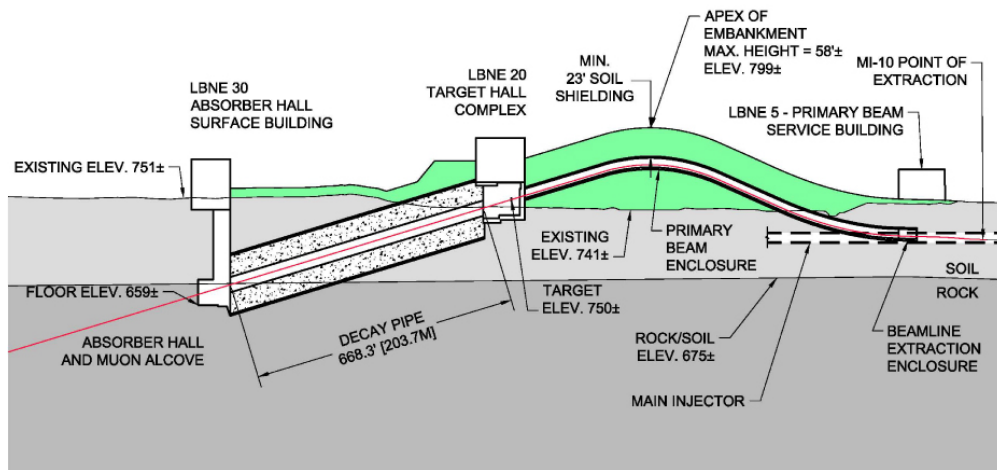


# Long-Baseline Neutrino Experiment (LBNE) Project

## Conceptual Design Report

### Volume 2: The Beamline at the Near Site

October 2012





# Contents

<b>Contents</b>	<b>i</b>
<b>Acronyms, Abbreviations and Units</b>	<b>vii</b>
<b>List of Figures</b>	<b>xi</b>
<b>List of Tables</b>	<b>xv</b>
<b>1 Introduction</b>	<b>1</b>
1.1 Introduction to the LBNE Project . . . . .	1
1.1.1 About this Conceptual Design Report . . . . .	1
1.1.2 LBNE and the U.S. Neutrino-Physics Program . . . . .	2
1.1.3 LBNE Project Organization . . . . .	3
1.1.4 Principal Parameters of the LBNE Project . . . . .	3
1.1.5 Supporting Documents . . . . .	5
1.2 Introduction to the LBNE Beamline (WBS 130.02) . . . . .	6
1.2.1 Overview and General Layout . . . . .	6
1.2.2 Primary Beam . . . . .	8
1.2.2.1 Extraction from Fermilab's Main Injector . . . . .	8
1.2.2.2 Beam Transport . . . . .	9
1.2.2.3 Beam Stability . . . . .	9
1.2.3 Neutrino Beam . . . . .	10
1.2.4 System Integration . . . . .	14
1.2.5 Near Site Conventional Facilities . . . . .	16
1.3 Participants . . . . .	17
<b>2 Primary Beam (WBS 130.02.02)</b>	<b>20</b>
2.1 Introduction . . . . .	20
2.2 Reference Design Overview . . . . .	20
2.3 Design Considerations . . . . .	22
2.3.1 Length and Elevation . . . . .	22
2.3.2 Existing Infrastructure and Shielding . . . . .	22
2.3.3 Beam Energy and Intensity . . . . .	23
2.3.4 Beam Control . . . . .	25
2.3.5 Estimation of Protons on Target . . . . .	25

2.4	Principal Design Elements and Parameters . . . . .	26
2.5	Lattice Optics (WBS 130.02.02.07) . . . . .	27
2.5.1	Introduction . . . . .	27
2.5.2	Design Considerations . . . . .	28
2.5.3	Reference Design . . . . .	28
2.5.3.1	Optics . . . . .	29
2.5.3.2	Sensitivity to Gradient Errors . . . . .	33
2.5.3.3	Beam Size at Target . . . . .	33
2.5.3.4	Trajectory Correction . . . . .	36
2.6	Magnets (WBS 130.02.02.02) . . . . .	39
2.6.1	Introduction . . . . .	39
2.6.2	Design Considerations . . . . .	39
2.6.3	Reference Design . . . . .	40
2.6.3.1	Main Dipole Magnets . . . . .	40
2.6.3.2	Main Injector Lambertson Magnets . . . . .	46
2.6.3.3	Main Injector C-Magnets . . . . .	48
2.6.3.4	Quadrupole Magnets . . . . .	48
2.6.3.5	Corrector Magnets . . . . .	53
2.6.3.6	Kicker Magnets . . . . .	54
2.6.3.7	Magnet Installation . . . . .	57
2.7	Magnet Power Supplies (WBS 130.02.02.03) . . . . .	61
2.7.1	Introduction . . . . .	61
2.7.2	Design Considerations . . . . .	62
2.7.3	Reference Design . . . . .	62
2.7.3.1	Power-supply Loops . . . . .	62
2.7.3.2	Power Supply Topology . . . . .	63
2.7.3.3	Dipole Power Supplies . . . . .	64
2.7.3.4	Quadrupole Power Supplies . . . . .	64
2.7.3.5	Corrector-Magnet Power Supplies . . . . .	64
2.7.3.6	Kicker Power Supplies . . . . .	65
2.7.3.7	Power Supply Control . . . . .	65
2.7.3.8	Power Feeder Loading . . . . .	67
2.7.3.9	Power Supply Large Equipment Installation . . . . .	67
2.8	Primary Water System (WBS 130.02.02.04) . . . . .	68
2.8.1	Introduction . . . . .	68
2.8.2	Design Considerations . . . . .	68
2.8.3	Reference Design . . . . .	69
2.8.3.1	Heat Loads and Heat Exchanger . . . . .	69
2.8.3.2	Pumps . . . . .	69
2.8.3.3	Piping, Valves, Fittings and Hardware . . . . .	69
2.8.3.4	De-ionizer / Filter Loop . . . . .	70
2.8.3.5	Instrumentation and Control . . . . .	70
2.8.3.6	Buswork . . . . .	71
2.8.3.7	Other Considerations . . . . .	71

2.9	Beam Instrumentation (WBS 130.02.02.05)	71
2.9.1	Introduction	71
2.9.2	Reference Design	72
2.9.2.1	Beam-Position Monitors	72
2.9.2.2	Beam-Loss Monitors	73
2.9.2.3	Beam-Intensity Monitors	74
2.9.2.4	Beam-Profile Monitors	74
2.10	Primary Vacuum (WBS 130.02.02.06)	74
2.10.1	Introduction	74
2.10.2	Design Considerations	75
2.10.3	Reference Design	75
2.10.3.1	Pumps	76
2.10.3.2	Beam Tubes	76
2.10.3.3	Valves and Gauges	76
2.10.3.4	Instrumentation and Control	77
2.10.3.5	Baking and Cleaning	77
2.11	Beam-Loss Calculations (WBS 130.02.02.08)	77
2.11.1	Introduction	77
2.11.2	Design Considerations	78
2.11.3	Reference Design	78
2.11.3.1	Primary-Beam Loss	79
2.11.3.2	Accidental Total Beam Loss	80
2.11.3.3	Activation of Components	84
<b>3</b>	<b>Neutrino Beam (WBS 130.02.03)</b>	<b>87</b>
3.1	Introduction	87
3.1.1	Design Considerations	88
3.2	Primary Beam Window and Baffle (WBS 130.02.03.02)	90
3.2.1	Introduction	90
3.2.2	Design Considerations	90
3.2.3	Reference Design	91
3.2.4	Target/Baffle Module	94
3.2.5	Target/Baffle Carrier	94
3.3	Targetry (WBS 130.02.03.03)	96
3.3.1	Introduction	96
3.3.2	Design Considerations	97
3.3.3	Reference Design	98
3.3.4	Target Options: R&D	102
3.3.5	Target and Horns Instrumentation	105
3.3.5.1	Design Considerations	106
3.3.5.2	Reference Design	107
3.4	Horns (WBS 130.02.03.04)	108
3.4.1	Design Considerations	109
3.4.2	Reference Design	110

3.4.2.1	Ancillary Components . . . . .	117
3.4.3	Horn Support Modules . . . . .	119
3.4.4	Support Module Stripling Blocks . . . . .	122
3.5	Horn Power Supplies (WBS 130.02.03.05) . . . . .	122
3.5.1	Design Considerations . . . . .	125
3.5.1.1	Capacitor Bank . . . . .	125
3.5.1.2	System Safety . . . . .	125
3.5.1.3	Controls . . . . .	126
3.5.1.4	Current Transducers . . . . .	126
3.5.1.5	Transmission Line . . . . .	126
3.5.1.6	Ground-Fault Protection . . . . .	128
3.5.1.7	Water Cooling . . . . .	128
3.6	Decay Pipe (WBS 130.02.03.06) . . . . .	128
3.6.1	Introduction . . . . .	128
3.6.2	Design Considerations . . . . .	129
3.6.3	Reference Design . . . . .	131
3.7	Hadron Absorber (WBS 130.02.03.07) . . . . .	132
3.7.1	Introduction . . . . .	132
3.7.2	Design Considerations . . . . .	132
3.7.3	Absorber Modeling . . . . .	134
3.7.3.1	Normal Operations . . . . .	134
3.7.3.2	Modeling Accident Cases . . . . .	136
3.7.4	Reference Design . . . . .	138
3.7.4.1	Absorber Core . . . . .	138
3.7.4.2	Absorber Shielding . . . . .	141
3.7.4.3	Absorber Water-Cooling System . . . . .	143
3.7.4.4	Absorber Temperature Monitoring . . . . .	144
3.8	Target Hall Shielding (WBS 130.02.03.08) . . . . .	144
3.8.1	Introduction . . . . .	144
3.8.2	Design Considerations . . . . .	144
3.8.3	Reference Design . . . . .	144
3.8.3.1	Target Hall Shield Pile . . . . .	144
3.8.3.2	Target Hall Air-Cooling Flows . . . . .	148
3.9	RAW Water Systems (WBS 130.02.03.09) . . . . .	151
3.9.1	Introduction . . . . .	151
3.9.2	Design Considerations . . . . .	151
3.9.3	Reference Design . . . . .	152
3.9.3.1	Target Hall Systems . . . . .	152
3.9.3.2	Absorber Hall Systems . . . . .	152
3.10	Radiological Considerations (WBS 130.02.03.10) . . . . .	153
3.10.1	Overview . . . . .	153
3.10.2	Shielding . . . . .	154
3.10.2.1	Primary Beamline . . . . .	154
3.10.2.2	Target Hall/Target Chase . . . . .	154

3.10.2.3	Decay Pipe . . . . .	154
3.10.2.4	Absorber Hall Complex . . . . .	155
3.10.3	Other Radiological Design Issues . . . . .	155
3.10.3.1	Groundwater and Surface Water Protection . . . . .	155
3.10.3.2	Tritium Mitigation . . . . .	156
3.10.3.3	RAW Systems . . . . .	156
3.10.3.4	Activated Air . . . . .	156
3.10.3.5	Outside Prompt Dose . . . . .	157
3.10.3.6	Offsite Dose . . . . .	157
3.10.3.7	Onsite Dose . . . . .	157
3.10.3.8	Residual Radiation . . . . .	157
3.11	Remote Handling Equipment (WBS 130.02.03.11) . . . . .	158
3.11.1	Introduction . . . . .	158
3.11.2	Design Considerations . . . . .	158
3.11.3	Reference Design . . . . .	159
3.11.3.1	Target Complex Remote-Handling Facilities . . . . .	159
3.11.3.2	Absorber Hall Remote Handling Facilities . . . . .	171
3.12	Modeling (WBS 130.02.03.12) . . . . .	175
3.12.1	Introduction . . . . .	175
3.12.2	Design Considerations . . . . .	175
3.12.3	Reference Design . . . . .	176
3.13	R&D Program . . . . .	176
<b>4</b>	<b>System Integration (WBS 130.02.04)</b>	<b>177</b>
4.1	Introduction . . . . .	177
4.2	Controls (WBS 130.02.04.02) . . . . .	177
4.2.1	Introduction . . . . .	177
4.2.2	Reference Design . . . . .	178
4.2.2.1	ACNET Controls . . . . .	178
4.2.2.2	Beam-Permit System . . . . .	179
4.3	Radiation-Safety Interlock Systems (WBS 130.02.04.03) . . . . .	180
4.3.1	Introduction . . . . .	180
4.3.2	Methods . . . . .	181
4.3.3	Reference Design . . . . .	182
4.3.3.1	Critical-Device Controller . . . . .	182
4.3.3.2	Exclusion Areas . . . . .	183
4.3.3.3	Electrical-Safety System . . . . .	183
4.3.3.4	Radiation-Loss Monitoring . . . . .	183
4.3.3.5	Airborne-Radioactivity Monitors . . . . .	184
4.3.3.6	Enclosure Radiation Monitors . . . . .	184
4.4	Alignment (WBS 130.02.04.04) . . . . .	184
4.4.1	Overview . . . . .	184
4.4.2	Design Considerations . . . . .	185
4.4.3	Reference Design . . . . .	186

4.4.3.1	Geodetic Determination of the Global Positions . . . . .	186
4.4.3.2	Primary Surface Geodetic Network at Fermilab . . . . .	188
4.4.3.3	High-Accuracy Sub-Surface Control Network . . . . .	190
4.5	Installation Coordination (WBS 130.02.04.05) . . . . .	191

**References** **193**

# Acronyms, Abbreviations and Units

AC	alternating current
ACNET	Accelerator Controls NETWORK
ASME	American Society of Mechanical Engineers
atm	atmosphere
AWG	American Wire Gauge
BLIP	Brookhaven Linac Isotope Producer
BLM	Beam-loss monitor
BNB	Booster Neutrino Beam
BNL	Brookhaven National Laboratory
BPM	Beam-position monitor
BuLB	Basic Micro Learning Box
CAMAC	Computer Automated Measurement and Control
CCD	charge-coupled device
CDC	Critical Device Controller
CDR	Conceptual Design Report
CORS	Continuously Observed Reference Station
CP	charge parity
CUB	Central Utilities Building
DAQ	data acquisition
DC	direct current

DCCT	DC current transformers
DI	de-ionization
DOE	Department of Energy
DS	downstream
DUSEL	Deep Underground Science and Engineering Laboratory
E-Net	Ethernet
ESS	Electrical Safety System
FEA	finite element analysis
FF	final focus
FFT	fast fourier transform
FODO	A repetitive configuration of focusing (F) and defocusing (D) magnetic elements separated by a fixed spacing of non-focusing elements (O)
FPGA	field programmable gate array
FRCM	Fermilab Radiological Control Manual
ft	foot or feet
gpm	gallons per minute
GPS	global positioning system
GRS	Geodetic Reference System
hBN	Hexagonal boron nitride
hp	horsepower
HRM	Hot-link Rack Monitor
HTO	tritiated water molecule
Hx	Heat Exchanger
ID	inner diameter
IHEP	Institute for high energy physics
IMU	Inertial Measuring Unit
INS	Inertial Navigation System

IPM	Ionization Profile Monitor
ITRF	International Terrestrial Reference Frame
L	used here to indicate the “level” underground, in feet
LC	inductive/capacitive
LCW	low-conductivity water
LHC	Large Hadron Collider
LOTO	lock-out/tag-out
MAD	Methodical Accelerator Design
MARS	a monte carlo code
MCC	Motor control centers
MECAR	Main Injector Excitation Controller and Regulator
MI	Main Injector
MI-10 (60, 64 etc)	Surface buildings above extraction point on Main
MIBS	Main Injector Beam Synchronous Clock
MPS	machine-protection system
MUX	multiplex
NAD	North American Datum
NGS	National Geodetic Survey
NOvA	NuMI Off-axis “nu sub e” Appearance Experiment
NuMI	Neutrinos at the Main Injector (Beamline facility at Fermilab)
OD	outer diameter
P5	Particle Physics Project Prioritization Panel
PLC	Programmable Logic Controller
POCO	name of graphite supplier (POCO Graphite)
POT	Protons on Target
Ppm	parts per million

psid	pounds per square inch differential
PW	Pond Water
RAL	Rutherford Appleton Laboratory
RAW	Radioactive water
RF	radio frequency
RH	remote handling
RSS	Radiation Safety Interlock Systems
SCR	silicon-controlled rectifier
SEM	secondary emission monitor
SI	Systems Integration
SURF	Sanford Underground Research Facility (in Lead, S.D., the LBNE Far Site)
TCLK	Tevatron Clock
TCV	Temperature control valve
TH	Target Hall
THI	Target Hall instrumentation
THSP	Target Hall shield pile
TLM	Total-loss monitor
UHV	Ultra High Vacuum
US	upstream
VA	Volt-Ampere (also kVA, MVA)
VAC	Volts AC (also mVAC, kVAC, MVAC)
VFD	variable-frequency drive
VME	VMEbus, VERSAmodule Eurocard bus, ANSI/IEEE 1014-1987; a computer bus standard
WBS	Work Breakdown Structure

# List of Figures

1-1	Organization chart for the LBNE Project to L3 . . . . .	4
1-2	Systems included in the LBNE Beamline . . . . .	7
1-3	The energy range of the first and second oscillation peaks . . . . .	12
1-4	The first horn magnet . . . . .	12
1-5	Neutrino fluxes at the Far Detector (focusing positive particles) . . . . .	13
1-6	Antineutrino fluxes at the Far Detector (focusing negative particles) . . . . .	13
1-7	Neutrino events as function of decay-pipe length (simulated) . . . . .	15
1-8	LBNE Overall Project Layout at Fermilab . . . . .	17
1-9	Organization chart for the Beamline L2 Project to L4 . . . . .	19
2-1	Primary beamline elevation view . . . . .	23
2-2	Main Injector beam power as a function of beam energy . . . . .	24
2-3	LBNE extraction Lambertsons and C-magnet straddling MI quadrupole . . . . .	29
2-4	Magnet parameters of the primary beamline . . . . .	30
2-5	Horizontal and vertical lattice functions of transfer line . . . . .	31
2-6	Magnet apertures and beam envelopes . . . . .	32
2-7	Tuning range of the Final Focus . . . . .	34
2-8	Final Focus gradients for the examples in Figure 2-7 . . . . .	35
2-9	Trajectories with random misalignments and dipole field errors . . . . .	37
2-10	Orbit offsets and corrector kicks for the trajectories in Figure 2-9 . . . . .	38
2-11	MI Dipole cross section. . . . .	42
2-12	Layout of one IDA and one IDB dipole in a half cell . . . . .	43
2-13	Beam tube cross section . . . . .	44
2-14	Typical IDA excitation curve. . . . .	45
2-15	MI Lambertson magnet end and cross section. . . . .	47
2-16	Excitation curve of a MI Lambertson magnet. . . . .	47
2-17	ICA MI C Magnet. . . . .	49
2-18	ICA beam tube shown in horizontal bending orientation. . . . .	49
2-19	ICA integrated strength as a function of current. . . . .	50
2-20	Cross-section of QQB and QQC quadrupoles. . . . .	52
2-21	Typical QQB excitation curve. . . . .	52
2-22	Typical QQC excitation curve. . . . .	53
2-23	Schematic of LBNE 3-in (76.2-mm) aperture gap trim dipole (IDS). . . . .	55
2-24	Integrated strength of NuMI dipole corrector. . . . .	56
2-25	Cross section of a NOvA extraction kicker, "RKB" type . . . . .	58

2-26	Magnet installation on sloping surfaces. . . . .	60
2-27	Magnet power-supply block diagram . . . . .	63
2-28	Ion chamber loss monitor. . . . .	73
2-29	SEM beam profile monitor . . . . .	75
2-30	Horizontal and vertical beam distributions at baffle entrance . . . . .	80
2-31	Halo particle loss distribution along the beamline . . . . .	81
2-32	Core beam population and distributions . . . . .	82
2-33	The halo and core beam loss . . . . .	83
2-34	Beam trajectory for beam loss due to magnet-strength degradation . . . . .	84
2-35	Instantaneous temperature rise and accidental beam loss . . . . .	85
2-36	Residual dose rates along the beam line and magnets . . . . .	86
3-1	Cartoon of the neutrino beamline . . . . .	88
3-2	Cut view of an engineering model of part of the target complex . . . . .	89
3-3	Shielding wall with embedded stepped liner. (b): After cartridge insertion. . . . .	92
3-4	Section view of replacement window assembly . . . . .	93
3-5	Section view of 2.3-MW-capable beryllium window . . . . .	93
3-6	708 kW (NOvA) baffle baseline design for LBNE . . . . .	94
3-7	Elevation view of target/baffle module and carrier design . . . . .	95
3-8	Proposed LT target for LBNE . . . . .	100
3-9	Cross-section of LT target . . . . .	100
3-10	Prototype of titanium cooling . . . . .	102
3-11	BLIP test sample holder . . . . .	104
3-12	Horn 1 section . . . . .	109
3-13	Horn 2 section. Horn 2 specifications are listed in Table 3-2. . . . .	109
3-14	Idealized shape of the Horn 1 inner and outer conductors . . . . .	111
3-15	Idealized shape of horn 2 inner and outer conductors . . . . .	112
3-16	Horn 1 inner conductor water spray coverage. . . . .	112
3-17	Additional support and stability for the thin inner conductor . . . . .	112
3-18	Horn 1 stripline connection at the downstream end . . . . .	113
3-19	Heating loads on the inner conductor of Horn 1 . . . . .	114
3-20	Heating loads on the inner conductor of Horn 2 . . . . .	115
3-21	Temperature of Horn 1 at steady state . . . . .	116
3-22	Temperature trends in the Horn 1 neck at beam cold start-up . . . . .	116
3-23	Temperature trends in the Horn 1 neck during a single pulse after equilibrium . . . . .	116
3-24	Magnetic pressure loading profile on the Horn 1 inner conductor at mid-pulse. . . . .	117
3-25	Stress due to magnetic loading at mid-pulse for Horn 1. . . . .	117
3-26	Horn cooling water manifolds. . . . .	118
3-27	Horn hanger structural analysis with tri-axial loading. . . . .	119
3-28	Horn support module concept . . . . .	120
3-29	Adjustment fixtures for the horn-support module concept . . . . .	121
3-30	Stripline Block structure assembly. . . . .	123
3-31	Stripline Block remote clamp assembly. . . . .	124
3-32	NuMI Capacitor Bank transport and installation, 2004. . . . .	124

3-33	Stripline cross-section: 8 conductor . . . . .	127
3-34	Stripline cross-section: 9 conductor . . . . .	127
3-35	Typical cross section of concentric decay pipe and shielding concrete. . . . .	129
3-36	Section of the decay pipe at its upstream end . . . . .	131
3-37	Simplified elevation view of the absorber within the Absorber Hall . . . . .	133
3-38	Longitudinal energy deposition in the absorber core, normal operation . . . . .	135
3-39	ANSYS simulation of Al core block . . . . .	136
3-40	Temperature distribution in the Al absorber-core block . . . . .	137
3-41	Model of the absorber conceptual design; top view . . . . .	139
3-42	Design of the absorber core blocks . . . . .	140
3-43	Design of the Al pre-core mask. . . . .	142
3-44	Beamline elevation view . . . . .	146
3-45	Cross section of target chase steel shielding . . . . .	147
3-46	Schematic of air-cooling for shielding . . . . .	150
3-47	LBNE Target Hall enclosure beamline elevation section . . . . .	160
3-48	Target Complex Plan View . . . . .	161
3-49	Target Complex Plan : expanded view of Figure 3-48 . . . . .	162
3-50	Target Hall work cell concept . . . . .	163
3-51	Target Hall work cell section, viewed from upstream . . . . .	164
3-52	Photo of cask-to-morgue cell transfer system . . . . .	170
3-53	Absorber Hall section . . . . .	172
3-54	Absorber Hall section with details of absorber core and shielding . . . . .	173
3-55	Absorber Hall beam view showing hadron-monitor replacement concept . . . . .	174
4-1	GPS network tying Fermilab and SURF to the CORS system . . . . .	187
4-2	Residuals in latitude/longitude and residuals in height. . . . .	188
4-3	Fermilab LBNE surface geodetic network. . . . .	189
4-4	Distribution observation residuals for the Target and Near Detector Halls in MINOS . . . . .	191



# List of Tables

1-1	LBNE Principal Parameters . . . . .	5
1-2	LBNE CD-1 Documents . . . . .	5
1-3	Summary of principal beam design parameters. . . . .	10
1-4	Beam stability requirements. . . . .	10
1-5	Parameters for Beamline Reference Design . . . . .	16
2-1	Summary of primary-beam magnet specifications . . . . .	39
2-2	Properties of IDA Dipoles [b]. . . . .	41
2-3	Properties of IDD Dipoles [b]. . . . .	41
2-4	Properties of the MI Lambertson magnets. . . . .	46
2-5	ICA Main Injector C-Magnet Properties. . . . .	48
2-6	QQB: Hollow conductor 3Q120 Properties. . . . .	51
2-7	QQC: Quadrupole magnet properties. . . . .	51
2-8	LBNE Trim Dipole Properties (IDS) . . . . .	54
2-9	Properties of the NOvA extraction kicker magnets (RKB) . . . . .	57
2-10	Characteristics of magnet installation. . . . .	59
2-11	Dipole (bending) magnet loops . . . . .	62
2-12	Quadrupole magnet loops . . . . .	64
2-13	Corrector magnet power supplies. . . . .	65
2-14	Specifications for the ion chamber loss monitor. . . . .	74
2-15	List of major vacuum components . . . . .	76
2-16	Aperture half-size of primary beam line elements used in simulations . . . . .	79
3-1	Properties of graphite and beryllium at 20°C . . . . .	98
3-2	Horn parameters. The inner and outer conductor parameters are abbreviated by IC and OC, respectively. . . . .	111
3-3	Heating loads on the horns . . . . .	114
3-4	Estimated circuit parameters for the horn power supply . . . . .	122
3-5	Operational/accident conditions for the absorber at 2.3 MW beam power . . . . .	138
3-6	Shielding requirements for the top of the target chase. . . . .	145
3-7	Shielding requirements for the walls and the floor of the target chase. . . . .	148
3-8	Airflows in the target pile and the decay pipe. . . . .	149
3-9	Target Hall crane characteristics. . . . .	167
3-10	Morgue storage requirements. . . . .	169

4-1 Alignment tolerance requirements ( $1-\sigma$ ) . . . . . 185

# 1 Introduction

## 1.1 Introduction to the LBNE Project

The Long-Baseline Neutrino Experiment (LBNE) Project team has prepared this Conceptual Design Report (CDR) which describes a world-class facility to enable a compelling research program in neutrino physics. The ultimate goal in the operation of the facility and experimental program is to measure fundamental physical parameters, explore physics beyond the Standard Model and better elucidate the nature of matter and antimatter.

Although the Standard Model of particle physics presents a remarkably accurate description of the elementary particles and their interactions, it is known that the current model is incomplete and that a more fundamental underlying theory must exist. Results from the last decade, revealing that the three known types of neutrinos have nonzero mass, mix with one another and oscillate between generations, point to physics beyond the Standard Model. Measuring the mass and other properties of neutrinos is fundamental to understanding the deeper, underlying theory and will profoundly shape our understanding of the evolution of the universe.

### 1.1.1 About this Conceptual Design Report

The LBNE Conceptual Design Report is intended to describe, at a conceptual level, the scope and design of the experimental and conventional facilities that the LBNE Project plans to build to address a well-defined set of neutrino-physics measurement objectives. At this Conceptual Design stage the LBNE Project presents a *Reference Design* for LBNE and alternative designs that are still under consideration for particular elements.

The scope includes

- an intense neutrino beam aimed at a far site
- detectors located downstream of the neutrino source

- a massive neutrino detector located at the far site
- construction of conventional facilities at both the near and far sites

The selected near and far sites are Fermi National Accelerator Laboratory (Fermilab), in Batavia, IL and Sanford Underground Research Facility (SURF), respectively. The latter is the site of the formerly proposed Deep Underground Science and Engineering Laboratory (DUSEL) in Lead, South Dakota.

This CDR is organized into six stand-alone volumes, one to describe the overall LBNE Project and one for each of its component L2 projects:

- Volume 1: The LBNE Project
- Volume 2: The Beamline at the Near Site
- Volume 3: Detectors at the Near Site
- Volume 4: The Liquid Argon Detector at the Far Site
- Volume 5: Conventional Facilities at the Near Site
- Volume 6: Conventional Facilities at the Far Site

Volume 1 is intended to provide readers of varying backgrounds an introduction to LBNE and to the following volumes of this CDR. It contains high-level information and refers the reader to topic-specific volumes and supporting documents, also listed in Section 1.1.5. Each of the other volumes contains a common, brief introduction to the overall LBNE Project, an introduction to the individual L2 project and a detailed description of its conceptual design.

### **1.1.2 LBNE and the U.S. Neutrino-Physics Program**

In its 2008 report, the Particle Physics Project Prioritization Panel (P5) recommended a world-class neutrino-physics program as a core component of the U.S. particle physics program [1]. Included in the report is the long-term vision of a large detector at the formerly proposed Deep Underground Science and Engineering Laboratory (DUSEL) in Lead, S.D. (now SURF), and a high-intensity neutrino source at Fermilab.

On January 8, 2010, the Department of Energy (DOE) approved the Mission Need for a new long-baseline neutrino experiment that would enable this world-class program and firmly establish the U.S. as the leader in neutrino science. The LBNE Project is designed to meet this Mission Need.

With the facilities provided by the LBNE Project, the LBNE Science Collaboration proposes to mount a broad attack on the science of neutrinos with sensitivity to all known parameters in a single experiment. The focus of the program will be the explicit demonstration of leptonic CP violation, if it exists, by precisely measuring the asymmetric oscillations of muon-type neutrinos and antineutrinos into electron-type neutrinos and antineutrinos.

The experiment will result in precise measurements of key three-flavor neutrino-oscillation parameters over a very long baseline and a wide range of neutrino energies, in particular, the CP-violating phase in the three-flavor framework and the mass ordering of neutrinos. The unique features of the experiment – the long baseline, the broad-band beam, and the high resolution of the detector – will enable the search for new physics that manifests itself as deviations from the expected three-flavor neutrino-oscillation model. The scientific goals and capabilities of LBNE are outlined in Volume 1 of this CDR and the 2010 Interim Report of the Long-Baseline Neutrino Experiment Collaboration Physics Working Groups [2].

Siting the Far Detector deep underground, a scope opportunity that LBNE may seek to pursue in the future with non-DOE funding, would provide opportunities for research in additional areas of physics, such as nucleon decay and neutrino astrophysics, in particular, studies of neutrino bursts from supernovae occurring in our galaxy.

### **1.1.3 LBNE Project Organization**

The LBNE Project Office at Fermilab is headed by the Project Director and assisted by the Project Manager, Project Scientist and Systems Engineer. Project Office support staff include a Project Controls Manager and supporting staff, a Financial Manager, an Environment, Safety and Health (ES&H) Manager, a Computing Coordinator, Quality Assurance, Procurement and Risk Managers, a documentation team and administrative support. The Project organization is shown in Figure 1-1.

The Beamline, Liquid Argon Far Detector and Conventional Facilities L2 Projects are managed by the Project Office at Fermilab, while the Near Detector Complex L2 Project is managed by a Project Office at Los Alamos National Laboratory (LANL).

More information on Project Organization can be found in Volume 1 of this CDR. A full description of LBNE Project management is contained in the LBNE Project Management Plan [3].

### **1.1.4 Principal Parameters of the LBNE Project**

The principal parameters of the major Project elements are given in Table 1-1.

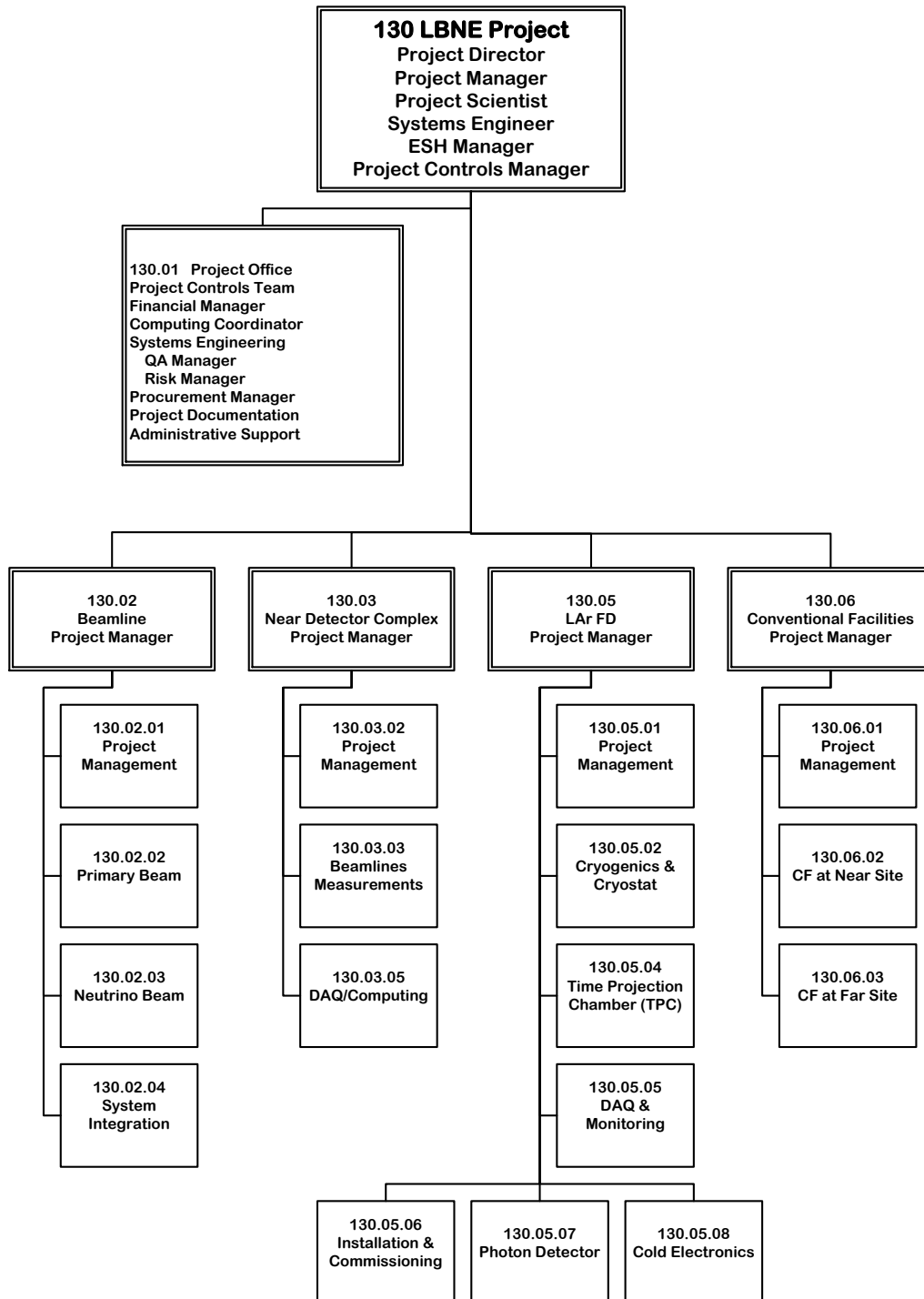


**Figure 1-1:** Organization chart for the LBNE Project (to WBS Level 3)

**Table 1-1: LBNE Principal Parameters**

Project Element Parameter	Value
Near- to Far-Site Baseline	1,300 km
Primary Proton Beam Power	708 kW, upgradable to 2.3 MW
Protons on Target per Year	$6.5 \times 10^{20}$
Primary Beam Energy	60 – 120 GeV (tunable)
Neutrino Beam Type	Horn-focused with decay volume
Neutrino Beam Energy Range	0.5 – 5 GeV
Neutrino Beam Decay Pipe Diameter $\times$ Length	4 m $\times$ 203.7 m
Far Detector Type	LArTPC
Far Detector Active (Fiducial) Mass	13.5 (10) kton
Far Detector Depth	3 m overburden

### 1.1.5 Supporting Documents

Additional information related to the CDR is available in a set of supporting documents. Detailed information on risk analysis and mitigation, value engineering, ES&H, costing, project management and other topics not directly in the design scope can be found in these documents, listed in Table 1-2. Each document is numbered and stored in LBNE’s document database, accessible via a username/password combination provided by the Project. Project documents stored in this database are made available to internal and external review committees through Web sites developed to support individual reviews.

**Table 1-2: LBNE CD-1 Documents**

Title	LBNE Doc Number(s)
Alternatives Analysis	4382
Case Study Report; Liquid Argon TPC Detector	3600
Configuration Management Plan	5452
DOE Acquisition Strategy for LBNE	5442
DOE Preliminary Project Execution Plan	5443
Integrated Environment, Safety and Health Management Plan	4514
LAr-FD Preliminary ODH Analysis	2478
LBNE Reconfiguration Final Report	Linked from LBNE web site (lbne.fnal.gov) under “Reports and Documents”

Global Science Objectives, Science Requirements and Traceback Reports	4772
Muon-induced Background for Beam Neutrinos on the Surface	6159
Parameter Tables, Far Detector	3383
Preliminary Hazard Analysis Report	4513
Preliminary Security Vulnerability Assessment Report	4826
Procurement Plan	5329
Project Management Plan	2453
Project Organization Chart	5449
Quality Assurance Plan	2449
Report on the Depth Requirements for a Massive Detector at Homestake	0034
Requirements, Beamline	4835
Requirements, Far Detector	3747
Requirements, Far Site Conventional Facilities	4958
Requirements, Near Detectors	5579
Requirements, Near Site Conventional Facilities	5437
Risk Management Plan	5749
The Science and Strategy for a Long-Baseline Neutrino Experiment Near Detector	8625
Value Engineering Report	3082
Work Breakdown Structure (WBS)	4219

## 1.2 Introduction to the LBNE Beamline (WBS 130.02)

### 1.2.1 Overview and General Layout

The LBNE Beamline at Fermilab will be designed to provide a neutrino beam of sufficient intensity and energy to meet the goals of the LBNE experiment with respect to long-baseline neutrino-oscillation physics. The design is a conventional, horn-focused neutrino beamline. The components of the beamline will be designed to extract a proton beam from the Fermilab Main Injector (MI) and transport it to a target area where the collisions generate a beam of charged particles. This secondary beam, aimed toward the Far Detector, is followed by a decay-pipe where the particles of the secondary beam decay to generate the neutrino beam. At the end of the decay pipe, an absorber pile removes the residual hadrons.

The facility is designed for initial operation at proton-beam power of 708 kW, with the capability to support an upgrade to 2.3 MW. In the reference design, extraction of the proton beam occurs at MI-10, a new installation. After extraction, this primary beam establishes a horizontally straight compass heading west-northwest toward the Far Detector, but will be bent upward to an apex before being bent downward at the appropriate angle, 101 milliradians ( $5.79^\circ$ ) as shown in Figure 1-2.

The primary beam will be above grade for about 550 feet; this design minimizes expensive underground construction and significantly enhances capability for ground-water radiological protection. The design requires, however, construction of an earthen embankment, or hill, whose dimensions are commensurate with the bending strength of the dipole magnets required for the beamline. The embankment will need to be approximately 950 feet long and 58 feet high above grade at its peak.

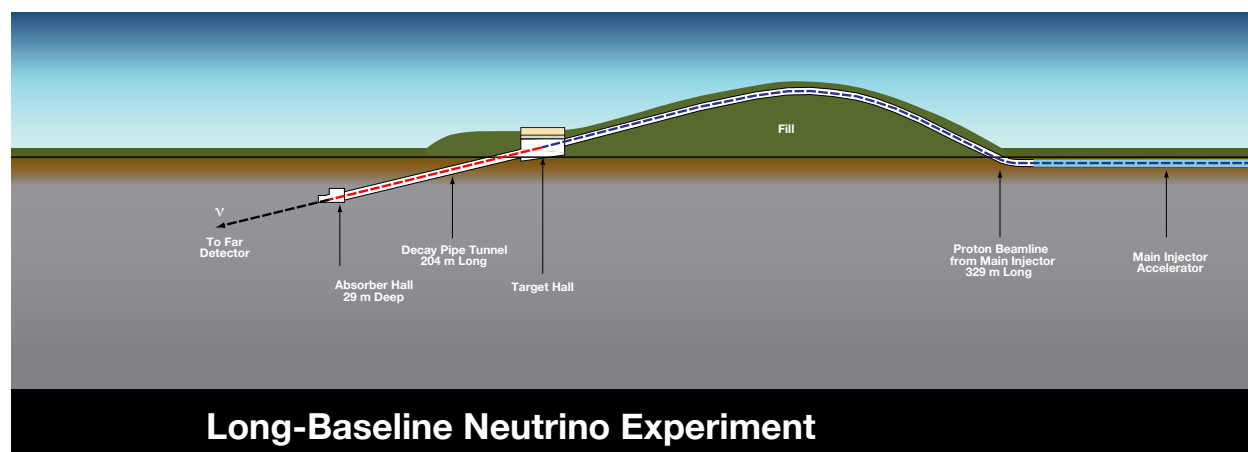


**Figure 1-2:** Schematic of the systems included in the LBNE Beamline. The top of the engineered hill is 18 m above grade.

The target marks the transition from the intense, narrowly directed proton beam to the more diffuse, secondary beam of particles that in turn decay to produce the neutrino beam. The secondary particles are short-lived and most decays generate a muon, which penetrates deep into the surrounding rock and a neutrino that continues on toward the Far Detector.

After collection and focusing, the pions and kaons that did not initially decay – the residual particles mentioned above – need a long, unobstructed volume in which to decay. This decay volume in the LBNE reference design is a pipe of circular cross section with its diameter and length optimized such that decays of the pions and kaons result in neutrinos in the energy range useful for the experiment. The decay volume is followed immediately by the absorber, which removes the remaining beam hadrons.

The LBNE Beamline is broken into three principal systems for organizational purposes: the Primary Beam (referring to the components required for the initial, high-intensity proton

beam), the Neutrino Beam (for the components used to create a high-intensity neutrino beam from the initial proton beam) and System Integration.

It is important to note that the design and construction of high-intensity neutrino beams has been an integral aspect of Fermilab's program for decades. The experience gained from the various neutrino projects has been employed extensively in the LBNE Beamline conceptual design. In particular, the NuMI beamline serves as the prototype design. Most of the subsystem designs and their integration follow, to a large degree, from previous projects.

Radiological protection is integrated into the LBNE beamline reference design in two important ways. First, shielding is optimized to reduce exposure of personnel to radiation dose and to minimize radioisotope production in ground water within the surrounding rock. Secondly, the handling and control of tritiated ground water produced in or near the beamline drives many aspects of the design. Production of tritium is unavoidable, and it is necessary to minimize its accumulation in the soil or rock in the form of tritiated water (HTO).

The reference design for the primary beam and the neutrino beam is suitable for the initial beam power of 708 kW in all respects. Some aspects of the reference design are also appropriate for a beam power of 2.3 MW. These include the radiological shielding and the size of the enclosures as well as the beam absorber, the remote handling, the decay-pipe cooling and the RAW system piping, none of which can be upgraded after exposure to a high-intensity beam.

The LBNE Beamline will become operational after the current planned six-year run of the NOvA experiment. With the concurrence of the Fermilab Directorate, LBNE assumes components from the NuMI Beamline will be available for removal and reuse [4].

## 1.2.2 Primary Beam

### 1.2.2.1 Extraction from Fermilab's Main Injector

The primary proton beam for LBNE will be extracted from the Main Injector (MI) using a method called "single-turn" extraction, in which all the protons accelerated in the MI synchrotron ring will be diverted to the dedicated LBNE beamline within one circuit. Although the NuMI beam operates at 120 GeV, further studies on optimizing the LBNE signal-to-detector backgrounds may indicate desirability of a lower energy. The design proton energy thus ranges from 60 to 120 GeV. Approximately  $4.9 \times 10^{13}$  protons are extracted every 1.33 seconds at 120 GeV, resulting in a beam power of 708 kW. The extraction point, located near the MI-10 surface building and called simply *MI-10*, will be a new installation, different from the one used for NuMI.

### 1.2.2.2 Beam Transport

The design of the primary proton beam transport is driven by both the goals of the LBNE physics program and radiological safety concerns. The beam must first of all be intense enough to create a flux of neutrinos at the Far Detectors sufficient to meet the physics objectives of the experiment. Secondly, the beam energy must be set to optimize the energy spectrum of the neutrinos, yet not produce excess background signals that could compromise the measurements. And the system must be safe. Together these requirements imply that the beam must reach the target with very low losses to ensure both efficient production of neutrinos as well as minimal radiological activation of components in the beamline. Due to accelerator duty-cycles, some reduction of total beam power at lower energies is likely. And of course sufficient shielding must be in place in case of any accidental mis-steering of the beam.

The primary beamline elements necessary for transport include dipole (bending) magnets, quadrupole (focusing) magnets, corrector magnets, monitoring instrumentation and vacuum equipment. LBNE will use conventional dipole and quadrupole magnets to guide the beam in the right direction and focus it on the target, respectively. Their optics will closely follow the design of the Main Injector elements. The magnets and their power supplies will be optimized for performance and cost, and will include both new and refurbished elements. The LBNE beam optics will be simulated and analyzed for optimum transport properties.

The general primary-beam specifications are listed in Table 1-3. The accelerator complex and the LBNE Beamline are planned to deliver  $6.5 \times 10^{20}$  primary protons to the neutrino target per year. This number includes allowances for scheduled shutdowns for maintenance and upgrades as well as unscheduled failures estimated from past experience. The fast, “single-turn” extraction technique delivers all the protons in one machine cycle (1.33 seconds) to the LBNE target in 10 microseconds. When synchronized to the detector electronics, this short spill helps ensure a high rejection of background events at the Far Detector that do not originate from the accelerator beam.

In this Conceptual Design Report, the beam trajectory points to a Far Detector positioned at the 4850L, whereas the detector is designed (and costed) to be near the surface. Due to the geometry of the decay pipe, the actual difference in the spectrum at the surface from a beam aimed 4850' underground is less than  $\pm 1\%$  for energies below 5 GeV as computed by physics simulations. The final design will align the beam with the Far Detector location.

### 1.2.2.3 Beam Stability

The primary beam needs to be stable in position and direction at the neutrino production target. Deviations in the beam position, for example, affect not only the spatial distribution of the distant neutrino flux, but can also affect the energy spectrum. These systematic

**Table 1-3:** Summary of principal beam design parameters.

Parameter	Value
Protons per cycle (120 GeV)	$4.9 \times 10^{13}$
Spill duration	$1.0 \times 10^{-5}$ sec
Energy	60 to 120 GeV
Protons on target per year	$6.5 \times 10^{20}$
Beam size at target	1.3 to 1.5 mm
$\Delta p/p$	$11. \times 10^{-4}$ 99% ( $28. \times 10^{-4}$ 100%)
Beam/batch (84 bunches)	$8 \times 10^{12}$ nominal; ( $3 \times 10^{11}$ commissioning)
Transverse emittance	$30\pi\mu\text{m}$ 99% ( $360\pi\mu\text{m}$ 100%)
Cycle time (120 GeV)	1.33 sec
Beam divergence ( $x,y$ )	17 $\mu\text{rad}$

**Table 1-4:** Beam stability requirements.

Parameter	Value
Position at target	$\pm 0.45$ mm
Angle at target	$\pm 70$ $\mu\text{rad}$
Size at target, rms	10% of $\sigma(x,y)$

effects must be minimized to the extent that they become negligible in the physics analyses. Although the full physics analysis procedures will not be available for some time, guidelines from simple analyses and experience from previous experiments provide a basis for estimating the effects of a poorly positioned beam. Table 1-4 lists the maximum allowable deviations from the design goals of beam position, angle and size. A set of beam-position monitors with control feedback will be installed at points along the primary beamline to ensure stability.

### 1.2.3 Neutrino Beam

The neutrino beam must be optimized for direction and energy to enable the neutrino-oscillation physics at the Far Detector. The neutrino beam will be created from the primary (proton) beam in a three-step process.

1. The primary beam strikes the neutrino production target in the Target Hall.
2. The charged products of these interactions, mostly pions and kaons, are collected in the Target Hall and focused in the direction of the Far Detector.
3. Those pions and kaons that are aimed correctly enter the long pipe of the decay volume, where they decay into neutrinos forming the neutrino beam.

The beamline elements involved in these three steps must be designed to work together to maximize the neutrino flux in the useful energy range for the experiment.

The target, the first element of the neutrino beam system, will be designed to interact with approximately 85% of the primary protons and to minimally absorb the charged pions and kaons created in those interactions. To accomplish this, the target needs to be relatively small in cross section. This requires a tight focus of the primary beam, resulting in a very dense energy deposition in the target material. The challenge is to design a long and narrow piece of material that can be adequately cooled and can survive these demanding conditions for as long as possible before being degraded by radiation and requiring replacement.

The neutrino-beam energy spectrum must be tailored to maximize the signal in the  $\nu_e$  appearance oscillation experiment, in which muon neutrinos oscillate to electron neutrinos. There are, in effect, two predicted energy intervals of interest in this experiment, referred to as the *first* and *second* oscillation maxima. The beam must provide a concentrated neutrino flux at the energies bounded by these oscillation peaks, shown in Figure 1-3. The higher-energy regime, 1.5- to 5-GeV neutrino energy (“1” in Figure 1-3), corresponds to focused pions of approximately 3.5 to 12 GeV, and is relatively straightforward to reach with toroidal, or horn, magnetic focusing elements. The lower-energy part of the neutrino spectrum (“2” in Figure 1-3) is more challenging to produce with high efficiency; it corresponds to pions and kaons of less than a few GeV which are scattered more and emerge at large angles making a sharp focus difficult. LBNE’s on-axis design, with the beam pointing directly to the detectors, optimizes the neutrino flux over the broad energy range needed to cover both oscillation maxima. The spectrum optimized for oscillation physics has the target fully inserted into Horn 1, however, it is possible to increase the energy of the spectrum significantly by adjusting the target’s position upstream by up to 2.5 m. See Figure 1-4.

The focusing of pions and kaons within the broad energy range of 2 to 12 GeV requires at least two horn magnets. The target and horns will be mounted inside a heavily shielded vault (called the “chase”) that is open to the decay pipe at the downstream end. Low-energy pions and kaons usually pass through a large section of the magnetic field in the first horn and are focused to a point between the horns. A schematic of the first horn is shown in Figure 1-4. The second horn acts to redirect these particles toward the decay pipe. Most of the higher-energy pions and kaons are collected with the second horn, due to the small angles at which they are produced. The reference design for the target and horns has been simulated, and the parameters, listed in Table 1-5, have been tuned to deliver a neutrino-beam spectrum adequate for the physics goals. The parameters may be further optimized for the physics of LBNE, subject to material and engineering constraints. The neutrino flux at the Far Detector site is shown in Figures 1-5 and 1-6, calculated for the NuMI horns at 200 kA, 6.6 m apart and at a distance of 17.3 m from Horn 1 to the decay pipe (4 m in diameter and 200 m long). The NuMI target starts  $-35$  cm from Horn 1.

Over the lifetime of the experiment, the target and focusing horns will need to be replaced. Accommodating the safe routine replacement of parts in a radioactive environment is an

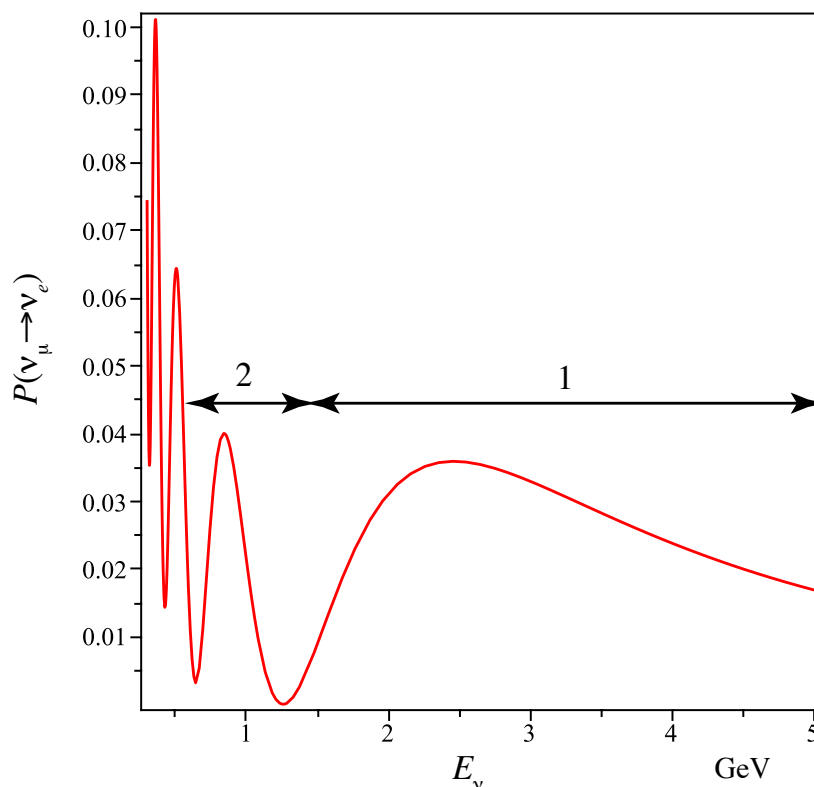


**Figure 1-3:** The energy range of the first and second oscillation peaks are denoted by the respective numerals. The beam design is optimized to produce neutrinos within this range. The true probability depends on a parameter,  $\theta_{13}$ .

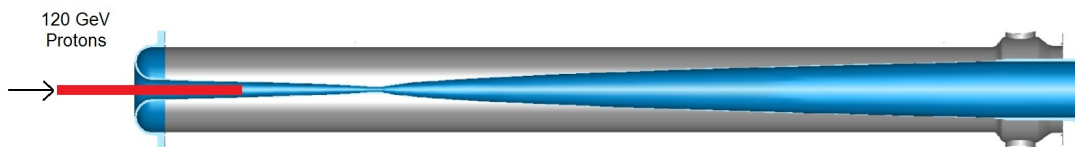


**Figure 1-4:** The first horn magnet. The conductor of the horn is shaded blue, and the graphite target (red) is inserted into the horn. The beam is incident from the left and the magnetic field region is between the shaped inner conductor and the cylindrical outer conductor (gray). Horn 1 is 336 cm long. The target is shown in the fully inserted position.

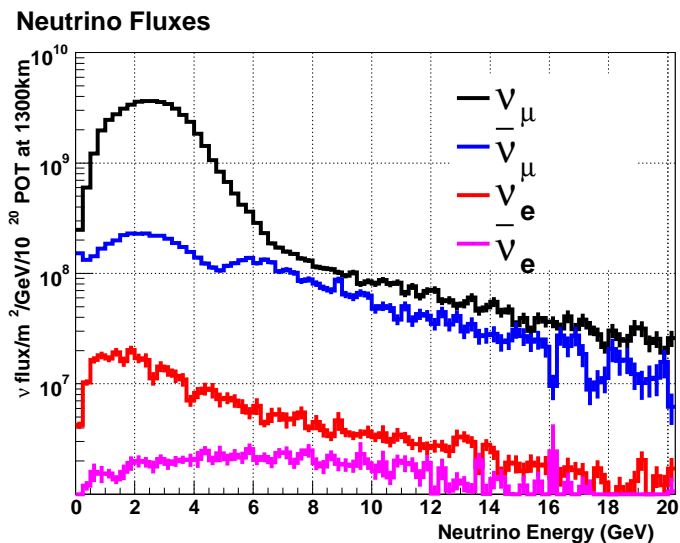


**Figure 1-5:** Neutrino fluxes at the Far Detector as a function of energy in the absence of oscillations with the horns focusing positive particles. In addition to the dominant  $\nu_\mu$  ( $\bar{\nu}_\mu$ ) flux, the minor components are also shown. Note the logarithmic scale.

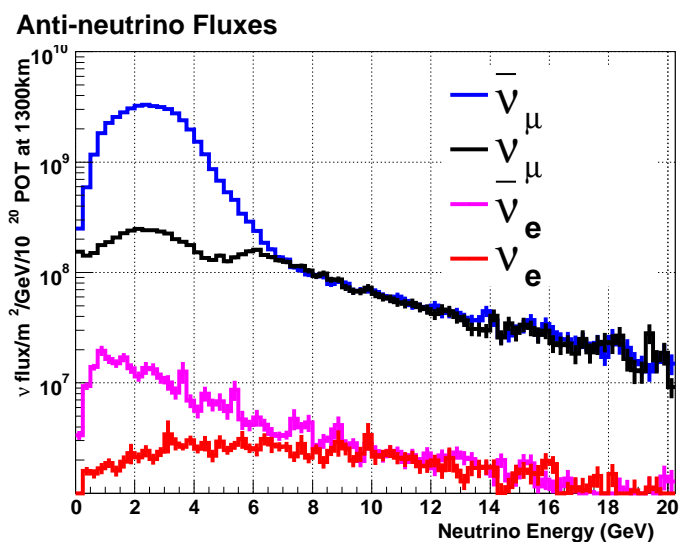


**Figure 1-6:** Antineutrino fluxes at the Far Detector as a function of energy in the absence of oscillations with the horns focusing negative particles. In addition to the dominant  $\nu_\mu$  flux, the minor components are also shown. Note the logarithmic scale.

essential part of the Target Hall design, and remote-handling procedures involving activated targets and horns are being developed.

After collection and focusing, the pions and kaons that did not initially decay – the residual particles mentioned above – need a long, unobstructed volume in which to do so. This decay volume in the LBNE reference design is an air-filled pipe of circular cross section, oriented toward the Far Detector. Its diameter and length are optimized to allow decays of pions and kaons such that they produce neutrinos in the useful energy range. In general, a longer pipe allows for the decays of higher-energy particles. These occur naturally at smaller production angles and are thus distributed close to the beam axis. Therefore longer pipes with smaller diameters are desirable for higher-energy beams. Lower-energy pions and kaons are not as well collimated and hence require a larger-diameter pipe. The two extrema in energy, as required by the physics measurements, provide the basis for optimization of the decay pipe geometry. The reference design calls for a 203.7 m long decay pipe of diameter 4 m; this represents an acceptable balance between obtaining the desired neutrino energies and cost. See Figure 1-7.

A considerable fraction of beam power, 23%, is deposited within the decay region. This heat energy will be removed by air convection with a system of blowers and heat exchangers. An alternative design under study would fill the main volume of the decay pipe with helium. The beam power deposited in the decay region implies creation of radioisotopes within the walls surrounding the pipe, requiring shielding and sealing from the surrounding ground water. The reference design uses a minimum of 5.5 m of concrete between the pipe and the native rock or soil (engineered fill or glacial till).

The roughly 15% of protons that do not interact with the target, along with the residual pions and kaons, must be absorbed to prevent them from inducing radioactivity in the surrounding rock or soil. This is accomplished with a specially designed aluminum and steel pile, called the *absorber*, that transforms the beam's kinetic energy into heat, thus protecting the rock or soil from beam-activated nuclides. The absorber occupies an excavated enclosure at the end of the decay pipe. The neutrino beam specifications are listed in Table 1-5.

#### 1.2.4 System Integration

Integration of installation plans and procedures across the Beamline sub-project is an essential task given the complexity and interconnectedness of the beam systems. The System Integration group is responsible for a variety of control, monitoring, alignment and other elements that must ensure safe and proper operation of the beam. Control systems, in particular, will be built specifically for the LBNE Beamline, but will be based on and must integrate into Fermilab's present accelerator-controls system. Chapter 4 is dedicated to System Integration.

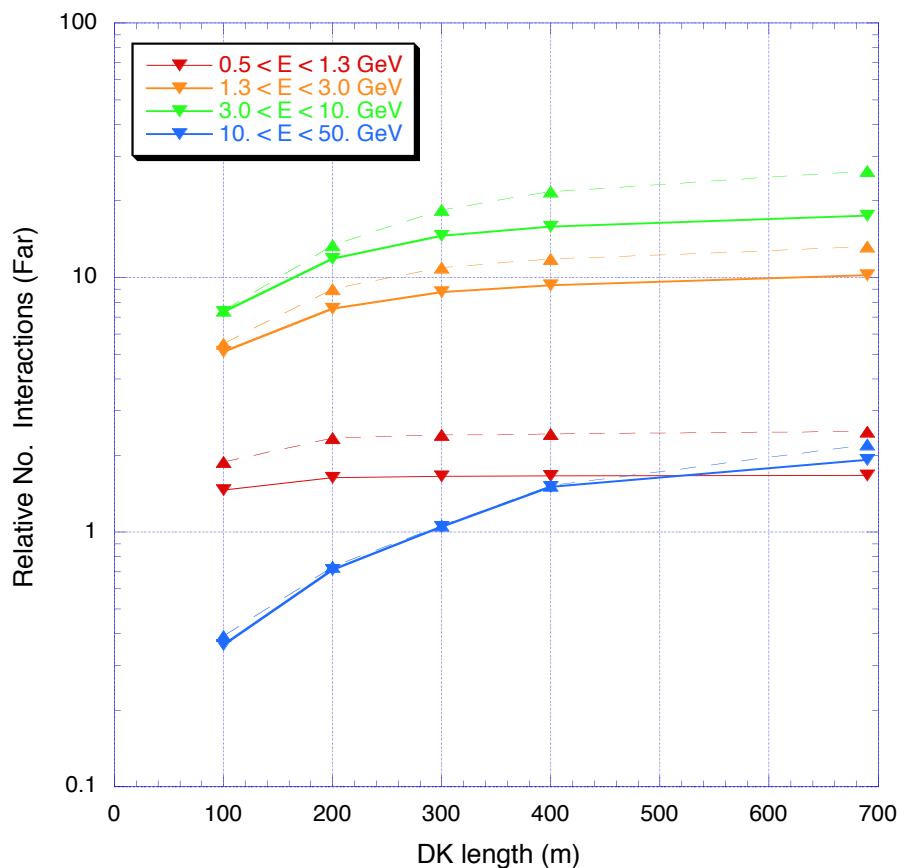


**Figure 1-7:** The number of neutrino interactions in the Far Detector depends on the length and diameter of the decay pipe. Here, the number of events is plotted as a function of length, with two curves for each colored energy range: solid is for a diameter of 2 m and dashed is for a diameter of 4 m. The reference design is a pipe 4 m in diameter and 203.7 m long.

**Table 1–5:** This table presents partial set of the relevant parameters for the elements of the reference design. Other important details such horn shapes are found in the subsystem sections herein. The third column lists the range of a parameter that has been studied for both physics or engineering considerations.

Element	Parameter	Range	Reference design value
Target	material	graphite, Be	graphite
	transverse size	5 to 16 mm	6.4 mm
	length	2 interaction lengths	951 mm
Focusing Horn 1	length	2500 to 3500 mm	3360 mm
	current	180 to 300 kA	200 kA
Focusing Horn 2	length	3000 to 4000 mm	3630 mm
	current	180 to 300 kA	200 kA
	dist. from Horn 1 (front)	6000 to 8000 mm	6600 mm
Decay Pipe	length	200 to 250 m	203.7 m
	radius	1.0 to 3.0 m	2 m
	atmosphere	Air, He, vacuum	air STP

### 1.2.5 Near Site Conventional Facilities

The Near Site Conventional Facilities not only provide the support buildings for the underground facilities, but also provide the infrastructure to direct the beamline from the below-grade extraction point to the above-grade target. The layout is shown in Figure 1–8. Following the beam from east to west, or from right to left in this figure, is the underground Primary Beamline Extraction Enclosure, the in-the-berm Primary Beamline Enclosure and its accompanying surface based Service Building (LBNE 5), the in-the-berm Target Complex (LBNE 20), the Decay Pipe and the underground Absorber Hall and its surface Service Building (LBNE 30). The Project limits are bounded by Giese Road to the north, Kautz Road to the east, Main Injector Road to the south, and Kirk Road to the west.

These facilities are described in detail in Volume 5 of this CDR.

Following is a list of references to text about conventional-facilities design choices in LBNE CDR Volume 5: *Facilities at the Near Site* that relates to the the following Beamline L2 Project elements. (All elements are also addressed in Volume 5 Section 1.2.)

- Primary beam enclosures: Section 5.1
- Service buildings LBNE 5, LBNE 20, LBNE 30: Sections 4.1, 4.2 and 4.3
- Target Hall target chase: Section 4.2



**Figure 1–8:** LBNE Overall Project Layout at Fermilab

- Target Hall support rooms: Section 4.2
- Near-surface storage and morgue: Section 4.2
- Decay pipe: Section 5.2
- Absorber Hall: Section 5.3

### 1.3 Participants

The conceptual design for the LBNE Beamline has been carried out by an LBNE L2 Project team, managed at Fermilab and to date made up entirely of physicists, engineers, designers and technicians from Fermilab. In addition, several contracts with other institutions and consultants have been completed for conceptual design work on particular beamline systems or components:

- Argonne National Laboratory (MOU, target)
- Brookhaven National Laboratory (MOU, target)
- Institute of High Energy Physics, Protvino, Russia (Accord, target)

- Oak Ridge National Laboratory (contract, remote handling)
- Rutherford Appleton Laboratory (Accord, target)
- Bartoszek Engineering (contract, Horn support structures)

The Beamline management coordinates the design activities of the consultants to assure that the efforts remain on track. The beamline is planned for construction at the Fermilab site, which is managed by the Fermi Research Alliance (FRA).

The LBNE Beamline effort is managed by the Work Breakdown Structure (WBS) Level 2 Manager for the Beamline Project. The supporting team includes a WBS Level 3 Manager for the Beamline's two principal systems, Primary Beam and Neutrino Beam, as well as for System Integration. WBS Level 4 Managers manage the design of the components in these beamline systems and the interfaces between them. Figure 1-9 shows an organization chart down to Level 4 (L4).

Assisting and advising the Beamline L2 Project are an ES&H Coordinator, two Radiation Physicists and a Project Controls specialist.

Interaction amongst the Beamline team, and between this team and the design consultants as well as the LBNE Near Site design team, has been done via weekly meetings, periodic design interface workshops, and electronic mail.

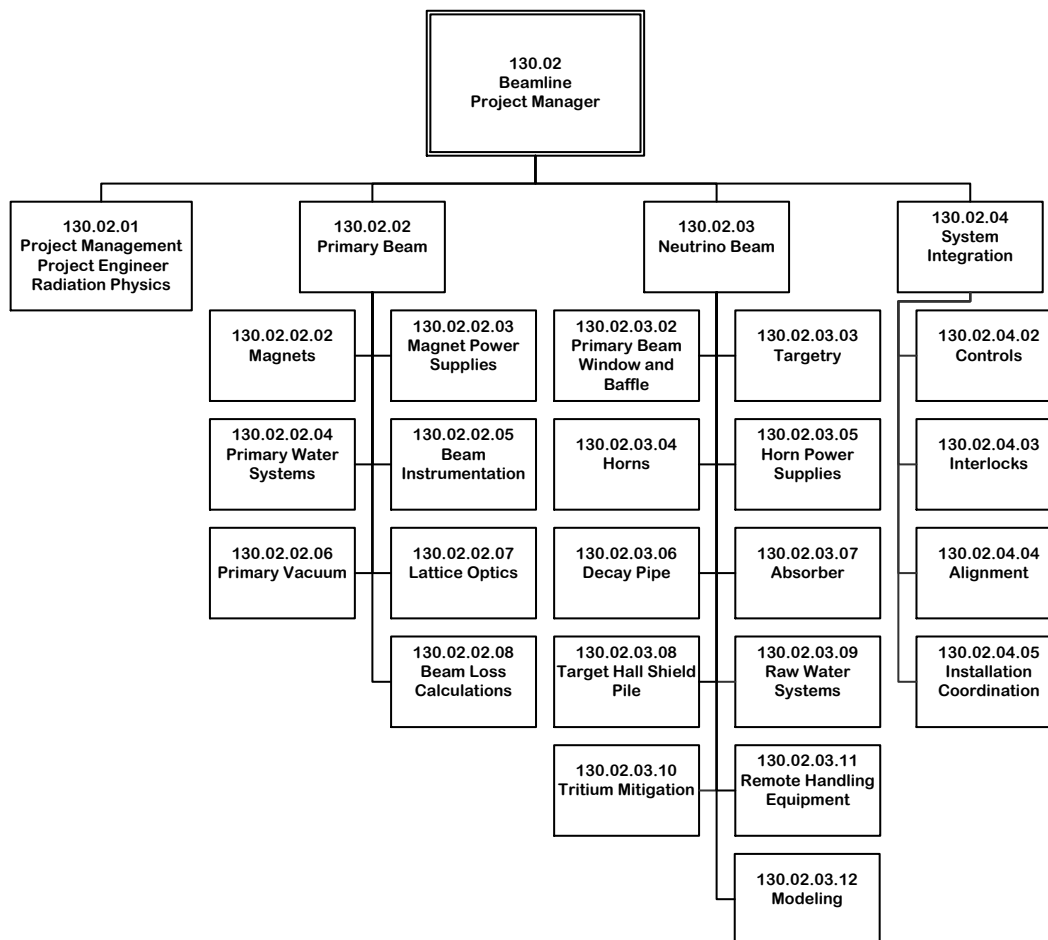


**Figure 1-9:** Organization chart for the Beamline L2 Project (to WBS Level 4)

## 2 Primary Beam (WBS 130.02.02)

### 2.1 Introduction

This chapter describes the reference design for the LBNE primary (proton) beamline. This system will extract protons from Fermilab’s Main Injector (MI) synchrotron, using a single-turn extraction method, and transport them to the target in the LBNE Target Hall. The nominal range of operation will be from 60 to 120 GeV.

The principal components of the primary beamline include specialized magnets at the MI-10 extraction point to capture all of the protons in the synchrotron and redirect them to the LBNE beamline: a series of dipole and quadrupole magnets to transport the proton beam to the target, power supplies for all the magnets, a cooling system, beamline instrumentation and a beam-vacuum system for the beam tube.

All of the LBNE primary-beam technical systems are being designed to support sustained, robust and precision beam operation. Careful lattice optics design (described in Section 2.5) and detailed beam-loss calculations (described in Section 2.11) are essential for the proper operation of the primary-beam system, as are a detailed understanding and monitoring of component alignment and development of the comprehensive beam-permit and control systems, described in Chapter 4.

### 2.2 Reference Design Overview

The LBNE primary beamline is extracted using single-turn, or “fast” extraction, in which all the protons accelerated in the MI synchrotron ring will be diverted to the LBNE beamline within one revolution after each acceleration cycle. The train of bunches of protons in the MI extends most of the way around the ring. After extraction, the beam is controlled by a series of dipole (bending) and quadrupole (focusing) magnets collectively called the “lattice optics.” This term refers to the overall design of the system, i.e., the magnet types, strengths, order, relative placement and other characteristics. The LBNE primary-beamline lattice optics is

designed to direct the beam toward the target and the downstream Far Detector, with a spot size appropriate for maximizing the physics potential of LBNE.

LBNE will implement a modular optics design comprised of three distinct lattice configurations in series: the specialized MI-to-LBNE matching section, the transport section and the final focus of the beam on the production target.

After the kicker magnets in the MI apply a horizontal kick to the beam, the beam passes through a set of three specialized magnets, called Lambertsons, that vertically extract the beam from the MI. The Lambertsons sit in the path of the beam, both when it circulates and when it is extracted, so they must accommodate both paths. The circulating beam passes through a field-free hole in the magnet yoke, and the extracted beam instead passes through the (separate) magnet aperture and is thus bent away (upward) from the MI trajectory. Each Lambertson in the line bends the beam more, such that after passing through all three (and one focusing quadrupole, a component of the MI lattice that sits between the first and second Lambertsons), the extracted beam is sufficiently separated from the MI orbit to pass through the first bending magnet external to the MI, a C-magnet. The C magnet barely clears the MI beam tube downstream of the third Lambertson and provides an additional upward bend, enough so that the extracted beam can pass above the outside of the next quadrupole in the MI lattice. The C-magnet is the last element of the specialized extraction channel.

The transport section includes a series of rolled dipole magnets (tilted about the beam axis to vary the direction of bend) interspersed with quadrupole magnets regularly spaced to ensure that beam size does not exceed that in the MI. The first dipole bends the beam horizontally further from the MI and reduces the rate of vertical rise. Several quadrupoles maintain the beam size as the beam tube passes through the wall between the MI tunnel and the LBNE primary-beam enclosure. The beam is then bent to the right and up, and back down from the apex at an angle of 101 milliradians ( $5.79^\circ$ ) toward the target, thus establishing the needed trajectory for the neutrino beam.

In the last section of the primary beamline, the beam size and its angular spread are tailored to the desired distribution for hitting the production target. This is accomplished by a set of eight quadrupoles in the final-focus section, which can be tuned to produce a wide range of beam spot sizes while maintaining a narrow angular spread.

Some magnets will be grouped into a single “magnet loop” and powered by a single power supply, whereas others will be powered individually, according to the lattice optics design. In order to maintain the lowest possible power consumption, all of the larger magnet loops will be ramped. A primary water system will feed cooling water to the magnets and power supplies. Beam instrumentation will characterize and monitor important beam parameters, for example, beam positions, stability, losses, intensity and transverse emittance. A vacuum system will maintain a vacuum of better than  $1 \times 10^{-7}$  torr residual gas pressure in the beam tube in order to reduce the beam loss due to proton-gas interaction.

## 2.3 Design Considerations

### 2.3.1 Length and Elevation

As discussed in the Alternatives Analysis document [5], primary-beam extraction at both MI-10 and MI-60 were considered, both for shallow and deep configurations, and the “MI-10 Shallow” design was selected after a thorough value-engineering process. It offers several advantages over the other designs, in particular over the “MI-60 Deep” design, its nearest competitor.

The shallow beam design offers a significant cost savings for the neutrino beam facility, plus significant advantages with tritium mitigation for the near-grade Target Hall. Also, given the limited available site footprint, a deep Target Hall, as exists for NuMI/ NOvA, would require the primary-beam transport to be considerably longer to reach the depth at which sufficient structural rock cover exists above the hall. This added distance is neither necessary nor available with MI-10 extraction for a 120-GeV beam.

The target elevation of 750 feet, a few feet above natural grade elevation, is chosen to optimize overall facility-construction technical and resource requirements [6]. The target elevation at 750 feet was selected as the best balance between minimizing Absorber Hall depth in the rock and the extent of the primary beam transport line above natural grade level. Additional constraints include limiting the maximum primary-beam enclosure elevation angles to 150 milliradians, and achieving the required trajectory for transport of the neutrino beam to the Far Detector site. A profile-view schematic of the target lineup for the primary-beam transport with Target Hall and decay region is shown in Figure 2-1. Colors in the figure illustrate the height of earth fill needed, including shielding for the primary-beam enclosure, along with the location of the Target Hall and decay region with respect to the underlying glacial till and rock strata.

The design requires support for the beam-enclosure regions above natural grade elevation. The addition of deep foundations to the underlying rock has been included in the facility design to ensure position stability of the technical components.

### 2.3.2 Existing Infrastructure and Shielding

The choice of a shallow beam extracted at MI-10 avoids beam crossings, which extraction at MI-60 would not, and it allows for a simpler extraction enclosure, enabling a cost-effective facility design of the entire extraction region. It interferes minimally with existing beam systems in this region, eliminates the need for small-aperture dipoles of the existing MI-60 extraction for the NuMI beam, and also provides some shielding separation from accelerator-tunnel beam losses at the beginning of the LBNE primary-beam transport enclosure. The

MI-10 primary-beam layout on the Fermilab site is shown in Figure 2-1.

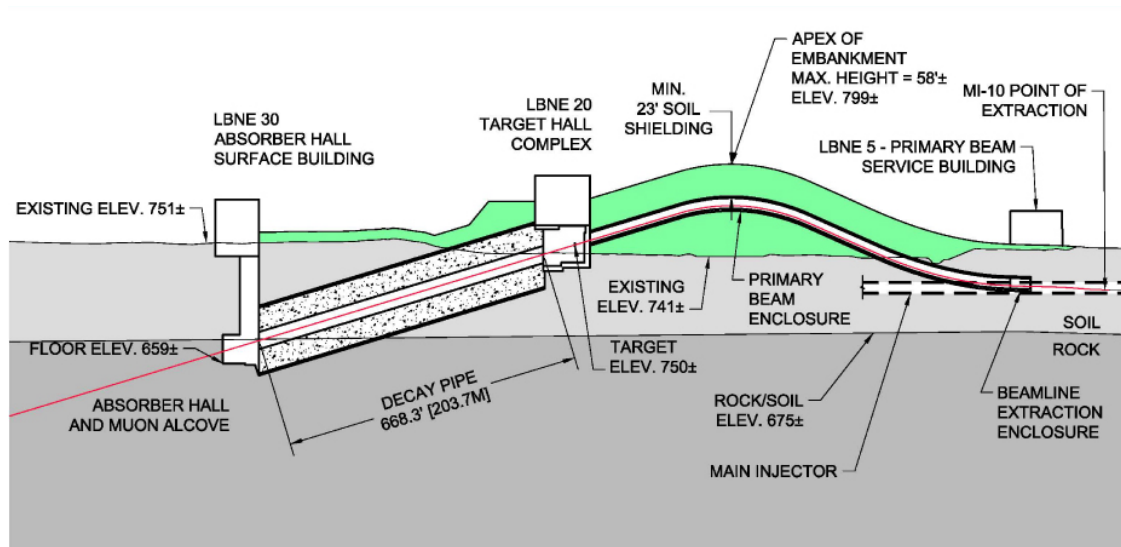


**Figure 2-1:** Elevation view showing the concept of elevating the beamline, thereby minimizing the amount of deep excavation and tunnels. The beam comes from the right through the primary beam enclosure and interacts at target within the Target Hall Complex. The green shaded part indicates fill used to elevate the beam.

### 2.3.3 Beam Energy and Intensity

The primary-beam energy that optimizes the physics of LBNE is an important aspect still under study. An energy lower than 120 GeV is preferable as long as the beam power is not compromised. The MI accelerates protons within a range of energies from injection energy (8 GeV) to 120 GeV and thus can transport protons anywhere in this range. However at lower energies, particularly under 60 GeV, acceleration-cycle times limit the number of protons per hour, and hence average power. Therefore energy less than 60 GeV is not currently being considered.

The expected beam intensity for a proton energy of 120 GeV (60 GeV) is  $4.9 \times 10^{13}$  ( $4.5 \times 10^{13}$ ) protons per pulse. At 120 GeV (60 GeV), the cycle time between pulses is 1.33 s (0.80 s), giving a proton-beam power of 708 kW (545 kW).

The calculated beam power as a function of beam energy [7] is shown in Figure 2-2 using assumptions outlined in the discussion of efficiency, above.

At this very high beam intensity, primary-beam control requirements must be stringent since only a few pulses of mis-steered beam will severely damage technical components. Residual activation of components must also be rigorously limited since, for example, replacing a multi-ton magnet on the steep enclosure slopes would require many hours of close-in work around

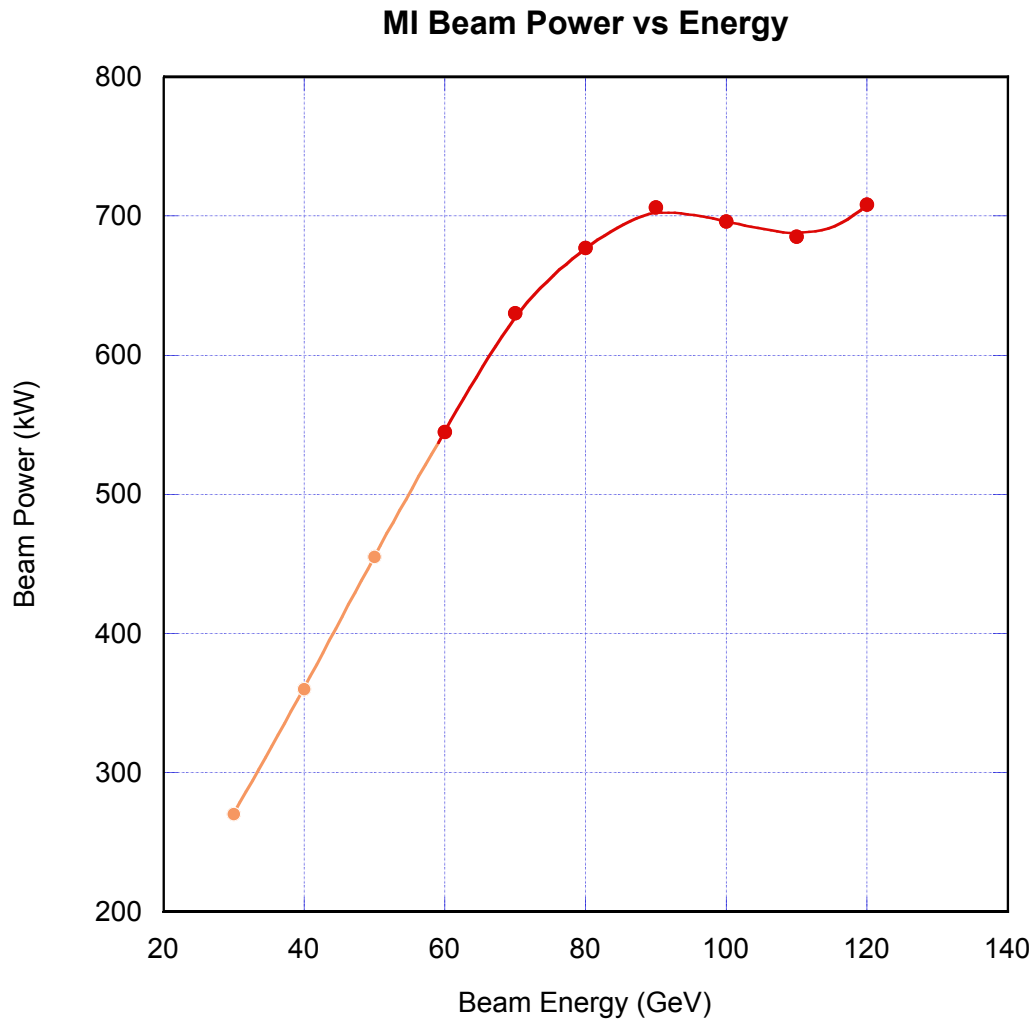


**Figure 2–2:** The Main Injector beam power as a function of beam energy. The decline of power at lower energies is typical of synchrotrons: all beam is injected into the machine at once at low energy and the acceleration time per GeV is fixed. The cycle rate in the Booster can be increased to 15Hz to compensate down to 90 GeV, but below  $\sim 70$  GeV the recycler ring limits the cycle time. The energy region of interest for LBNE is shown by the red line.

the components. Severe limits on proton-beam transport loss will be imposed, requiring normal fractional beam loss of less than a few parts per million. The primary beam design is fully compatible with operations at higher beam power, up to 2.3 MW.

### 2.3.4 Beam Control

Techniques, hardware and control applications for accomplishing primary-beam control at the required level were developed for the NuMI 400-kW proton beam. These features have been demonstrated to perform very well during the six years of NuMI beam operation and are therefore being used in the design for the LBNE primary beam. Included are:

- A comprehensive beam-permit system (described in Section 4.2) with more than 250 parameters that are to be verified prior to each beam extraction
- Open-extraction channel and primary-transport magnet apertures capable of accepting a range of extracted beam energies
- Primary-extraction channel and LBNE beam-transport component apertures sized to accept a beam envelope larger than the MI dynamic aperture of  $360 \pi$  mm-mrad, without beam loss
- Excellent magnetic-field uniformity to match the beam-envelope apertures
- Major power-supply regulation to a few parts per million to achieve good beam-transport stability
- A strong focusing-beam optics design, with excellent control of beam size and dispersion
- Fully automated beam-position control, with no manual adjustment of beam positions required during operation
- Robust beam instrumentation to enable maintenance of beam-targeting accuracy to approximately  $100 \mu\text{m}$

### 2.3.5 Estimation of Protons on Target

The goal for accumulating 120-GeV protons at the neutrino target with beam power of 708 kW is  $6.5 \times 10^{20}$  protons-on-target (POT) per year. This assumes 12 Booster batches with a per-batch intensity of  $4.3 \times 10^{12}$ . Given an MI throughput of 0.95, this results in  $4.9 \times 10^{13}$  protons per MI cycle (1.333 sec). The up-time includes the total expected efficiency of the accelerator complex as well as scheduled maintenance.

The total accelerator operational efficiency is the product of efficiencies of the Proton Source, Linac, Booster and MI. The product of the first three stages (Source, Linac and Booster) has historical average efficiency of 0.87 [8]. The number of protons delivered from the MI to NuMI has been limited by delivery to other programs (anti-protons source for collider operations and test beams). The up-time of the MI is very high, with efficiency of approximately 0.97. The annual scheduled maintenance, a facility shutdown, averaged 2.4 months (72 days) over the period FY2007-2010 (annual fraction of 0.8).

The estimated unscheduled down time, using data from the operation of NuMI, including power failures and downtime for chillers, dehumidifiers and tritium mitigation systems, is small; the efficiency is 0.97. Assuming that LBNE target and horn replacements take 30 days per year in addition to the facility shutdown, the LBNE “efficiency” due to component replacement is estimated to be 0.90. This efficiency takes into account two target replacements per year and one horn replacement where the target/horn replacement takes 2.5/3.5 weeks respectively including the cooldown period. It is assumed that one of the two target replacements will take place within the scheduled annual shutdown and that the horn replacement has 50% probability to take place within the scheduled shutdown. An additional 0.95 efficiency is assumed due to programmatic issues and very short downtimes (less than a few minutes). Thus, the total efficiency for LBNE is estimated to be approximately  $0.87 \times 0.97 \times 0.80 \times 0.97 \times 0.90 \times 0.95 = 0.56$ . It is also assumed this overall efficiency can be maintained over a ten-year period, from beam startup to completion of the oscillation physics goals.

The total expected POT per year, given above, is thus the product of the total efficiency (0.56), the number of protons per second ( $3.68 \times 10^{13}$ ) and the number seconds in a (perfect) year ( $3.15 \times 10^7$ ) [8].

The reliable delivery of a 708-kW beam to the target should be aided greatly by the operation of NOvA, which will use the same accelerator sequence as LBNE, except for the final beam transport to the target. Therefore, the primary risk in beam delivery to the target can be isolated to the final primary-beam section built for LBNE. The reliability of very low-loss transport through the LBNE section will be enhanced by state-of-the-art beam monitors and an active control-feedback system. With deliberate beam commissioning and start-up, the efficiency in the LBNE primary beam should be very high. The corresponding operating efficiency for the NuMI primary beam over a six-year period has been greater than 0.99.

## 2.4 Principal Design Elements and Parameters

The principal design elements and parameters of the Primary Beamline reference design include:

- Single-turn extraction of primary beam at MI-10 and an extraction rate of  $4.9 \times 10^{13}$  protons per MI cycle (120 GeV)
- Beam transport to target in the Target Hall exiting the MI-10 enclosure via an evacuated pipe heading west-northwest toward the Far Detector at SURF in Lead, S.D., followed by a vertical bend upward, to a final downward pitch of  $5.79^\circ$
- Construction of earthen embankment approximately 950 ft long and of peak height 58 ft acting as support and shielding
- Shielding for radiological protection, for all possible accidental beam losses and for long-term residual beam exposure

The general primary-beam specifications are listed in Table 1-3.

## 2.5 Lattice Optics (WBS 130.02.02.07)

### 2.5.1 Introduction

LBNE will implement a modular optics design comprised of three sections in series: MI extraction with a specialized MI-to-LBNE matching section, the transport section and the final focus of the beam near the production target.

A series of five fast-pulsed magnets in the MI ring, called kickers (Section 2.6.3.6), extract the beam. The kicker magnets have a fast ramp-up to the required current followed by a ramp-down; the ramps occur during gaps in the circulating MI beam. The kickers are followed by the set of three Lambertson magnets that bend the extracted beam away further (upward) from the MI trajectory. To match the MI optics to the optics of the transport section, a string of individually controlled quadrupole and dipole magnets is used.

The transport section steers the beam from extraction/matching section up to and over the hill toward the Target Hall. The matching section is followed by an optical lattice consisting of a series of six periodic focusing units, “FODO” cells, which terminates 119 m upstream of the target. A set of eight independently tunable quadrupoles form the achromatic final-focus (FF) optics to obtain the desired beam size on the target. This final focus is tunable to produce a spot-size ( $\sigma$ ) from 1.00 to 4.00 mm over the entire momentum range 60 to 120 GeV/ $c$ .

## 2.5.2 Design Considerations

The design of the lattice for LBNE, as detailed in the next section, is constrained by the experimental needs, civil construction requirements and operational factors in transporting an intense beam over long periods of time. These include:

- large changes in elevation in order to keep the Target Hall above grade
- extraction and transport over a range of beam momenta (60 to 120 GeV/ $c$ )
- beam position and focus at target which is finely adjustable
- transport of beam with very low average losses

These constraints drive most of the fundamental aspects of the technical design. The optics presented here were computed using Methodical Accelerator Design (MAD) [9] and the design reflects the large amount of experience of the designers.

## 2.5.3 Reference Design

Protons are extracted from the MI-10 straight section. The extraction magnets are of the standard MI design with five kicker modules at the upstream end of the MI-10 straight section to kick the beam horizontally into three vertically-bending Lambertsons plus a C-magnet straddling the MI quad Q102 located 90° in betatron phase downstream; see Figure 2-3.

A single, rolled, long (6 m) MI-style IDA/IDB dipole (Section 2.6.3.1) steers the beam horizontally towards the MI enclosure wall between MI quads Q105 and Q106, while leveling the beam off somewhat to a gentle vertical slope of +0.60°, thereby bisecting the space separating the MI and Recycler Ring magnets. A 15.6-m-long carrier pipe transports the beam through the MI tunnel wall into the new primary beam extraction enclosure that houses the main body of the line.

From that point the protons are transported a further 257.9 m to the target, located 10 ft above grade (750 ft above sea level) and aimed towards the Far Detector. In the main body of the beamline, 12 IDA/IDB dipoles plus 12 short (4-m) MI-style IDC/IDD dipoles together bend the beam  $-7.180^\circ$  horizontally and  $-5.789^\circ$  net vertically. Bends are grouped into twelve 4 + 6 meter pairs. The first three cells accomplish the horizontal alignment to the Far Detector while generating a +143-mrad vertical trajectory. This upwards trajectory continues through the subsequent empty FODO cell, reaching maximum beam elevation 30 ft above grade. This is followed by three full cells that create the 244 mrad of downward bend necessary to obtain the final  $-101$  mrad trajectory to the Far Detector.

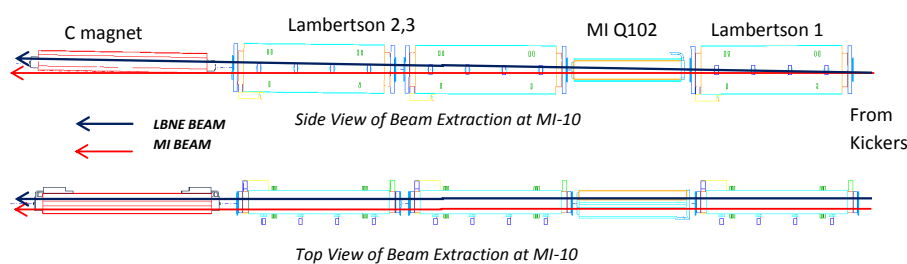


**Figure 2-3:** Configuration of the LBNE extraction Lambertsons and C-magnet straddling MI quad Q102

Optical properties are defined by 21 quadrupoles (grouped as 20 focusing centers) of the proven MI-beamline-style 3Q60/3Q120 series (Sections 2.6.3.4 and 2.6.3.5). All focusing centers are equipped with redesigned MI-style IDS orbit correctors (Section 2.6.3.5) and dual-plane beam-position monitors (BPMs) (Section 2.9). Ample space is available in each cell to accommodate ion pumps and diagnostic instrumentation. Parameters for the main magnets are listed in Table 2-4.

### 2.5.3.1 Optics

This 60-120 GeV/c transfer line design is comprised of distinct optical modules, as illustrated in Figure 2-5: extraction/matching section, transport section and a widely tunable quadrupole triplet module to control beam size on target.

The first six quadrupoles in the beamline are powered individually to perform the optical match between lattice functions of the MI and those of the LBNE transfer line (the roll angles of dipoles in the first three half-cells are selected specifically to contribute to the dispersion matching of  $(\eta_x, \eta'_x)$  and  $(\eta_y, \eta'_y)$ ). This matching section is followed by six 120° FODO half-cells characterized by quadrupoles Q208 through Q213. Cell length and phase advance are chosen such that beam size does not exceed that of the MI 90° lattice cell structure, while also optimizing efficient use of space for the achromatic insertions. Dispersion generated by variations in the beam trajectory are corrected locally and can not bleed out to corrupt the optics elsewhere in the line. Quadrupoles Q214 through Q221 form the tunable final-focus optics capable of producing a spot-size of  $\sigma = 1.00$  to 4.00 mm over the entire momentum range 60 to 120 GeV/c.

Magnet apertures (including the impact of rolls) and beam envelopes are shown in Figure 2-6. One contour corresponds to nominal MI beam parameters of  $\epsilon = 30\pi \mu\text{m}$  (99%, normalized) and  $\Delta p_{99}/p = 11. \times 10^{-4}$ . The larger envelope shown is calculated for  $\epsilon = 360\pi \mu\text{m}$  (100%, normalized) and  $\Delta p_{100}/p = 28. \times 10^{-4}$ . The latter values reflect the admittance of the MI at

DIPOLE TYPE (#)	L (m)	B (T)	TILT (deg)		QUAD NAME (#)	TYPE	L (m)	G (T/m)
<b>MI-10 EXTRACTION → LBNE</b>								
LAM1	2.8000	0.53242	-90.000		Q102	3Q84	2.1336	+16.16016
LAM12 (2)	2.8000	1.00000	-90.000					
V100	3.3528	1.00284	-90.000					
<b>MATCH FROM MI → LBNE FODO LATTICE &amp; 143 mr UP BEND</b>								
					Q201→202 (2)	3Q60	1.524	-11.13509
IDA/B	6.09981	1.22335	+62.844		Q203	3Q120	3.048	+12.48756
					Q204	3Q120	3.048	-9.18907
					Q205	3Q120	3.048	+13.06221
IDC	4.06654	1.38347	-44.126					
IDB	6.09981	1.38347	-44.126					
					Q206	3Q120	3.048	-13.52413
IDA	6.09981	1.10813	-44.126					
IDD	4.06654	1.10813	-44.126					
					Q207	3Q120	3.048	+16.16931
IDC	4.06654	1.10813	-48.179					
IDB	6.09981	1.10813	-48.179					
<b>FODO CELLS</b>								
					Q208	3Q120	3.048	-15.83240
IDA	6.09981	1.10813	-48.179					
IDD	4.06654	1.10813	-48.179					
					Q209	3Q120	3.048	+15.83240
IDC	4.06654	1.00297	-56.109					
IDB	6.09981	1.00297	-56.109					
					Q210	3Q120	3.048	-15.83240
IDA	6.09981	1.00297	-56.109					
IDD	4.06654	1.00297	-56.109					
					Q211→213 (3)	3Q120	3.048	+15.83240
<b>244 mr ACHROMATIC DOWN BEND &amp; FINAL FOCUS ON TARGET</b>								
IDC	4.06654	1.60431	+90.000					
IDB	6.09981	1.60431	+90.000					
					Q214	3Q120	3.048	-13.96520
IDA	6.09981	1.60431	+90.000					
IDD	4.06654	1.60431	+90.000					
					Q215	3Q120	3.048	+16.54570
IDC	4.06654	1.60431	+90.000					
IDB	6.09981	1.60431	+90.000					
					Q216	3Q120	3.048	-15.26976
IDA	6.09981	1.60431	+90.000					
IDD	4.06654	1.60431	+90.000					
					Q217	3Q120	3.048	+13.81046
IDC/D	4.06654	1.60431	+90.000					
					Q218	3Q60	1.524	-17.08214
IDA/B	6.09981	1.60431	+90.000					
IDA/B	6.09981	1.60431	+90.000					
IDC/D	4.06654	1.60431	+90.000					
					Q219	3Q120	3.048	-10.53138
					Q220	3Q120	3.048	+15.80329
					Q221	3Q60	1.524	-13.39482

**Figure 2-4:** Magnet parameters of the LBNE proton beamline at 120 GeV/c and  $\beta^*=86.328$  m.

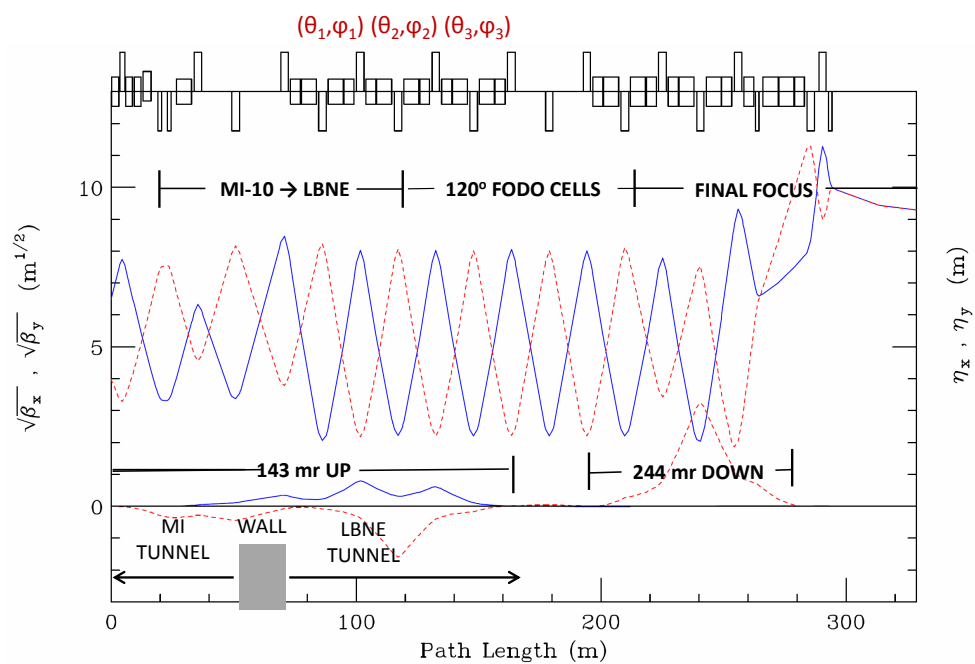


**Figure 2-5:** Horizontal (solid) and vertical (dashed) lattice functions of the LBNE transfer line. The final focus is tuned to produce a spot size of  $\sigma_x = \sigma_y = 1.50$  mm at 120 GeV/c and  $\epsilon = 30\pi$   $\mu\text{m}$  (99%, normalized).

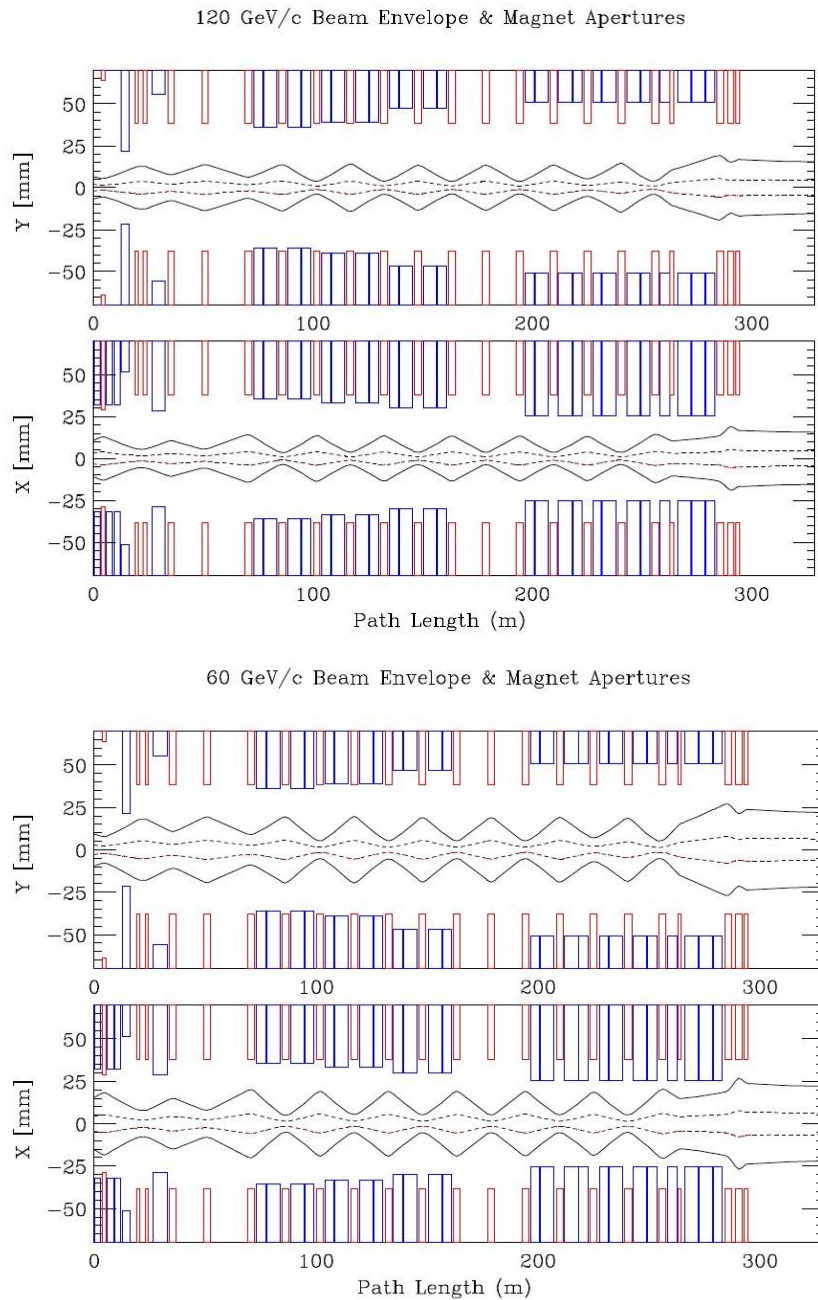


**Figure 2-6:** Magnet apertures and beam envelopes: The 99% contour (dashed) with nominal MI beam parameters, and the 100% envelope (solid) corresponding to the MI admittance at transition ( $\gamma t = 21.600$ ).

transition ( $\gamma t = 21.600$ ), and the transfer of such a beam to LBNE could only result from a catastrophic failure of the MI and LBNE safety and regulatory systems. The maximum transverse emittance of  $360\pi \mu\text{m}$  is determined by the restricted horizontal aperture in the Lambertson magnets seen by the circulating MI beam. The momentum spread is the maximum value that can be contained in a radio frequency bucket through acceleration. The  $\epsilon = 360\pi \mu\text{m}$  and  $\Delta p_{100}/p = 28. \times 10^{-4}$  envelopes, therefore, demonstrate that the LBNE primary beamline should be able to transport without losses the worst quality beam that the MI could transmit.

### 2.5.3.2 Sensitivity to Gradient Errors

It is assumed that the optical integrity of the primary beamline will not be compromised by magnet-to-magnet variations in the integrated quadrupole fields. Experience with the MI-style 3Q120 magnets has shown that these magnets are very high quality, with a spread in gradient errors on the order of  $\sigma(\Delta G/G) \sim 0.08\%$  or less [10]. Such a narrow error distribution cannot appreciably impact the beam characteristics or transport capabilities. Implementing even the most rudimentary strategy for sorting production quadrupoles, such as selecting those from the middle of the distribution for installation in the FODO cells, will reduce the spread even further. For nominal beam parameters at 120 GeV/c, a simple thin-lens calculation predicts that the largest error-wave expected in the 99% beam envelope ( $\pm 3.89$  mm nominal at  $\beta = 64.5$  m) would be less than 75 microns.

### 2.5.3.3 Beam Size at Target

An essential design requirement of the final focusing section is the ability to tune the spot size  $\sigma$  over a wide range. The optimum spot size is thought to fall in the range  $\sigma \sim 1.3$ -2.0 mm, which would grow to  $\sim 2.5$ -3.0 mm for a 2.3-MW upgrade. Spot size is still an evolving parameter. Ultimately, the choice will be driven to a large extent by details of the final target design, but other factors must also be considered. In addition to the 40% difference in beam size between 60 and 120 GeV/c, under real operational conditions the beam parameters ( $\epsilon, \Delta p/p$ ) will certainly be different from the ideal nominal values assumed here. Currently, the MI 99% normalized emittance at 120 GeV/c is  $\sim 20\pi \mu\text{m}$ , but it is not clear how this value might change in the future. It is essential that the FF design be sufficiently robust and versatile to anticipate these possibilities.

Figure 2-7 illustrates the wide tuning range of the FF. In principle, spot-size can be tuned to a maximum of  $\sigma^* = 4.00$  mm before magnet powering limitations take over. In practice, though, the maximum attainable  $\sigma^*$  is  $\sim 3.20$  mm. This limit is imposed by the restricted horizontal aperture (1.90 in) seen by the beam in the last 4-m vertical dipole. Results are shown for the two extremes of operational requirements. Calculations were performed assuming nominal beam parameters but the plot demonstrates that the FF is clearly adaptable

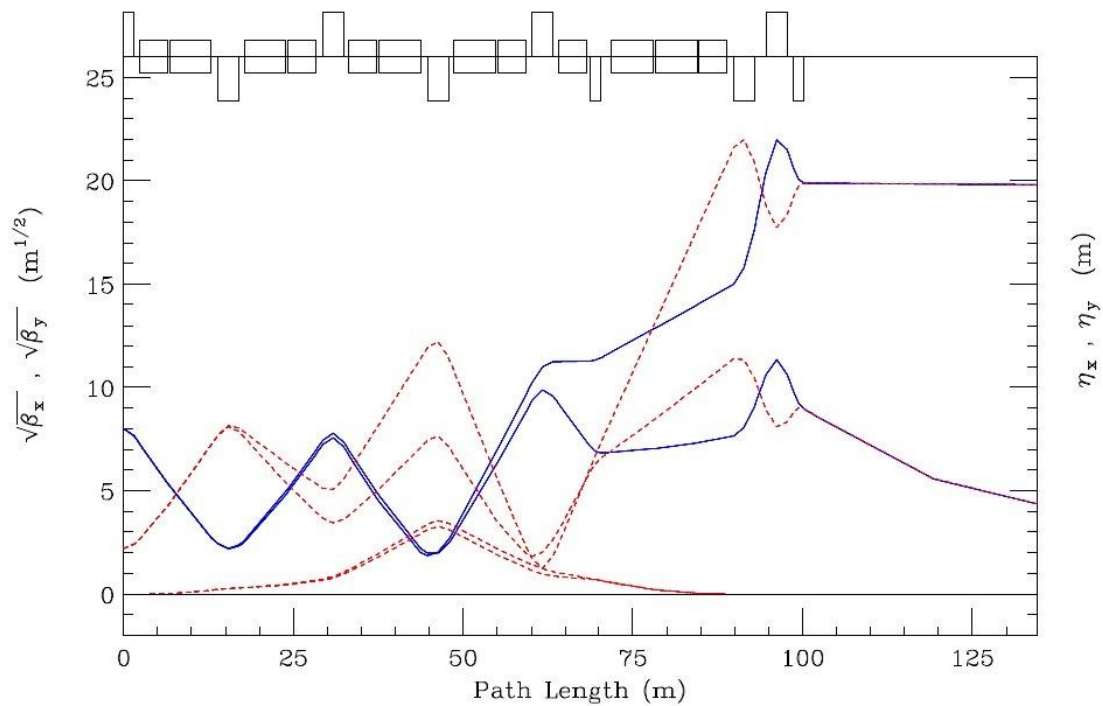


**Figure 2-7:** Tuning range of the Final Focus: The two examples assume nominal MI beam parameters. These extremes correspond to 60 GeV/c with  $\sigma^* = 1.0$  mm;  $\beta^* = 19.184$  m and  $\beta_{max} = 104$  m (lower), and at 120 GeV/c and  $\sigma^* = 3.20$  mm;  $\beta^* = 393$  m and  $\beta_{max} = 483$  m (upper). Vertical dispersion, shown across the bottom, rises from zero at the entrance to the dipole string, reaches a maximum of  $\eta_y \approx 3$  m, and is completely corrected to  $(\eta_y, \eta_{y'}) = (0,0)$  by the end of the bends.

			$\sigma = 1.00\text{mm @ } 60 \text{ GeV/c}$ $\beta^* = 19.184 \text{ m}$	$\sigma = 3.20\text{mm @ } 120 \text{ GeV/c}$ $\beta^* = 392.89 \text{ m}$
QUAD	TYPE	L (m)	G (T/m)	G (T/m)
Q214	3Q120	3.048	-6.97624	-12.01223
Q215	3Q120	3.048	+8.40581	+17.38185
Q216	3Q120	3.048	-7.64787	-14.48899
Q217	3Q120	3.048	+7.03514	+7.68385
Q218	3Q60	1.524	-8.56034	-3.99561
Q219	3Q120	3.048	-6.66201	-11.74485
Q220	3Q120	3.048	+10.76572	+15.68461
Q221	3Q60	1.524	-10.11021	-12.62987

**Figure 2-8:** Final Focus gradients for the examples in Figure 2-7

to any reasonable set of beam parameters. To meet the two extremes of spot-size criteria considered here,  $\beta^*$  at the target must be continuously tunable over a range of  $\times 21 \mu\text{m}$ . The corresponding quadrupole gradients are listed in Figure 2-8. The advantages of a modular optics design are evident – variations in the extracted MI beam parameters can be accommodated solely within the FF and do not involve tuning adjustments elsewhere in the line.

#### 2.5.3.4 Trajectory Correction

Trajectory correction is an issue which, of course, must be addressed in the design of any transfer line, but for the ultra-clean transport requirements of LBNE it is critical that precise position control be available throughout the primary beamline.

Correction of central trajectory errors have been simulated for dipole field errors and random misalignments assigned to all beamline elements (including BPMs). Realistic error values are on the order of  $\sigma(\Delta x, \Delta y) = 0.25 \text{ mm}$ , and  $\sigma(\psi_{roll}) = 0.50 \text{ mrad}$  [11]. Figure 2-9 shows the trajectory deviations resulting from randomly generated Gaussian error distributions (dashed). After correction using the LBNE trim dipoles the new orbits are also shown (solid), emphasizing the dramatic reduction in offset errors. Results of the tracking are summarized in Figure 2-10. All corrector strengths are well within the  $250 \mu\text{rad}$  (60% of peak) design specification for the new IDS trims. That orbit deviations are approximately twice as large in the vertical plane reflects the fact that dipole bending is predominantly vertical throughout the line. Dipole angular errors generated by  $\Delta B/B = 10^{-3}$  are as significant as the contributions from quadrupole misalignment.

Beam position on the target is accurate to a few microns – far below the  $150\text{-}\mu\text{m}$  tolerance set by horn focusing. The worst angular error found is  $\sim 0.7 \mu\text{rad}$  which, 1,300 km away at the Far Detector, translates into  $\sim 3 \text{ ft}$  of position error, which is clearly negligible.

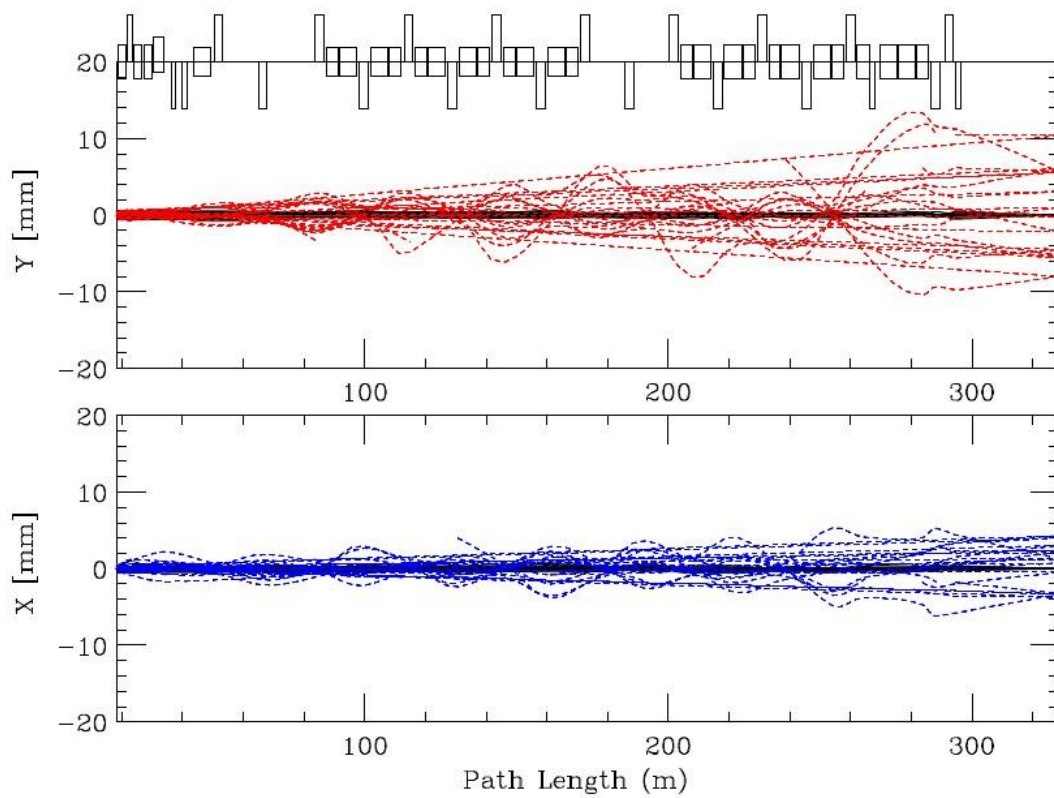


**Figure 2-9:** Uncorrected/corrected trajectories with random misalignments and dipole field errors; the plot begins at the upstream end of the first extraction Lambertson at MI-Q102

	ORBIT (mm)		CORRECTORS ( $\mu$ r)		ORBIT (mm)		CORRECTORS ( $\mu$ r)	
	$X_{\max}$	$X_{\text{RMS}}$	$\theta_{\max}$	$\theta_{\text{RMS}}$	$Y_{\max}$	$Y_{\text{RMS}}$	$\varphi_{\max}$	$\varphi_{\text{RMS}}$
<b>UNCORRECTED</b>	6.200	1.614	–	–	14.732	3.414	–	–
<b>CORRECTED</b>	0.996	0.285	110.670	26.653	1.101	0.281	114.430	37.901
<b>BEAM JITTER ON TARGET</b>								
	X ( $\mu$ m)		X' ( $\mu$ r)		Y ( $\mu$ m)		Y' ( $\mu$ r)	
	$X_{\max}$	$X_{\text{RMS}}$	$X'_{\max}$	$X'_{\text{RMS}}$	$Y_{\max}$	$Y_{\text{RMS}}$	$Y'_{\max}$	$Y'_{\text{RMS}}$
<b>CORRECTED</b>	1.079	0.400	0.694	0.230	0.437	0.139	0.330	0.110

**Figure 2–10:** Orbit offsets and corrector kicks for the trajectories in Figure 2–9

## 2.6 Magnets (WBS 130.02.02.02)

### 2.6.1 Introduction

This section discusses the magnets that will be used in the primary beamline to steer and focus the beam. The set of magnets includes five extraction kickers, three Lambertson magnets, one current septum C-magnet (the first magnet that is external to the MI ring), 25 main dipole magnets, 21 quadrupole magnets and 23 dipole corrector magnets for fine-tuning. From the extraction point, the lattice optics have to transport the primary beam to the target with the highest possible intensity. The magnet counts are summarized in Table 2-1.

### 2.6.2 Design Considerations

**Table 2-1:** Summary of primary-beam magnet specifications

Magnet	Common Name	Steel Length	Nom. Strength at 120 GeV	Count
RKB Kicker	NOvA extraction	~1.720 m	0.0237 T	5
ILA	MI Lambertson	2.800 m	0.532 / 1.000 T	3
ICA	MI C Magnet	3.353 m	1.003 T	1
IDA/IDB	MI Dipole 6 m	6.100 m	1.003 - 1.604 T	13
IDC/IDD	MI Dipole 4 m	4.067 m	1.003 - 1.604 T	12
QQB	3Q120 quadrupole	3.048 m	9.189 - 16.546 T/m	17
QQC	3Q60 quadrupole	1.524 m	11.135 - 17.082 T/m	4
IDS	LBNE trim dipoles	0.305 m	Up to 0.365 T	23

There are two technical considerations for the beamline magnets beyond providing the integrated dipole field and quadrupole gradient to establish the design lattice. First, the magnet apertures must be large enough to allow for an upgrade of beam power to 2.3 MW and alignment of the magnets should be sufficiently precise so as to not require any further enlargement due to the relative placement of the apertures. Secondly, the magnets must support rapid ramping of excitation. Beam only passes through the magnets for 10  $\mu$ s of spill time out of each 1.33 s beam acceleration cycle, so the current between spills can be turned down to save power. This reduces the cost of the magnets (by reducing the amount of conductor needed), the cost of the power supplies, and the cost of the cooling systems, though the ramping does impose additional requirements. The rates at which the magnets can be ramped affect the average power consumption, which, in turn, affects the heat load and operating cost of the beamline.

The intention is to make use of existing magnets and designs as much as possible for both cost containment and a general commitment to recycling. For each magnet function, the existing uncommitted magnets available at Fermilab and elsewhere have been reviewed.

Suitable candidates have been identified for the Lambertsons, C-magnet, QQB and QQC quadrupoles; they will be refurbished or rebuilt as needed for use in the primary beamline. Existing designs to which additional magnets can be built will be used with no design changes except to the mechanical-support system. The main dipoles and quadrupoles fall into this category. The trim dipole magnets will be constructed according to a new design based heavily on current magnets. The kickers will be a minor modification to existing NOvA kicker design. Existing tooling will be used to the extent possible for all magnets.

### 2.6.3 Reference Design

#### 2.6.3.1 Main Dipole Magnets

The dipole magnets are responsible for directing the primary beam to the target. As the biggest magnets in the beamline, they must be reliable and energy-efficient. They must also provide sufficient strength and aperture to cleanly transport the beam at any energy in the range of 60–120 GeV.

The same type of magnets as used for the MI dipoles are the logical choice for this function, in particular a combination of the 6-m IDA magnet and the 4-m IDD magnet designs. They have performed successfully since the MI's commissioning in 1998. The LBNE magnets will be newly constructed to the existing designs, as mentioned above. The basic properties of these magnets are listed in Table 2-2 and 2-3. The magnet cross section is shown in Figure 2-11 and the layout of an IDA/IDB pair of dipoles, as used in the MI, is shown in Figure 2-12. An IDA/IDD pair has the same interconnection.

The MI dipoles are slightly curved to match the path of the bending particles. The sagitta (the distance between that curve and a straight line) in the 6-m dipoles is about 16 mm.

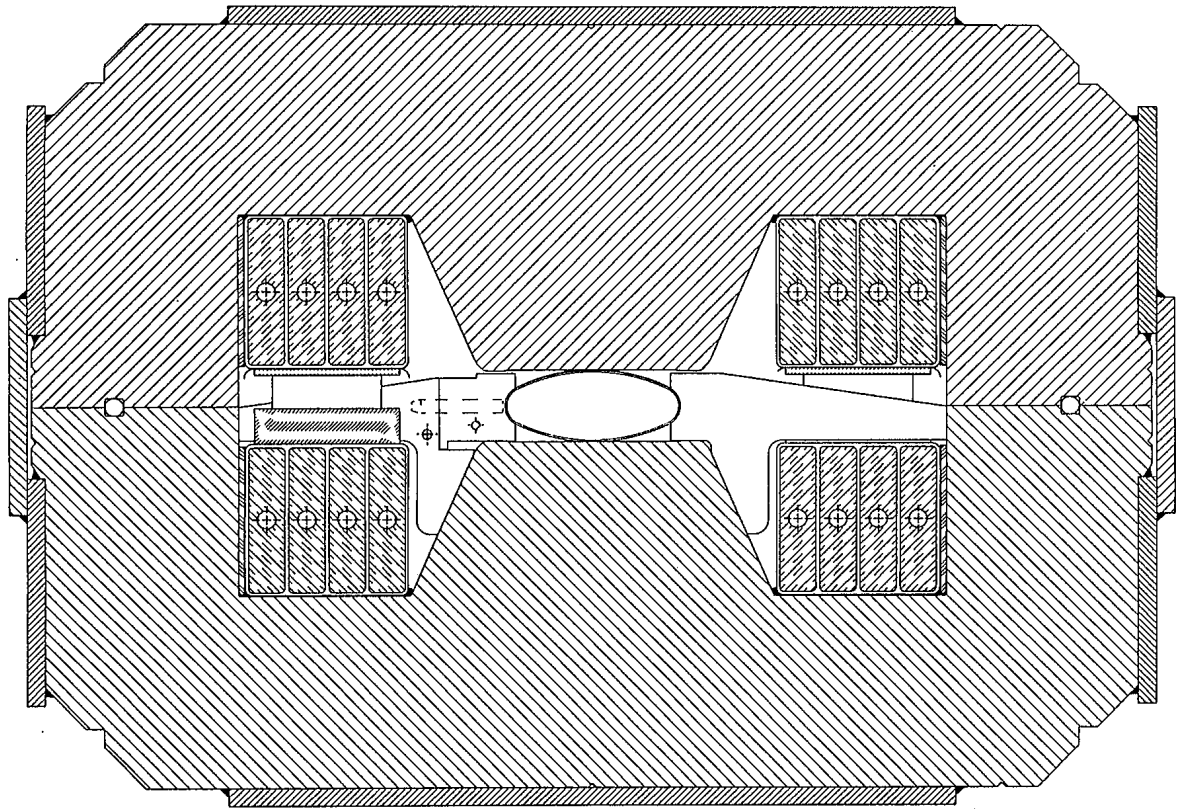
The beam-tube cross section used in the MI dipoles is shown in Figure 2-13 for reference. The beam-tube cross section is oval, wider in the magnet's horizontal dimension, to accommodate the width of the beam due to protons of (slightly) different momenta bending differently in the magnetic field. (Note that the magnets may be oriented at different angles depending on their locations in the beamline, so "magnet's horizontal" may not necessarily mean horizontal in an absolute sense. "Width" refers to the bending direction, perpendicular to the gap dimension between the poles.) Under vacuum, the beam tube's smaller dimension decreases to enough under 2.000 inches to allow its insertion into a magnet aperture and then to allow bending to match the beam sagitta. The MI tubes were cold-drawn through successive dies to produce the required shape. LBNE plans to take the less costly approach, employed in the Fermilab Recycler, of squashing round tubes to a roughly oval shape. The initial tube size will be selected based on aperture requirements. For example, a squashed 3-in (76 mm) outside diameter (OD) tube would yield an aperture width of about  $\pm 47$  mm and a 3.5-in OD tube would yield a width of about  $\pm 58$  mm.

**Table 2-2:** Properties of IDA Dipoles [b].

Property	Value
Steel length	6.100 m
Magnetic field (nominal at 120 GeV)	1.003 to 1.604 T
Integrated field (nominal at 120 GeV)	6.76 to 10.03 T-m
Gap	50.80 mm
Number of turns	8
Aperture height (with beam tube)	47 mm
Aperture width (with beam tube)	120 mm
Current (nominal at 120 GeV)	5106 to 8748 A
Resistance (at 20°C)	0.8 mΩ
Inductance (at 100 Hz)	2.0 mH
Power dissipation (max, I <sub>rms</sub> = 0.5 I <sub>max</sub> )	16.4 kW
Water flow (at 100 psid)	0.93 l/s
Temperature rise (max at 100 psid)	4.2°C
Weight	18,180 kg
Fermilab drawing numbers	5520-ME-274896, 5520-ME-274897
Color	Light blue

**Table 2-3:** Properties of IDD Dipoles [b].

Property	Value
Steel length	4.065 m
Magnetic field (nominal at 120 GeV)	1.003 to 1.604 T
Integrated field (nominal at 120 GeV)	4.51 to 6.68 T-m
Gap	50.80 mm
Number of turns	8
Aperture height (with beam tube)	47 mm
Aperture width (with beam tube)	120 mm
Current (nominal at 120 GeV)	5108 to 8748 A
Resistance (at 20°C)	0.52 mΩ
Inductance (at 100 Hz)	1.3 mH
Power dissipation (max, I <sub>rms</sub> = 0.5 I <sub>max</sub> )	10.6 kW
Water flow (at 100 psid)	1.10 l/s
Temperature rise (max at 100 psid)	2.3°C
Weight	12,300 kg
Fermilab drawing numbers	5520-ME-274910
Color	Light blue



FMI DIPOLE  
TYPICAL CROSS SECTION

**Figure 2-11:** MI Dipole cross section.

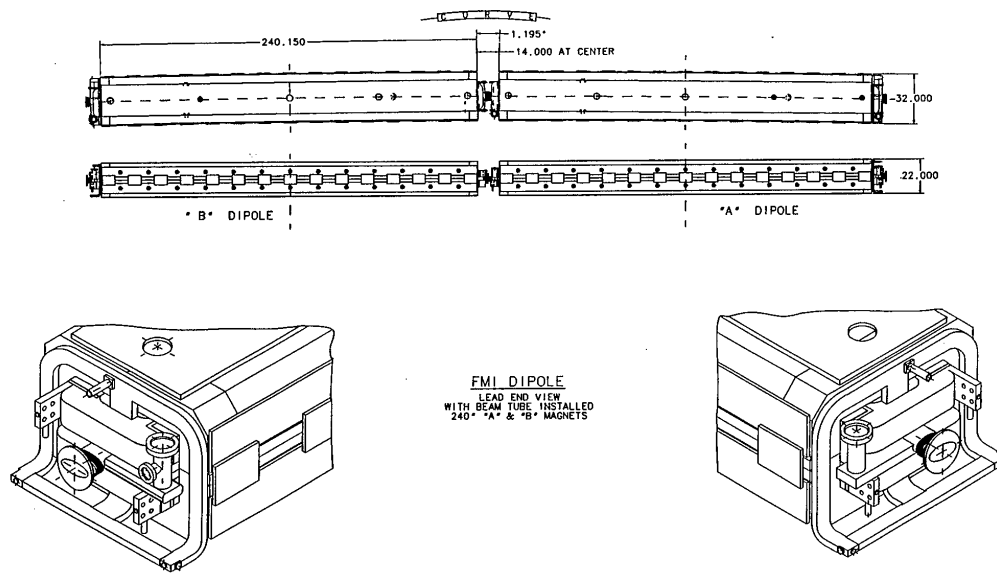
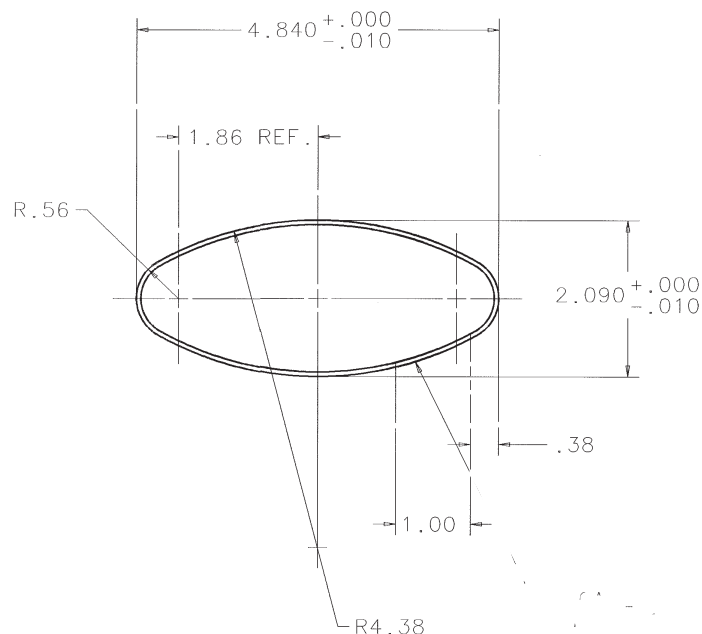


Figure 2-12: Layout of one IDA and one IDB dipole in a half cell .

The excitation curve of a typical IDA magnet, in Tesla-meters versus Amperes, measured during production is shown in Figure 2-14. The integrated strength of IDD dipoles was measured to be 2/3 the strength of IDA dipoles to better than 0.1%.



**Figure 2-13:** Beam tube cross section

The dipole magnets have four terminals, significantly reducing the length of inter-magnet bus work in the main arc; see the center portion of the top image in Figure 2-12. Each length of magnet (6 m and 4 m) comes in two variants that differ only in the placement of the through-bus in the magnet and in the end of the magnet that has the more complicated bus and manifolding. The 6-m magnet variants are designated IDA and IDB; the 4-m magnet variants are designated IDC and IDD. In the MI, one IDA and one IDB (or one IDC and one IDD) magnet are compactly placed back-to-back, with their yokes approximately 0.35 m apart, leaving just enough room for the electrical jumpers between magnets and an ion vacuum pump where the beam tubes are welded together. An IDA can be just as well mated with an IDD. This pairing of a 6-m magnet with a 4-m magnet prevails in the LBNE primary beamline. The water connections and the power connections for the bus around the quadrupoles are made at the outside ends of the pair of magnets.

LBNE plans to follow the procurement strategy used during construction of the MI, developed to minimize the cost and maximize the magnet quality while making extensive use of outside vendors. The major components and subassemblies were fabricated in industry, with all contracts build-to-print (except the steel, which was based on performance) and awarded through a mix of straight bids and a source evaluation board. The cores, coils and beam tubes were assembled into complete magnets at Fermilab. This approach allows Fermilab to control the critical steps in the magnet fabrication and to assume the responsibility for

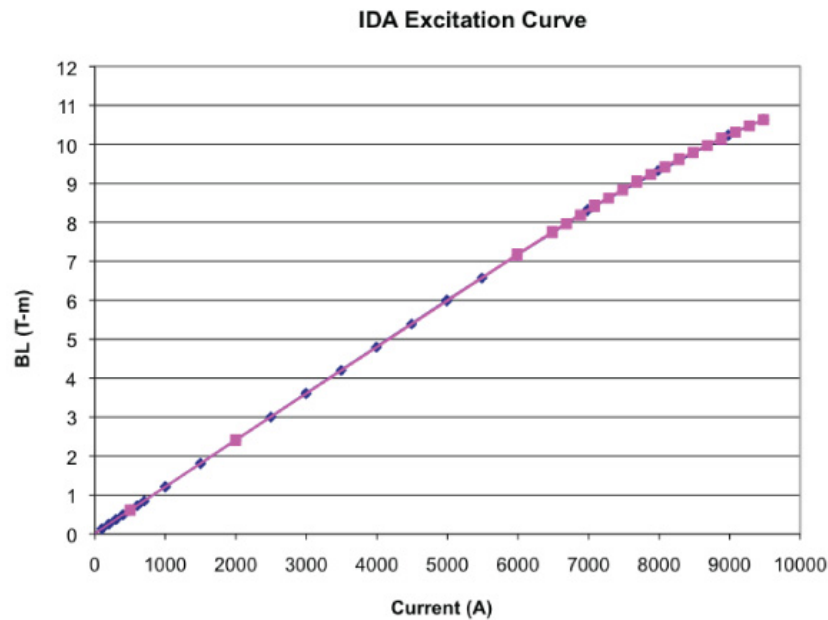


**Figure 2-14:** Typical IDA excitation curve.

the final performance with confidence, rather than trusting the vendors and paying for the vendors' potential liabilities. By taking ownership of the LBNE components, Fermilab will readily be able to make thorough inspections of the components before assembly and ensure that the final magnets meet the needs of the project.

For the MI, Fermilab purchased the coils of coated sheet steel, as that is a critical component whose magnetic properties need close control. Fermilab contracted for the stamping of the steel into laminations for the core and exercised tight oversight and monitoring of the critical lamination dimensions. Fermilab contracted with a fabrication shop to build the magnet half cores using Fermilab-provided stacking equipment, with Fermilab specifying which boxes of laminations were used in each half core based on steel and lamination data. Fermilab contracted with two specialized vendors to produce the coils, one to fabricate the bare coils and another to insulate them, though for LBNE the coil procurements may be combined. As in the Fermilab Recycler, it is expected that the beam tube will be formed from stock dimension tubes, and Fermilab welders will attach the various bellows, flanges, pump-out ports and other features.

For quality control purposes, all magnets will be subjected to magnetic tests.

During operation, the circuits must be ramped between beam pulses to maintain a conservative temperature rise in the magnets and avoid overheating. It is assumed that an *RMS* current of half the peak current can be achieved.

**Table 2-4:** Properties of the MI Lambertson magnets.

Property	Value
Steel length	2.800 m
Magnetic field (nominal at 120 GeV)	0.532 / 1.000 T
Integrated field (nominal at 120 GeV)	1.49 / 2.80 T-m
Gap	50.80 mm
Number of turns	24
Aperture height (with beam tube)	50.80 mm
Aperture width (with beam tube)	406 mm
Current (nominal at 120 GeV)	922 - 1815 A
Resistance (at 20°C)	12.9 mΩ
Inductance (at 100 Hz)	3.9 mH
Power dissipation ( $I_{rms} = 0.5 I_{max}$ )	11.3 kW
Water flow (at 100 psid)	0.96 l/s
Temperature rise (at 100 psid)	2.8°C
Weight	23,500 lb
Fermilab drawing number	5520-ME-331492
Color	Siver

### 2.6.3.2 Main Injector Lambertson Magnets

LBNE will use three existing MI Lambertson magnets (ILA) for extraction from the MI and injection into the LBNE primary beamline. The magnets were built by Fermilab staff for the MI and NuMI projects. Due to the decommissioning of the Tevatron, a suitable pool of spares will become available, including the four ILA magnets in the Tevatron injection system. They will be inspected, with particular attention to the high-voltage insulation and the water circuits, and refurbished as necessary in preparation for long-term service in the LBNE primary beamline. The basic properties of the Lambertson magnets are listed in Table 2-4, and a sketch of the magnet is shown in Figure 2-15. A typical ILA excitation curve is shown in Figure 2-16.

To minimize the thickness of the septum between the hole for the circulating beam and the aperture for the extracted beam, no beam tube is used. Rather, vacuum in the aperture is maintained by a stainless-steel skin that encases the inner core. The large surface area of the laminations inside the evacuable volume necessitates an in situ bake after installation, using the attached electrical heating elements.

To maintain a conservative temperature rise in the magnet and to minimize the impact of any leakage field on the low-energy injected beam, the magnets will be ramped. It is assumed that an *RMS* current of half the peak current can be achieved.

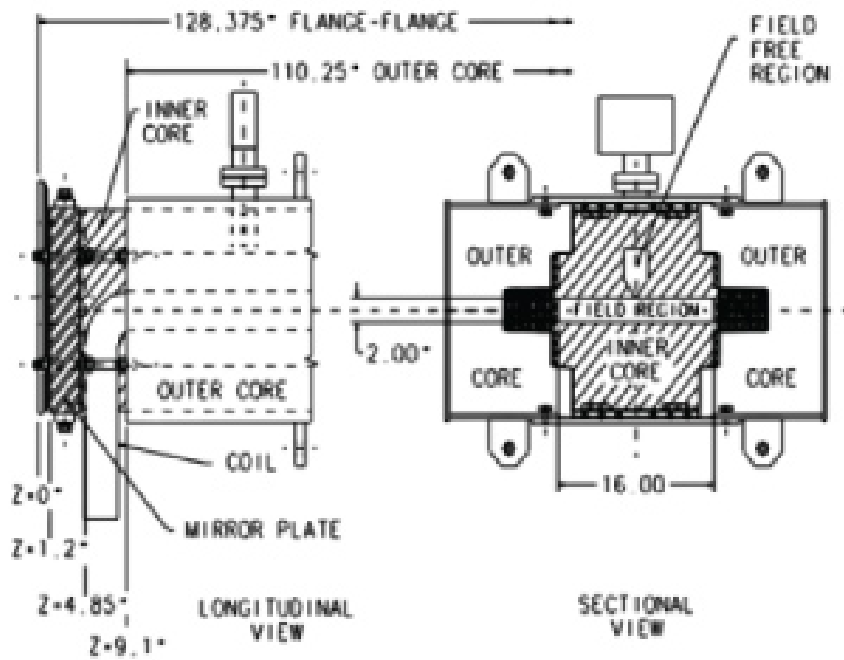


Figure 2-15: MI Lambertson magnet end and cross section.

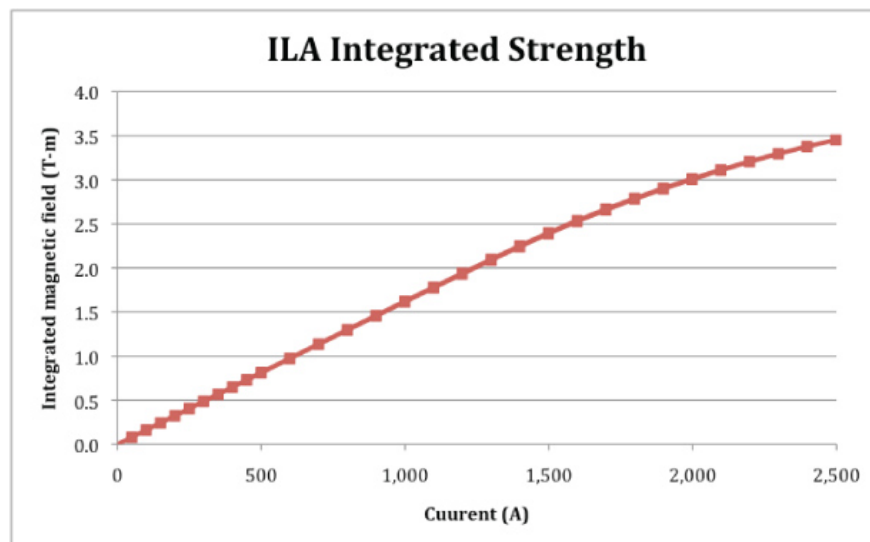


Figure 2-16: Excitation curve of a MI Lambertson magnet.

**Table 2-5: ICA Main Injector C-Magnet Properties.**

Property	Value
Steel length	3.353 m
Magnetic field (nominal at 120 GeV)	1.003 T
Integrated field (nominal at 120 GeV)	3.36 T-m
Gap	40.61 mm
Number of turns	12
Aperture height (with beam tube)	37.5 mm
Aperture width (with beam tube)	98.3 mm
Current (nominal at 120 GeV)	2679 A
Resistance (at 20°C)	2.11 mΩ
Inductance (at 100 Hz)	14 mH
Power dissipation ( $I_{rms} = 0.5 I_{max}$ )	12.6 kW
Water flow (at 100 psid)	0.57 l/s
Temperature rise (at 100 psid)	5.3°C
Weight	8,500 lbs
Color	Light blue

### 2.6.3.3 Main Injector C-Magnets

As at the other high-energy extraction points in the MI, the Lambertson magnets are followed by a current septum C-magnet. The MI C-Magnet, the ICA, was based on the F17 C-Magnet design for the Tevatron I project. Several C-magnets were used in the A150 anti-proton beamline from the MI to the Tevatron and will be available for use in the LBNE beamline. The basic properties of these magnets are listed in Table 2-5, and a sketch of the magnet is shown in Figure 2-17. The beam tube cross section is shown in Figure 2-18. The excitation curve of a typical ICA magnet is shown in Figure 2-19.

In preparation for use in LBNE, the C-magnets will be inspected, and refurbished as necessary, with particular attention to the high-voltage insulation and the water circuits.

To maintain a viable temperature rise and avoid overheating, the magnets must be ramped between beam pulses. It is assumed that an *RMS* current of half the peak current can be achieved.

### 2.6.3.4 Quadrupole Magnets

The LBNE primary beam will be focused with 3Q120 and 3Q60 quadrupole magnets of the specific styles QQB and QQC. These styles of quadrupoles are reliable, compact, energy-efficient and suitably strong. The basic properties of the magnets are listed in Tables 2-6

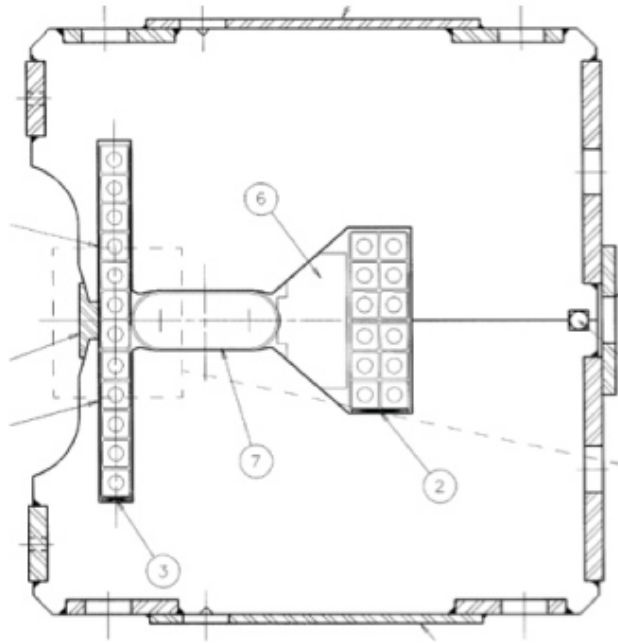


**Figure 2-17:** ICA MI C Magnet.

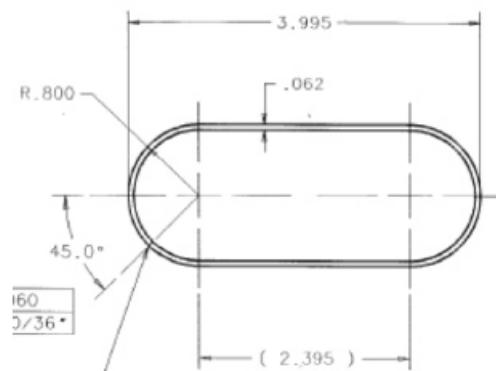


**Figure 2-18:** ICA beam tube shown in horizontal bending orientation.

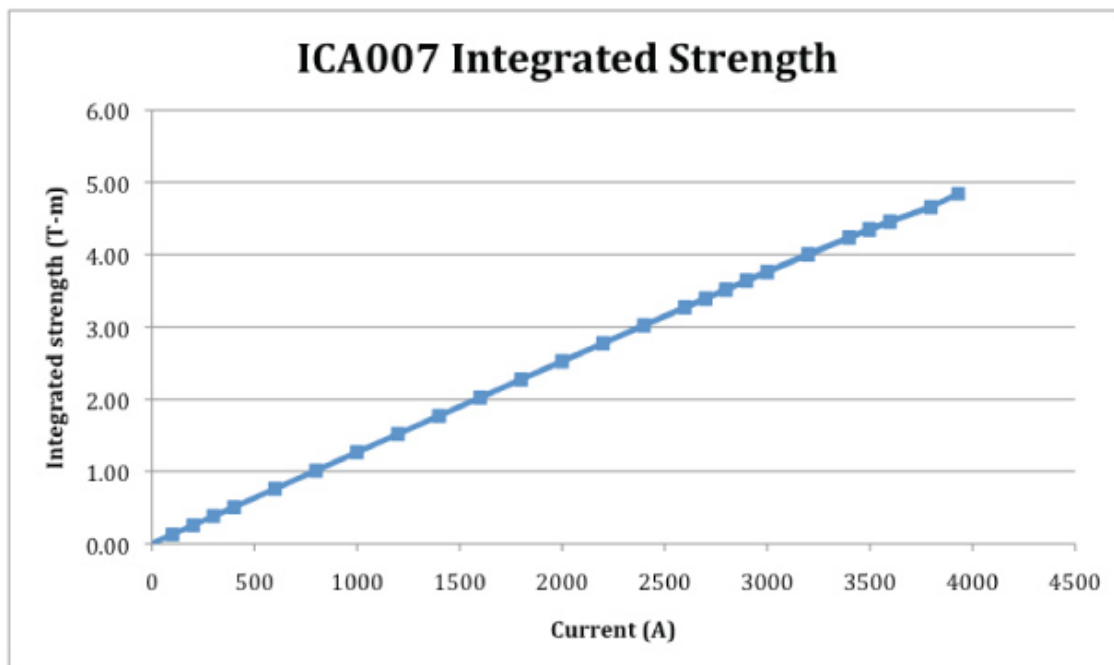


**Figure 2-19:** ICA integrated strength as a function of current.

and 2-7. The magnet cross section is shown in Figure 2-20 and the excitation curves are shown in Figures 2-21 and 2-22. The beam tube is round, with a 71.9-mm (2.82-in) minimum inner diameter.

The 3-m QQB magnets are the main focusing quadrupoles of the primary beamline. Shorter QQC quadrupoles are used at four locations because of spacing. At the upstream end of the beamline, just following the C-magnet, the functionality of a single 3-m quadrupole is implemented with two 1.5-m quadrupoles; this avoids interference with a quadrupole in the MI ring. At the other end of the line, two of the five quadrupoles in the final focus are sufficiently weak to suggest a shorter magnet. The basic design of the 3Q120 and 3Q60 dates from the 1970s, when they were first used extensively in the external beamlines of the Fermilab fixed-target program. They are still commonly used, although the yoke and coil configuration have evolved over the years. The QQB and QQC magnets have a slightly larger yoke than the earliest versions (15 in  $\times$  17 in rather than 13 in  $\times$  17 in), providing more mechanical stability. They also use hollow, water-cooled coils, which allow a higher current density than the original indirectly cooled, solid-conductor models. The water manifolds will be of the same style as designed for the MI. The coil will be vacuum-impregnated in the core.

For quality-control purposes all magnets will be subjected to magnetic measurements.

The circuits will be ramped between beam pulses to maintain a conservative temperature rise in the magnets. It is assumed that an *RMS* current of 53% of the peak current can be

**Table 2-6:** QQB: Hollow conductor 3Q120 Properties.

Property	Value
Steel length	3.048 m
Magnetic gradient (nominal at 120 GeV)	9.189 to 16.546 T/m
Integrated gradient (nominal at 120 GeV)	28.01 to 50.43 T-m/m
Pole diameter	76.02 mm
Number of turns	28 per pole
Aperture (with round beam tube)	72 mm
Current (nominal at 120 GeV)	192 to 353 A
Resistance (at 20°C)	156 mΩ
Inductance (at 100 Hz)	82 mH
Power dissipation (I <sub>rms</sub> = 0.533 I <sub>max</sub> )	5.9 kW
Water flow (at 100 psid)	0.35 l/s
Temperature rise (at 100 psid)	4.0°C
Weight	7,400 lbs
Color	Orange

**Table 2-7:** QQC: Quadrupole magnet properties.

Property	Value
Steel length	3.048 m
Magnetic gradient (nominal at 120 GeV)	13.39 to 17.08 T/m
Integrated gradient (nominal at 120 GeV)	20.41 to 26.03 T-m/m
Pole diameter	76.02 mm
Number of turns	28 per pole
Aperture (with round beam tube)	72 mm
Current (nominal at 120 GeV)	233 to 369 A
Resistance (at 20°C)	156 mΩ
Inductance (at 100 Hz)	82 mH
Power dissipation (I <sub>rms</sub> = 0.533 I <sub>max</sub> )	4.4 kW
Water flow (at 100 psid)	0.35 l/s
Temperature rise (at 100 psid)	2.1°C
Weight	7,400 lbs
Color	Orange

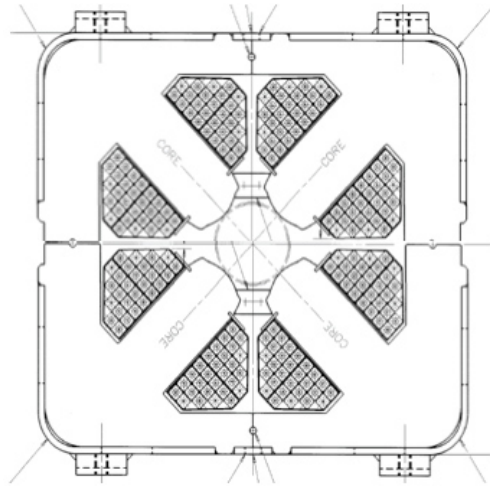


**Figure 2-20:** Cross-section of QQB and QQC quadrupoles.

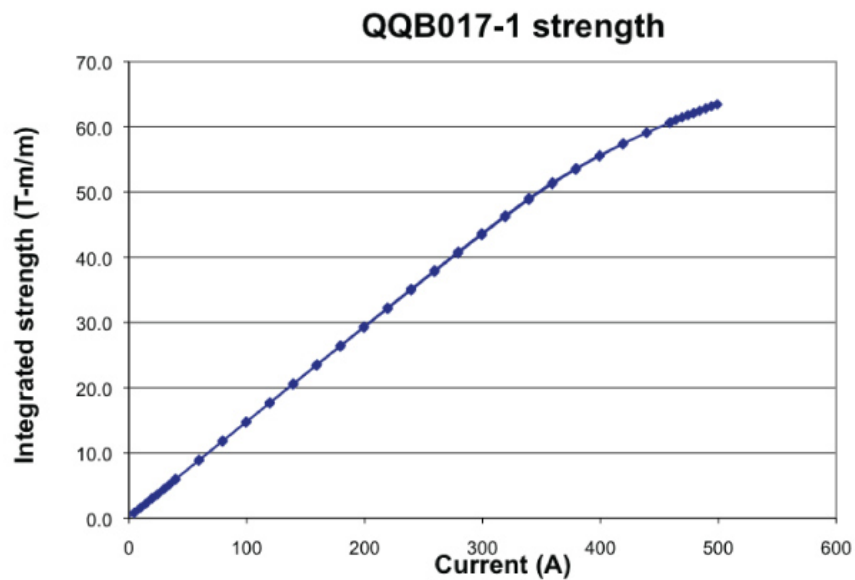


**Figure 2-21:** Typical QQB excitation curve.

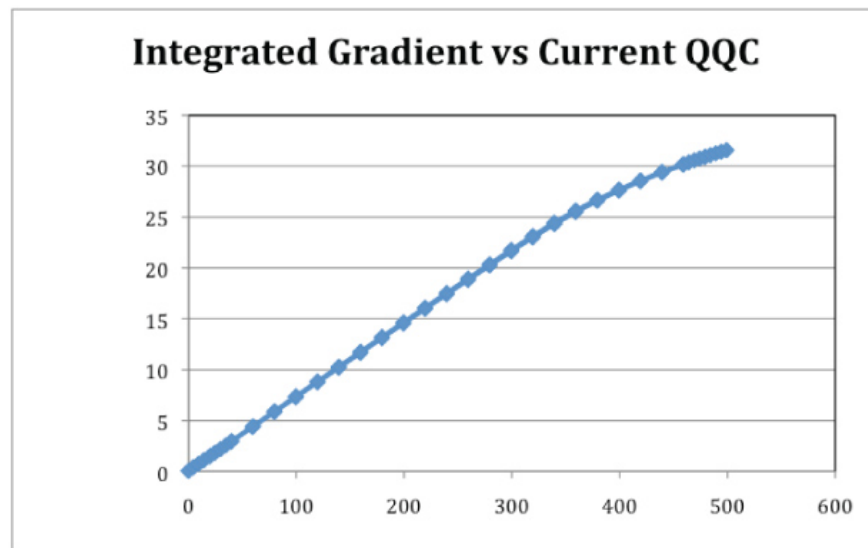


**Figure 2-22:** Typical QQB excitation curve.

achieved.

### 2.6.3.5 Corrector Magnets

A trim dipole (fine-tuning) magnet, called an IDS, is located at every focusing location. One of these locations has two quadrupoles functioning as one element and two locations are sufficiently sensitive to require steering in both planes, so the trim magnet count does not exactly match the quadrupole count.

This is a new design based on the IDH horizontal trim dipole correctors built for the MI and subsequently used, with modifications, in the NuMI beamline. To allow operation over a wider range of excitations without overheating, the conductor size will be increased from 10-gauge square copper to 8-gauge square copper. To maintain better linearity over the extended operating range, the back leg thickness will be increased.

The corrector magnets have the same pole width at the MI horizontal correctors, but a gap increased from 50.8 mm to 76.2 mm gap to accommodate a round beam tube matching the quadrupole aperture at any rotational angle around the beam. MI correctors with an increased gap are used in the NuMI beam. In NuMI, the increased current needed to reach the desired field strengths required attaching indirect water cooling channels to the core. In the MI, the linear range of the excitation curve has been successfully extended by strapping extra steel plates onto a few magnets to increase the flux return path. Because the water-cooling and added steel plates are cumbersome and labor-intensive to install, it was decided to address both of these issues with a new design. The basic properties of the magnets are listed in Table 2-8, and a conceptual drawing of a trim dipole is shown in Figure 2-23. Initial

**Table 2-8: LBNE Trim Dipole Properties (IDS)**

Property	Value
Steel length	0.305 m
Magnetic field (maximum peak)	0.365 T
Integrated field (maximum peak)	0.130 T-m
Pole gap	76.2 mm
Number of turns	812
Aperture height (with beam tube)	72 mm
Aperture width (with beam tube)	120 mm
Current (maximum peak)	30 A
Resistance (at 20°C)	1.4 $\Omega$
Inductance (at 100 Hz)	750 mH
Power dissipation (maximum)	315 W
Cooling	Air cooled
Temperature rise (internal)	32°C
Weight	295 kg
Color	To be determined

design work has been done assuming both a 50.8 mm to 76.2 mm gap, adjustable with back leg spacers. Figure 2-23 reflects the 76.2 mm configuration.

The measured excitation curve of a MI trim dipole magnet with the increased gap used in NuMI is shown in Figure 2-24. Since the pole shape, length, and number of turns in the coil are the same, and the yoke is comparable, this closely matches the expected performance of the LBNE IDS.

To maintain a conservative temperature rise in the magnets during operation, the stronger circuits must be ramped between beam pulses. It is assumed that an *RMS* current of half the peak current can be achieved. Because heat dissipation is a primary motivation of the new design, the thermal performance has been modeled in detail. To validate the modeling, a prototype magnet will be subjected to extensive thermal tests. The prototype will also be thoroughly measured magnetically to ensure conformance with the design requirements, as will at least a quarter of the production magnets, for quality assurance purposes.

### 2.6.3.6 Kicker Magnets

To extract the beam at the MI-10 straight section, a five-kicker-magnet system is needed. This system substitutes the 3 2.2 m-long NuMI kickers. The decision to use shorter kickers is dominated by the available NOvA ceramic tubes. These magnets will be similar to the recently built RTV-potted NOvA extraction kickers (“RKB” type). Table 2-9 summarizes the parameters of these kickers. The cross-section of the kicker is shown in Figure 2-25.

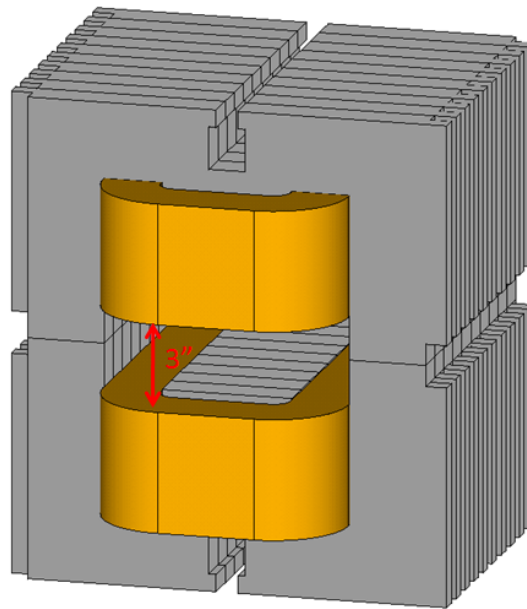


**Figure 2-23:** Schematic of LBNE 3-in (76.2-mm) aperture gap trim dipole (IDS).

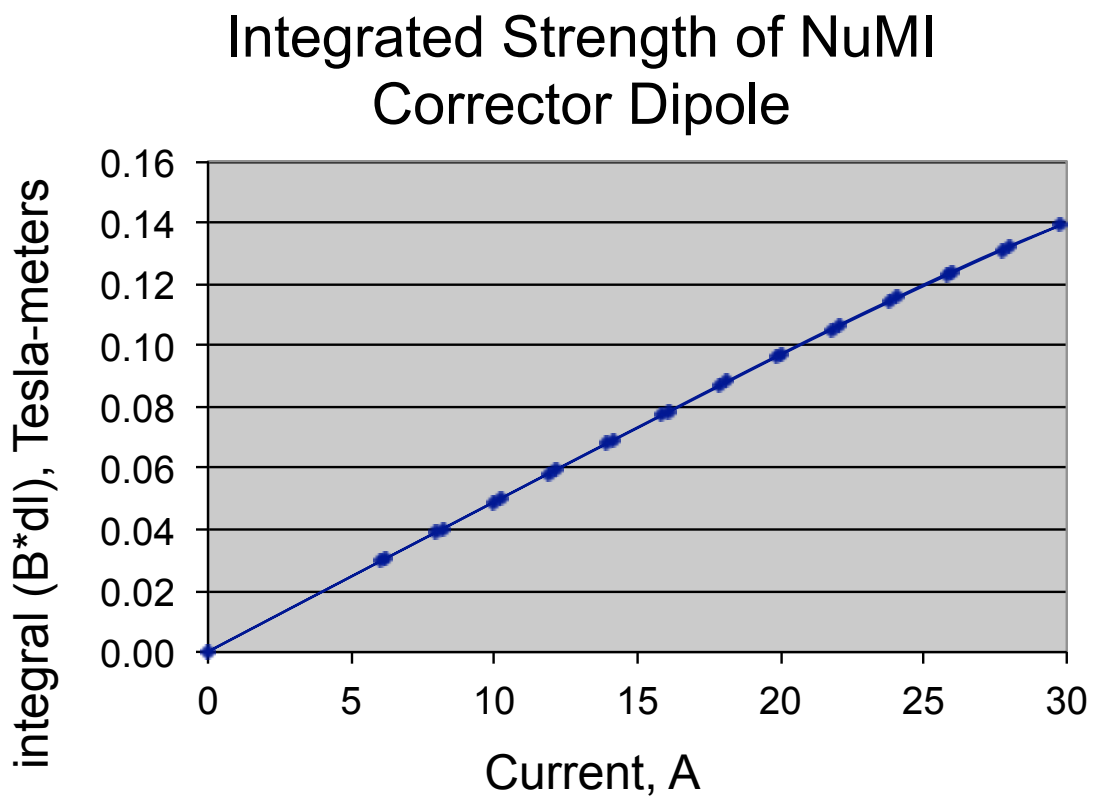


**Figure 2-24:** Integrated strength of NuMI dipole corrector.

**Table 2-9:** Properties of the NOvA extraction kicker magnets (RKB)

Property	Value
Length	1.7 m
Magnetic field (maximum peak)	0.0237 T
Integrated gradient (maximum peak)	0.0281 T-m
Number of turns	1
Aperture height	38 mm
Aperture width	86 mm
Current (maximum peak)	1000 A
Kick Angle (@120 GeV)	815 $\mu$ rad
Field rise time (1% to 99%)	1.6 $\mu$ s
Field flattop time	9.8 $\mu$ s
Power dissipation (maximum)	250 W
Flattop stability	$\pm 1\%$
Cooling	Air cooled
Drawing number	5520.000-ME-460906
Color	Silver

A temperature-regulation system is required for the loads of the kicker magnets to meet the stability requirement on kicker amplitude and to remove heat from the loads. A regulation of  $\pm 0.5^\circ\text{C}$  is needed on the fluid to meet the stability requirement. Fluorinert is used because it is a good high-voltage insulator and thermal conductor, and it has low viscosity.

The LBNE Fluorinert recirculation system will be very similar to the one currently located in MI-10 which is used for the 8-GeV Injection Kickers. It will run parallel to it, terminating at the LBNE kicker loads. It will be cooled by LCW as if it were simply another power supply load. The skid will also have a heater, along with a temperature-control valve and circuit, for fine-tuning of the operational temperature.

### 2.6.3.7 Magnet Installation

LBNE magnet installation covers installing 78 magnets, listed in Table 2-1, in the Main Injector and primary beamline enclosure. For the purposes of this discussion, the roughly 1,080-ft primary beamline consists of three sections: the MI/extraction, the vertical up-bend section and the vertical down-bend section. Based on experience with NuMI and other MI projects, LBNE beamline installation will use a combination of methods. The methods for transportation and positioning will vary for different sections, however the scheme of supporting and adjusting will be the same. Each magnet will have a stand that provides three-point support and six degrees of freedom for precise adjustment; the characteristics of magnet installation are shown in Table 2-10.

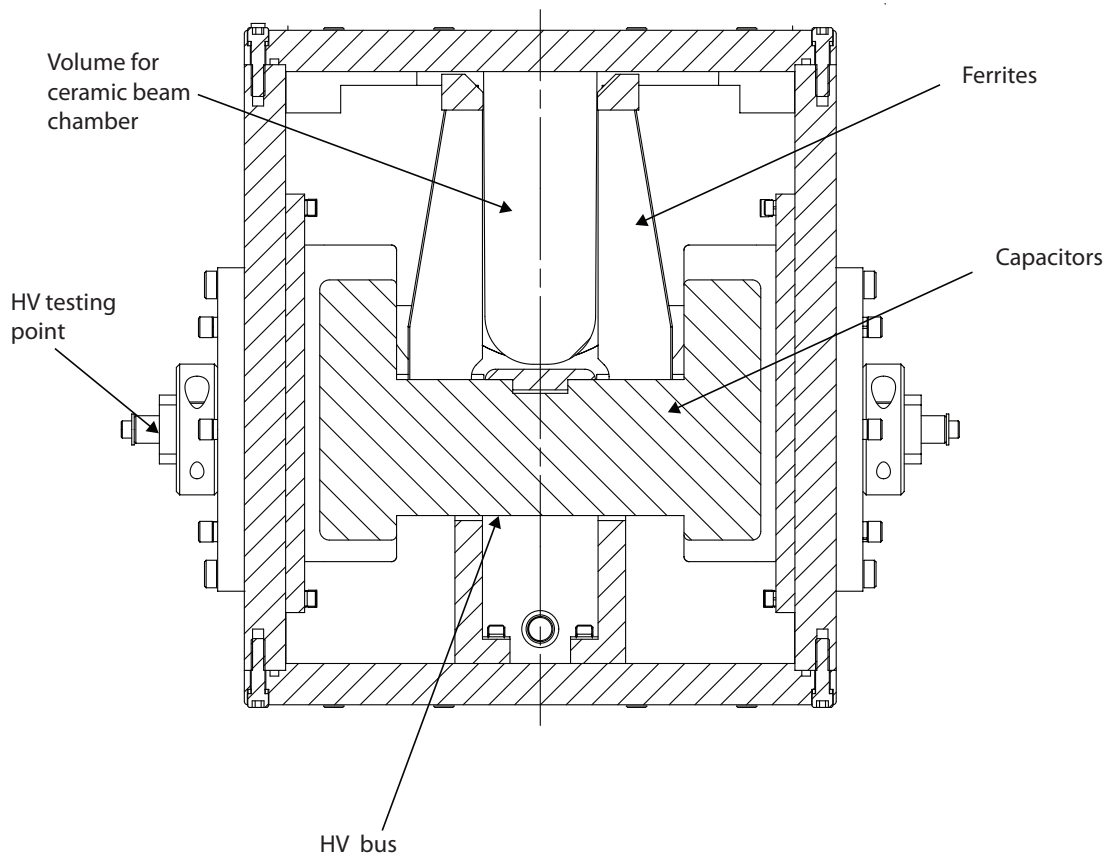


**Figure 2-25:** Cross section of a NOvA extraction kicker, "RKB" type

**Table 2-10:** Characteristics of magnet installation.

	Extraction Stub	Vertical Up-Bend	Vertical Down-Bend
Section Length	150 ft	500 ft	430 ft
Enclosure Notes	Co-existing with other beam lines in existing enclosure, location high in enclosure	Various slopes up to 150 mrad.	Various slopes up to 101 mrad
# of Major Magnets	9	30	11
Support/Adjustment	Stand/hanger of new design	MI stands with modification	MI stands with modification
Transportation Method	Tugger, dolly via MI-10	Tugger, dollies and winch via LBNE Ent.	Tugger, dollies and Winch, via Target Hall
Positioning Method	Lift table + track	MI hydraulic carriage with modification	MI hydraulic carriage with modification

This section focuses on the technical aspects of installation. Chapter 4, on system integration, explains how to best sequence the installation steps relative to each other and other tasks. Because magnet installation is a very significant part of the beamline installation, it must be integrated into the overall plan to ensure that it is done safely and efficiently, but the scope of magnet installation is the responsibility of the Primary Beam.

A tugger and dolly will move each magnet to its designated tunnel location in the MI. Most of the magnets will be transported to the Magnet Installation Tunnel just downstream of LBNE by flatbed trucks, where they will then be moved into the primary beam enclosure. For magnets in the sections of vertical bend, the tugger is not suitable because of the large declination in the floor (150 mrad at maximum), so each magnet and its loading dollies will be moved by a winch system.

The winch system has a similar line speed (35 feet per minute) as the one used in NuMI for a similar installation, but with larger capacity (up to 40,000 lbs), a longer range (1,100 ft) and new features such as variable speed control, self-guidance and dual-directionality. After installation is finished, the winch system will be removed from the tunnel and will be reinstalled only as necessary for future use.

The dollies will require redesign so they are able to work in two different situations: together with a tugger to transport magnets across non-sloping floors and together with the winch system to transport magnets across sloping floors.

Before positioning a magnet in its final position, the locations of the beamline and magnets

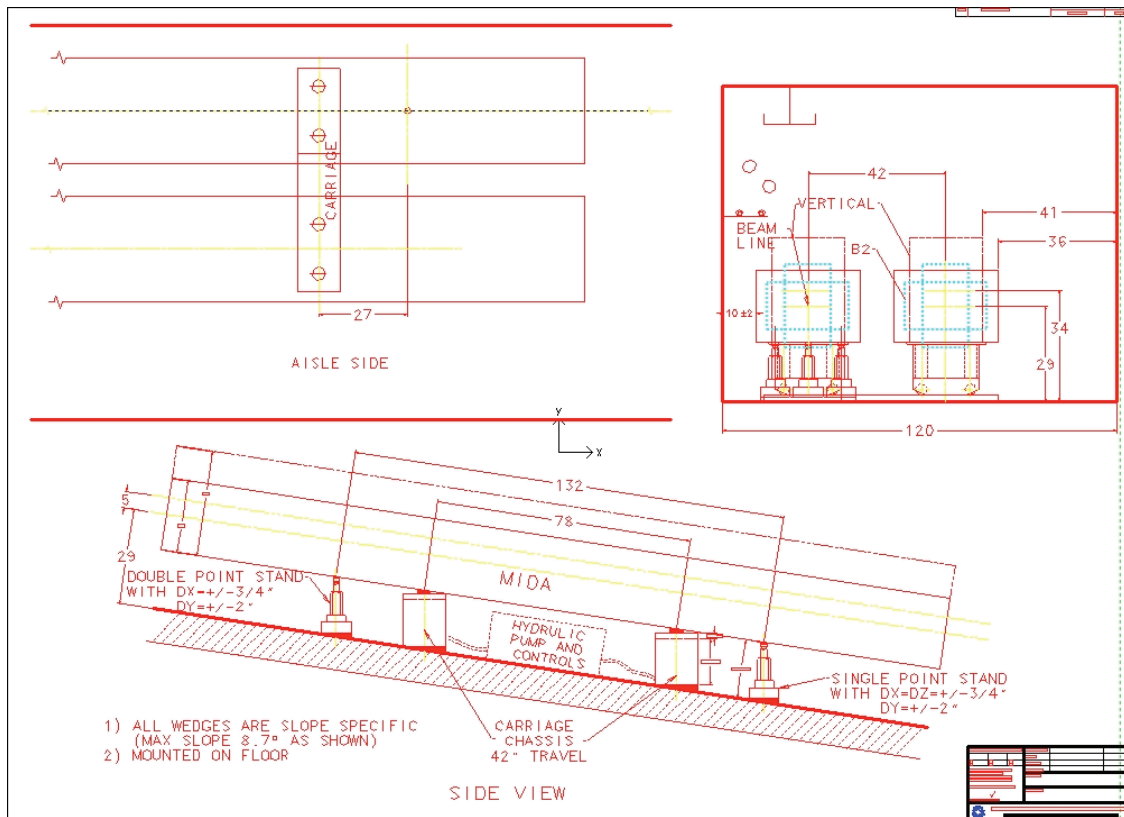


Figure 2-26: Magnet installation on sloping surfaces.

will be marked on the floor with the help of a survey crew. Each stand or hanger will be installed within  $\pm 0.25$  in of its ideal position; a mounting template may be necessary to achieve this. The stands will be set to the proper position to receive the magnets. The magnets will then be transported and secured at their aisle location, and the hydraulic carrier can be set and secured in its designated position. The carrier can then extend its carriage underneath each magnet and transfer the magnet transversely to its beamline location. The stands can then be adjusted to engage with the magnet and take the load from the carrier. At that point, the magnet dollies and the carrier can be removed. The stands are then adjusted to their neutral positions, and the final precise adjustment will be performed by a survey crew. For the magnets in the MI, a lift table and transverse tracks will be used to position each magnet.

In general, MI magnet stands will be used. Their features include: thrust bearing for heavy magnets (up to 40,000 lbs), a low-friction-coefficient insert for easy sliding and a bronze bearing for easy adjustment. The stands have a transverse axial adjustment of  $\pm 0.75$  in and a longitudinal axial adjustment of  $\pm 2$  in because of a deviation of the tunnel floor from its nominal elevation due to construction tolerance and settlement. Cradles will be designed to accommodate magnets in their rotated positions.

Wedging will be used to modify the bottom part of stands located on slopes based on the degree of slope, so that each stand sits upright. Shimming may be needed to level wedges due to imperfections in the floor. With the wedges at the bottom of the magnet stand, these stands provide vertical support against gravity, so there are no lateral forces even though a magnet may be located on a slope (see Figure 2-26). However, the addition of wedges at the bottom of the magnet and at the bottom of stands requires five more inches to be added to the distance between the beamline and the floor.

## 2.7 Magnet Power Supplies (WBS 130.02.02.03)

### 2.7.1 Introduction

This section describes the power supply system for the magnets that comprise the lattice optics of the primary beamline. Fermilab has a long history of developing and procuring power supplies for large magnet systems and this experience will guide the design of the LBNE magnet power systems. Some magnets will be grouped and powered by a single “magnet loop” (many magnets powered with one set of supplies), the rest will be powered individually, according to the lattice optics design. The power supply system design seeks to minimize power consumption, reuse existing supplies from the Tevatron and the NuMI beamline, whenever possible, to better manage the cost.

**Table 2-11:** Dipole (bending) magnet loops

Magnet Loop Name	Number of Magnets	Power Supply Location	Power Supply Type	Power Supply Voltage	Peak Magnet Current	RMS Current	Average Power
E:LAM1	1	MI-10	500 kW	50	922	432	8,259 kW
E:LAM12	2	MI-10	500 kW	200	1,815	882	64,702 kW
E:V1001	1	MI-10	500 kW	50	2,649	1,212	16,587 kW
E:H202	1	LBNE 5	375 kW	50	7,339	3,601	24,256 kW
E:H204	2	LBNE 5	2x375 kW	100	5,878	4,640	72,473 kW
E:H206	6	LBNE 5	2x375 kW	100	5,320	3,724	72,473 kW
E:H208	4	LBNE 5	500 kW	200	5,320	2,975	35,368 kW
E:H214	12	LBNE 5	2.8 MW	420	8,510	4,406	124,735 kW

## 2.7.2 Design Considerations

Power consumption is a cost driver during operation, and thus a design driver. In order to maintain the low power consumption, all of the magnet currents will be ramped. Each power-supply design will be selected to provide the best balance between the voltage stresses on the magnet and average power consumption. Also, each power supply will be constructed to use the maximum voltage necessary to reach the peak current and settle into regulation before the beam is extracted from the MI.

## 2.7.3 Reference Design

### 2.7.3.1 Power-supply Loops

The primary beamline will contain a kicker supply, three extraction power-supply loops, five major bending-magnet loops, one large quadrupole loop, eleven minor quadrupole loops and a series of corrector-magnet power supplies. A simplified diagram for a power supply loop is shown in Figure 2-27. Table 2-11 shows a complete listing of the dipole magnet loops, and Table 2-12 lists the quadrupole-magnet loops and the assumed location of the equipment. Table 2-13 shows the corrector-magnet system, which will use “Booster-style” corrector supplies.

A kicker system, two extraction Lambertson magnet loops and a C-magnet will be placed at the beginning of the beamline. The power supplies for these magnets will need to be powered from the MI-10 service building and will be part of the MI electrical safety system. This ensures that during access to the MI that these supplies are de-energized using the normal MI procedures. The magnets and the power supplies will be removed from the NuMI beam line extraction and installed at MI-10. The large magnet supplies will be located in

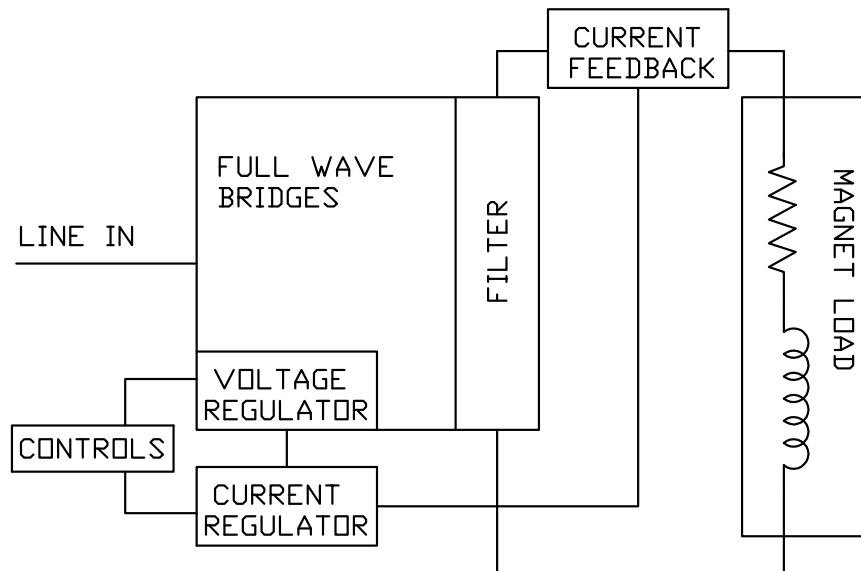


**Figure 2–27:** Magnet power-supply block diagram

the MI-10 service building and will be powered using a relocated, existing transformer from the MI pulse power feeders.

Magnets located in the LBNE Primary Beam Enclosure all power supplies will be in the LBNE 5 Service Building.

### 2.7.3.2 Power Supply Topology

The ramped power supplies will be constructed using 12-pulse rectifiers with a passive filter connected to the output. Only supplies using 12-pulse rectifiers will be connected to the pulse power feeder because a tuned harmonic filter is installed on the feeder to reduce the voltage stress on the 13.8-kVAC components. The feeder will be extended to connect to the MI beamline feeder system (under the Conventional Facilities scope), which has a harmonic filter with the capacity to power the LBNE beamline. The feeder will need to be extended from MI-10 to the new LBNE-5 service building. The details of the feeder and filter construction are given in Volume 5 of this CDR. The on/off switch for the 13.8-kVAC feeder system will be controlled locally at the LBNE 5 Service Building using a motor-driven disconnect to make access to the MI and LBNE easier for the operation crews. This will allow for access into the LBNE enclosure without turning off the MI.

**Table 2-12:** Quadrupole magnet loops

Magnet Loop Name	Number of Magnets	Power Supply Location	Power Supply Type	Power Supply Voltage	Peak Magnet Current	RMS Current	RMS Power
E:Q201/2	1	MI-10	75 kW	150	234	110	2.6 kW
E:Q203	1	LBNE 5	75 kW	150	263	125	3.3 kW
E:Q204	1	LBNE 5	75 kW	150	194	96	1.9 kW
E:Q205	1	LBNE 5	75 kW	150	275	132	3.7 kW
E:Q206	1	LBNE 5	75 kW	150	285	138	4.0 kW
E:Q207	1	LBNE 5	75 kW	150	340	173	6.3 kW
E:Q208	1	LBNE 5	400 kW	800	333	190	48.5 kW
E:Q216	11	LBNE 5	75 kW	150	341	186	8.2 kW
E:Q217	1	LBNE 5	75 kW	150	283	140	4.7 kW
E:Q218	1	LBNE 5	75 kW	150	361	153	1.9 kW
E:Q219	1	LBNE 5	75 kW	150	224	178	7.5 kW
E:Q220	1	LBNE 5	75 kW	150	339	172	6.2 kW
E:Q221	1	LBNE 5	75 kW	150	288	109	1.6 kW

### 2.7.3.3 Dipole Power Supplies

The dipole power supplies will all be re-used Tevatron and NuMI existing equipment, relocated to LBNE. Most of the equipment being moved from either the Tevatron or NuMI will be usable as is, however the large Tevatron dipole supply will operate at a higher current than in the Tevatron so it will need a new current-regulation system.

### 2.7.3.4 Quadrupole Power Supplies

None of the Quadrupole power-supply equipment has an equivalent component in the Tevatron, but NuMI has just installed five new quadrupole supplies. LBNE will relocate and use these supplies and procure six new copies for the Quad magnet loops. A single current-regulator card will be installed in the voltage regulator, just as in the present system for the magnet loops. These supplies have proven to be reliable and will continue to be used.

### 2.7.3.5 Corrector-Magnet Power Supplies

The LBNE primary beamline will utilize upgraded MI-type correction-element magnets. These magnets will all be IDH style, oriented horizontally or vertically, and placed at both ends of each Quadrupole magnet in the beamline. The power supplies will use the newly designed Booster correction elements regulator board to provide the fastest ramping opera-

**Table 2-13:** Corrector magnet power supplies.

Magnet Loop Name	Number of Magnets	Power Supply Location	Power Supply Type	Power Supply Voltage	Power Supply Current
E:xT201 thru E:xT221	23	LBNE 5	FNAL Booster 40 A Trim	180	40

tion. These are individual switch-mode units that utilize a common bulk supply similar to those used in the present MI installations. A single bulk power supply installation is capable of driving all of the proposed 23 individual magnets. The power supply is intended to be used as a ramping supply and will provide full four-quadrant operation. The magnets will be ramped to the 40-A peak as needed to achieve the longest life in the magnets, and to minimize high-current DC operation and system heating.

### 2.7.3.6 Kicker Power Supplies

New kicker magnets and a kicker-magnet power supply will be needed to extract the beam from the MI. The present NuMI extraction kicker magnets at MI-60 use three long magnets, but five short magnets are planned for the MI-10 extraction (see Section 2.6.3.6). This change has little effect on the power supply, but it affects the number of cable terminations on/at the loads. This power supply system will be copied from the NuMI extraction kicker, a proven and reliable design, with few changes. The power-supply design consists of a pulse-forming network (PFN), charging supply, resonant charger, switch tube in an oil tank and terminated transmission-line loads. To maintain regulation, high-resistance cooling liquid is circulated through the loads, requiring a heat exchanger to maintain load temperature. All of the controls for this system will be identical to the latest design installed for the NoVA upgrade to the MI and any usable equipment from the NuMI extraction will be relocated to the MI-10 service building.

### 2.7.3.7 Power Supply Control

The power-supply control system will use the latest design of the controls interface from the Electrical Engineering Support department of the Fermilab Accelerator Division (AD E/E Support). This controller includes a built-in transient recorder and a single E-Net connection that provides the status and control back to the front-end computers. The current reference design is similar to the ramp generator series commonly used today and referred to as a C46x card. However in the future LBNE will be moving to a VME-based control system that will provide a ramp generator that emulates the present system. The current regulation and controls can support either system without any changes.

### 2.7.3.7.1 Voltage Regulator

A standard voltage-regulator chassis was developed to improve maintenance and operation of power supplies in the accelerator complex. This Fermilab voltage regulator is specified in 12-pulse supply procurements. This has reduced the maintenance load on Fermilab's engineering staff because, having over 150 copies, the lab is not subject to unique designs supplied by different vendors. The primary beamline will continue to use this chassis design in all of the 12-pulse high-current supplies in the line as well as in the Fermilab high-stability current-regulation system. All of the regulators will come with the Tevatron and NuMI supplies, and LBNE will procure additional units for the seven new quad supplies.

### 2.7.3.7.2 Current Regulator

The ramps for the beamline magnets move very quickly to high currents, so for the magnet loops with two supplies, both must be programmed to operate at the same voltage. This is in contrast to the MI where, instead, a controller MECAR (the Main Injector Excitation Controller and Regulator) removes supplies from the magnet loop to reduce feeder-loading during the ramp. MECAR regulation and control is currently installed in the NuMI beamline for HV101 (two supplies) and V118 (three supplies).

The current-regulation system for the large supplies will use the latest version of the BuLB v2.0 current regulator that is a subset of the MECAR regulator and will have a response in current regulation comparable to the MI. These regulators have been installed in the present NuMI beamline high-current supplies to improve the accuracy from pulse to pulse. This regulator is used to provide the highest pulse-to-pulse stability in the LBNE current-regulation system design. It is constructed with a built-in learning system that is used to correct the systematic errors in the current. The power supplies will have filters; the fast changing voltage will ring during the step-down and affect flattop current. It will be impossible to "learn out" the effect of the ring, so the shorter the flattop is, the more structure will be seen in the current. The learning system will make this repeatable ramp-to-ramp and should not affect beam transfer any more than the changes in MI bend-magnet current do. This regulation limit is not unique to LBNE but is fundamental to ramped-power systems, including that of the MI. In addition to providing the current regulation, this system has a built-in transient recorder to capture single-event trips, allowing for faster analysis of random events.

### 2.7.3.7.3 Series Power Supply Controller

Connection of multiple power supplies in series or parallel increases the risk of back-feed from the other devices. A system of knife switches and disconnect switches will be used to isolate the supplies from the load and the beamline for maintenance of the H214 magnet loop. The knife switches, taken from the Tevatron, will be installed in the large dipole-magnet systems

to improve the maintainability of the supply and magnet load.

For the series-connected supplies, a new, custom controller will provide the voltage drive to both supplies and manage their ON/OFF status as a single supply. Controllers of this type, used on three magnet loops in NuMI with up to three 500-kW supplies in series, use a commercial controller (based on a Programmable Logic Controller, PLC) during operation. This controller will also manage the magnet-loop monitors, temperature, voltage-to-ground, bus-water differential pressure and ground current.

All of the high-current power supplies will use a distributed ground system to check for excessive ground current (ground fault) in the power supplies and magnet, and if detected will trip off the supplies. The ground-fault system is built into the smaller supplies but will be part of a separate controller in the series-connected supplies. All of the support hardware in the existing power supplies will be relocated with the supplies and used with the new controller.

#### **2.7.3.8 Power Feeder Loading**

The feeder system that provides power to the primary beamline supplies will be routed from the Kautz Road substation, via an extension of the MI beamline feeder 96/97 to both of the LBNE service buildings (as part of the Conventional Facilities scope). This feeder system already incorporates a harmonic filter to reduce the voltage stress on the 13.8-kVAC devices. The peak loading on the feeder is expected to be 6.8 MVA and the harmonic filter has 5 MVARs of correction to the beamline-feeder system. Beam will not be sent through the NuMI or F-sector beamlines during LBNE pulses, so the supplies in the MI beamline will be at 'idle' and not drawing high power. This will allow the needed pulse power to be drawn from the existing capacity of the MI, and continued running with a mix of beamline choices on a time-line generator mix, as is done now, without changes to the feeder system.

#### **2.7.3.9 Power Supply Large Equipment Installation**

The large power supplies consist of multiple sub-assemblies that will need final assembly in place in the service buildings. The outdoor equipment is large and will be put in place by a local rigging company. As equipment is taken from the Tevatron and NuMI it will be disassembled using a combination of Fermilab labor and local contractors. All electrical work will be performed by local contractors. Fermilab will locate and assemble the large subsystems and perform all testing and integration into the controls system. Fermilab will act as the general contractor to have the large sub-assemblies constructed and complete the final assembly work on site for only the large supplies, new and MR/Tevatron size equipment. The smaller, high-current supplies will be constructed off-site and come in fully operational. They will be installed by Fermilab personnel and the power connections will be made by

local contractors. The final testing and integration to the controls will be done by Fermilab staff.

## 2.8 Primary Water System (WBS 130.02.02.04)

### 2.8.1 Introduction

The primary water system will feed cooling water to the magnets, power supplies and other equipment of the primary beamline. The system will include a heat exchanger, filtration systems, pumps, expansion tank, instrumentation, buswork, and piping, valves, fittings and other hardware.

This system will supply low-conductivity water (LCW) of a resistivity in the range of 16 to 18 M $\Omega$ -cm, at a supply temperature of 95°F. The majority of the system's components will be located in the pump room at ground-level in LBNE 5. From there, LCW will be fed to components in LBNE 5, as well as into and throughout the beamline enclosure, and finally to LBNE 20 Service Building and Target Hall horn power supplies. This system may be used to supply the make-up water to the Target Hall radioactive water (RAW) systems. Beamline components at the extraction point in the Q-100 area of the MI will be fed from the MI Global LCW System.

### 2.8.2 Design Considerations

Full system modeling needs to be accomplished once all component requirements are well understood and all configuration options are decided. System schematics will be created in parallel and should include a piping and instrumentation diagram (P&ID). Piping-installation drawings and specifications will be created from this, with sufficient documentation to provide for outside bidding practices.

Piping will be designed and installed in accordance with ASME B31.3 Code for Process Piping. Pressure vessels shall be designed in accordance with ASME Boiler and Pressure Vessel Code Section VIII Division 1. Both will adhere to FESHM [12] Chapter 5031, as well as the Fermilab Engineering Manual [13].

## 2.8.3 Reference Design

### 2.8.3.1 Heat Loads and Heat Exchanger

Total heat loads for the system will be in the range of 0.8 to 1.0 MW, depending upon the final choice of dipoles and power supplies used and the final configuration of all other equipment. Final removal of this heat will be through transference in pond water to an LCW heat exchanger, to be located at LBNE 5. This will be a tube-and-shell style exchanger, with pond water on the tube side and LCW on the shell side to facilitate the cleaning of the pond-water side.

A three-way valve setup will be used to control the LCW temperature, by directing LCW flow either to the heat exchanger or to bypass the heat exchanger. This will regulate the temperature of the LCW supply leaving the pump room. Flow on the pond water side will remain at full throughput.

### 2.8.3.2 Pumps

LCW will be supplied to the magnets in the enclosure with a pressure differential of 100 psid or greater. This will require pump output at 150 psid to compensate for losses along the route and equates to a dynamic head of 350 ft. Flow will be determined by the final system configuration, but is estimated at this time to be about 950 gpm. LCW pumps will be located in LBNE 5. The arrangement will be for four 50-hp pumps to be piped in parallel, with normal configuration as three pumps in operation and one offline in standby mode. It may be possible to reuse pumps from the Tevatron LCW system, although this is not included in the current scope.

### 2.8.3.3 Piping, Valves, Fittings and Hardware

Piping for LCW will be schedule 10 304/304L stainless steel, with full penetration welds. Because the total run length in the direction of the beamline will be about 750 ft, as well as runs to and from the service buildings of roughly 230 ft otherwise, thermal stresses and the need for expansion should be addressed in the design. At this time, it appears that a 5-in iron pipe size will be adequate for enclosure flows, requiring 6 in from the LBNE 5 pump room to the tunnel connection.

Piping for the pond water lines to and from the heat exchanger within the LBNE 5 pump room are to be schedule 40 carbon steel. These will have a strainer upstream of the heat exchanger (Hx) and a bypass around the strainer. In addition, building isolation valves will

be necessary. Ponds, pond water pump vaults, and piping from the pond vaults to the pump room are to be supplied by Conventional Facilities.

Individual magnet and power-supply component connections will have ball valves on both supply and return taps wherever possible. Where standard FODO cells provide magnets in a dipole-quad-dipole string, secondary manifolds such as used in the MI would be a very good consideration, and are included in the estimate. When this is not possible, such as for the bus lines feeding the dipoles, suitable valving to ensure local isolation will be implemented. At this time, all LCW connections to all magnets are planned to be hoses connections, and will be separate from the electrical connections of the bus.

Hangers and brackets will be stock, such as Unistrut or B-Line, where possible. Custom 3-in-a-row vertical brackets may make the best use of enclosure space, and have been costed for the enclosure run. All nut-bolt-washer hardware is to be 304 stainless steel. All brackets not stainless steel will have a rust-preventing finish such as paint or plating.

#### **2.8.3.4 De-ionizer / Filter Loop**

Cooling water will require filtration and deionization polishing to maintain the “low-conductivity” status. This filtration will be located in LBNE 5 and will include pre- and post-filters, as well as several 3.6-ft<sup>3</sup> bottles of mixed-bed de-ionizing (DI) resins in parallel between the filters.

This system will require a fill line to make up water using LCW supplied from the MI. This water will come into the system through the filtration loop. This system will also require a storage and expansion tank, of around 1,000 gal, that will be an ASME U-stamped coded vessel, supplied with a level indicator and a pressure-relief device. LCW is cycled by passing a small part of the pump discharge stream through the filtration loop and into the expansion tank. This flow then exits the tank as a mix and returns to the main system on the suction side of the pumps. This ensures that the LCW in the tank remains as polished as it is in the remainder of the system.

#### **2.8.3.5 Instrumentation and Control**

The pumps will require Motor Control Centers (MCCs) in the LBNE 5 pump room. Variable-frequency drives (VFDs) will be investigated for this purpose. These, and the Temperature Control Valve (TCV) power, are high-voltage devices, requiring panels similar to what is used in the MI pump rooms.

Both LCW and pond-water systems should have suitable pressure, temperature and flow-measuring instruments, and LCW will require at least two inputs for DI status. All readings

should feed to ACNET (described in Section 4.2) for remote reading and data-logging.

### 2.8.3.6 Buswork

Since buswork must be leak-tight and is similar to piping, its installation is within the scope of the LCW systems. This will include the purchase and installation of the bus that runs from the power supplies into the enclosure and to the magnets. Final connections between the bus and magnets are addressed in Section 2.6.

Where standard FODO cells provide magnets in a dipole-quad-dipole string, 1-in  $\times$  4-in rectangular bypass bus lengths such as used in the MI will be required. Existing MI designs may be sufficient. Bus discard from the magnet-building process could be used as material. Also, a location for a bus run of 370 ft in length (140 ft along the enclosure, plus 230 ft from the enclosure to the power supplies in LBNE 5) will need to be determined. This bus should be water-cooled as well, and of 2-5/8-in OD bus. In addition, all exposed bus between the power supplies in LBNE 5 and the enclosure must be contained in aluminum shielding panels such as those used in the MI Service Buildings.

### 2.8.3.7 Other Considerations

Because of the large vertical hump in the beamline trajectory, significant fluid-dynamics modeling of the entire system will need to be done, representing all the components as completely as possible, before committing to a final design.

## 2.9 Beam Instrumentation (WBS 130.02.02.05)

### 2.9.1 Introduction

The LBNE primary beamline includes instrumentation and diagnostics to characterize important beam parameters, for example, beam positions, stability, losses, intensity and transverse emittance, and to continuously monitor the operation of all the beamline elements under operating conditions, i.e., with a high-power beam. During the first commissioning and machine studies, the diagnostics systems also have to operate with a low-intensity beam (approximately  $3 \times 10^{11}$  protons per batch).

The four core instrumentation systems for the primary beamline are:

1. Beam-Position Monitors (BPM): 24 dual-plane BPMs for beam-trajectory measurement, based on button-style pickups and digital-receiver read-out electronics
2. Beam-Loss Monitors (BLM): 30 ion-chamber BLMs for local beam-loss monitoring, and four long (approx. 250-ft) total-loss monitors (TLM)
3. Beam-Intensity Monitors: two toroidal transformer-based beam-intensity monitors
4. Transverse-Beam Profile Monitors: six dual-plane secondary emission monitors (SEM) to measure the transverse beam profile (effectively a 2D intensity plot of the beam at a given location), from which the beam emittance can be derived.

BPMs and BLMs are part of an integrated machine-protection system (MPS), where a beam-based technical interlock is used to prevent damage from a mis-steered or out-of-control, high-power beam.

Possible additions (not part of the current 708-kW design) to this set of beam instruments include, for example:

- A broadband wall-current monitor for beam-timing measurements
- An imaging system to monitor the 2D beam profile at the exit window
- Non-invasive transverse beam-profile monitors, for example, IPMs or e-beam scanners, as required

## 2.9.2 Reference Design

Table 1-3 summarizes important beam parameters, to which all installed beam diagnostics must be sensitive. All read-out hardware (signal processing, data acquisition, timing, triggers, power supplies, and so on) will be located outside the enclosure and wired using low-insertion-loss, high-shielding cables for the detection elements in the tunnel. Housing these electronics systems in service buildings MI-10 and LBNE 5 along with the Target Hall Complex (LBNE 20) will minimize the cable length. Wherever feasible, components from existing NuMI instrumentation will be re-purposed for LBNE to reduce costs.

### 2.9.2.1 Beam-Position Monitors

The BPM system will be based on simple electrostatic “button-style” pickup detectors. The measurement of integration time will be a few 100 nsec, which allows for observation of beam displacements within the batch. The anticipated resolution is 25 to 30  $\mu\text{m}$  in a beam pipe

with a 3-in circular cross section. The read-out system is based on digital downconverter and signal-processing technologies very similar to the existing installations at other Fermilab accelerators, for example, the Tevatron, MI, Recycler, transport beamlines and experimental beamlines (e.g., NuMI, BNB). An automatic gain-correction system will continuously monitor and calibrate the electronics, and correct slow drifts due to temperature and aging effects of electronics components.

### 2.9.2.2 Beam-Loss Monitors

The BLM system will be very similar to the installation in the NuMI beamline. Figure 2-28 shows an ion-chamber beam-loss detector, the basic element for the 30 BLMs in the primary beamline for detecting local beam losses. These sensors will be placed on the dipole and quadrupole magnets. They offer a  $10^6$  dynamic range, and will be operated in a window between  $10^{-8}$  fractional beam loss (lower limit) and  $10^{-2}$  fractional beam loss (saturation). The current plan is to re-purpose the existing ion chambers from the NuMI beamline. A digital FPGA-based read-out system may also be considered, similar to the one in the Large Hadron Collider (LHC) at CERN.

A set of four TLMs, based on argon-filled Heliax cables, will complement the BLMs and monitor the integrated beam loss along the beamline. The readout and gas-monitoring systems for the NuMI TLMs will be re-purposed for LBNE.

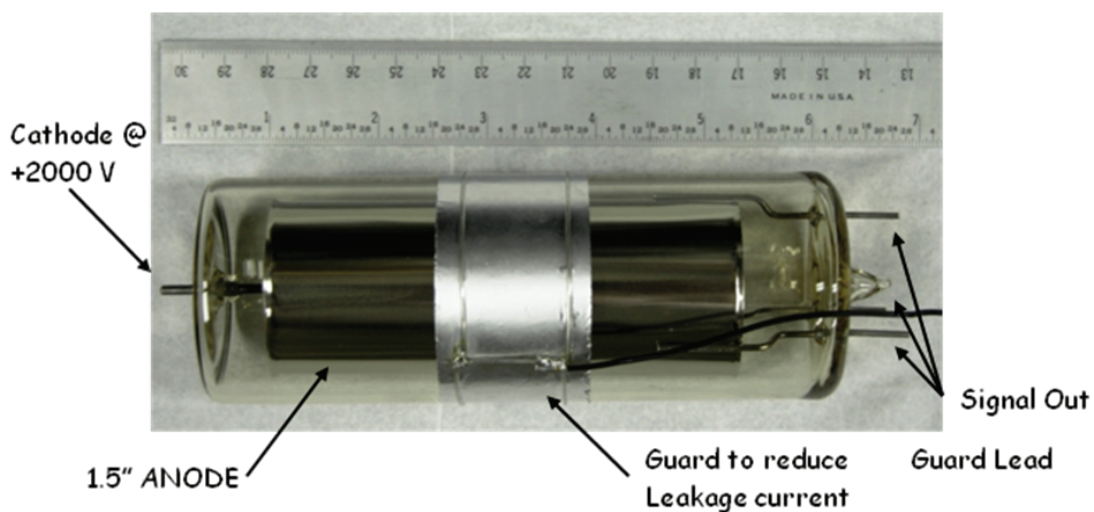


**Figure 2-28:** Ion chamber loss monitor.

**Table 2–14:** Specifications for the ion chamber loss monitor.

Materials	Glass, Nickel
Volume	110 cm <sup>3</sup> Argon gas at 1 Atm
Calibration	70 nC / rad
Response time	1-2 $\mu$ sec
Leakage current	< 10 pA
Operating range	1 mrad -100 rad

### 2.9.2.3 Beam-Intensity Monitors

Two beam-intensity monitors are needed for the primary beamline and will be based on 3.5-in Pearson toroidal transformers. Monitors used for NuMI will be re-purposed for LBNE. The analog gain and filter stages may need to be located in the enclosure and the digital signal-processing and calibration systems will be located in the service building.

### 2.9.2.4 Beam-Profile Monitors

The beam-profile monitors are based on the secondary-emission principle. Two orthogonal arrangements of 48 thin titanium wires or foils are used, spaced 0.5-1 mm apart, mounted on a fork-like ceramic carrier substrate, as shown in Figure 2–29 (left). A rotary-motion system sweeps the SEM wire or foil frame into the beam and performs a pulse-by-pulse measurement of the transverse beam profile. Figure 2–29(right) shows an estimation of the heating using thin, 5- $\mu$ m by 150- $\mu$ m titanium foils with 1-mm pitch as target for a 708-kW beam. With the inserted SEM foil, the maximum tolerable fractional beam loss is limited to  $2.5 \times 10^{-6}$ . Monitors used for NuMI will be reused in LBNE. For operation at a higher beam power, carbon filaments may need to be used as the SEM target or non-invasive monitoring techniques may be necessary.

## 2.10 Primary Vacuum (WBS 130.02.02.06)

### 2.10.1 Introduction

The primary vacuum system is intended to maintain a vacuum of better than  $1 \times 10^{-7}$  torr residual gas pressure in the beam tube in order to reduce the beam loss due to proton-gas interaction. The entire primary beamline, about 1,200-ft long from extraction at MI-10 to the pre-target enclosure, will be divided into several independently evacuated sections according to the physics requirements, installation and pump scheme. Each section of approximately 300 to 400-ft will have about 20 ion pumps to achieve and maintain this pressure level.

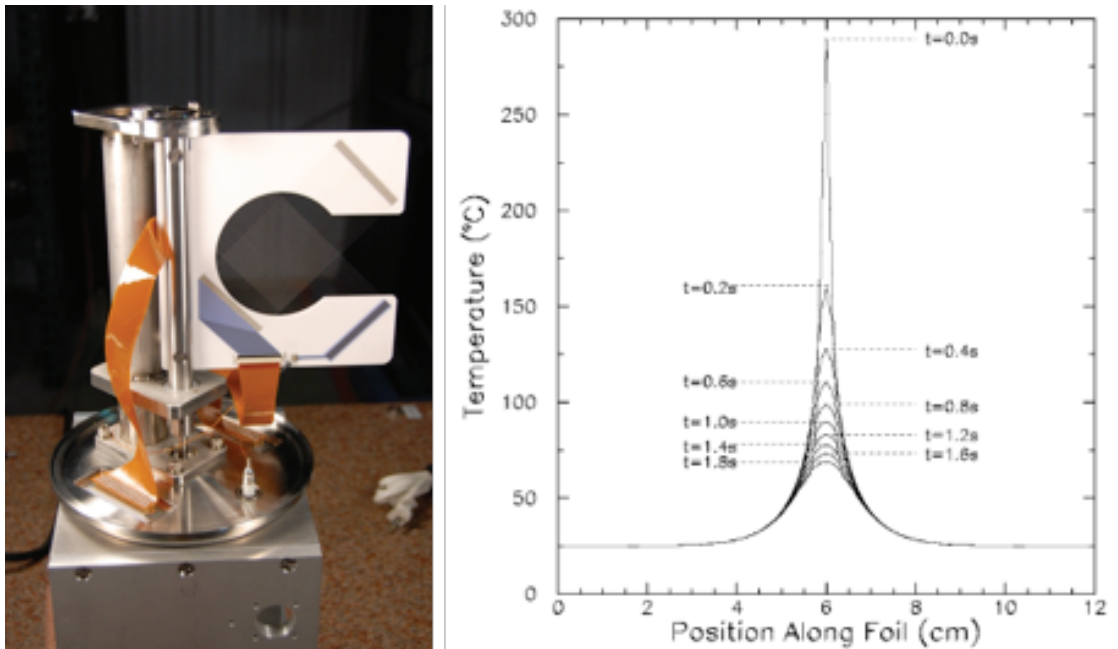


**Figure 2-29:** SEM beam profile monitor. Left: rotary mechanics with Ti multiwire frame; Right: Ti foil heating estimation for 708 kW beam power.

### 2.10.2 Design Considerations

LBNE's design is of a typical single-pass beamline. The requirement on residual gas pressure in the beam tube is not difficult to meet, however, NuMI's experience shows that a highly reliable, low-maintenance vacuum system is critical for minimizing outgassing and the potential for leaks, and thus for improving the overall operational efficiency of the beamline.

### 2.10.3 Reference Design

The system will consist of 62 45-l/s ion pumps, four section valves and eight gauges for separation and interlocking. All beamline devices exposed to vacuum will have to comply with UHV practice regarding material choices, cleaning and handling, in order to minimize outgassing and contamination. Although there is no plan to bake the entire primary beamline, prebaking may still be required for some devices. The following pumping scheme will be applied at each section: (1) pump down to  $10^{-6}$  torr solely by turbo stations at two pumping ports along the whole section, and perform a leak check with a minimum sensitivity of  $2 \times 10^{-10}$  torr l/s, (2) start all ion pumps, and (3) valve out turbo stations (i.e., close the valves and remove the temporary turbo pumps) when  $10^{-7}$  torr of average pressure is achieved.

In making the beamline-vacuum connections, as many of them as possible will be welded,

**Table 2-15:** List of major vacuum components

Ion Pumps	Section Valves	Instrumentation	Bellows	Tubes
62	4	8	80	4" dia, 550 feet
Distributed pumping, distance should be not larger than 20 ft	Interlocked gate valve, Section length is less than 300 feet.	For pumping/venting port, Pirani gauges, ion gauges, and diagnosis.	Oval, and 3", 4" round	SS 304

especially in areas where a low maintenance is required. In addition, all beam instrumentation, such as BPM, toroids, and multi-wire will use conflate flanges, as well vacuum gauges and pumps.

### 2.10.3.1 Pumps

The 62 ion pumps will be distributed along the beamline with spacing of 20 feet or less. Once a given section is evacuated to  $10^{-6}$  torr by two portable turbo carts and the section is thoroughly leak-checked, the ion pumps in that section will be turned on.

### 2.10.3.2 Beam Tubes

The shape and size of beam tubes will vary along the beamline. The vacuum interface between dipoles, dipole-quadrupoles and beam-tube sections will be welded. The interfaces related to beam-diagnosis instrumentation are a type of Conflat-copper gasket. The beam tubes that reside inside the magnets will be part of the magnet. Dipole beam tubes have an elliptical cross section of 2 in by 4.8 in, and quadrupole beam tubes have an outer diameter cross-section of 3 in. The beam tubes in other areas have an outer diameter cross-section of 4 in. Various quantities of bellows, flanges, tees, crosses, stands, vacuum-grade bolts, nuts and gaskets are also needed.

### 2.10.3.3 Valves and Gauges

Four 4-in, fast-action gate valves will be used for protection from failures, convenience of installation and maintenance. They will be interlocked with beam operation and triggered by Pirani gauges or cold cathode gauges in each segment. About 10 all-metal right-angle UHV valves will be used for pumping ports.

### 2.10.3.4 Instrumentation and Control

Three standard 8-ft racks for the controllers of ion pumps, gauges and valves, will be located in a designated service building, and their outputs will be logged via ACNET. All the ion pumps, gauges and valves will be remotely controlled. Also needed are leak detectors, residual gas analyzers, and local controllers of ion pumps, gauges and valves for diagnosis and maintenance.

### 2.10.3.5 Baking and Cleaning

In-situ vacuum baking for the whole beamline is not required, but pre-baking some components may be necessary, especially for beam-instrumentation components. All components must go through UHV cleaning procedures before installation. Equipment includes heat tapes, temperature controllers, thermal couples, VariAC transformers, thermal insulating blankets, sheets, foils, UHV gloves, lint-free wipers, cleaning fluids, etc.

## 2.11 Beam-Loss Calculations (WBS 130.02.02.08)

### 2.11.1 Introduction

This section provides an overview and important examples for simulations that give information about the mechanisms and results of an improperly controlled primary beam. The high-intensity beam needs to be modeled and understood to a very high precision to ensure that beamline components are kept to low activation levels and to be confident that accidental losses are rare and not damaging. The model is as complete as possible, from extraction through the Target Hall, where beam particles (protons) and their interactions are tracked individually and in full detail. Simulated magnets are controlled in groups appropriate to the designed power-supply bus configuration. Errors in magnetic fields for individual magnets can be inserted as random manufacturing errors and as simulated current fluctuations from power-supply errors. Beam loss studies provide one key input in the requirements for the magnet power-supply stabilities.

In addition to providing validation of operational beam-loss control for environmental and component protection, the simulations can provide a level of confirmation for the design of the beam-interlock systems (Section 4.3).

Additional studies are needed to determine criteria appropriate for LBNE enclosure and building construction, as well as equipment installation during the MI operation.

Calculations that provide distributions of losses along the primary beamline are obtained with STRUCT code [14]. The STRUCT output goes into calculations, done by MARS [15], of energy deposition and groundwater and component activation.

### 2.11.2 Design Considerations

The main design criteria for the primary beamline are (1) the transmission of high-intensity beam with minimum losses, (2) precision of targeting and (3) minimization of component activation. Mitigation of groundwater activation is relatively straightforward for the above-grade beam, however protection from prompt radiation, such as muon plumes, requires mitigation.

Serious consideration must also be given to accidental beam losses that, within just a few beam pulses, can cause beamline-component damage. Significant sources of beam-position instability on the target as well as increased beam loss along the beam line include the power supplies for the extraction kicker, and the quadrupoles and dipole magnets. Variations in the element strength that occur over a period of minutes or hours can be corrected. However, for variations on shorter time scales, such as pulse-to-pulse jitter, the specification on beam instability would have to be met directly at the power supply.

### 2.11.3 Reference Design

The proton beam extracted from the MI-10 straight section is transported 329 m to the LBNE target located 11.4 m above the MI elevation. The design is based on a 708 kW beam with intensity of  $4.9 \times 10^{13}$  for a 1.33-second MI cycle. The design must be compatible with an upgraded capability of 2.3 MW beam power with intensity of  $1.6 \times 10^{14}$  per cycle.

The worst-case conditions are simulated using a  $3\sigma$  emittance of  $30\pi$  mm-mrad for the beam core, with halo cut-off at  $360\pi$  mm-mrad or  $10.4\sigma$ , and momentum spread ( $1\sigma$ ) of  $dp/p = 0.0004$  with cut-off at  $dp/p = 0.0028$ . In the simulations, 1% of the beam in halo is distributed with horizontal and vertical amplitudes in a range from  $A_{min} = 3\sigma$  to  $A_{max} = 10.4\sigma$  as  $F=1/A_{x,y}$ . The beam intensity is assumed to be  $1.6 \times 10^{14}$  per 1.33-s MI cycle (2.3 MW case), that is a factor of six higher compared to the NuMI design. The effects of magnet power-supply instabilities to beam distributions at the target and baffle, discussed in Chapter 3 are calculated for nominal emittance of  $30\pi$  mm-mrad.

The beamline aperture half-sizes used in simulations are presented in Table 2-16.

**Table 2-16:** Aperture half-size of primary beam line elements used in simulations

Element	L (m)	Hor. (mm)	Vert. (mm)	Aperture
LAM10	2.80	32.0	25.4	rectangular
Q102 quadrupole	2.1336	63.0	29.0	special
beam line quads (3Q120)	3.048	36.6	36.6	round
beam line quads (3Q60)	1.524	36.6	36.6	round
V100 (vertical dipole)	3.3528	51.6	21.7	rectangular
MI dipole (IDA/IDB)	6.09981	60.0	23.5	elliptical
MI dipole (IDC/IDD)	4.06654	60.0	23.5	elliptical
H-corrector	0.3048	60.0	23.5	elliptical
V-corrector	0.3048	36.6	36.6	round
Long drift sections	-	36.6	36.6	round
Baffle	2.50	7.5	7.5	round
Horn 1 entrance	-	12.0	12.0	round
Target (round target)	0.966	7.5	7.5	round
Horn 1 exit (conical, 10mr, round)	2.00	23.0	23.0	10mr, conical
drift Horn 1 to Horn 2	3.20	50.0	50.0	round
Horn 2	3.00	39.0	39.0	round

### 2.11.3.1 Primary-Beam Loss

Beam distributions representing a sum of 100 distributions have been produced for independent random values of magnet strengths in the beamline. The calculations are done assuming a common power supply for several magnets, with instabilities as follows: LBNE quadrupole,  $dG/G = \pm 0.001$ ; extraction kicker,  $dB/B = \pm 0.005$ ; Lambertson magnet,  $dB/B = \pm 0.002$ ; MI quadrupoles,  $dG/G = \pm 0.001$ ; and MI closed orbit,  $dA = \pm 1\sigma_{x,y}$  or  $\pm 1.3$  mm. Figure 2-30 shows the calculated horizontal and vertical  $3\sigma$  beam distributions at the baffle entrance as a function of dipole and quadrupole power-supply instability. The effect of quadrupole strength instability to the resulting beam size is much less significant than that for the dipole magnets.

The halo particle-loss distributions along the beamline as a function of dipole and quadrupole strength instability with (1) an individual power supply for each magnet and with (2) a common power supply for several magnets are shown in Figure 2-31. The resulting distribution is a sum of 100 distributions for independent random values of magnet strengths in the line. The  $360\pi$  mm-mrad amplitude corresponds to  $10.4\sigma = 13.2$  mm at the baffle. For an aperture radius of 7.5 mm, the baffle intercepts  $\sim 15$  kW of power from beam halo.

Figure 2-32 shows a  $3\sigma$  beam population and distributions at the baffle (left), and at the Far Detector located 1,300 km distant from the target (right) for a dipole power-supply instability of  $dB/B = \pm 0.0001$ ,  $\pm 0.0003$ ,  $\pm 0.001$  and  $\pm 0.002$ . Calculations are done for assuming

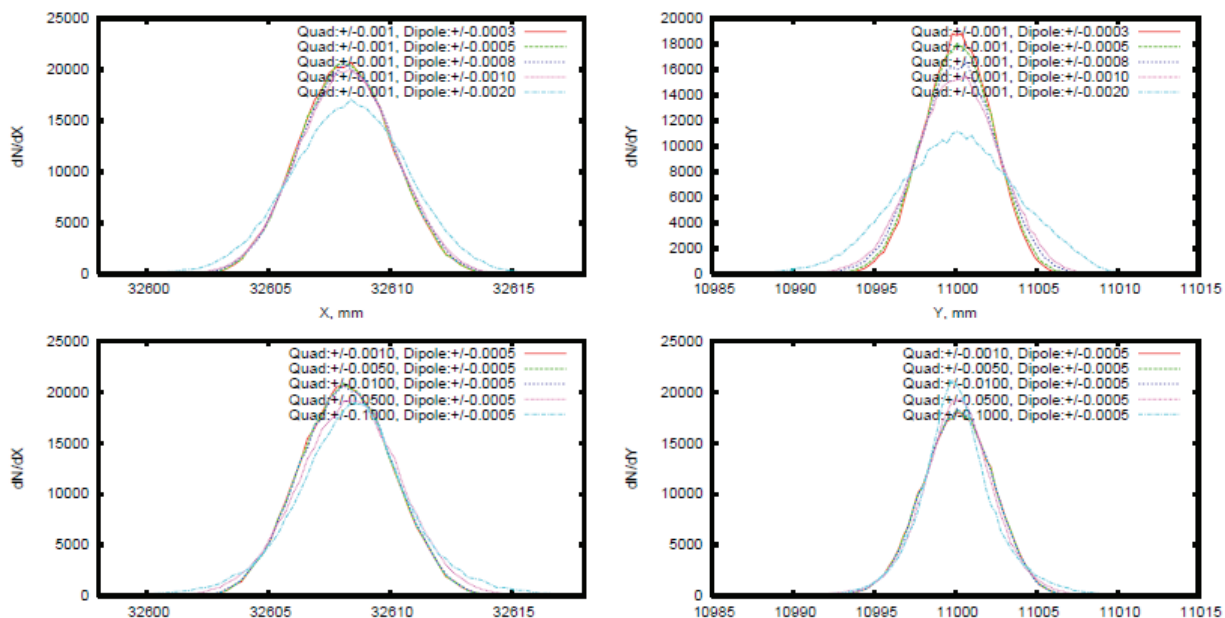


**Figure 2-30:** Horizontal (left) and vertical (right) beam distributions at baffle entrance as a function of dipole (top) and quadrupole (bottom) power supply instability.

a common power supply for several magnets with instabilities as follows: LBNE quadrupole,  $dG/G = \pm 0.001$ ; extraction kicker,  $dB/B = \pm 0.005$ ; Lambertson magnet,  $dB/B = \pm 0.002$ ; MI quadrupoles,  $dG/G = \pm 0.001$ ; and MI closed-orbit,  $dA = \pm 1\sigma_{x,y}$  or  $dA_m = \pm 1.3$  mm. It is assumed in these calculations that there is no proton-beam interaction with matter in the target and in the ground downstream of it. Beam distributions are shown for 100 independent, random distributions of magnet strength deviations. The beam spot size is  $\sigma_{x,y} > 30$  m in the far detector at  $dB/B = \pm 0.0004$ .

The halo and core beam losses along the primary beamline and at the baffle as a function of dipole magnet power-supply instability with a common power supply for several magnets are presented in Figure 2-33. NuMI operates now at 0.4 MW with maximum allowed fractional beam loss of  $10^{-5}$  from the total intensity. For LBNE's 0.7 MW, the safety level will be  $5 \times 10^{-6}$ , and for 2.3 MW it will be  $1.5 \times 10^{-6}$ . To have a viable operational margin, the goal is to keep normal beam loss an order of magnitude better than this, or  $5 \times 10^{-7}$  for 0.7 MW and  $1.5 \times 10^{-7}$  for 2.3 MW, that is  $\sim 0.4$  W. From this point of view, the dipole instability should be less than  $dB/B < \pm 0.0025$ , which keeps losses below 1 W/m.

### 2.11.3.2 Accidental Total Beam Loss

An accidental total beam loss will likely cause component heating and damage, may induce groundwater activation and cause radiation concerns outside the tunnel. The lost-beam trajectories along the beamline due to an accidental degradation of bending-magnet strength

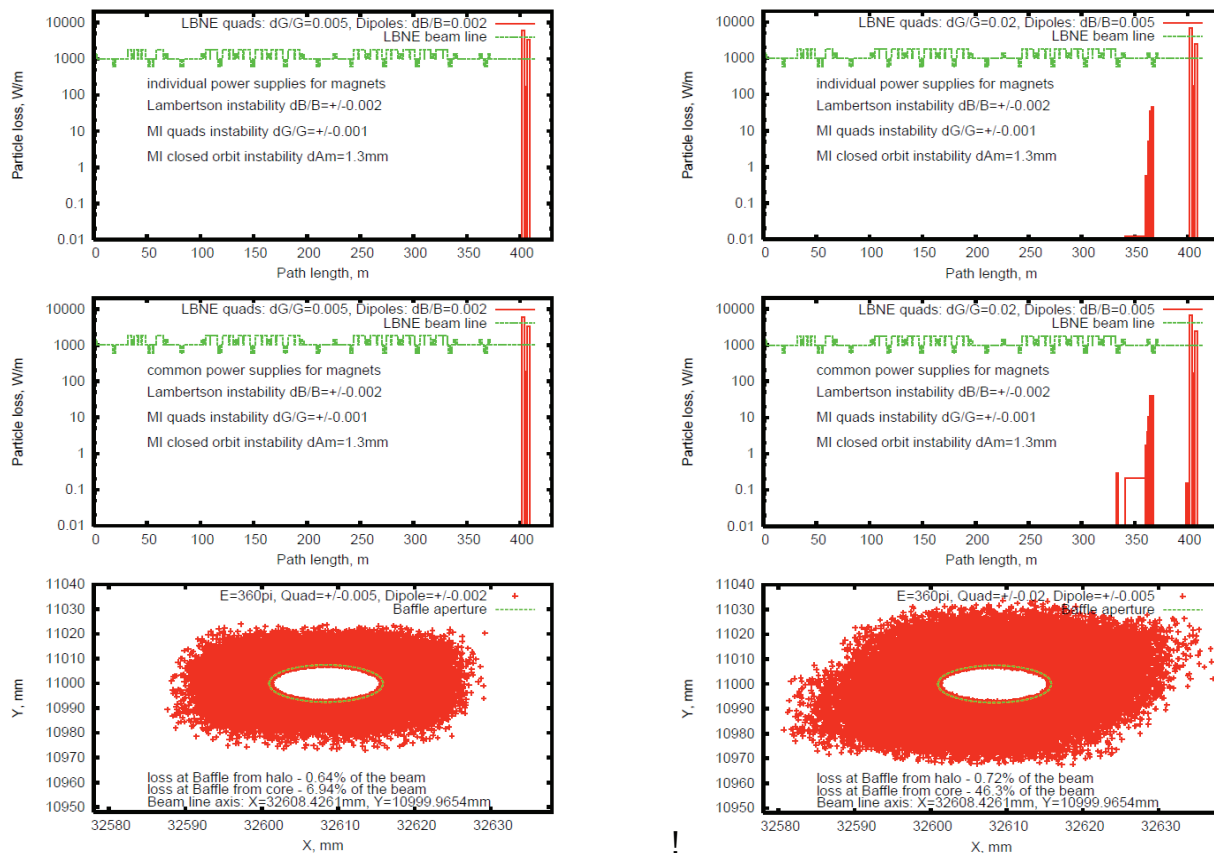


**Figure 2-31:** The halo particle loss distribution along the LBNE beamline at dipole strength instability of  $dB/B=\pm 0.002$  (left),  $dB/B=\pm 0.005$  (right) and quadrupole strength of  $dG/G=\pm 0.005$  with individual power supply for each magnet (top) and with common power supply for several magnets (second line). Beam loss population at the baffle is shown on the bottom.

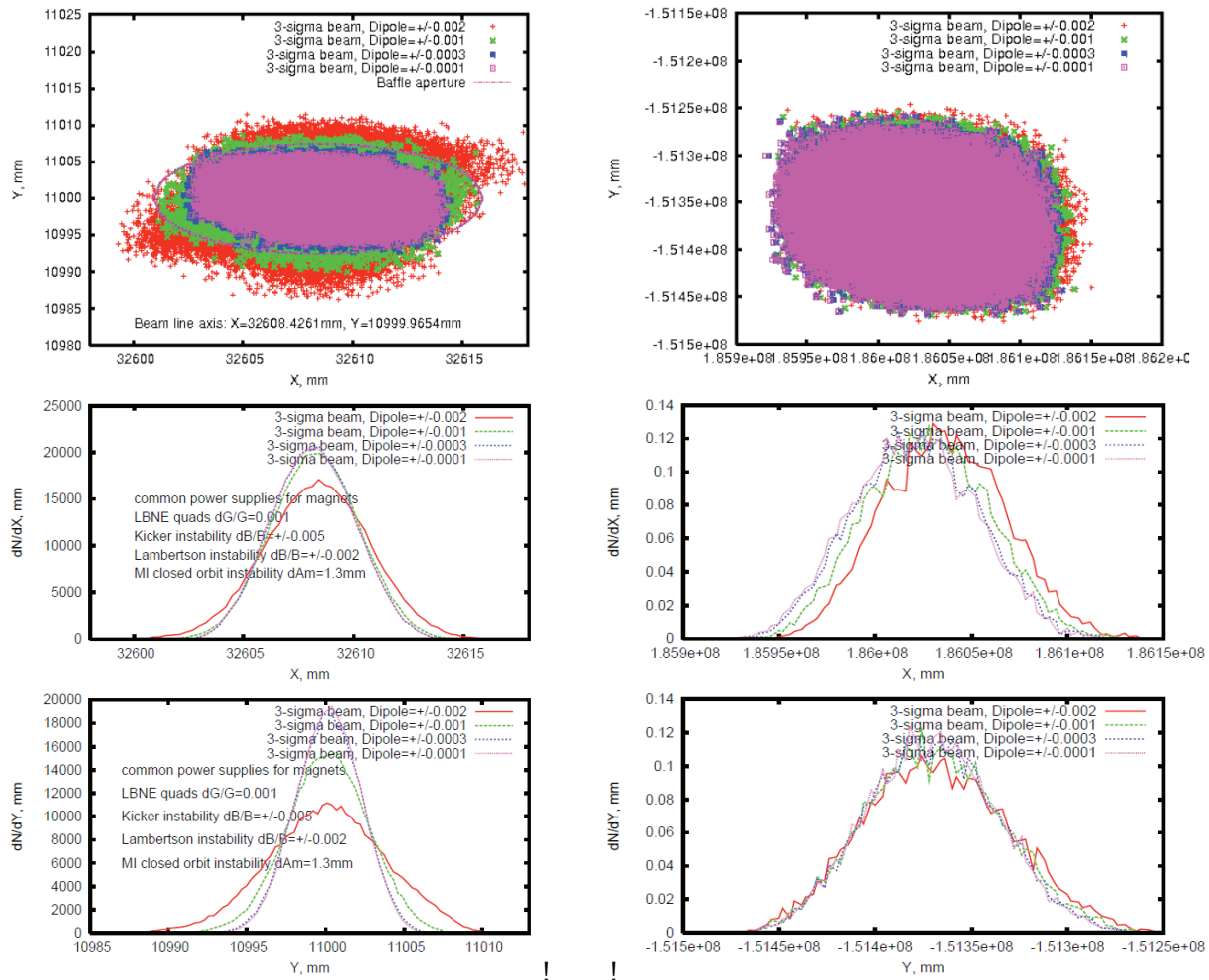


**Figure 2-32:** The  $3\sigma$  core beam population (top) and distributions (middle and bottom) at the Baffle (left), and at the far detector (right).

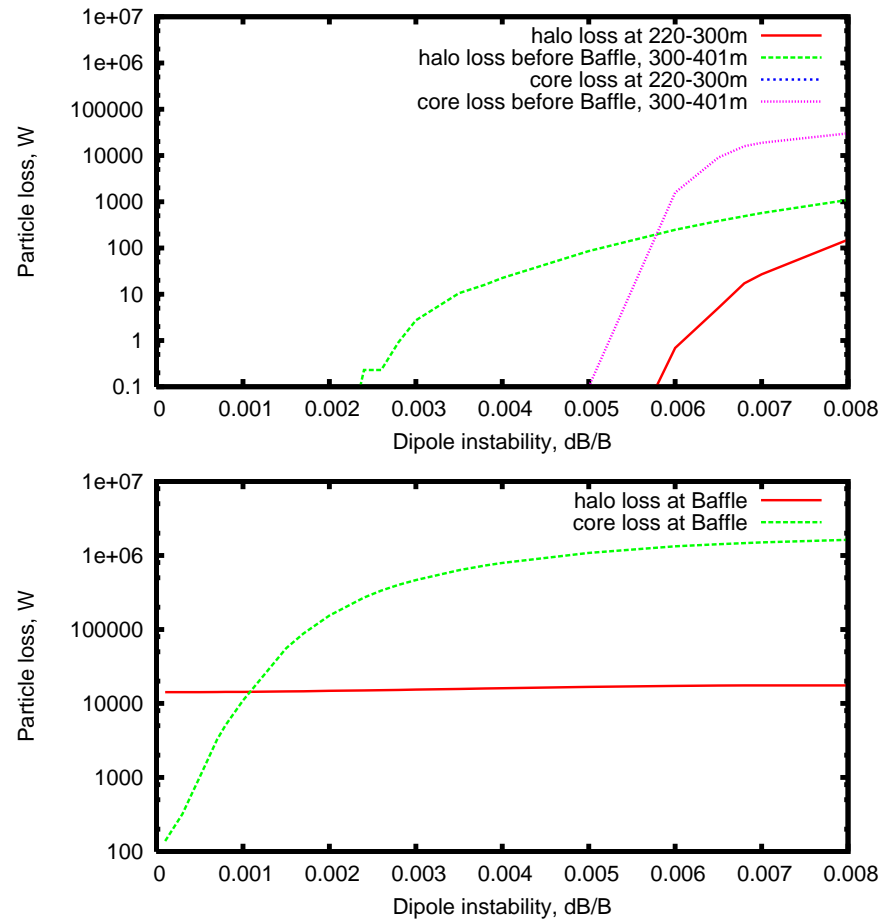


**Figure 2-33:** The halo and core beam loss at 120 GeV along the LBNE primary beam line (top) and at the Baffle (bottom) as a function of dipole magnet power supply instability, with common power supply for several dipoles.

have been calculated and are shown in Figure 2-34.

The instantaneous temperature rise in a dipole-magnet beam pipe (Figure 2-35), following the loss of the entire beam (2.3 MW), is  $\sim 2500$  K, which is a factor of two higher than the melting point of stainless steel. The beam vacuum pipe or a magnet would be effectively destroyed in one beam pulse (or a few pulses at 708 kW). This possibility must be eliminated by analyzing all parameters of the system just before extraction, and then abort the beam to the MI beam dump if any critical parameter is out of the safety region (for details of the LBNE beam-permit system see Section 4.2).

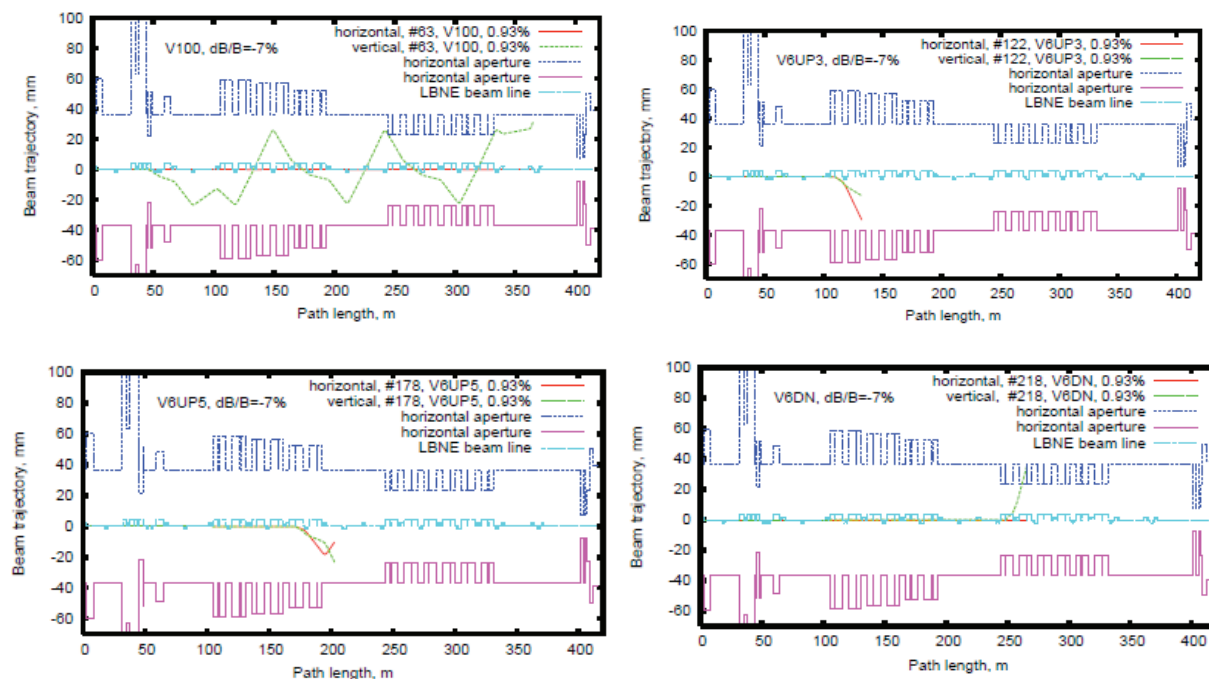


**Figure 2-34:** An example of beam trajectories along the beamline for a beam lost due to accidental degradation of bending magnet strength

### 2.11.3.3 Activation of Components

Beamline-component activation is a critical issue in a high-intensity beamline whose operational life is measured in decades. A sample case is presented here, where 0.3% of a 2.3 MW beam is lost continuously, as the outer-most part of the beam envelope interacts with the vacuum pipe, magnets and other installed components. The magnitude of this loss is chosen to be typical of what one might have anticipated in lower-intensity beamlines of the past. Of course for LBNE, this value is unacceptably high, but results from this study can be scaled to estimate tolerable losses. Residual dose rates for losses of 0.003 of total intensity

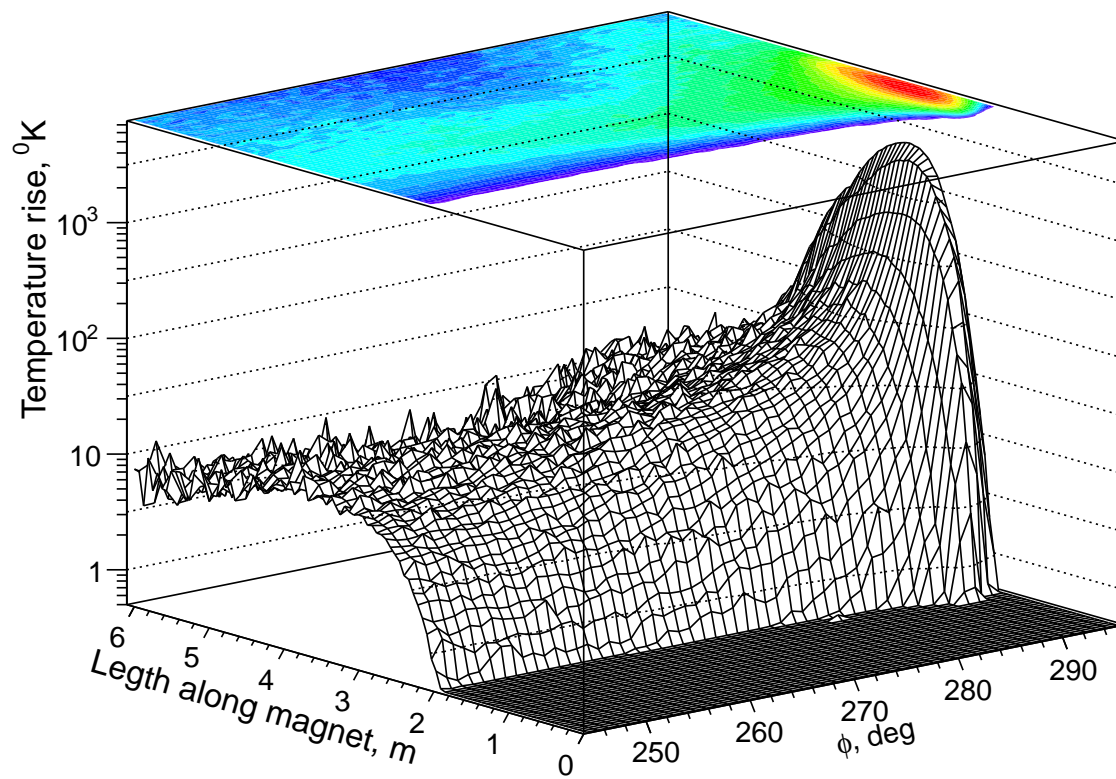


**Figure 2-35:** An instantaneous temperature rise along and across the dipole magnet beam pipe at accidental loss of entire beam.

for 30 days, followed by one day cool-down, is shown in Figure 2-36. Residual dose rates on the surfaces of bending and quadrupole magnets reach 50 rem/hr, which is three orders of magnitude higher than the goal of less than 50 mrem/hr. Scaling these results to acceptable limits implies that losses need to be no greater than order  $10^{-6}$ . The methods proposed to achieve this are listed in Section 2.3.4.

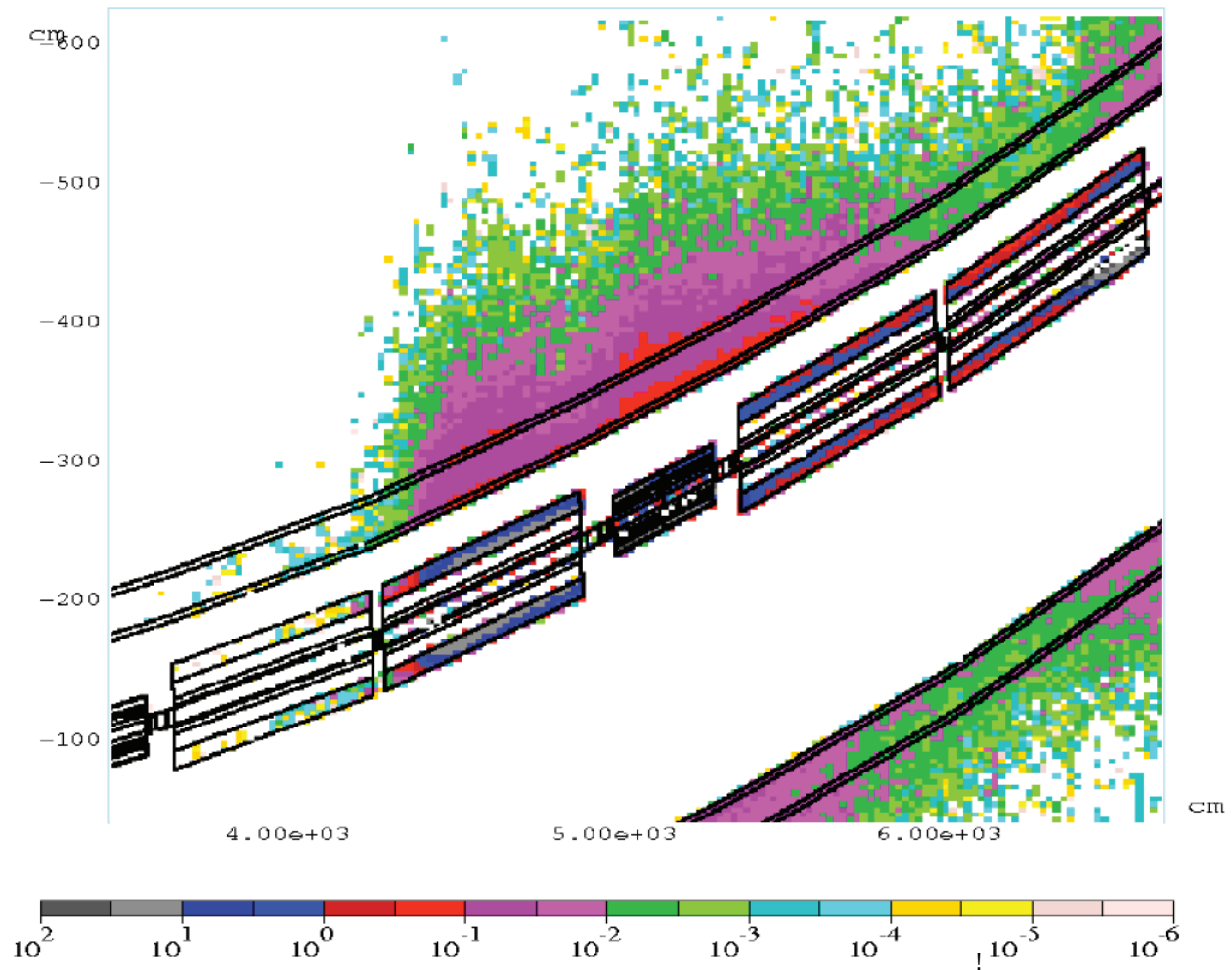


**Figure 2-36:** Residual dose rates along the beam line and magnets following a loss of 0.3% of the beam for 30 days followed by one day cool-down. The color-coded logarithmic scale has units of m-Sv/h (1 m-Sv/h is equivalent to 100 mrem/h)

## 3 Neutrino Beam (WBS 130.02.03)

### 3.1 Introduction

This chapter discusses the conceptual design of the second main system within the LBNE Beamline, the Neutrino Beamline, which refers to the set of components and enclosures designed to efficiently convert the initial proton beam into a high-intensity neutrino beam aimed at the far detector, 1,300 km away.

The LBNE neutrino beam would be the fourth large neutrino beam facility designed and built at Fermilab. Its design is very similar to the NuMI beam constructed in 2004 [16]. All major elements of the LBNE design have their analogs in the NuMI beamline. Thus, the experience gained in constructing and operating the current facility can be incorporated into LBNE design as improvements. The LBNE neutrino beam must necessarily be of even more robust design since the initial beam power is expected to be increased threefold after some years of operation at 708kW. For most elements, the increased capacity will be met by incremental improvements and replacement strategies.

A proton-beam pulse from the primary-beam system enters the neutrino beamline system (from the left in Figures 3-1 and 3-2) through a beryllium “window.” This window seals off the evacuated beam pipe of the primary beamline, and the protons enter the air-filled target chase (the volume surrounding the target and focusing mechanisms). Initially they pass through a small aperture in a 1.5-m-long graphite cylinder, called a baffle, which protects equipment downstream from mis-steered beam. A meter and a half past the end of the baffle, they reach the target, a long, thin graphite cylinder in which about 85% of the protons interact and produce secondary particles. The target is surrounded by the first horn, a magnetized structure which provides initial focusing for the secondary particles, predominantly pions and kaons. A second horn, a few feet downstream, provides additional focusing for the secondary particles before they enter the decay pipe, where a large fraction of the pions will decay to neutrinos, forming the neutrino beam. The final portion of the neutrino beamline is the absorber, downstream of the decay pipe. The absorber is intended to stop the protons that failed to interact in the target and the secondary particles that failed to decay to neutrinos; it must be designed to sustain the beam energy deposition

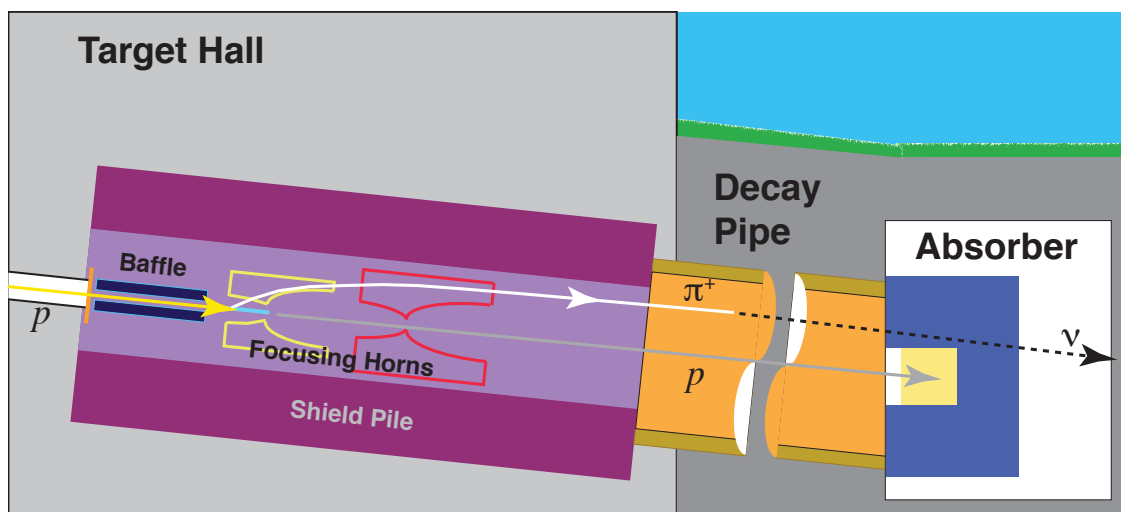


**Figure 3-1:** A cartoon of the neutrino beamline showing the major components of the neutrino beam. From left to right, the beam window, horn-protection baffle, target, the two toroidal focusing horns, decay pipe and absorber. The air volume surrounding the components between the window and the decay pipe is called the target “chase”. The target chase and rooms for ancillary equipment (power supplies, cooling, air recirculation and so on) is included in the area called the target complex (not pictured).

under expected normal operational conditions as well as under accident situations.

Section 1.2.3 presents a more thorough introduction to the Neutrino Beamline.

### 3.1.1 Design Considerations

Primary design considerations include the need to provide a wide-band beam to cover the first and second neutrino-oscillation maxima and the need to plan for an eventual upgrade in incident primary beam power from 708 kW to 2.3 MW without retrofitting. The designs for the neutrino beam components detailed in this Chapter are appropriate only for a primary beam energy of 120 GeV.

To avoid both technical and cost/schedule problems in the future, the potential beam-power upgrade has design implications for several subsystems, including: the baffle and window-replacement infrastructure, the two-horn system, the dimensions of the target pile, decay pipe and absorber as well as the cooling systems for the target chase, decay and absorber.

Radiological concerns, such as prompt dose, residual dose, air activation and tritium production are also important considerations. They have been extensively modeled, and these issues have been addressed in the system design.

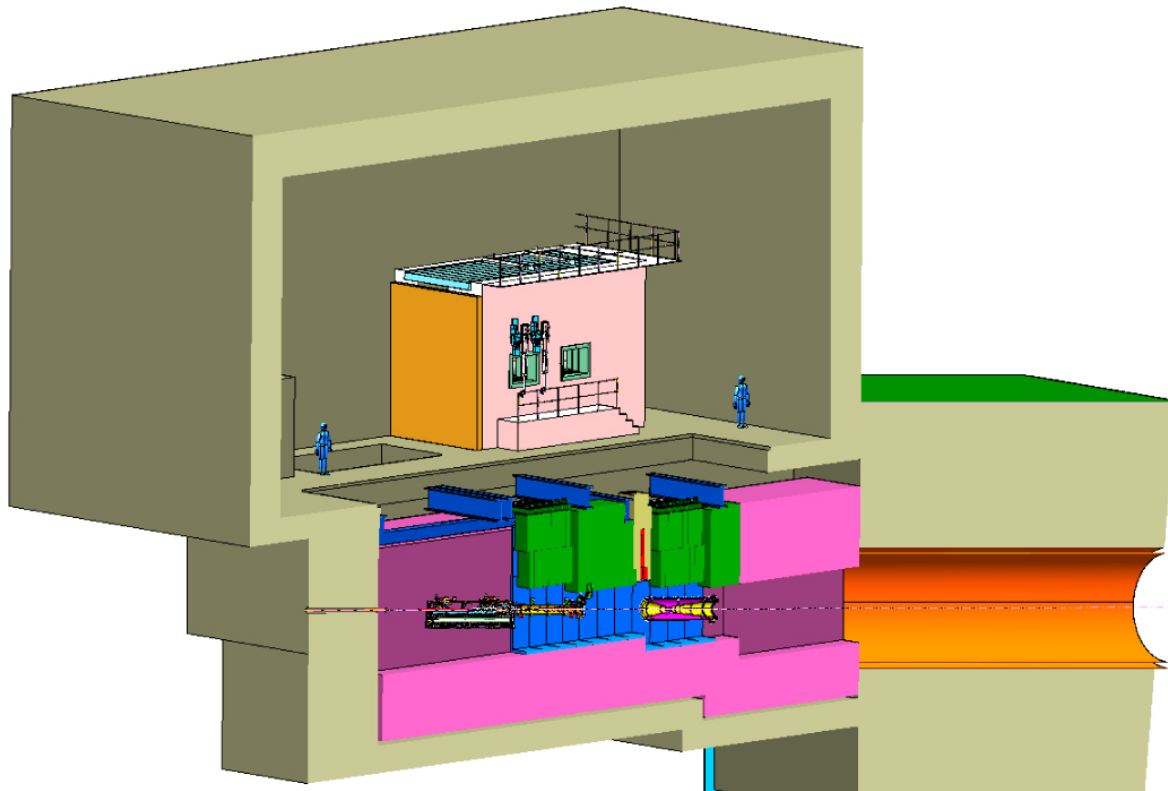


**Figure 3–2:** A cut view of an engineering model of part of the target complex, showing the relationship of the components depicted in Figure 3–1 to scale. The target chase shielding is shown by purple and green zones, the chase cooling panels are blue. The top of the chase shielding is removed. Above, and to the beam-left of the chase is the work cell. The start of the decay region is shown at the right. The absorber is not represented here.

## 3.2 Primary Beam Window and Baffle (WBS 130.02.03.02)

### 3.2.1 Introduction

The upstream beamline enclosures are separated from the target chase by a 3.9-m-thick concrete shielding wall to isolate the upstream (evacuated) beamline from high radiation dose rates. The primary protons enter the target chase through a window in the wall; it is a beryllium hemisphere that seals the evacuated primary beampipe.

The baffle, just downstream from the window, is a passive device that works essentially as a collimator. It is a graphite structure intended to prevent any mis-steered beam pulse from causing damage. In particular, it protects the inner conductors of the horns from the primary beam directly striking the aluminum. The baffle design depends on the geometry of the parts it protects as well as beam size, so the reference baffle design follows from the beam, horn and target specifications.

### 3.2.2 Design Considerations

An important consideration is allowing for replacement of the primary beam pipe and the mating flange to the window in the event of damage to the latter. A primary beampipe cartridge design with an embedded liner within the concrete shielding wall will allow this, with a primary beampipe pressure of  $1 \times 10^{-8}$  Torr.

A second important consideration is the potential beam-energy upgrade from the initial 708 kW to 2.3 MW. First, this affects the window design since the spot size for the 708 kW beam energy design, 1.3 mm (*rms*), similar to the NOvA design [17], may increase by a factor of two for a 2.3 MW beam. The aperture will be scaled by a factor of two, as a conservative estimate. The window housing and mating primary-beampipe aperture also require a larger size. Secondly, the window itself will need to be interchangeable. Experience from NuMI shows that the primary-beam window has an estimated lifetime limit of three years at 708 kW. The 708-kW primary-beam window design validated by NOvA considers an air cooled, 0.25-mm-thick, 25.4-mm-diameter beryllium grade PF-60 membrane.

Thirdly, the window itself (also referred to as the beryllium membrane) may require active cooling at the 2.3-MW value.

In either beam-energy case, the construction tolerance is 0.2 mm (*rms*); the goal for overall baffle position accuracy is 0.5 mm, including thermal effects, survey tolerance, and carrier instability. The construction and alignment tolerance of the hole through the baffle must be 0.5 mm or better [18].

In general, each baffle design must withstand two thermal conditions induced by the proton beam: normal operation under  $\sim 2\%$  continuous beam loss (DC) and a one-pulse accidental event. To accommodate both these conditions, the 708-kW baffle design relies on heat transfer to the existing airflow through 18-pin radiator sections clamped along the baffle's length. In addition, conductive filler will be used to bridge the thermal-resistance gap between each radiator pin section surface and the 61-mm-diameter aluminum tube outer surface. These thermal conditions increase for both normal operation and one-pulse accidental event going from 708 kW to 2.3 MW, as well, and the conductive filler may require further investigation. The baffle's lifetime is not a concern since it will be changed out with the target (and target carrier) during 708-kW beam operation.

Early detection of a beam mis-steering event and beam termination through the upstream Beam Position Monitor (BPM), described in Section 2.9.2.1, and baffle thermocouple instrumentation, described in Section 3.2.3, limit the amount of errant pulses received. Both the window and baffle will need to be replaced for 2.3 MW beam operation.

### 3.2.3 Reference Design

The embedded 273-mm O.D., 6.4-mm-thick, stainless-steel stepped liner pipe implemented during the civil construction is shown in Figure 3-3(a). The primary beam pipe cartridge consists of an internal 76-mm O.D., 1.5-mm-thick beam pipe suspended within an outer 260 mm O.D. stepped pipe housing, both constructed from stainless steel as shown in Figure 3-3(b). Spider collars at each end provide adjustment between the cartridge housing and internal beam pipe. These collars will lock following pre-alignment and the annular void between cartridge inner housing and outer beam pipe surfaces is filled with epoxy to prevent US radiation back-scatter. Silver plating the exterior cartridge surface and implementing a 550-mm O.D., 25-mm-thick, stainless-steel cartridge extraction flange eases removal. This extraction flange also provides indexing of the cartridge to establish longitudinal position and fixed rotation.

Alignment of the primary beam pipe is a multi-stepped process. First, the embedded liner is fiducialized and mapped from the US beamline enclosure prior to beamline commissioning. Remote pre-alignment of the cartridge is necessary relative to the mapped liner. Then, after securing the primary beam pipe position within the cartridge (locking end collars and filling void with epoxy), a cart and cable system transports the assembly to the US beamline enclosure for installation. Insertion of the cartridge involves a combination of support from the cart and overhead rigging operation while moving axially.

Initial alignment of the beam pipe cartridge and attached window is obtained by using a DS docking feature shown in Figure 3-4 and attachment at the US extraction flange. This support-alignment system provides repeatable positional alignment within a final alignment resolution of  $\pm 0.5$  mm. There is a provision for the insertion of an US and DS aperture

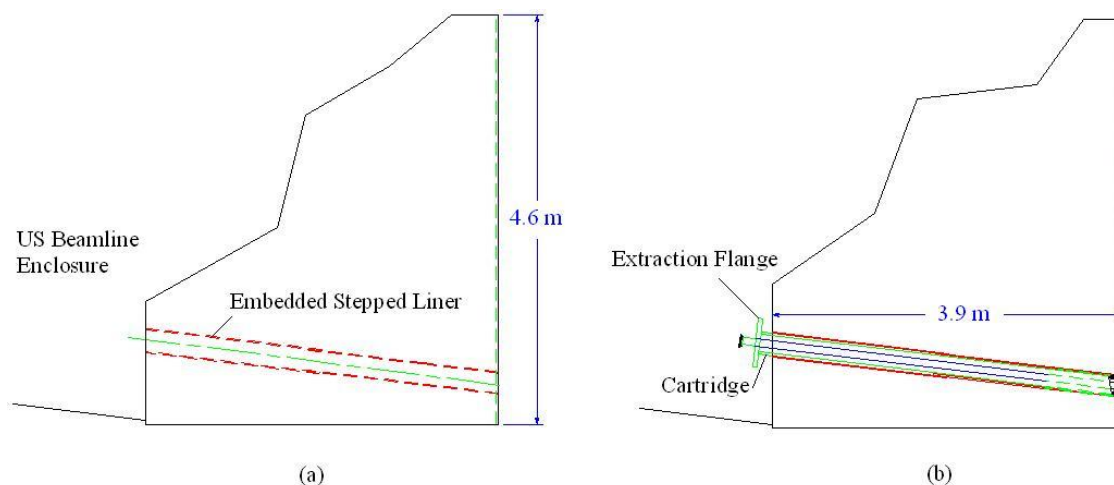


**Figure 3-3:** Shielding wall with embedded stepped liner. (b): After cartridge insertion.

shielding plug used for protection during primary beam pipe cartridge replacement. These aperture shielding plugs would be constructed from steel and moved into the US beamline and target chase only during periods of cartridge replacement. DS remote handling of the aperture shielding plug within the target chase is possible through a rail/cable system, which attaches to an embedded stainless-steel plate within the concrete wall at the target chase US face.

The 708-kW primary beam beryllium thin window design is able to withstand the stress waves and also pressure and thermal loading given a 1.3-mm spot size while periphery air-cooled. At 2.3-MW beam energy, a 50-mm diameter partial hemispherical beryllium window with a 3.5-mm spot size and natural convective cooling also is sufficient. A 1.3-mm spot size at 2.3 MW is not acceptable since the combined maximum shock stress, transient stress and transient temperature induced within the window are above the ultimate tensile stress for beryllium. Optimization of a periphery air-cooled, hemispherical tapered beryllium window shape with a thin center and gradually thicker outer crown which allows greater conduction could be applied with further investigation [19].

A conceptual section view of a 50-mm diameter, 0.2-mm-thick, partial-hemispherical beryllium window whose periphery is water-cooled given the 2.3-MW (1.5 to 3.0 mm spot size) case, is shown in Figure 3-5. The primary beam window design is constructed from a 117.5 mm O.D., 19.1 mm thick 316 stainless-steel Conflat flange. This flange is a bolted connection which attaches to the primary beam pipe mating Conflat flange with a knife edge seal. The window construction and knife edge seal must maintain a leak rate of  $10^{-9}$  Pa-m<sup>3</sup>/s or less required to achieve primary beam pipe design pressure.

The baffle is a passive device, essentially a collimator, which protects the inner conductors of the horns from the primary beam directly striking the aluminum. A critical aspect is determining the size and position of the aperture with respect to the target and horns. The

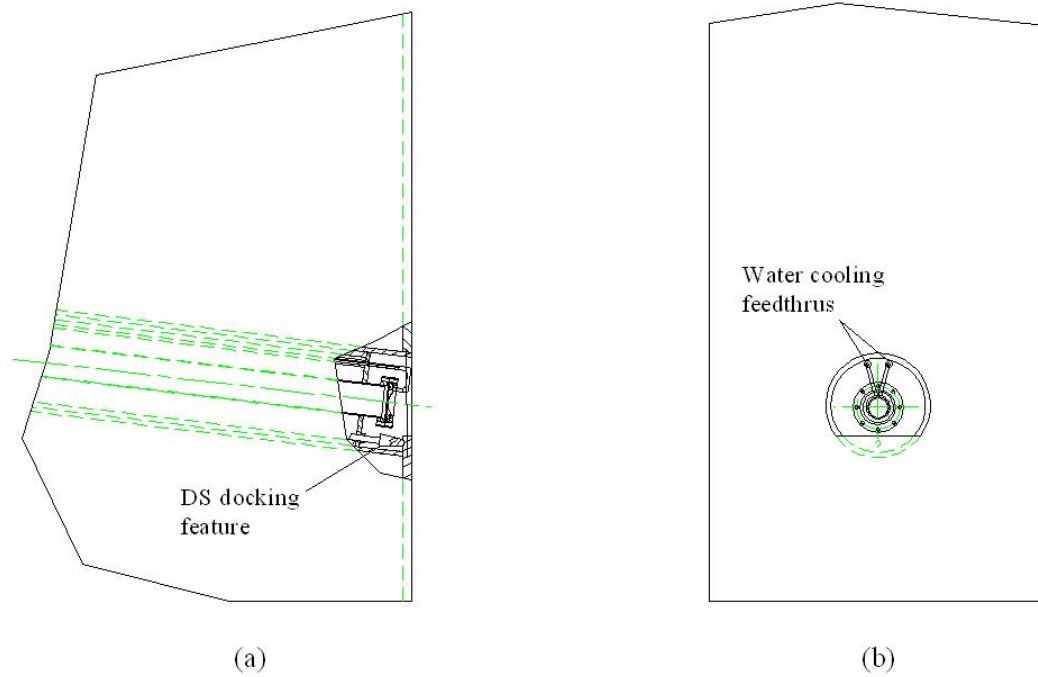


**Figure 3-4:** Section view of replacement window assembly. (b): End view of window assembly.

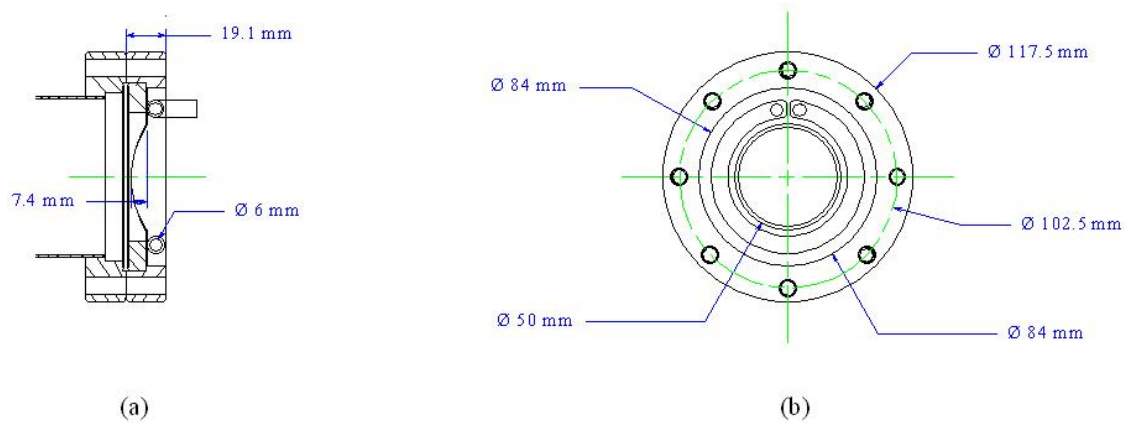


**Figure 3-5:** Section view of 2.3-MW-capable beryllium window. (b): End view of window assembly.

baffle design depends on the geometry of the parts it protects, so the reference baffle design follows from the horn and target specifications.

The 708 kW baffle baseline design consists of ten 57 mm O.D.  $\times$  13 mm I.D.  $\times$  150 mm long graphite R7650 grade cores which are enclosed by a 61 mm  $\times$  3 mm thick  $\times$  150 cm long aluminum tube after annealing. Eighteen 66-mm long radiator pin sections are evenly placed along its length at 11.5 mm intervals with a provision for two 33.4 mm openings supporting the baffle  $\sim$ 22% of the length from each end as shown in Figure 3-6.

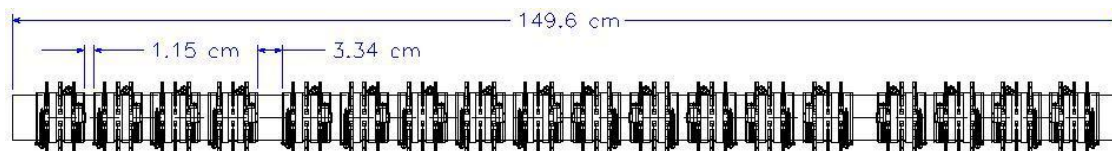


**Figure 3-6:** 708 kW (NOvA) baffle baseline design for LBNE

Performing horizontal and vertical beam scans across the baffle and using the hadron monitor for primary instrumentation will provide an accurate check on the baffle centroid position with respect to the beam axis. However, this technique has limited sensitivity to the baffle angle. We will mount the target and baffle together as a rigid unit, so that scanning the target and aligning it on the beam center assures that the baffle angle (and target angle) will be set correctly as well. (Such a scheme was used for the NuMI target). The beam should be able to scan to at least  $\pm 12$  mm at low intensity. At NuMI, these scans are done with  $8 \times 10^{11}$  protons per pulse, which is 2% of full intensity; a similar intensity should also work for LBNE beam scans.

### 3.2.4 Target/Baffle Module

A “module” refers to the heavy shielding module that supports beam components below it. The module has motor drives to provide vertical and transverse horizontal motion for precise alignment of the component/carrier below it. Modules are described in section 3.4.3. (The target/baffle module design is basically the same as a horn module, except it does not need the stripline block). The module is expected to last the life of the facility, and its shielding thickness is designed for 2.3 MW operation.

### 3.2.5 Target/Baffle Carrier

The target and baffle are mounted on a carrier that hangs off of shafts extending through the module. The carrier supplies motion of the target along the beam direction that allows (i) insertion of the target into the horn for standard running and (ii) the flexibility to move the target up to 2.5 m upstream of its standard location for special runs. The baffle is mounted

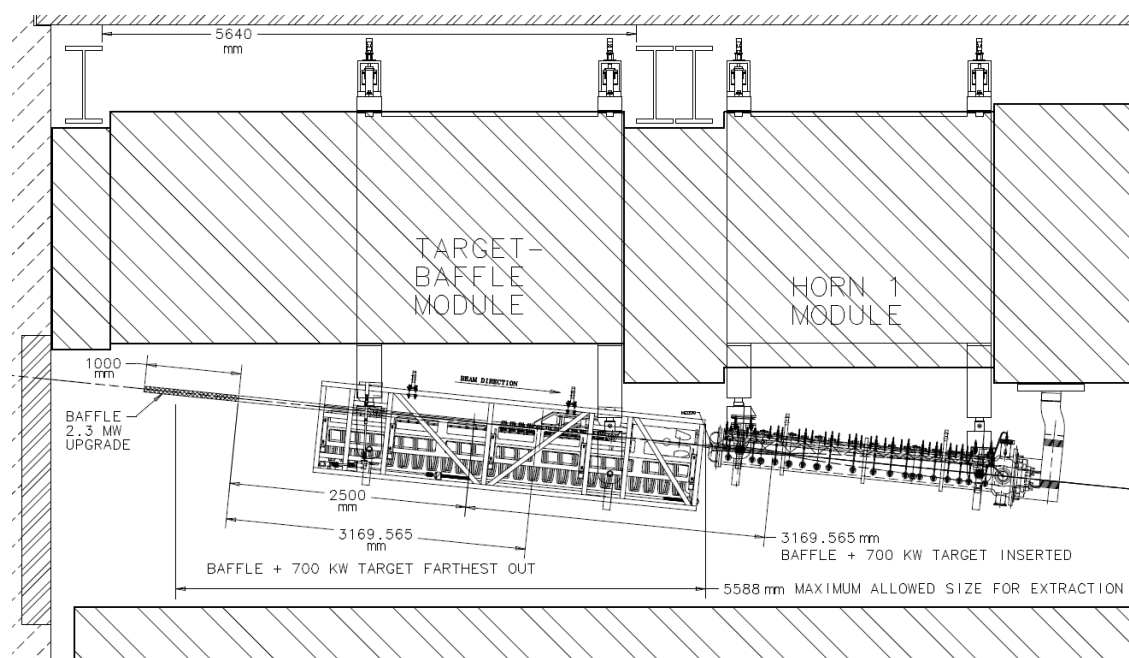


**Figure 3-7:** Target carrier in target pile shielding. The length of the baffle plus target assembly is shown in the fully inserted downstream position, and also in the furthest out position 2.5 m upstream of that. 5588 mm is taken as the maximum reasonable carrier length to extract between the carriage cross beams that are 5640 mm apart. The extra 1000 mm length of a baffle for 2.3 MW operation is also sketched in, showing that the usable range of target motion may be modestly reduced by that upgrade.

rigidly to the target, and moves with it, relative to the outside carrier frame. When a target is replaced, the carrier and baffle are replaced with it as a unit. This conceptual design copies exactly the NuMI target/baffle carrier design.

Attachment/removal of the target+baffle+carrier unit to/from the module is done in the target hall work cell.

For 2.3 MW operation, it is expected that the baffle will have to be  $\sim 1$  m longer. This will impact the possible range of motion of the target, which may be reduced to  $\sim 2$  m. The limitation comes from the worry that the carrier drive could freeze up with the baffle fully extended, and could not be extracted past the carriage beams when in the 2.5 m position (see Figure 3-7).

## 3.3 Targetry (WBS 130.02.03.03)

### 3.3.1 Introduction

This section details the neutrino-production target and the accompanying instrumentation for commissioning, alignment and monitoring of the target and focusing system in the beam. The target is the source for the pions and kaons which later decay to produce neutrinos. Although the production of these particles may be increased with more beam power, engineering and material properties place a limit on beam power for a practical target. These practical concerns include removing beam heating, withstanding thermal shock, and resisting radiation damage. Target replacement strategies also play a role in design. For LBNE, a conceptual design for a target operating at 708 kW is given, which has adequate margins for reliability in this regime. Research and development of target designs is also pursued, with the goal of greater longevity and reliability.

The LBNE target is substantially based on the NuMI target design which has operated since 2005, with some modifications to accommodate higher beam power. The target core is graphite segmented into short rectangular segments oriented vertically, with the short dimension transverse to the beam. The heat from the core is removed by two titanium water lines brazed to the top and bottom of the graphite. The entire assembly is encased within a beryllium containment tube. The segments are 6.4 mm in width and 20 mm in length. A total of 47 segments, spaced 0.2 mm apart, result in a total graphite length of 95 cm, corresponding to two interaction lengths. Drawings of the target are shown in Figure 3-8 and Figure 3-9. The target will be cantilevered into the horn and inserted via a carrier similar to that used in NuMI which also carries the baffle.

During the initial commissioning of the beam, the Target and Horns Instrumentation (THI) discussed in Section 3.3.5, will be used to establish that the components and systems are

working and will allow a beam-based alignment of their positions. Later, the instrumentation will be used to re-commission the beam whenever major components (e.g., targets, horns) are replaced. The instrumentation will also perform long-term monitoring of the beam properties to provide signs of degradation or failure.

### 3.3.2 Design Considerations

The neutrino-production target design is determined by balancing the ideal production of mesons for neutrino production and the survivability of the device for tens of millions of beam pulses. The target must have the following features:

- Adequate material to convert the protons into mesons, while not absorbing too many of the produced particles
- The ability to withstand the instantaneous thermal and mechanical shocks due to the beam
- The ability to withstand the sustained thermo-mechanical stresses and temperatures
- A cooling system to remove the heat deposited by the beam interaction (approximately 20 kW, or 3% of the beam energy)
- Resistance to the effects of radiation damage so as not to encounter substantial change in mechanical properties during the run

These considerations lead to a long, thin target design, for which the exact length must be determined by optimization of the entire beamline, but is approximately two nuclear-interaction lengths (1 m for materials with density  $\sim 2 \text{ g/cm}^{-3}$ ). The target width must be sufficient to cover the beam spot, but is otherwise minimized, except for the practical concerns of heat removal and mechanical integrity. The primary target material must have high mechanical strength, high specific heat, high thermal conductivity, a low coefficient of thermal expansion, and good radiation properties. Although a number of single-element materials generally fit the above requirements, the two materials best fitting those parameters for neutrino beams are beryllium and graphite. Their properties are listed in Table 3-1.

Target longevity is a major issue for the performance of the LBNE facility. Graphite, the material used in the NuMI target, has been adopted as the LBNE reference-design target material, but alternatives are under study. Whereas the NuMI target performance has been on-the-whole successful, a total of six targets have failed or shown deterioration in the neutrino-production rate over a span of months.

Each of these incidents caused operational and experimental complications, required beam downtime for repairs or replacements, or led to a slow decrease in production efficiency.

**Table 3-1:** Properties of graphite and beryllium at 20°C, from manufacturers (POCO Graphite and Brush Wellman).

	Graphite (POCO ZXF-5Q)	Beryllium (S-65C)
Apparent density ( $\text{g cm}^{-3}$ )	1.81	1.82
Compressive Strength (MPa)	195	260
Tensile Strength (MPa)	90	370
Modulus of Elasticity (GPa)	12.5	310
Thermal Conductivity ( $\text{W m}^{-1} \text{K}^{-1}$ )	70	200
Coeff. of Thermal Expansion ( $\mu\text{m m}^{-1} \text{K}^{-1}$ )	8.1	10.7
Specific Heat ( $\text{J kg}^{-1} \text{K}^{-1}$ )	710	1770

Features of the NuMI target were changed in later-series targets to improve lifetime. These improvements were in the cooling lines or other parts of the target assembly that were identified as potential weak points. Further features of the LBNE target are under study to reduce the failure and degradation rates. The primary target material, however, has not yet been modified and is the subject of R&D within LBNE.

Regarding the target's mechanical properties, deviations in size, shape or density of a few percent will impact the experiment's measurement capabilities. The source of these changes can be structural damage (change in material strength leading to disintegration), direct decomposition of the material (radiolysis), oxidation of the material, swelling, contraction, and other changes.

The primary target material must be integrated into a structure that provides cooling, structural integrity and environmental isolation. For LBNE, the target is positioned within the upstream portion of the horn to preferentially focus low-energy pions; this configuration has been used in NuMI and other neutrino beams. A position within the horn adds two complications: 1) the horn focuses some secondaries back into the target, increasing the heat load; and 2) the target must be supported either through cantilevering or contact with the horn conductor. The outer target structure provides either the stiffness for the cantilever or the interface with the horn inner conductor. Typically, the simplest solution is cantilevering the target.

### 3.3.3 Reference Design

The reference target design for LBNE is an upgraded version of the NuMI-LE target that was used for seven years of beam delivery to the MINOS experiment. The NuMI-LE target (NT series) was designed for 400-kW beam power. This new LBNE design takes advantage of some of the work done for the 700 kW ANU-NOvA target (MET series) that will be used in NuMI starting in 2013, as well as R&D done towards making the NuMI-LE target more robust. We are designating this target series LT. Figure 3-8 and Figure 3-9 show the new

target design.

The target material is POCO graphite ZXF-5Q. The target consists of 47 segments, each 2 cm long. Including the space between segments, the total length of the graphite core is 95 cm. The segmentation is to prevent buildup of stress that would be found in a single long segment. The graphite segments are 6.4 mm wide in the horizontal (transverse to the beam) plane. They are brazed to the water cooling tubes at the top and bottom of each segment; the distance between the edges of the water cooling tubes is 15 mm. The top and bottom of the graphite segments are sculpted to the radius of the cooling tubes; the vertical edges of the graphite are rounded to prevent stress buildup in corners.

The graphite is in helium gas, slightly above atmospheric pressure. The inert atmosphere prevents oxidation of the graphite. Helium helps to cool the outer containment tube, transporting heat to the water cooling tubes.

The NUMI LE target was designed for  $4.0 \times 10^{13}$  protons per pulse; this will increase to  $4.9 \times 10^{13}$  for LBNE 700 kW beam power. Two previous design studies calculated the stress in the 6.4 mm wide graphite segments assuming  $5.5 \times 10^{13}$  protons per pulse; one with the LE target at 480 kW, and the other for the ANU-NOVA target at 880 kW. Both studies indicate that increasing the beam spot size from the 1.0 mm RMS used in the original NUMI calculations to 1.3 mm RMS is adequate to address the issue of stress in the graphite for the more intense beam. So the LBNE target will use the same 1.3 mm RMS beam spot size that has been adopted for ANU-NOVA.

The water tubes are 6 mm O.D. 0.4 mm wall titanium. The entire tube loop inside the target can is from a single piece of tubing; there are no joints inside the helium vessel. The lack of joints reduces the risk of water leaking into the helium vessel, which would be fatal to the target. The water tube bends to the side of the containment tube at the downstream end for water-turn-around, so that it is not directly in the path of the remnant proton beam.

The helium-containment tube around the target segments is 30 mm O.D. 0.4 mm wall beryllium. The upstream and downstream windows are also beryllium. The upstream window has a stainless steel flange. The rest of the upstream vessel is aluminum.

The base plate of the helium containment tube provides the fixed mechanical reference for the target and is flanged to connect to the upstream portion of the target can. The base plate is stainless steel, and helium containment where the water-lines penetrate this plate is supplied by a compression fitting. The base plate also holds the helium supply tube. The target vessel will be evacuated before being filled with helium.

There are five aluminum rings spaced out along the graphite-plus-cooling-tube core to keep it aligned within in the helium containment tube.

The target will be inserted into the horn by carrier system, described in Section 3.2. The

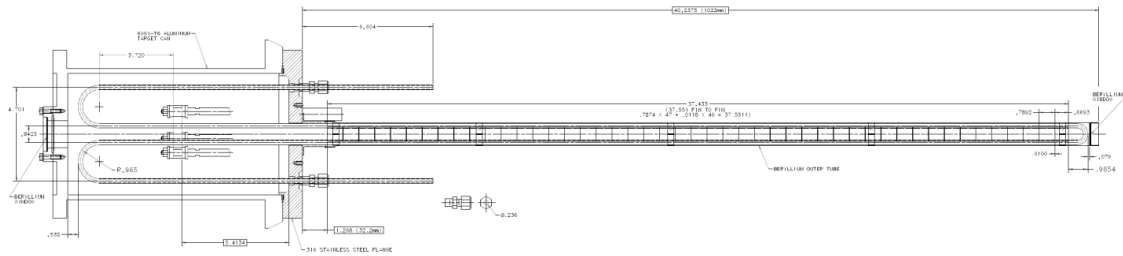


**Figure 3-8:** Proposed LT target for LBNE. Beam enters through the beryllium window on the left, encounters the graphite core, and exits through the beryllium window on the right. Units are inches unless otherwise noted.

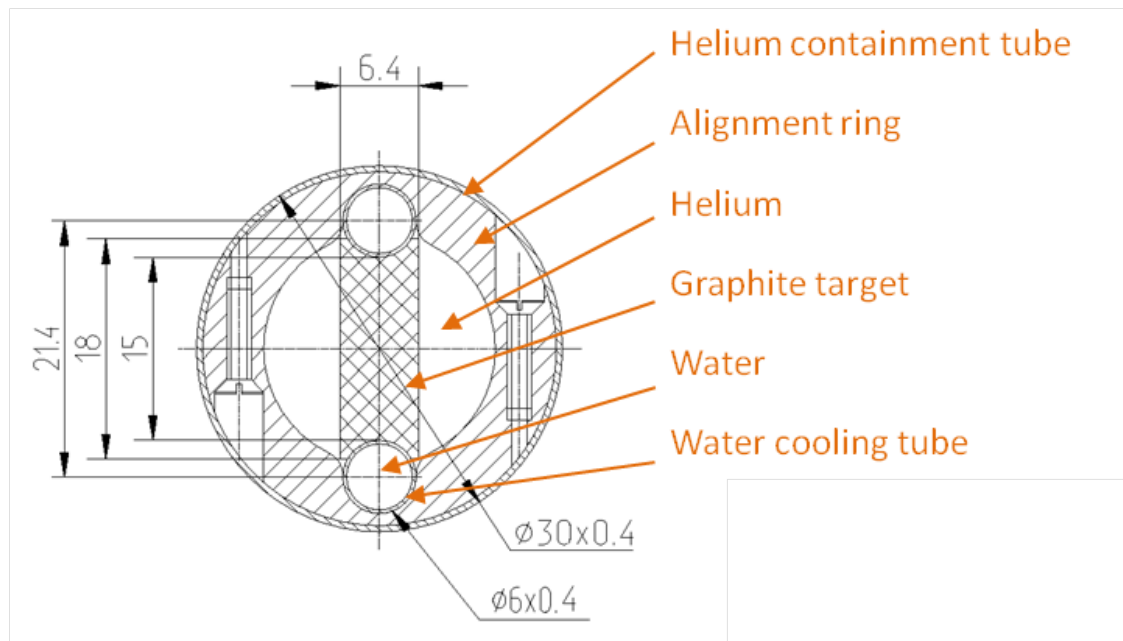


**Figure 3-9:** Cross-section of LT target for LBNE. Note the alignment rings do not run the full length of the target. Units are mm.

carrier is supported by a module upstream of the horn module. Both the baffle and target are firmly fixed to the carrier. As a unit, the target and baffle can be moved into the horn and transversely moved for alignment and beam tests.

One issue with water cooling is the near-instantaneous heating of the water. Water, being relatively incompressible, can produce large pressures when heated in a confined area. This is known as the “water hammer” effect. A straightforward calculation at 30°C suggests the pressure increase could be as much as 50 atm, although further study has indicated that the flexibility of the walls will reduce this factor substantially. While the pressure level itself is not of concern, the cyclic loading is. To ameliorate this problem, the plan is to introduce bubbles of a gas (probably helium) to absorb the shock. Additionally, lowering the temperature of the water can reduce the water hammer effect, as water’s coefficient of thermal expansion decreases at lower temperatures (zero at 4°C).

The LBNE target can be compared to the targets used or planned for the NuMI beamline. The MINOS target was inserted into the NuMI horn, but designed for a beam power of 400 kW. The MINOS target would be problematic in two ways at 700 kW beam power. (i) The downstream part of the outer aluminum tube that contains the helium atmosphere and holds the downstream beryllium window would overheat at 700 kW. (ii) At the current water flow rate, the increased differential temperature between the top and bottom water lines would increase the bending of the target between cool and operating conditions. To address these issues:

- The outer tube will be made from beryllium instead of aluminum. The beryllium can withstand much higher temperatures than the aluminum. It offers other advantages, such as generating less showering and so reducing the heating of the horn inner conductor.
- The water cooling lines will be made from titanium instead of the steel used for MINOS targets. Titanium has a lower coefficient of thermal expansion, so the allowable temperature rise of the cooling water is higher. The balance of the compensation is achieved by increasing the water flow rate via increasing the water pressure differential.

Six MINOS targets have failed. The actual causes of failure are not understood in detail because the target cannot be easily inspected due to residual radiation. Once the radiation levels decrease, post-mortems are planned to further investigate the failures. At least five failures seem to result from weak points in the device itself: in the cooling lines or the exterior vessel. The other, more relevant, failure is in the second MINOS target (NT-02). NT-02 had the greatest run period and showed a gradual degradation of neutrino production during its  $6 \times 10^{20}$  proton run. The degradation was not uniform in neutrino energy (consistent with various models) but amounted to 15% at the peak. NOvA has indicated that a 10% degradation would be an upper bound, and that 5% would be preferable. As such, target lifetimes of  $4 \times 10^{20}$  protons or less must be considered, if the degradation mode cannot be

addressed. For LBNE, this implies up to two targets per year will need to be replaced and these failures must be considered as part of the normal operation of the beam.

The NOvA target was developed from a design for the MINOS medium-energy target. It is designed for 708 kW, but does not fit inside the horn, thus widening the design options. The NOvA 708-kW target makes use of long (70 mm) segments that connect to a cooling plate that is well outside the baffle aperture. This longer cooling path simplifies construction and improves the thermal characteristics of the target, thus allowing target segments to handle much higher temperatures (up to as much as 800°C). The mechanical and radiation resistance of graphite is known to improve at higher temperatures (with the exception of oxidation). Additionally, the temperature gradients within the graphite are reduced.

The LBNE target cannot make use of all the improvements that the NOvA target includes, as it must fit inside the LBNE horn. As a result, the LBNE target is much more similar to the MINOS target, with only the above modifications of titanium cooling lines and a beryllium containment vessel. Two Titanium-water-cooling-tube-plus-graphite cores were built during the investigation of NuMI target water leaks. The second one was considered entirely successful and ready to be assembled into a target can for a production target (see Figure 3-10). The key development issues were brazing of the graphite to the tubes, bending of the tubes, and precise alignment tolerances. The LBNE-LT target core is practically identical to this.



**Figure 3-10:** Early prototype of a target graphite core bonded to a titanium cooling line.

### 3.3.4 Target Options: R&D

Target longevity is a major issue for the performance of the LBNE facility. A target R&D program will explore options of target material, geometry, cooling, and other design issues.

As mentioned in the previous section, a target replacement rate of two per year is likely, based on experience with the NuMI target. The logistics of target replacement in NuMI cost 2-3 weeks of runtime; the LBNE duration may be similar. Two target replacements per year compromises the facility performance by 10-15%. Additionally, there is substantial additional cost in the storage facilities and radioactive handling required for that volume of targets.

Reducing the frequency of target replacement could reduce the cost of the project, reduce the cost of operations and produce a more capable facility.

The goal of the target R&D program is to be able to produce targets of greater longevity through design choices that negligibly impact neutrino production, however, the choices are somewhat limited. The R&D program of work has three major components:

- Radiation testing of potential target materials at the BLIP facility at Brookhaven.
- Material studies through the Radiation Damage In Accelerator Target Environments (RaDIATE) collaboration.
- Single pulse thermal shock testing in the HiRadMat facility at CERN.

A first round of radiation testing has been performed at the Brookhaven Linac Isotope Producer (BLIP). A series of materials were tested, including different grades of graphite, a carbon-carbon composite and hexagonal boron nitride (hBN): a graphitic form of Boron Nitride that theoretically has superior mechanical properties. These materials have been irradiated to a fraction of the NuMI irradiation of NT-02, well into the range that mechanical properties should be affected. Material studies have been performed in which the samples were gauged for integrity, tensile strength, thermal conductivity, density and other mechanical properties. Figure 3-11 is a picture of the sample holder for the BLIP test.

Initial results from the irradiated samples give support to the historical use of a small grain size, anisotropic grade of graphite from POCO (ZXF-5Q). Additionally the results invalidated previous tests that had shown quite severe radiation damage. Those sample had been irradiated directly in water. The present BLIP test [20] demonstrated that identical samples experienced much greater degradation when irradiated in water instead of an inert environment (argon). The alternative material hBN fared poorly, seemingly to ablate in the radiation. Among graphites, POCO was among the best in terms of its retained strength and ductility. Another grade of graphite and a 3D carbon-carbon composite also appeared attractive. The carbon-carbon composite has a very low coefficient of thermal expansion, minimizing the effects of thermal shock. However, the CTE of the carbon-carbon changes substantially upon irradiation. This change can be reversed with annealing at moderate irradiation, but it is unclear whether the changes can be withstood in a target where annealing is not possible. Further investigations will study temperature-dependent effects, particularly annealing.

Additional radiation testing may be warranted, though few facilities can provide comparable irradiation. Reactor irradiation is easily available, but the effects of neutron irradiation can depart widely from that of high-energy protons. The BLIP facility was a good compromise, except for its limited exposure.



**Figure 3–11:** BLIP test sample holder. This figure shows cassettes of material samples irradiated in the BLIP facility. The beam enters from the right.

The other activities are to investigate alternative materials for the target and its support assembly. A particular aim is to consider beryllium as an alternative target material to graphite. Beryllium has some history as a target material, notably as the Fermilab MiniBooNE target, which has been exposed to in excess of  $1.5 \times 10^{21}$  protons at 8 GeV. A naive examination of beryllium's basic materials properties suggests that its single-pulse resistance to damage will be somewhat less than graphite. However, the precise modeling of beryllium damage is somewhat more involved. Particularly, beryllium as a metal has substantially greater tensile strength than graphite and thus may be more immune to fracture. Also, the radiation damage threshold of metals such as beryllium is substantially higher than the crystalline forms of graphite (the data are imprecise, but the difference is about an order of magnitude).

While beryllium has several known advantages over graphite, it has the overwhelming disadvantage of not being the material that has operated in the NuMI beam or other high-power neutrino beams (CNGS, T2K). An invaluable test would be to include beryllium as an operational neutrino production target in NuMI and verify its performance over an appreciable run period. Options are under consideration to modify a NOvA target to test beryllium as a target material. If successful, this material would have all the listed advantages to the LBNE Project and facility, as well as potentially being implemented for the NOvA experiment.

The Radiation Damage In Accelerator Target Environments (RaDIATE) collaboration is a program to investigate various materials of interest in the high energy proton irradiation regime primarily using the Materials for Fission and Fusion Power group at Oxford University. This group has the capability to fully analyze small, highly irradiated samples for mechanical changes due to irradiation. Several samples specifically chosen for LBNE will be irradiated and investigated at Oxford.

Single pulse thermal shock testing will be performed in the HiRadMat facility at CERN. The response of solid materials to short pulses of proton beam (or quickly moving targets in CW beam) is often simulated and used to predict failure. However anecdotal evidence suggests that failure predictions are significantly conservative for certain materials (such as beryllium). Particularly, the strength and other properties of beryllium are substantially different at high strain rate, that is: at the very short duration strains caused by beam irradiation beryllium's mechanical properties depart from their static values such that it is more resistant to thermal shock. Testing materials in the high intensity pulsed beam available at HiRadMat at CERN will validate simulations and failure criteria, potentially proving beryllium as a valid alternative to graphite.

### 3.3.5 Target and Horns Instrumentation

The Target and Horns Instrumentation (THI) is a set of detectors that provide measurements of the secondary beam for commissioning, alignment, and monitoring purposes. It supplements the primary beam instrumentation and the neutrino detectors. The THI's role

is to provide experimental and operational information to aid in the maximization of neutrino production and to limit the experiment's systematic uncertainties due to beam mis-modeling and variation. The major roles can be broken down as follows:

- **Commissioning:** on initial operation of the beam, the commissioning team will go through a series of tasks to demonstrate that the beam can be delivered to the absorber, target, horn and baffle. The THI will be able to provide live verification of these tasks. For example, the primary beam will be delivered to the beam absorber before installation of the target, and the THI will measure the beam distribution at the absorber. Additionally, this instrumentation will be used to recommission the beam whenever major components are replaced.
- **Alignment:** many of the neutrino beam components will have tight tolerance on their alignment at the start of and during the run. The THI measures the locations of the devices through beam-based alignment, which entails determination of the positions of the devices with respect to the primary proton beam. This alignment is particularly relevant for evaluating the uncertainties on neutrino production without propagating the uncertainties of several optical surveys.
- **Monitoring:** long-term monitoring of the beam characteristics will give indications or measurements of slow variations in the beam. The most significant variation will likely be target degradation. The NuMI NT-02 target was known to degrade up to the point where 15% of the peak flux had been depleted. Monitoring this depletion is necessary for modeling the neutrino beam.
- **Investigation:** the THI can be used to investigate the failure or malfunction of beam production components. In NuMI, the THI system was invaluable in several such investigations where on separate occasions the target containment vessel warped and filled with water.

### 3.3.5.1 Design Considerations

The detailed tolerances for components, and thus the measurement requirements, must be derived from a physics-based analysis of the effects of misalignments, target degradation and other deviations. The treatment of systematic errors in the MINOS experiment provides guidance, but the nature of the measurements is not precisely the same (MINOS was primarily a muon-neutrino disappearance experiment, while LBNE is an electron-neutrino appearance experiment; additionally, the detectors are substantially different in composition and modality). Another requirement for the Target and Horns Instrumentation is that results must be readily apparent and available. A package of software integrating the instrumentation must be available to personnel performing the above analyses online. This software must also be able to interface to primary beam instrumentation and (ideally) the neutrino beam detectors. Correlation of the various data is necessary for the THI measurements.

### 3.3.5.2 Reference Design

The model for LBNE Target and Horns Instrumentation are the comparable NuMI systems. The suite of instrumentation planned for LBNE are:

- A Budal monitor which directly measures the portion of the beam on target through electrical signals.
- Crosshair monitors which detect the shower of secondary particles produced through interaction of the primary beam together with crosshair-alignment features on the horns.
- A hadron monitor at the end of the decay pipe to measure the remaining secondary particles.
- Also, the functionality of a target decay monitor is within the scope of the tertiary beam detectors of the Near Detector.

A Budal monitor detects the beam on target by electrically isolating the target, and measuring the charge ejected or deposited. This device worked well in NuMI for commissioning and alignment. However, the electrical isolation involves certain design compromises that can increase the risk of target failure. Therefore, the LBNE target will not be entirely electrically isolated, but will have two segments isolated at the start of the target where the heat deposition is less than maximal. Additionally, a beryllium thermometer may be included at the front of the target to measure the vertical position of the beam. This device is being prototyped with the upcoming NOvA target.

The crosshair monitors are the primary tools for horn alignment and are similar to primary-beamline loss monitors. They will be integrated into the horn modules. During horn alignment, the target will be removed, allowing the primary beam to pass through the horn apertures. The beam is scanned across crosshair features fixed to the horn's upstream and downstream ends, producing a modest shower of particles that is detected by these loss monitors.

The hadron monitor resides at the end of the decay pipe, upstream of the hadron absorber and within the secondary beam. It measures the intensity, location and shape of the hadron beam just upstream of the absorber. In NuMI, the hadron monitor was used extensively for alignment by analyzing the change in the remnant beam as the primary beam was scanned transversely across the target, baffle, and horn features. It was used for commissioning, alignment, monitoring and for diagnosing failures. The NuMI hadron monitor was a  $1 \text{ m}^2$ ,  $7 \times 7$  array of parallel-plate ionization chambers. The ionization medium was helium at atmospheric pressure. The NuMI hadron monitor design cannot simply be reused for LBNE, however, as LBNE will have a shorter decay pipe and will thus produce a smaller and

more intense beam spot at the hadron monitor. The hadron monitor must withstand the heating and irradiation of this more intense beam. Additionally, it must be able to produce measurements at the higher particle fluxes. The NuMI hadron monitor was known to show saturation effects at high intensity; it also was known to show variability with temperature, pressure and impurity level in the helium supply. An evolved concept for the LBNE hadron monitor is to use argon at low pressure ( $\sim 1$  torr) to reduce the ionization intensities, and to reduce the variation with gas supply quality. A higher channel count is necessary as the pixel size will need to be at least a factor of three smaller, probably a factor of five.

Long-term degradation of the target material under beam irradiation can be monitored by comparing the ratio of muon fluxes of different energies. This system is vital for monitoring the detailed health of the target while not waiting for the analysis of neutrino of other tertiary beam monitors. The functionality of a target decay monitor can be realized through appropriate use of the muon monitors planned as part of the Near Detector scope. The system will consist of two arrays of ionization chambers at different locations within the shielding downstream of the hadron absorber. These devices will be configured in such a way as to produce a live measurement of target degradation through the ratio technique, wherein the ratios of muon-monitor signals provide an immediate indication of target degradation, after compensating for other detector effects.

The whole system of the above devices will be integrated with data from primary-beam devices and neutrino devices, if available. The software to integrate these devices will be readily available as a live accelerator-controls application, as well as recording all these data into the appropriate accelerator and experimental databases.

### **3.4 Horns (WBS 130.02.03.04)**

The horns are focusing devices for secondary particles produced by the interaction of the primary proton beam on the target; they act as magnetic lenses that focus these particles, primarily charged pions and kaons, toward the decay pipe. This focusing of particles is achieved through a pulsed toroidal magnetic field, which is present in the air volume between the co-axial inner and outer conductors that form the horn structure. LBNE will have two horns in series; the first of which partially surrounds the target, then extending more than 2 m further downstream in a parabolic shape, as can be seen in Figure 3-12. The second horn, shown in Figure 3-13 is located 6.6 m downstream from reference point MCZERO (defined in Figure 3-12), and also utilizes a double paraboloid inner conductor profile.

Conductor designs used are identical to those being manufactured for the NOvA experiment, which were developed from the NuMI neutrino beam. The horns are designed to operate with a beam power up to 708kW. The inner conductor profiles are designed to produce a neutrino beam with an energy spectrum appropriate for the primary physics goals of LBNE[21], subject to engineering and material constraints. The horn systems will be supported and

positioned by support modules, described in Section 3.4.3, which hang from carriage rails in the target hall chase. Electrical current supplied to the horns is transported via an aluminum stripline to the downstream end faces where connections to the horn conductors are made.

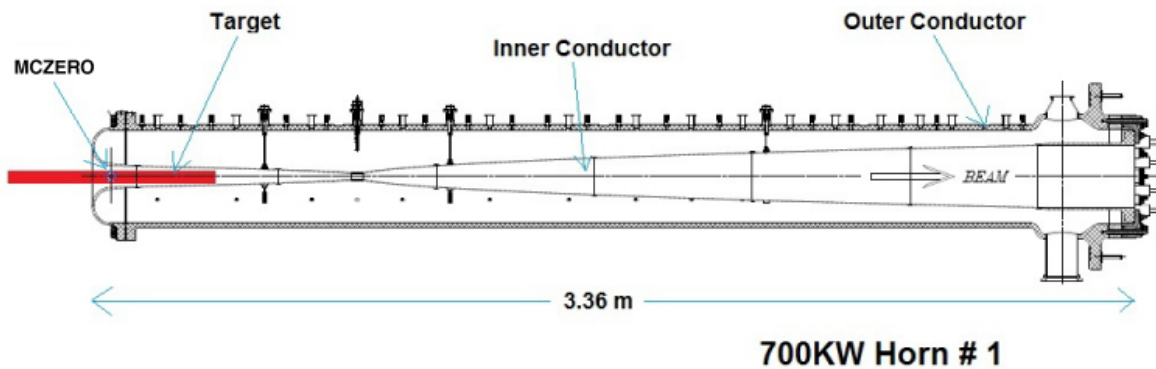


**Figure 3-12:** Horn 1 section. The reference “MCZERO” is the point along the beam that sets the coordinate system origin for Monte Carlo simulations. Horn 1 specifications are listed in Table 3-2.

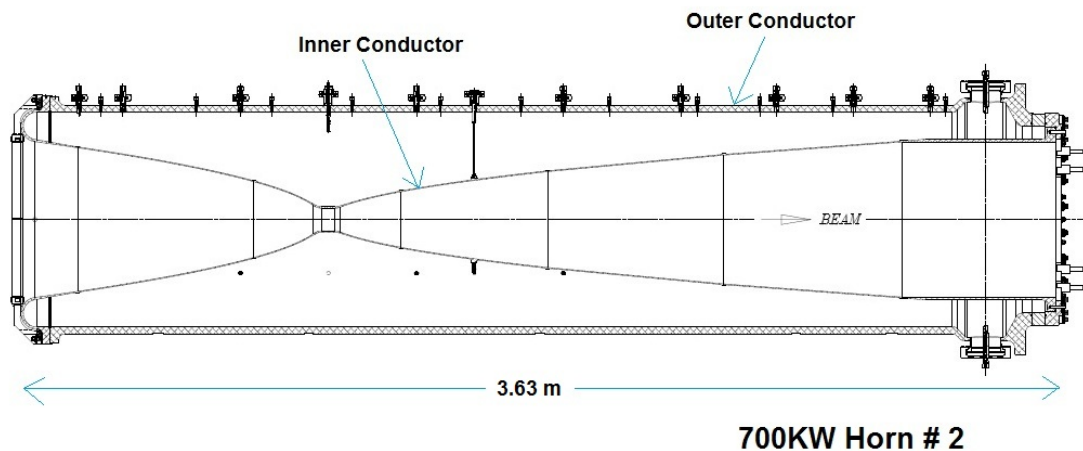


**Figure 3-13:** Horn 2 section. Horn 2 specifications are listed in Table 3-2.

### 3.4.1 Design Considerations

The horns (i.e., the conductors) must be able to endure the combined heat load from the secondary particle interactions in the horn material and resistive heating by the current flowing through them. To address the former, the thickness of the inner conductor should be minimized to reduce absorption and scattering of secondary particles in the conductor material. Resistive heating can be minimized by keeping the pulse length short, while water-spray cooling is used to keep the conductors at an acceptable operating temperature. Given

careful design of the stripline, air cooling is sufficient for the stripline. In addition to the cooling requirements, the inner conductor must withstand repetitive thermal and magnetic stresses over tens of millions of current pulses.

Lifetime expectations for horns are typically described in millions of pulses, with a safety factor associated with that rating. Stress results from finite element analysis can be used to determine the fatigue life of various components, and thus estimate horn lifespan. The component most subject to lifespan limitations is the Horn 1 inner conductor. It is important to demonstrate with analytical simulations that a horn will not fail after a minimum of  $1 \times 10^8$  cycles due to fatigue in the inner conductor. The design will be simulated and possibly adjusted to achieve this lifetime with a minimum safety factor of three. For this conceptual design, both horns are assumed to be replaced every two years.

Cooling considerations must also extend to the module mainframe and drive components, as dimensional stability while in operation is critical. Additionally, the weight of the horn, its support module and stripline block together must not exceed 50 tons, the Target Hall crane capacity. The horn systems assembly must be removable and transferable to the target hall work cell for initial installation, end of life removal, and potential repair activities. Horns are expected to be replaced every few years, while modules are considered permanent and will be designed as such.

### 3.4.2 Reference Design

The focusing system will be a two-horn design, with the upstream end of the second horn (Horn 2) located 6.6 m from the reference point MCZERO (near the upstream end of Horn 1). Both horns consist of an inner conductor, an outer conductor, a current-supply stripline, a cooling system and a support structure. The inner conductor of Horn 1 has a parabolic upstream section that surrounds the target tube up to the neck of the horn. This neck is followed by a parabolic downstream profile[21] that ends at the downstream face where the stripline is mounted. Horn 2 follows this layout, although varies in parabolic lengths, placement, and wall thicknesses[22]. Both Horn 1 and Horn 2 inner and outer conductors are of aluminum 6061-T6 construction. The inner conductor shapes are generated from the parameterization shown in Figs. 3-14 and 3-15.

The outer surfaces of the inner conductor will be cooled by water spray nozzles distributed along the beam axis and  $120^\circ$  azimuthally. Nozzles at the top of the outer-conductor cylinder will spray water to form a film running down from both sides, illustrated in Figure 3-16. The radioactive cooling water will be collected at the bottom of the horn and will return to an external heat exchanger through a closed circuit. The external surfaces of the horn will be exposed to the target chase airflow. To resist water corrosion and possibly electrical breakdown, the surface of inner conductors will be coated with electroless nickel.

**Table 3–2:** Horn parameters. The inner and outer conductor parameters are abbreviated by IC and OC, respectively.

	Horn 1	Horn 2
Material	Al 6061-T6	
Peak Current	200 kA	
Min. aperture “neck” radius	9 mm	39 mm
IC Thickness	2 mm	3 mm
Length	3.36 m	3.63 m
OC radius (outer)	165 mm	395 mm
OC Thickness	16 mm	25 mm

Horn 1 (700 kW version)	Upstream	transition	Neck	transition	Downstream	Equalization section
Z (cm)	0 to 44.047	44.047 to 80	80 to 83.982	83.982 to 95.128	95.128 to 300	300 to 331.437
I.C. $R_{in}$ (cm)	$\sqrt{\frac{92.8454-Z}{7.0483}} - 0.2$	$\sqrt{\frac{85.7091-Z}{7.0483}}$	0.9	$\sqrt{\frac{Z-82.2123}{2.1850}}$	$\sqrt{\frac{Z-80}{2.1850}} - 0.2$	9.843
I.C. $R_{out}$ (cm)	$\sqrt{\frac{92.8454-Z}{7.0483}}$		1.35	$\sqrt{\frac{Z-80}{2.1850}}$		10.795
O.C. $R_{in}$ (cm)	14.92					Varies, > 14.92
O.C. $R_{out}$ (cm)	16.51					Varies, > 16.51

**Figure 3–14:** Idealized shape of the Horn 1 inner and outer conductors.  $z=0$  is the beamsheet location MCZERO. The actual shape of the inner conductor includes rounding of the upstream corner over  $\pm$  a few cm (the curved end-wall extends to  $Z = -3.19$  cm), three places where the inner conductor is thicker to hold spider supports to the outer conductor, and seven places where the inner conductor is thicker for weld beads.

Horn 2	Upstream	Neck	Downstream	Equalization section
Z (cm)	0 to 97.617	97.617 to 104.803	104.803 to 300	300 to 353.515
I.C. R <sub>in</sub> (cm)	$\sqrt{\frac{100-Z}{0.1351}} - 0.3$	3.90	$\sqrt{\frac{Z-100}{0.2723}} - 0.3$	26.801
I.C. R <sub>out</sub> (cm)	$\sqrt{\frac{100-Z}{0.1351}}$	4.40	$\sqrt{\frac{Z-100}{0.2723}}$	27.753
O.C. R <sub>in</sub> (cm)	37.00			varies
O.C. R <sub>out</sub> (cm)	39.54			varies

**Figure 3-15:** Idealized shape of horn 2 inner and outer conductors.  $z=0$  is the insertion point of Horn 2, which is 6.6 m downstream of MCZERO, the  $z=0$  point of horn 1. The actual shape of the inner conductor includes rounding of the upstream corner (where the upstream-most edge of the curved end-wall is 4.8 cm upstream of  $z=0$ ), rounding at the transitions several cm upstream and downstream of the neck, one place where the inner conductor is thicker to hold spider supports to the outer conductor, and six places the inner conductor is thicker for weld beads.

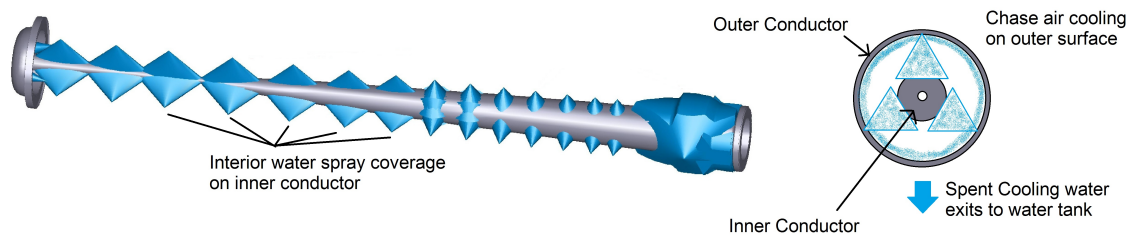


**Figure 3-16:** Horn 1 inner conductor water spray coverage.

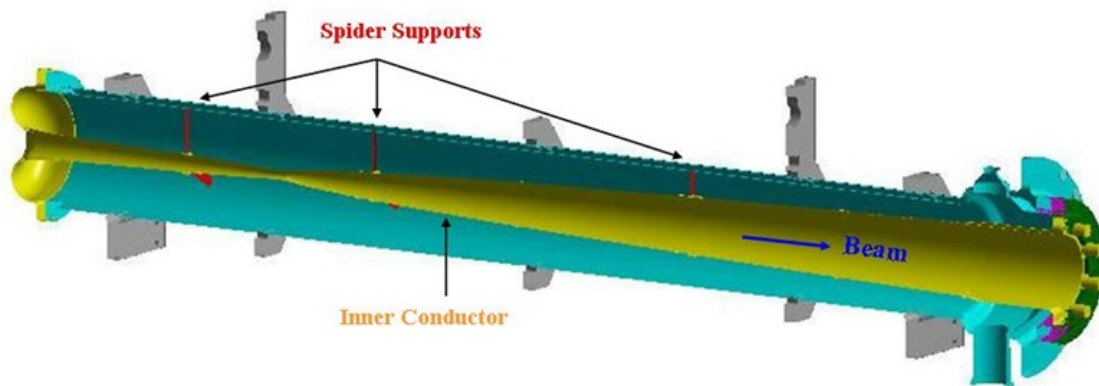


**Figure 3-17:** Additional support and stability for the thin inner conductor are provided by welded struts or "spider" (web) supports (thin red pieces).

The inner conductor will consist of seven segments welded together with in-house CNC TIG welding machine. Welds will be completed with a thicker wall at the joints, located away from the high-stress areas to compensate for the reduced strength in the heat-affected zone. Single pass, full-penetration welding will minimize the conductor distortion. Cosmetic passes will be applied if needed to achieve an overall straightness of  $\pm 0.020$  in. A few sets of spider supports, illustrated in Figure 3-17 will provide the position adjustment of the inner-conductor center line and meanwhile allow free thermal expansion of the conductors along the beam direction.

The electrical connection between the power supply and the horn is provided by a planar-design stripline, which has minimal inductance and resistance, and allows thermal expansion/contraction of the horns and transmission lines. The stripline between the horns consists of eight layers of aluminum 6101-T61 bus bars that are spaced by zirconia ceramic insulators, as shown in Figure 3-18. The stripline is flared out to connect to the horn inner and outer conductors at the downstream end and is insulated by an alumina (ceramic) ceramic ring. The upper portion is connected to the transmission line via a remotely controlled stainless-steel clamp assembly. The horn current pulse is a half-sine wave with a peak current of 200 kA, pulse width of 2.3 ms and a repetition rate of 1.33 s.

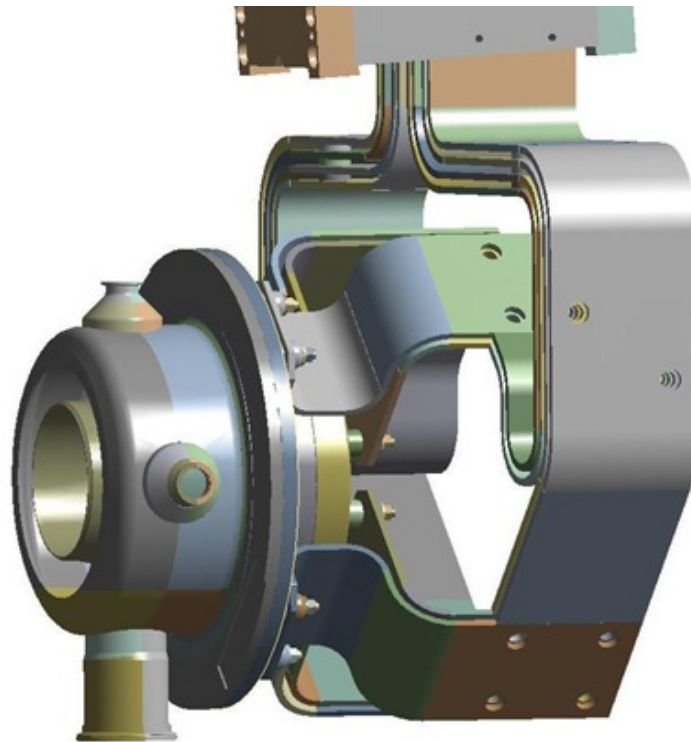


**Figure 3-18:** Horn 1 stripline connection at the downstream end

The horn striplines must be matched in length for pulse uniformity, and must be profile-matched to lessen the effects of magnetic loading. This profile-matching also helps to elimi-

**Table 3-3:** Summary of heating loads on the horns. The results are separate for the inner conductor (IC) and the outer conductor (OC).

LBNE	Horn1		Horn2	
	IC	OC	IC	OC
Beam Heating Loads	10 kW	12.5 kW	2.7 kW	9.6 kW
Resistive Heating Loads	9.1 kW		1.5 kW	

nate stray magnetic fields during the beam pulse that can adversely affect the beam optics. Ring-down times for the Horn striplines must be analyzed to ensure the vibrations completely dissipate in the 1.33-second cycle time. Any vibration condition left past the 1.33 second period will have the potential to develop a resonant frequency and decrease the service life of the horn.

The heating sources on the horn conductors include electrical-resistive heating by current and instantaneous beam heating due to secondary particle interactions in the material. The beam energy deposition rates in materials are calculated with MARS, a Monte Carlo code[23]. Because of its smaller radius and proximity to the target, the heating loads on Horn 1's inner conductor are much higher than those on Horn 2's inner conductor. Horn 1's maximum heating-load density occurs on the neck immediately upstream of the transition to parabola. See Figures 3-19 and 3-20 and Table 3-3. The steady-state temperature of Horn 1 is shown in Figure 3-21.

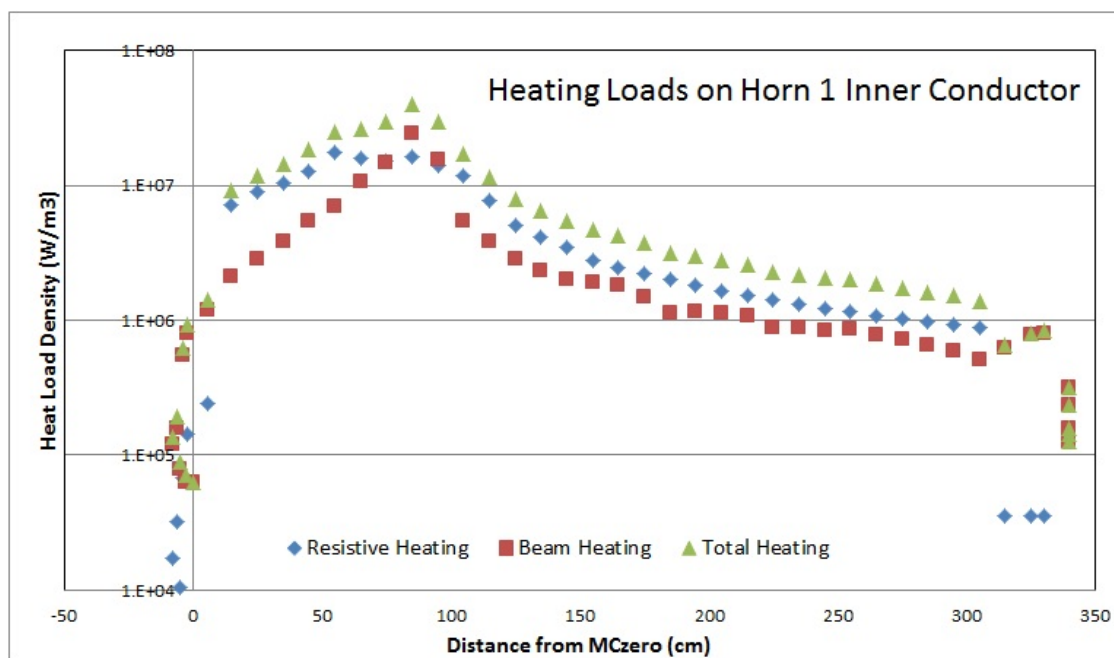


**Figure 3-19:** Heating loads on the inner conductor of Horn 1

Heating of the inner conductors produces thermal stresses, and electromagnetic forces gener-

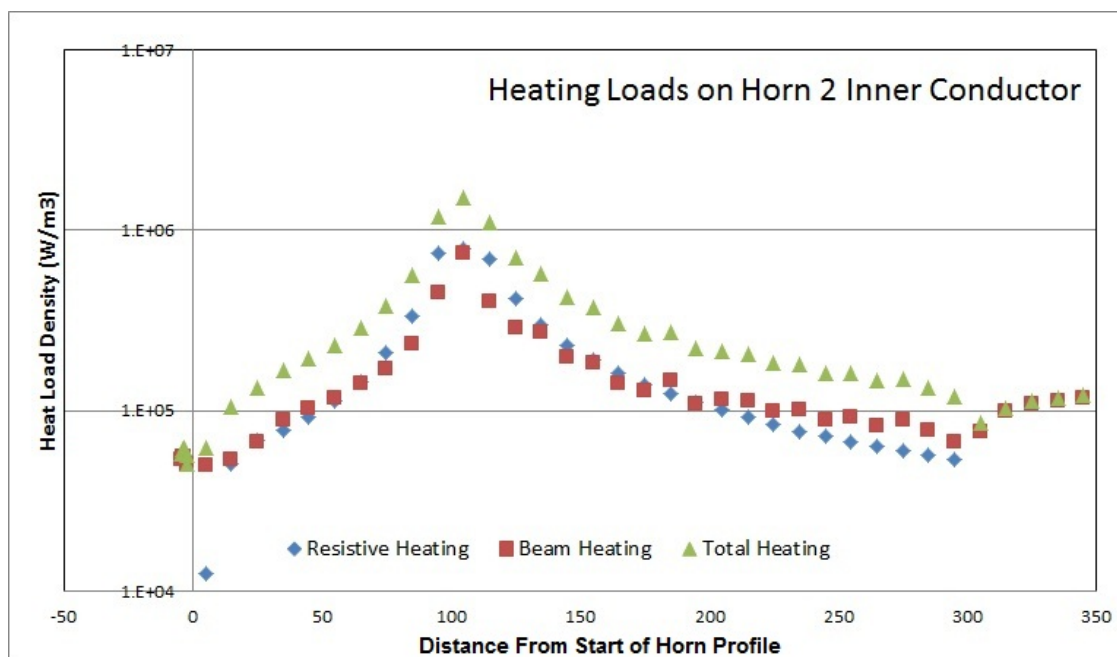


**Figure 3–20:** Heating loads on the inner conductor of Horn 2

ate magnetic stresses on the inner conductor during current pulsing. Thermal and structural finite element analysis (FEA) will be carried out to verify the design and study the fatigue strength of the inner conductors, the alignment stability of the horns, and the temperature profile of the striplines. Modal and buckling analysis will be performed to study the vibration and buckling characteristics of the horns.

Preliminary FEA calculations indicated that with the current design and a convective heat transfer coefficient of  $7,500 \text{ W}^\circ\text{C}/\text{m}^2$ , the neck would reach an equilibrium temperature of  $44^\circ\text{C}$  after five beam pulses as seen in Figure 3–22. After reaching equilibrium, during each pulse at full beam power the neck’s maximum temperature would rise to  $61^\circ\text{C}$  halfway into the current pulse after the instantaneous beam spill (mid-pulse) and would reach  $65^\circ\text{C}$  at the end of current pulse (end-pulse) as shown in Figure 3–23. Horn conductor and critical component temperatures must be engineered to remain below  $100^\circ\text{C}$ , as the fatigue strength (the stress level a material can endure for millions of cycles) begins to drop as operating temperatures pass this limit.

While the neck gets hot during current/beam pulsing, both end caps of the inner conductor remain cool. Thermal gradients produce compressive stress on the inner conductor, and electromagnetic forces generate compressive circumferential/radial stresses and tensile axial stress. The combination of thermal and magnetic loading results in a range of stress magnitudes and types of stress at different locations and times on the inner conductor. Stress calculations were performed to study the scenarios of steady state, mid-pulse and end-pulse for the normal beam operation at full power of 708 kW.

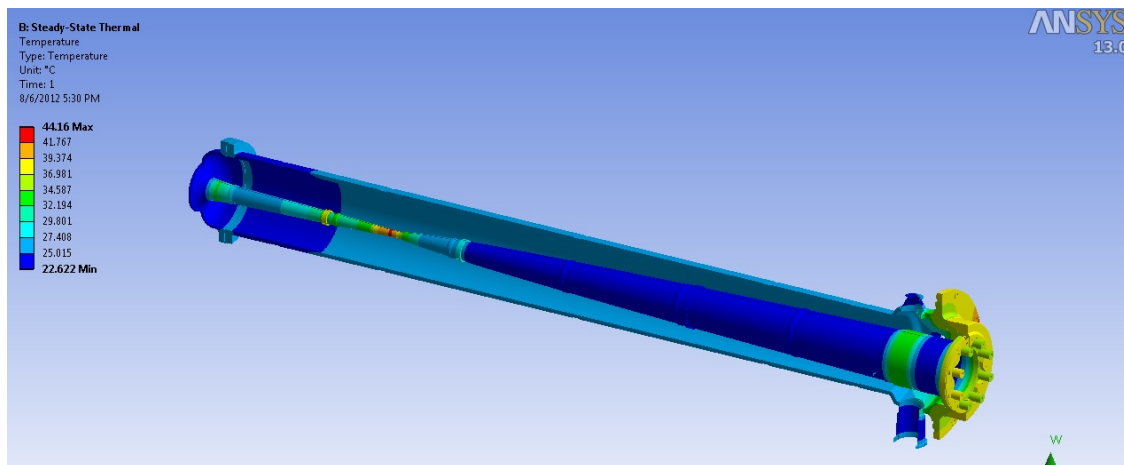


**Figure 3-21:** Temperature of Horn 1 at steady state

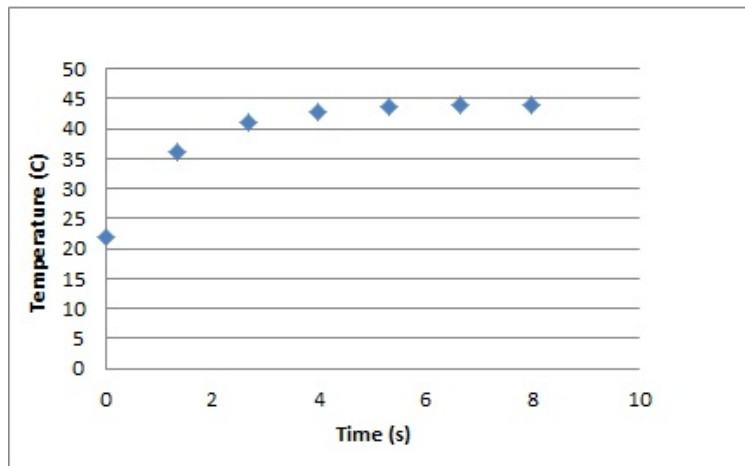


**Figure 3-22:** Temperature trends in the Horn 1 neck at beam cold start-up

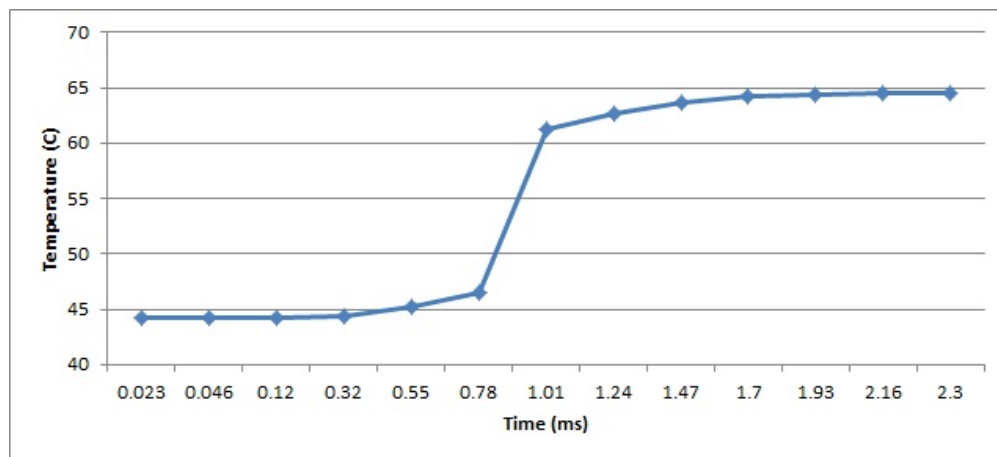


**Figure 3-23:** Temperature trends in the Horn 1 neck during a single pulse after equilibrium

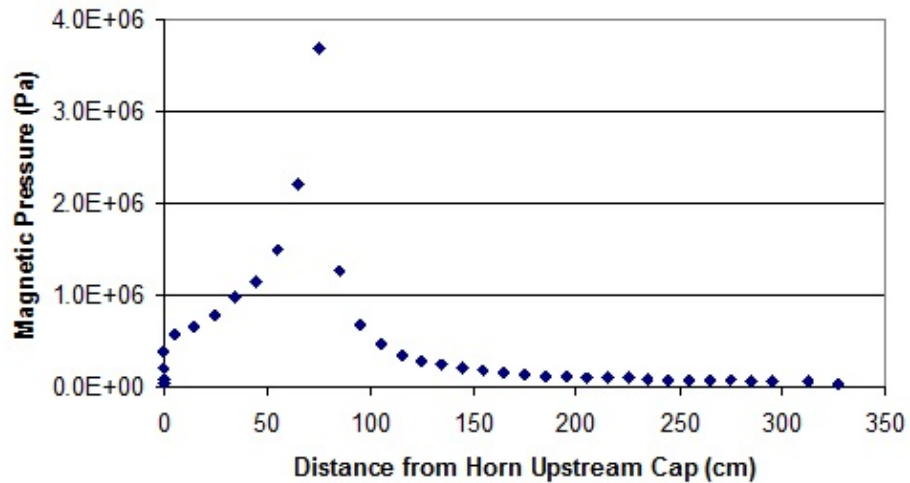


**Figure 3–24:** Magnetic pressure loading profile on the Horn 1 inner conductor at mid-pulse.

The following figures 3–24 and 3–25 show calculations of stress on Horn 1.

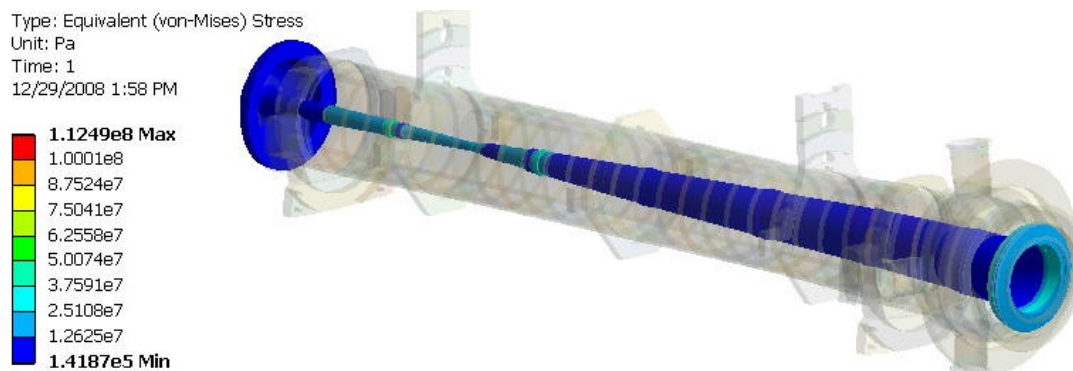


**Figure 3–25:** Stress due to magnetic loading at mid-pulse for Horn 1.

The cyclic thermal and magnetic loading over millions of beam/current pulses may lead to microscopic physical damage to the inner conductor material, even at stresses well below the ultimate strength. Due to the increased cross sectional area of the Horn 2 neck, as well as the lower beam energy deposition in the material, temperatures and stresses are comparatively lower than in Horn 1, and generally do not require as extensive of an analysis.

### 3.4.2.1 Ancillary Components

Outside of inner and outer conductors, several other ancillary systems exist to support the horn during operation. These components include the water manifolds and collection tank,

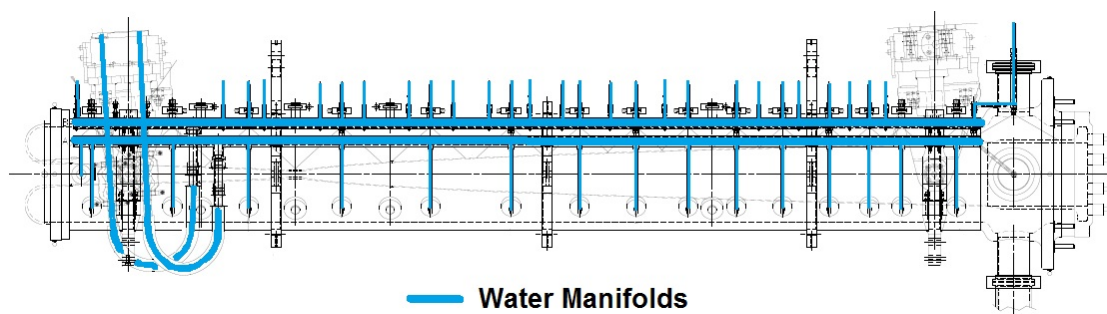


**Figure 3–26:** Horn cooling water manifolds.

upstream and downstream support hangers, as well as “crosshair” assemblies (for beam-aided alignment) and instrumentation.

The water manifolds run the length of the horn outer conductors and provide cooling water to the spray nozzles. All water manifolds must be electrically isolated by an alumina ceramic assembly that prevents horn current from traveling back to RAW systems and instrumentation. These manifolds and water cooling passages can be seen in Figure 3–26.

The upstream and downstream support hangers hold the horns in position, while providing a degree of freedom for vertical adjustment. Internal hanger bushings are constructed of metalized graphite, as to avoid corrosion problems seen with other bushing materials. The metalized graphite is also radiation hard and has proven to be a very successful material in hazardous environments. Water line connections, as well as all instrumentation lines run through the hangers, which demands a well-designed layout and specialized fittings for rad-hard, leak free service. A structural analysis has been performed on hangers to ensure material scalloping for weight reduction does not affect overall dimensional stability. This analysis will undergo several iterations as loading conditions for the horns become more defined. An example of this can be seen in Figure 3–27.

A Horn crosshair engineering analysis must also be performed to determine maximum operating temperatures. An aluminum crosshair design has been used successfully in the past, and beryllium has been specified for the NOvA Horn 1 crosshair due to the large amount of beam energy deposition. Beryllium is the most logical choice for the LBNE Horn 1, as it can withstand high temperatures with little deformation. Dimensional stability of the crosshair is the main consideration however, and additional cooling contacts or geometrical changes from their operation in the NOvA experiment might be needed. These changes would allow for a sufficiently low operating temperature, providing low thermal expansion and resistance to material creep.

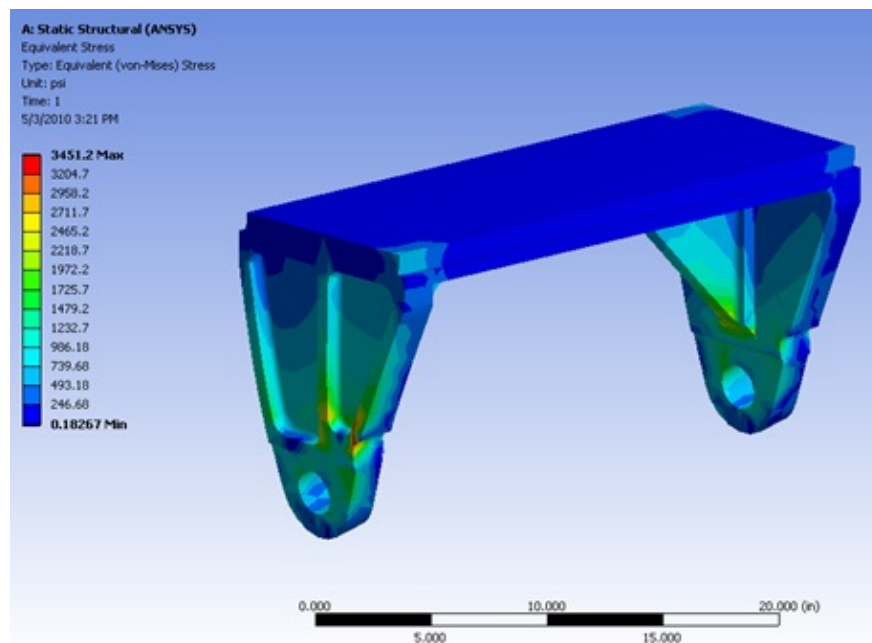


**Figure 3–27:** Horn hanger structural analysis with tri-axial loading.

### 3.4.3 Horn Support Modules

Horns will be supported and positioned by support modules. The intensely radioactive environment of the target chase requires that the horn-support module be adjustable and serviceable by remote control. The horn-support modules provide radiation shielding, and allow the mounting and dismounting of feed-through connections for the stripline, cooling water and instrumentation cabling from the top of the module mainframe, away from the most highly activated areas.

The horn module support concept is shown in Figure 3–28.

Horn-support modules are rectangular boxes open at the top and bottom, and are constructed from plate steel. The walls perpendicular to the beam at the upstream and downstream ends of the box will be up to 10-in thick. The side walls oriented parallel to the beam line will be up to 2-in thick with two plates welded together to form overhangs that create a labyrinth to shield radiation.

The modules fix the horn with respect to the module in the horizontal degrees of freedom, but not in the vertical. The module is adjusted with respect to the beam for transverse horizontal position and yaw. The horn is adjusted with respect to the module for vertical and pitch alignment. This is accomplished by two separate motorized systems shown schematically in Figure 3–29.

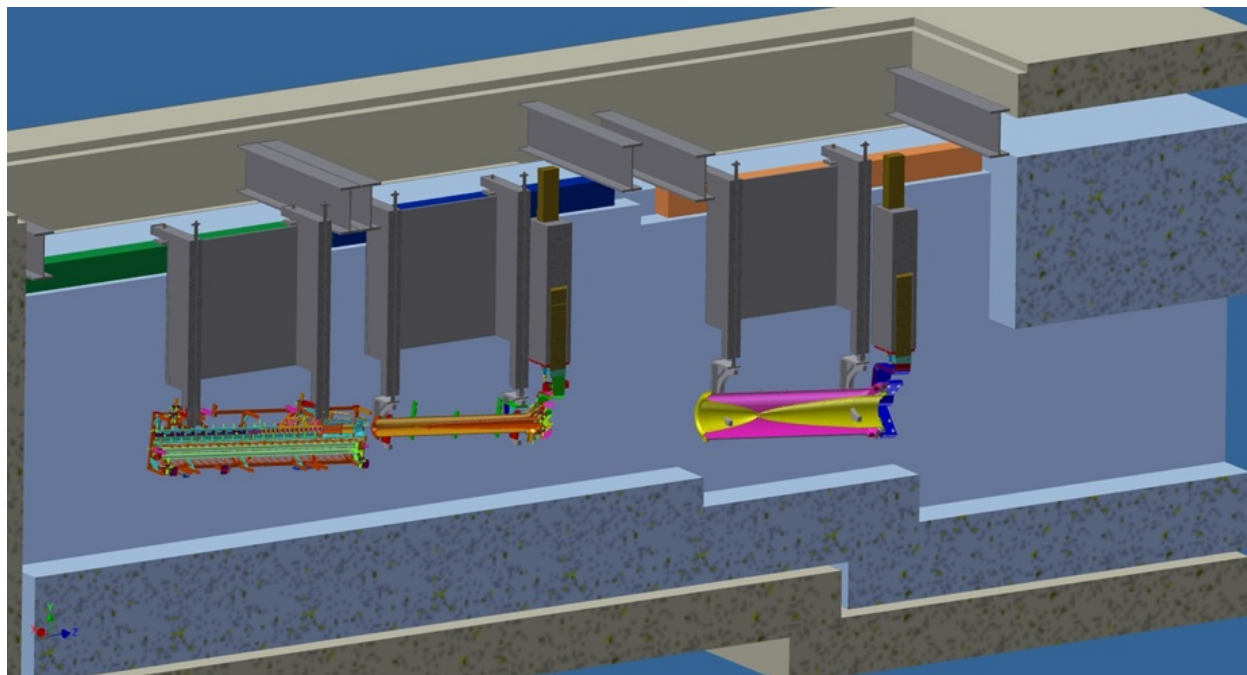


**Figure 3–28:** Horn support module concept. The beam comes from the left, through the target carrier assembly, followed by the Horn 1 and Horn 2 module assemblies.

The horizontal system is mounted to the carriage rails to allow the module to be pushed or pulled horizontally perpendicular to the beam with two independent five-ton screw jacks. The screw jack is powered by a radiation-hard stepper motor. The design is based on the existing hardware for the Booster Collimators installed at Fermilab. By differentially driving the horizontal motors at each end of the module, yaw is controlled. The vertical adjustment system is a simple screw-jack-gear-box-motor configuration conceptually similar to the horizontal mechanism. To allow the horn to be crane-lifted out of the beamline for repairs and then replaced without changing its position in the beam line, the module adjustment mechanism includes a kinematic mount. A standard kinematic mount is a three-point support with the third support point sitting on a flat plate to allow free horizontal motion. The modules are on four point supports, so both of the beam left support points are simple flat plates. Once the modules have been surveyed into place the first time, the motorized adjustment mechanisms can be used to scan the horn across the beam for final alignment. High-strength steels – alloys whose yield strength is above 87 ksi – have been found to be a problem in high-radiation areas because of “stress corrosion cracking”. This class of materials will not be used on any component of the modules or their adjustment systems.

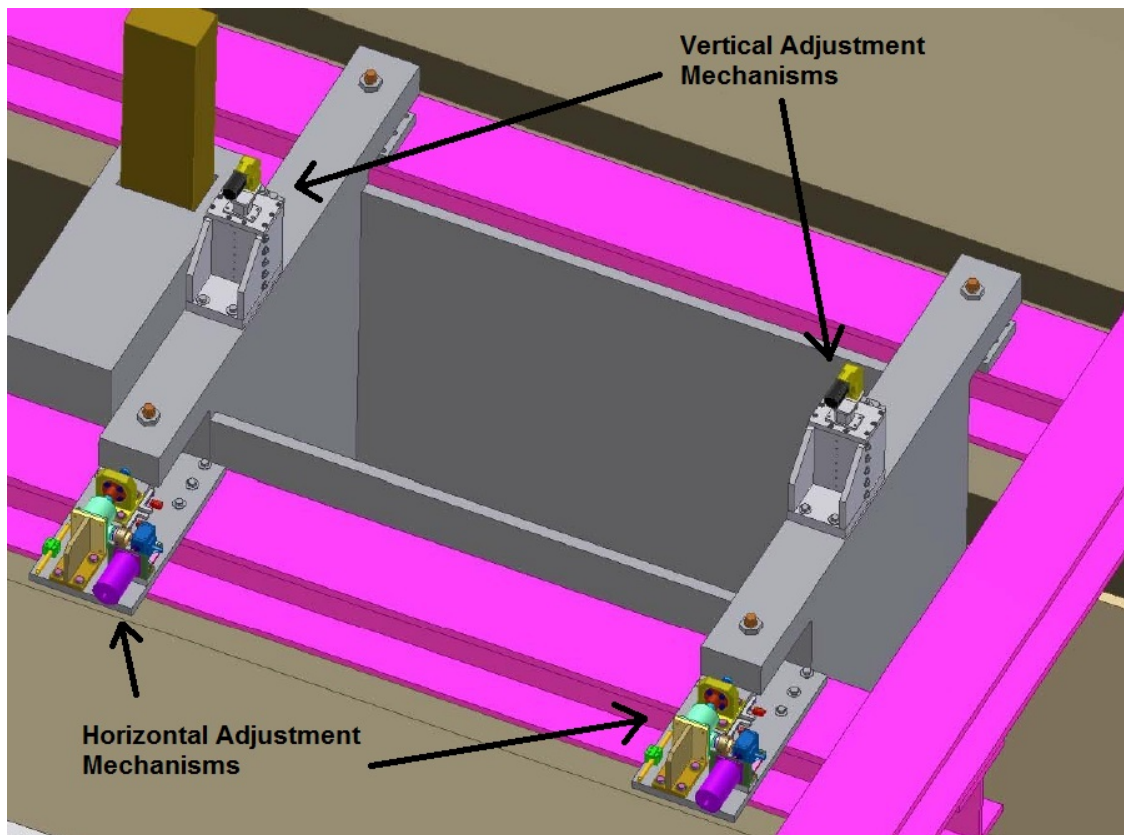


**Figure 3–29:** Adjustment fixtures for the horn-support module concept. The modules are fixed only horizontally along the beam direction.

**Table 3-4:** Estimated circuit parameters for the horn power supply; based upon NuMI system.

	Inductance ( $\mu\text{H}$ )	Resistance ( $\mu\Omega$ )	Power (kW)
Horn 1	0.685	249	7.9
Horn 2	0.51	71	2.4
Capacitor bank and connects	0.1	15	0.5
Transmission Line			
8 layer (30m)	0.45	312	9.9
9 layer (17m)	0.119	162	5.1
Totals	1.867	809	25.8

### 3.4.4 Support Module Stripling Blocks

Attached to each horn and supported by the module mainframe, the stripline block provides radiation shielding, as well as a containment structure for the striplines that supply current to the horn conductors. The blocks must have an integral labyrinth for these aluminum layers due to radiation shielding concerns, and also must remotely attach and unattach from the horn stripline through use of a remote clamp which is mounted to the lower end of the block. The conceptual stripline block assembly can be seen in Figure 3-30. This allows a complete horn system assembly to be assembled and unassembled through remote handling, providing minimal exposure to technicians during horn change-outs.

The stripline block will primarily consist of steel construction, having a stainless steel outer casing to provide corrosion resistance and containment for any internal components. The remote clamp assembly will be manufactured from 316 stainless steel to resist corrosion, as it must be able to disengage the horn stripline upon release. The remote clamp can be seen in Figure 3-31.

## 3.5 Horn Power Supplies (WBS 130.02.03.05)

This section discusses the horn power supplies, which will be designed to supply the horns with a minimum of a 200-kA sine-wave peak, within tolerances set for a minimum beam pulse of 10 microseconds. One supply will power both horns.

A damped LC discharge circuit will achieve the peak current when the silicon controlled rectifier (SCR) switch releases stored energy from the capacitor bank to the horns via a planar transmission line (“stripline”). The estimated circuit parameters are as listed in Table 3-4.

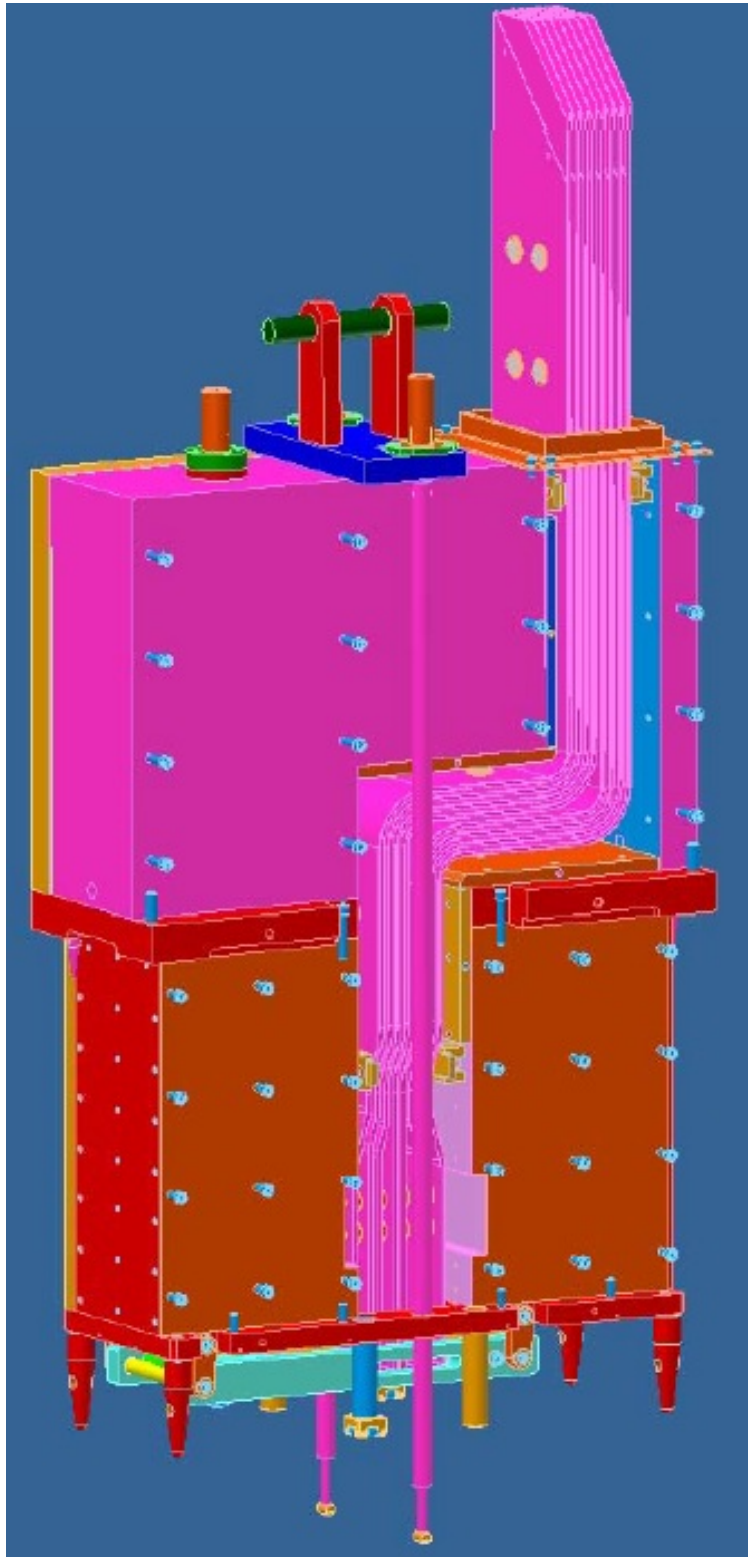


**Figure 3-30:** Stripline Block structure assembly.

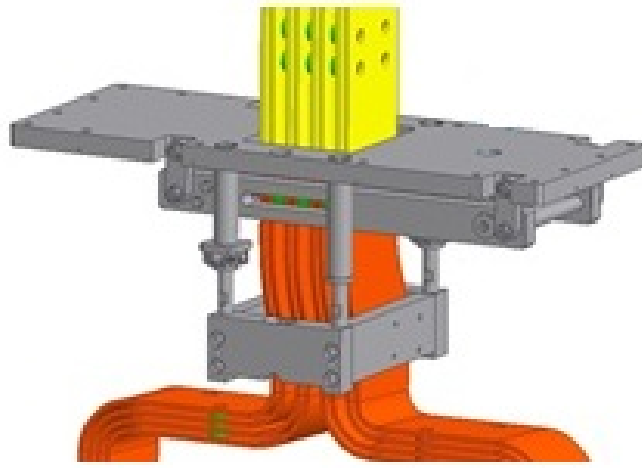


**Figure 3-31:** Stripline Block remote clamp assembly.

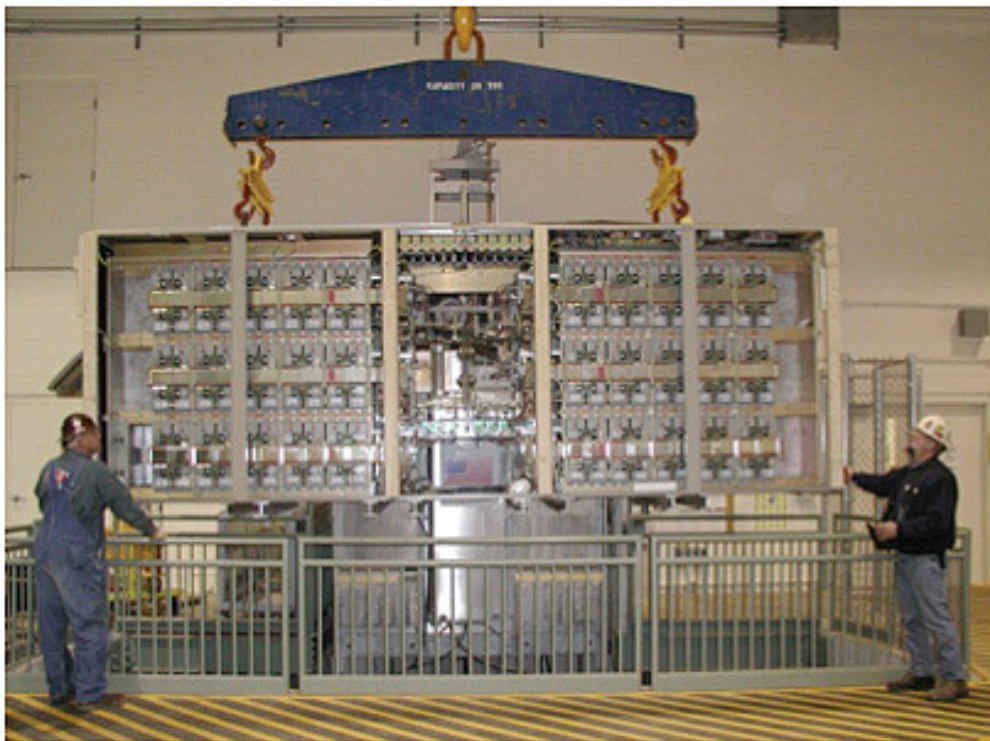


**Figure 3-32:** NuMI Capacitor Bank transport and installation, 2004.

### 3.5.1 Design Considerations

For powering LBNE focusing horns for 708-kW operation, the horn power supply built for NuMI will be reused in the LBNE beamline after cessation of the NOvA experiment. Extensively tested at 205 kA but used for most of its life at 180 kA to 200 kA, its reliable service is expected to continue through the NOvA experiment and on to LBNE service, including routine maintenance. Two areas of wear are the Silicon Controlled Rectifiers, (SCRs) and energy storage capacitors. Both items are designed into the existing equipment in a manner allowing ready removal and replacement. A stress analysis of the 22,000 lb. capacitor bank was completed and documented prior to it being moved into its current NuMI underground target hall support room location, shown in Figure 3-32

#### 3.5.1.1 Capacitor Bank

Operating with the NuMI capacitor bank powering the horns will provide a half-sine pulse width of 2.1 ms base-time. Pulse width is reduced from the 2.6 ms of NuMI due to a shorter and lower inductance stripline design planned for LBNE. The NuMI stripline components are not candidates for reuse in LBNE due to corrosion and activation.

DC capacitor charging is presently accomplished by a single 240-kW, 800-volt phase controlled supply manufactured by Power Energy Industries (PEI). A second unit of the same model was installed adjacent to the operating unit as a stand-by spare. This will also be done for LBNE, allowing rapid change-over in the event of failure of the in-service unit.

#### 3.5.1.2 System Safety

The safety system designed into the NuMI horn power supply will meet all the needs of the LBNE experiment. It has been approved by the Fermilab ES&H Section and also by the Directorate prior to start-up of operations in the NuMI beamline.

Local controls continuously monitor numerous parameters during the charge-discharge cycle, safely shutting down the system if out-of-tolerance conditions are detected. Monitored parameters include personnel entry, charging source over-current, over-voltage, over-current on any one of the 12 sub-cells, total load current, over-current in any stripline conductor, out of balance conditions between cells, ground fault currents, excessive water, air, or stripline temperatures. Stored energy in the capacitor bank is immediately dissipated in redundant resistive dumps via redundant, appropriately rated HV relays and an SCR for microsecond response.

A system transient recorder monitoring as many as 32 parameters of every pulse is incorporated to assist with diagnostics. Specific parameters of interest are user selectable, allowing

detailed observation of intermittent events as deemed necessary.

Included, too, is a slow-start controller, regulating horn current from zero to its preset operating level over a period of 30 seconds, allowing the system to trip at low level conditions during initial turn-on in the event the load has been compromised by any form of fault.

### 3.5.1.3 Controls

The existing low-level electronic controls as part of the NuMI system will likewise be repurposed and installed in LBNE. Once there, a complete performance check and calibration will be carried out. Connections to the ACNET controls will require new cabling, set up and performance verification.

### 3.5.1.4 Current Transducers

Passive current transformers installed within each capacitor bank cell monitor the cell performance to 0.4% accuracy. These 12 signals are also summed to provide individual stripline currents plus total load current for over-current monitoring for horn protection.

### 3.5.1.5 Transmission Line

New stripline is to be constructed to connect the capacitor bank to the two series connected NuMI style horns. To preclude any redesign of the stripline-to-horn interface for 708-kW operation, NuMI eight-layer design, Fig. 3-33, will be installed under and within the target hall chase shielding. A more efficient nine-layer MiniBooNE style stripline, Fig. 3-34, will be constructed from the capacitor bank to and through the penetration and continuing on along the target hall wall, connecting to the NuMI style stripline. Appropriate nine-to-eight layer adaptor links are to be utilized.

The aluminum bus alloy of choice is 6101-T61. Specifically intended for electrical use, it has nearly the conductivity of pure aluminum but with enhanced mechanical properties. The stripline design must have minimal inductance and resistance, allow for thermal expansion and contraction at horn and capacitor bank connections while allowing rapid reliable connection and disconnection at each horn location. In high radiation field portions of stripline, the conductors will be spaced with alumina ceramic insulators. In minimal or no radiation portions, lower cost inorganic materials will be sought. Lengths between spacers are separated by air gap. The assembly will be held together in compression by overall aluminum bar clamps at each spacer location. Stripline electrical joints are held in compression by the proven 3200 psi steel bar clamp technique. Vertical floor-mounted stanchions will support the completed stripline assembly along the target hall wall portion.

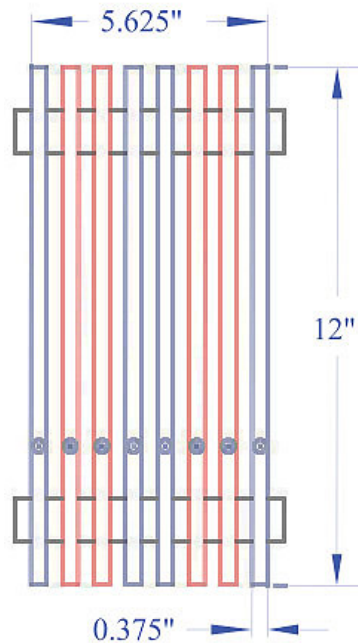


**Figure 3-33:** Stripline cross-section: 8 conductor (NuMI-style). Color indicates polarity of current. This design connects from the nine to eight layer transition to the horns.

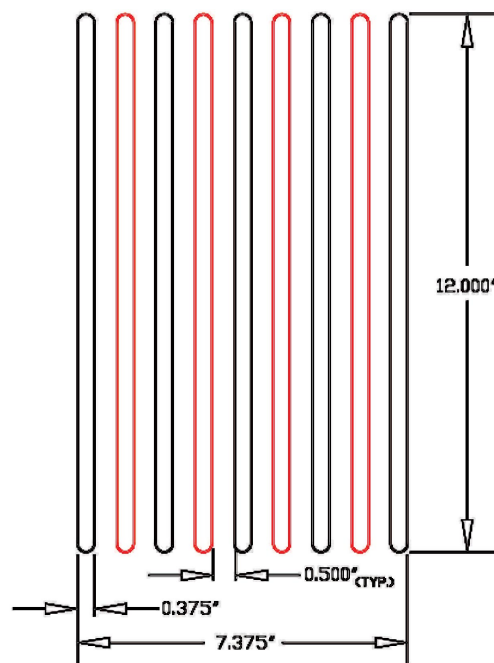


**Figure 3-34:** Stripline cross-section: 9 conductor. Color indicates polarity of current. This design will be installed from the power supply to the 8-conductor stripline transition in the chase.

While the two different stripline cross-sections have a factor of two difference in inductance, the nine-layer design being lower, they have nearly the same resistance. Power loss in the stripline is 560 W/m, 26 kW total, based upon an estimated total stripline length of 47 meters. The stripline will be sized to carry the normal 7,700 A<sub>rms</sub> operating current (300 kA<sub>peak</sub>) of horn operation plus a 20% design margin in terms of current. Overall ducting and filtered forced-air cooling will protect personnel and control temperatures.

### 3.5.1.6 Ground-Fault Protection

Since horns and horn support modules are isolated from ground due to their operation at high voltage, 940 mcm (thousand circular mils) grounding cables connect each of the horn modules directly to the capacitor bank single-point ground. This ground point is monitored to detect ground fault current. Detected faults initiate immediate termination of system operation and, via electronic crowbar with mechanical back up shorting relays, redirects all remaining stored energy to the internal dump resistor banks.

More importantly all high voltage equipment enclosures will be connected directly to Earth ground utilizing low impedance techniques. This protects personnel making incidental contact with the exterior of any system enclosures from transient “ground bounce” should such faults occur during routine operation or maintenance activities.

### 3.5.1.7 Water Cooling

LCW at the same 12-gpm flow rate will be available for the capacitor bank and DC charging power supplies as was done for NuMI.

## 3.6 Decay Pipe (WBS 130.02.03.06)

### 3.6.1 Introduction

The decay pipe is the region where the pions and kaons generated from the target decay into neutrinos. The length is determined by the distance at which most of the pions decay, producing neutrinos near the maximum energy required by the physics goals of LBNE. The pipe must be of sufficient diameter to allow for decay of the lowest-energy pions required by the experiment. The decay-pipe reference-design length is 203.7 m.

Concrete radiation shielding surrounds the decay pipe to minimize activation of surrounding ground water. Heat generated in materials due to beam reactions will be removed by airflow

through the decay pipe. A geomembrane system surrounds the decay-pipe concrete to act as a barrier for minimizing ground-water inflow. Any ground water that penetrates the barrier system will be collected in pipes and conveyed to sumps located in the Absorber Hall, described in Section 3.7.

The scope of work described in this section includes specifying (1) the length, material, diameters and wall thicknesses for the concentric decay pipe, (2) the thickness for the shielding concrete, (3) cooling parameters, and providing the end closure. Conventional Facilities (see Volume 5 of this CDR) designs and provides the corrosion-protected concentric decay pipe, shielding concrete and the geomembrane ground-water barrier and drainage system.

### 3.6.2 Design Considerations

The decay pipe and its shielding are built underground and their size cannot be significantly modified or upgraded after completion. Therefore, this part of the neutrino beam has been designed for 2.3-MW beam-power operation, corresponding to the maximum anticipated power. The concentric decay pipe and shielding concrete are illustrated in Figure 3-35, which shows the system designed by the Conventional Facilities at the Near Site to satisfy the Beamline requirements [24]. The CF design is described in more detail in Volume 5 of this CDR.

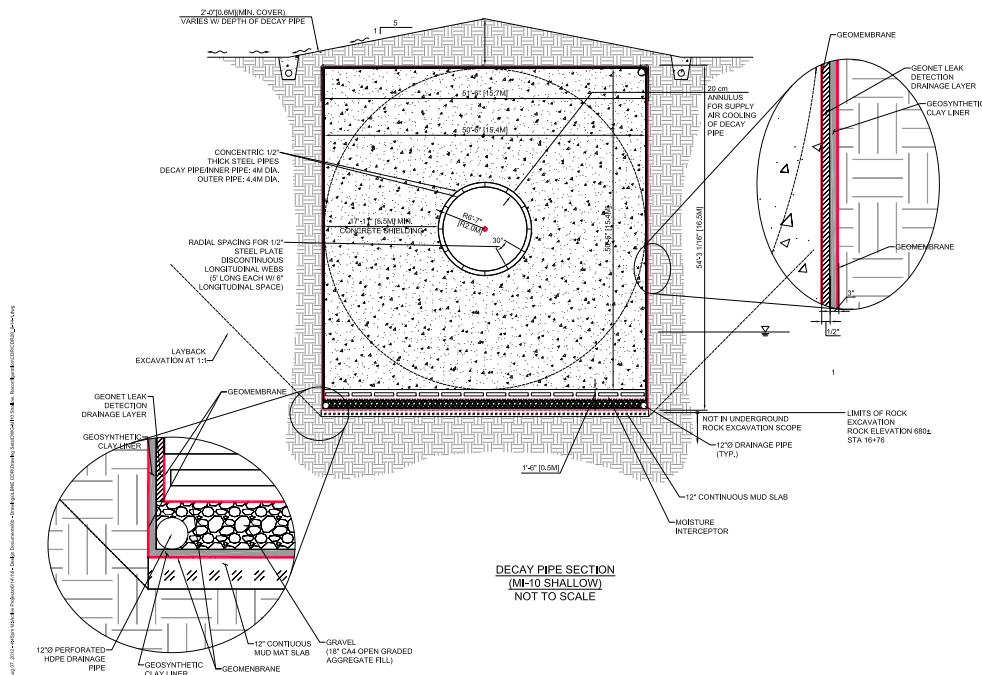


**Figure 3-35:** Typical cross section of concentric decay pipe and shielding concrete.

The decay pipe CF construction must be built to meet these requirements:

- 203.7-m length
- 4-m inside-diameter steel pipe installed concentrically in a 4.43-m inside diameter steel pipe; the radial annular gap between the tubes is 0.2 m
- commercial-grade pipe with thickness of 12.5 mm
- spacers welded between the two pipes to maintain concentricity and to not interfere with the airflow
- a geomembrane ground-water barrier system to drain water away from the decay pipe as part of the overall tritium-mitigation strategy discussed in Section 3.10
- alignment accuracy maintained at 20 mm
- resistance to temperature rise of 50°C which generates compressive stress of 15,600 psi with fully constrained concrete end walls
- external and internal steel-corrosion protection for radiation resistance and corrosion lifetimes
- concrete radiation-shielding thickness of 5.5 m with upstream and downstream 6-m ends

The decay-pipe region begins 17.3 m downstream of the target. The upstream end of the decay pipe opens to the chase within the Target Hall (see Figure 3-36), accepting cooling-air return-flow from the target chase on its way to the combined air-return duct at the upstream end of the decay pipe, as discussed in Section 3.8. Heat generated by beam interaction has been calculated to be 511 kW, distributed non-uniformly down the length of the decay pipe. Approximately half of this heat is generated in the inner steel tube, with the remainder generated in the outer steel tube and first 0.5-m depth of concrete. A maximum temperature of 35°C is estimated in the steel tubes and a maximum temperature of 40°C is estimated at the geomembrane layers with the cooling airflow of 50,000 scfm discussed in Section 3.8 and air supply temperature of 15°C (59°F). The downstream end of the decay pipe must be closed as part of the air cooling of the pipe.

It is anticipated that the CF design will include concrete at normal strength of 4,000 psi with appropriate flow characteristics for pouring. It is also expected that the stiffeners will be positioned between the inner and outer pipes to maintain concentricity.

### 3.6.3 Reference Design

The decay pipe ends in the upstream wall of the Absorber Hall, as shown in Figure 3-37. The Beamline L2 Project will provide the end closure at the downstream end of the decay pipe for the outer steel tube. This will be a steel, formed head with a central 1-m-diameter region of 6-mm-thick aluminum. The head will be sized to minimize deflections due to air pressure. The central aluminum window will be air-cooled as the air flows out of the annular radial gap and turns 180°, flowing against the end closure, to head upstream in the 4-m-diameter inside steel tube. This window will be welded in place and will not be replaceable.

Supply and return air ducts connected to the concentric decay pipe (Fig. 3-36) for the cooling airflows are discussed in Section 3.8.

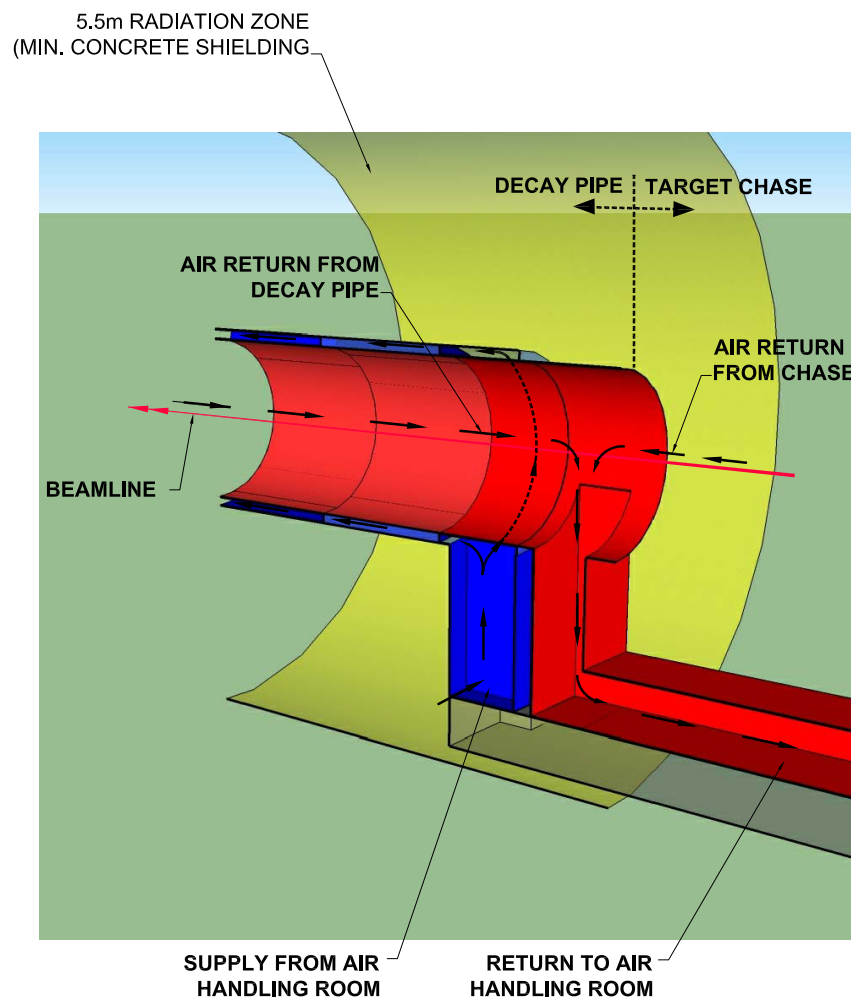


**Figure 3-36:** Section of the decay pipe at its upstream end. The airflow directions within the pipes are indicated.

## 3.7 Hadron Absorber (WBS 130.02.03.07)

### 3.7.1 Introduction

The hadron-absorber structure (also called simply the “absorber”) is located directly downstream of the decay pipe. The absorber, a pile of aluminum (Al), steel and concrete, is intended to absorb the residual energy from uninteracted protons and the secondary particles (hadrons) which do not decay. The power absorbed is a large fraction of the total beam power and thus needs to be contained to prevent activation of subsurface soils and groundwater.

The absorber consists of the following components: the absorber core (including the Al and steel sections, and the Al pre-absorber core mask), the absorber shielding (including steel blocks and concrete), and the temperature-monitoring and cooling infrastructure.

Figure 3–37 shows a simplified view of the absorber within the Absorber Hall. The yellow zone represents the absorber core where the vast majority of the non-interacted protons and secondary particles that reach the absorber will start hadronic and electromagnetic showers.

### 3.7.2 Design Considerations

The LBNE absorber is designed to support a beam power up to 2.3 MW at an energy range from 60 to 120 GeV. The absorber should operate without maintenance during the lifetime of the experiment; extensive upgrades at a later time would be impractical.

The absorber must be designed to sustain the beam-energy deposition under expected normal operational conditions as well as under all accident situations that may occur with some reasonable probability. In the case of normal operation, the absorber should dissipate 560 kW of power per beam spill. In the case of an accident, the absorber should sustain at least 15 pulses at full 2.3-MW beam power for a total duration of 20 s. During this time, the thermal protection embedded in the core blocks should generate a signal to inhibit the beam permit. Such power requires special attention to the cooling of the absorber components, especially its central part - the Al core.

The interaction of the protons and residual secondary particles with the absorber media creates thermal neutrons that are mostly absorbed by the external concrete. The majority of the muons pass through the absorber, depositing negligible amounts of energy before they stop in the rock downstream of the Absorber Hall. According to the simulation [25], 24% of the total beam power is deposited in the absorber, 60% of which comes from the primary protons.

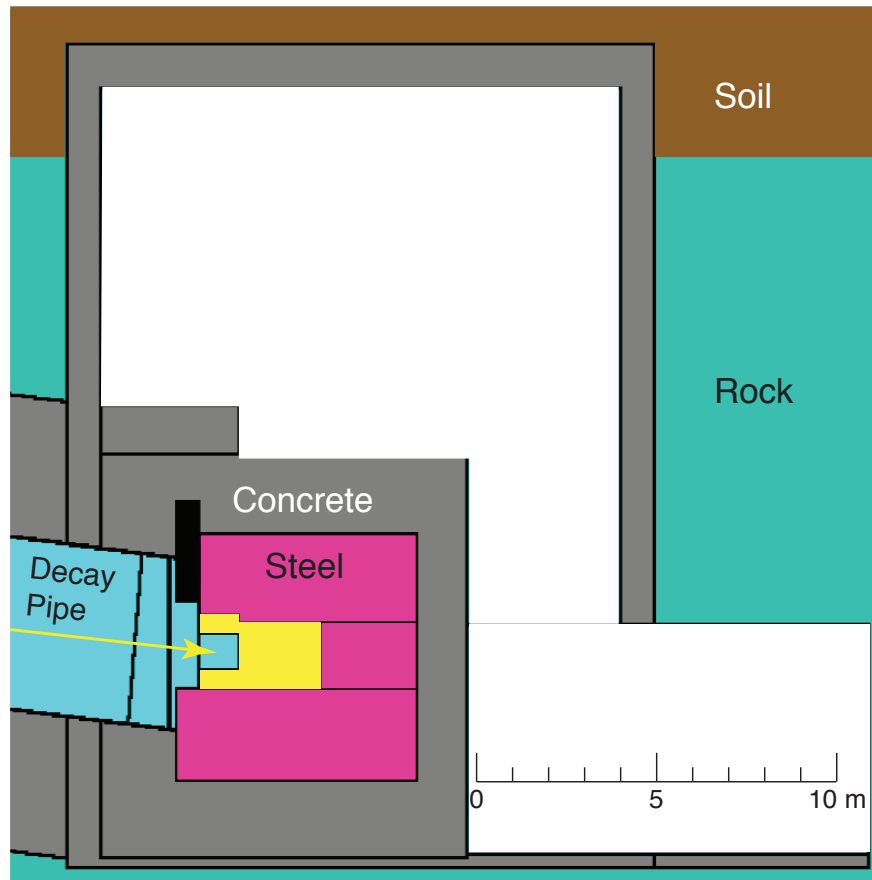


**Figure 3-37:** Simplified elevation view of the absorber within the Absorber Hall. The white zones are air. Most of the energy (from the uninteracted protons) is deposited into the Al absorber core (yellow). The excavation at the lower right is an alcove for beam muon monitors (described in Volume 3 of this CDR). The soil-rock interface is approximately 23 m below the surface.

### 3.7.3 Absorber Modeling

#### 3.7.3.1 Normal Operations

The longitudinal energy deposition in the Al core in the case of normal operation is shown in Figure 3-38. The maximum energy deposition is between the third and fourth blocks (hatched zone, Figure 3-38). Accordingly, the reference design places the center of the third block in the transverse center of the hadronic shower. For this block, the calculated energy deposition was transferred to finite element analysis software (FEA using ANSYS) to simulate the temperature distribution and the necessary cooling conditions. Figure 3-39 (left), shows the maximum temperature in the absorber-core block over 10,000 normal beam pulses. The temperature reaches a plateau at approximate 187° C. Figure 3-39 (right) shows the final temperature distribution in the block. For this simulation, the cooling lines were placed around the perimeter of the block and water temperature was assumed constant at 25° C. This analysis shows that maximum operational temperature is below any critical temperature of the Al material. This relieves a point of concern that exposure of Al material to high temperatures ( ~275° C) for long period of time could raise the issue of creep (time-dependent plastic deformation) and possible thermal distortion.

Similar simulations were performed for all other absorber blocks, and the results were taken into consideration in the overall design of the cooling scheme. To simplify the design, the steel blocks of the absorber core have the same cooling channel pattern as the Al ones.

The absorber core, like the target and decay pipe, needs to be adequately shielded to prevent a build-up of radionuclides in the water contained in the surrounding rock. To satisfy this requirement, the core, like the NuMI absorber [16], should be surrounded with steel and concrete blocks, which form the absorber shielding. Additional specification for the amount of shielding comes from a requirement that the residual radiation dose in the Absorber Hall, after decay of the short-lived radionuclides, should be on the level of 100 mrem/h. This requirement is imposed by the necessity of servicing the detectors placed in the Absorber Hall, e.g., the hadron and muon monitors. To satisfy these requirements for the LBNE absorber, the MARS simulation indicated that at least seven feet of steel and three feet of concrete shielding are needed.

The hadron monitor, which is placed in the front of the absorber core, is expected to have an average lifetime of one year (see Volume 3, Section 3.2 of this CDR). To store both the highly activated monitors after their service life and any faulty absorber blocks, a specially designated radioactive material storage place is included in the absorber concrete wall. It has three slots to store the activated Monitors and/or absorber blocks before their removal to the surface.

It is unlikely, but possible, that the water-cooled absorber modules and steel shielding blocks will fail. Although the absorber components are designed to last the lifetime of the facility

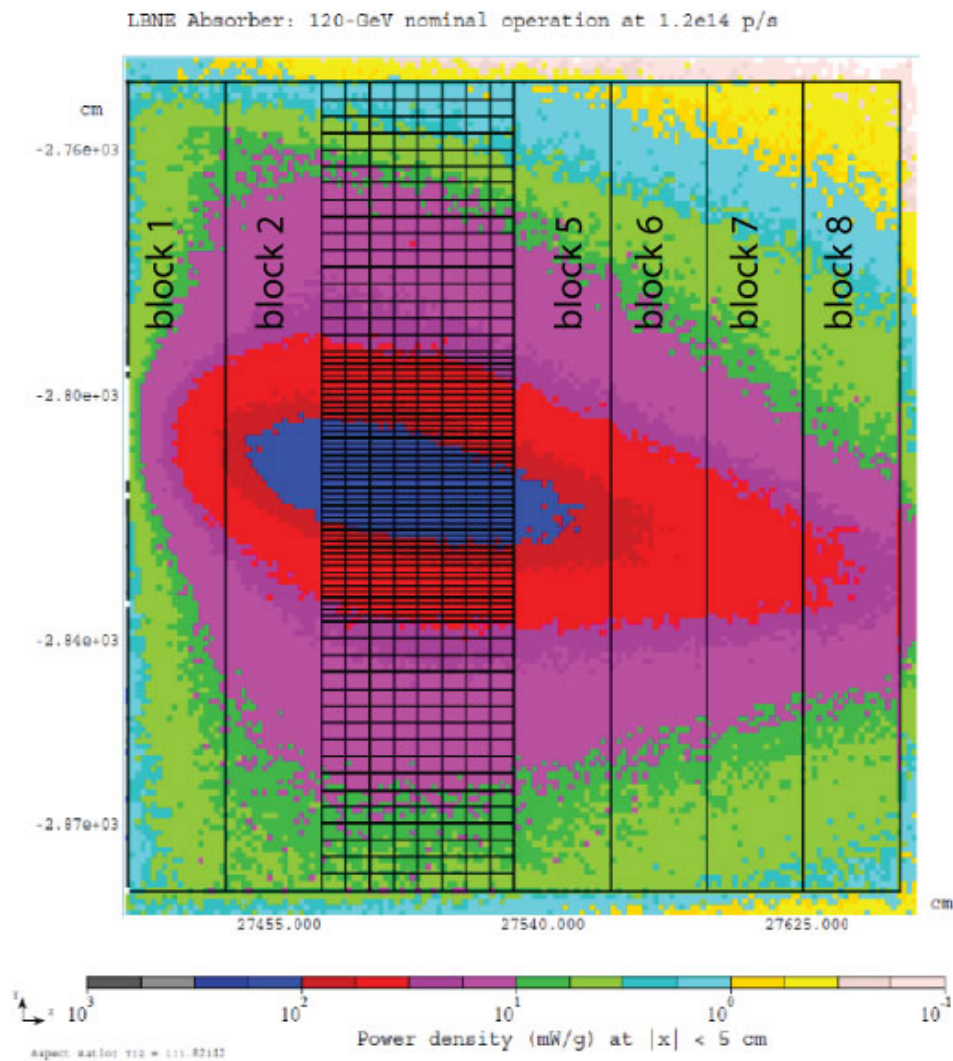


**Figure 3–38:** Result from MARS modeling showing the longitudinal energy deposition in the Al core of the absorber for normal operation.

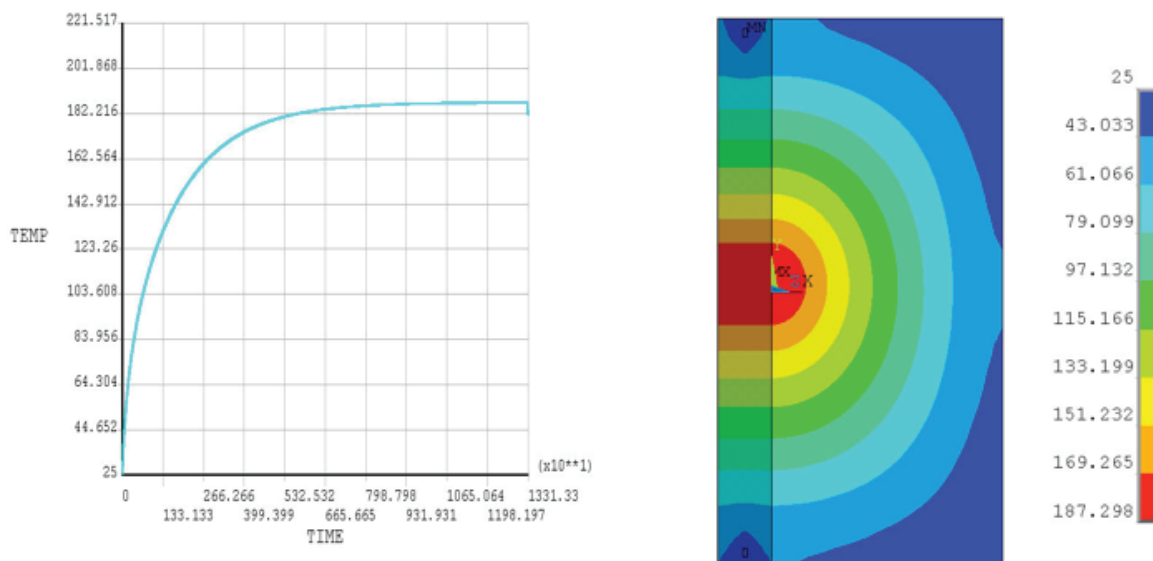


**Figure 3–39:** Results from ANSYS simulation. The maximum temperature ( $^{\circ}\text{C}$ ) versus time  $\times 10$  (s) for the third Al core block is shown (left) after 10,000 normal pulses. The temperature distribution in the same block is shown to the right.

and will include at least three redundant water-cooling lines, the consequences of complete failure might be significant. Because of the low probability of complete failure, the design and construction of remote handling equipment for the absorber modules and water-cooled shielding will not be included in the current design. If complete failure of a water-cooled block occurs during operation, a long downtime (6 months to 1 year) would then be required to design, build, develop procedures and safely replace the failed component(s). Following repair, failed components could be stored in the slots provided to keep the activated hardon monitors in the Absorber Hall.

### 3.7.3.2 Modeling Accident Cases

Two accident conditions have been modeled.

The first accident case assumes that a mis-targeted primary proton pulse hits directly in the central part of the absorber. In this case the full beam power of 2.3 MW is deposited directly into the absorber structure. An analysis was performed to determine how many direct beam pulses the Al core can take before the maximum temperature reaches over  $600^{\circ}\text{C}$  (the melting temperature for pure Al is  $660^{\circ}\text{C}$ ). Figure 3–40 shows the temperature distribution in the third block after ten direct beam pulses imposed over the operational regime with temperature of  $187^{\circ}\text{C}$ . The FEA shows the temperature increasing to  $490^{\circ}\text{C}$ , or

every beam spill increases the temperature in the center of the core by approximately 20°C. The requirement is that the absorber should sustain at least 15 accident pulses, for the total duration of 20 s. An extrapolation of this dependence showed that after approximately 20 faulty pulses the maximum temperature in the center of the third Al-core block will reach ~ 600°C which is still below the melting temperature for the Al core. To prevent such a high temperature, every core block will be instrumented with a number of thermocouples (eight by current design) connected to a National Instrument data-acquisition system [26]. It is worth mentioning that the first steel block in the absorber-core (block number 9) will reach operational temperature of 265°C and 387°C after 15 faulty pulses.

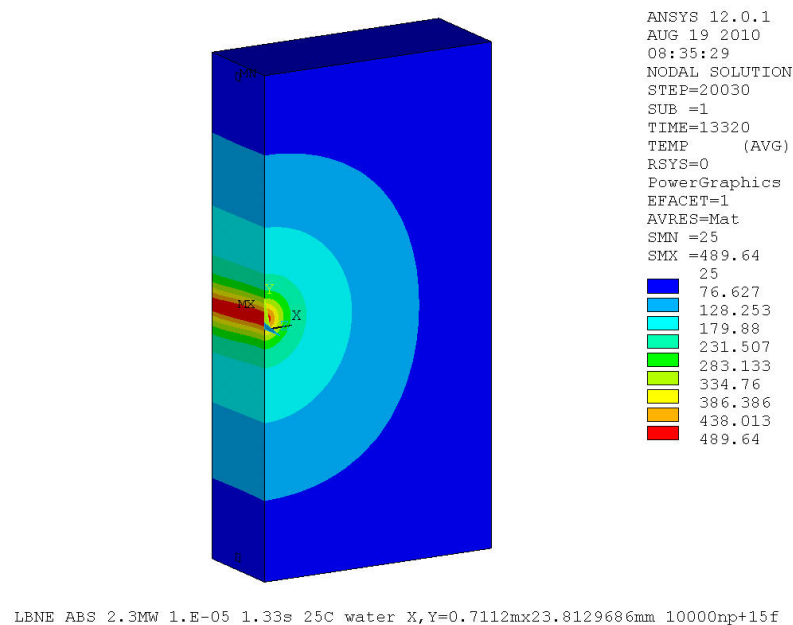


**Figure 3–40:** Temperature distribution in the Al absorber-core block. Fifteen beam pulses under the fault condition are superimposed on 10,000 normal ones. The maximum temperature in the center of the block is 490° C after 15 faulty pulses.

The second accident case assumes the beam is mis-steered relative to its original direction, causing a beam-control failure. This is a single pulse accident condition and it is assumed that primary-beam instrumentation will trip the beam permit before a second or at most a third pulse. Using a simple target/baffle model (one baffle and one passive aperture restrictor, 10 m apart, with diameters 40 mm upstream and 20 mm in front of the target) a maximum “hittable” radius of 900 mm at the absorber is estimated. The primary concern for this accident case is hitting a water-cooling channel, possibly setting off a water hammer effect. MARS [23] energy-deposition modeling, followed by an ANSYS [27] Finite Element Analysis (FEA) simulation indicated that if the water-cooling channels are kept outside the 900-mm-radius, the absorber core will overheat (the water-cooling channels must remain at ~750 mm radius to prevent overheating). To prevent a direct beam hit on the core cooling channels

**Table 3–5:** Operational and accident conditions for the absorber used in the design study with 2.3-MW beam power.

Beam Power in absorber normal operation	500kW
Beam Power in absorber accident condition	2.3MW
Primary beam size at absorber (target in)	20mm H × 12mm V ( $\sigma$ )
Primary beam size at absorber (target out)	15mm H × 12mm V ( $\sigma$ )
Accident condition - direct beam	15 pulses (20 s)
Accident condition - mis-steered beam	2 pulses (2.6 s)
Max. temp. in Al core - normal	187° C
Max. temp. in steel core - normal	265° C
Max. temp. in Al core - accident	490° C
Max. temp. in steel core - accident	387° C
Temperature rise per accident pulse Al (steel)	20 (13) ° C

placed inside this radius, a pre-absorber-core mask will be used to protect the water-cooling channels (see Section 3.7.4.1).

Table 3–5 summarizes the operational and accident conditions for the absorber.

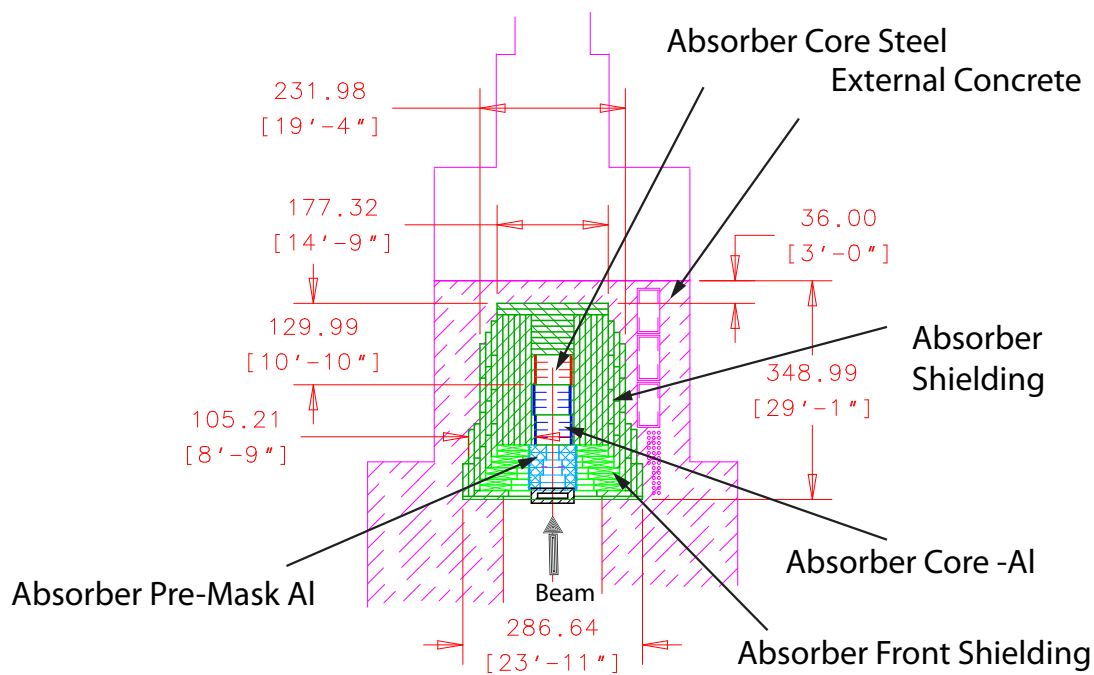
### 3.7.4 Reference Design

Figure 3–41 shows the top view of the absorber. The magenta represents the walls of the concrete shielding. The Al pre-mask and core is shown in blue, while the steel core blocks are represented with red. The green color around the core represents the steel shielding. On the right, three storage slots are reserved for the activated hadron monitors and faulty absorber-core blocks, in case they require replacing.

#### 3.7.4.1 Absorber Core

The absorber core consists of eight Al blocks (each 60-in × 60-in × 12-in). The core receives approximately half of the total energy deposited within the absorber pile, and thus requires water-cooling. The design of the block is shown in Figure 3–42. At least three continuous Al water-cooling lines are welded to the four sides of the block. By design, one cooling line is enough to support the absorber operation. In case of an emergency water leak from one of them, the second or/and third cooling line will be used.

The core dimensions depend on the energy, size and intensity of the incident hadron beam. A MARS simulation, using a simple target and decay-pipe geometry, of the LBNE beam incident on the absorber was used to define the parameters of the core [25]. The parameters



**Figure 3-41:** Model of the absorber conceptual design; top view. The core of water-cooled Al blocks is 96-in deep, followed by 130 in of steel (first 32 in are water-cooled) and 36 in of concrete at the rear. The routing of the cooling pipes is not shown.

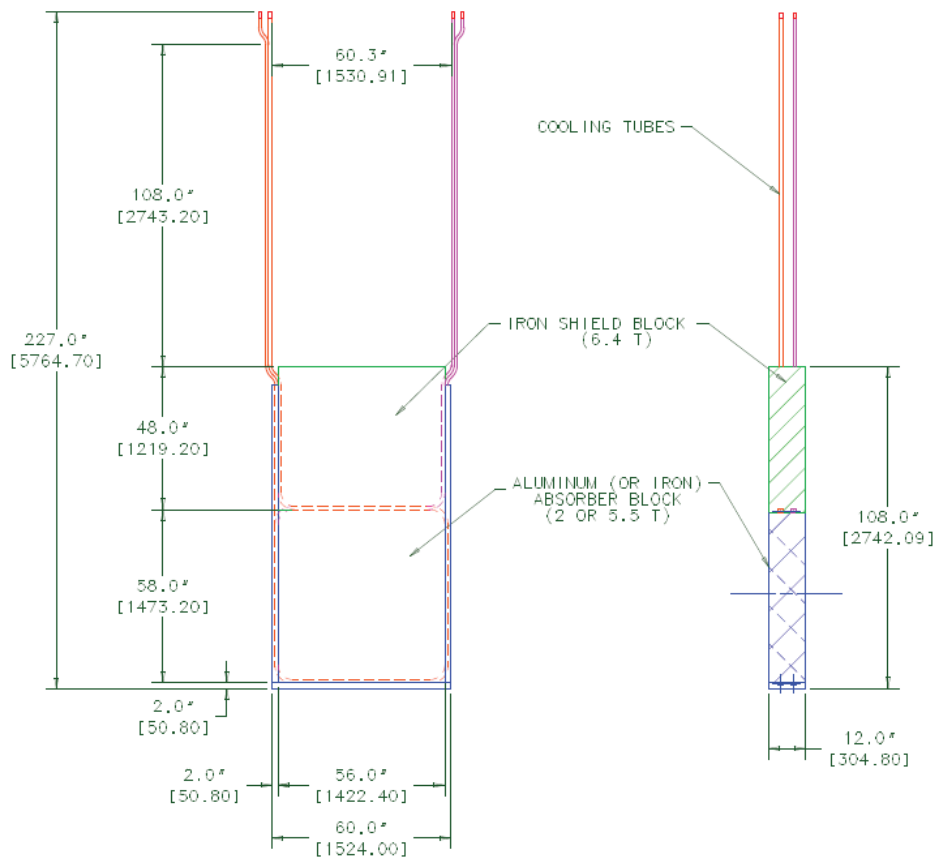


**Figure 3-42:** Design of the absorber core blocks. Note that the part of the top steel shielding (green box, left) is attached to it for easy replacement.

lead to an LBNE absorber core similar to the NuMI ones with an increase of the transverse cross section to 60-in  $\times$  60-in, including the water-cooling channels. The core is leveled horizontally and the beam hits it at an angle of 101 mrad, crossing the absorber horizontal middle plane between the third and fourth core blocks at maximum energy deposition.

To absorb the longitudinal tails of the hadronic showers initiated in the core, the core is extended by an extra seven feet of steel; see Figure 3-41, red and green blocks behind the Al core. Four of these blocks (red blocks) form the steel part of the absorber core. By design, they are identical to the Al blocks except that their Al cooling tubes are clamped to the edges of the block. The other part of the steel shielding (green blocks) is made from continuous-casting salvage steel (CCSS), with a thickness of 9.11 in. The total number of steel blocks behind the Al core is chosen to maintain a safe amount of residual radiation in the Absorber Hall, since service work will need to be performed behind the absorber pile.

This entire structure must be encased in concrete of sufficient thickness to moderate or absorb thermal neutrons and to keep the flux at the absorber shaft entrance at acceptable radiation levels. This design may allow a core block change in case of a total failure of the all three cooling channels. To perform this operation the 30-ton crane installed in the Absorber Hall would be used.

During normal operation, the FEA [28] of the energy deposition in the first steel block (number 9) shows a maximum temperature of 265° C (see Table 3-5). To avoid such a high-temperature condition for this block (ninth block), an option to increase the thickness of the Al part of the core by adding one more block has been investigated. This block will further spread the hadronic shower, thus decreasing the amount of the deposited energy in the first steel block. Furthermore, some minor optimization to the geometry of the absorber core is in progress.

To avoid accidents in which beam directly hits a core cooling line, as described in Section 3.7.3.2, an Al pre-core mask has been introduced. The design of this module is shown in figure 3-43. Six of these pre-core blocks are installed in front of the Al core blocks. The masks are similar in design to the absorber-core blocks, but with larger cross-section. The diameter of the through-hole decreases from 40 in to 20 in over 6 foot distance and center of the hole is offset to follow the beamline slope. The cooling tubes of the pre-core mask blocks are outside of the possible accidental beam-hit area.

#### 3.7.4.2 Absorber Shielding

To decrease the absorber cost, the external shielding around the core also uses CCSS slabs (shown in green, Figure 3-41). The other dimensions of the slabs can be custom ordered; the only limitation is the capacity of the Absorber Hall crane of 30 ton. The absorber core and these blocks are staggered horizontally by  $\pm 1$  inch to exclude the possibility of creating

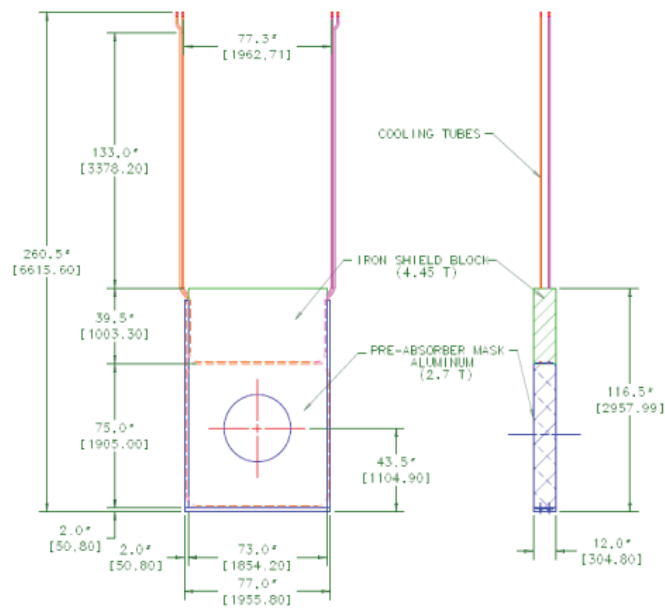


**Figure 3-43:** Design of the Al pre-core mask.

a longitudinal air gap where the hadron shower could propagate. There is no staggering in the vertical direction because the beam is tilted vertically. Some of the front shielding blocks should be water-cooled; the power dissipation in them is too large to rely on just the air convection cooling. The minimum thickness of the absorber core shielding is 87 inches.

In comparison with the NuMI absorber, where the external shielding is built mostly from standard concrete square blocks, for LBNE, the absorber will be surrounded by a cast-in-place concrete bed to provide external shielding of (minimum) thickness 36 in (shown in magenta in Figure 3-41). This concrete is provided by the Conventional Facilities at the Near Site, and is discussed in Volume 5 of this CDR. The only removable blocks will be in the area above the absorber core, which is covered with two overlapping layers of standard concrete blocks (3-ft  $\times$  3-ft  $\times$  6-ft), the area above the radioactive-material storage place, covered with two overlapping layers of concrete blocks (3-ft  $\times$  3-ft  $\times$  7.5-ft); and the area above the Hadron Monitor in front of the first block of pre-absorber core mask, covered with two overlapping layers of standard concrete blocks (3-ft  $\times$  3-ft  $\times$  6-ft).

### 3.7.4.3 Absorber Water-Cooling System

The water-cooling system is based on the detailed simulation of the power losses in different parts of the absorber. The total calculated loss in the core at normal operation is 347 kW (120 kW in the Al blocks and 227 kW in the steel blocks). To dissipate these losses with the cooling water, 165 gpm of water flow is needed through the absorber blocks. At this flow, the water temperature will rise approximately 10°C, varying from block to block. Some additional cooling is anticipated for the front steel shielding blocks.

A closed loop of distilled water with a nominal pressure of 100 psi is assumed. Depending on the cooling and heat-exchanger scheme, the pressure may be adjusted between 60 and 100 psi, and the water-cooling tube size will be selected accordingly. The water-cooling system must be equipped with pressure-relief valves to prevent any damage to the radioactive-water system; a loss of water flow could be serious during an accident condition, for example, while significant energy is stored in the absorber blocks.

For redundancy, the absorber-cooling infrastructure is divided into three or four independent loops. Each loop supplies water to one of the cooling lines for each absorber block. If a problem occurs in one of the cooling lines of any absorber block, the supply cooling loop will be switched off until a shutdown time can be scheduled. Meanwhile, the absorber will continue to work using a spare cooling loop.

A metal containment pan will be installed underneath the absorber to collect cooling radioactive water in the event of a leak from a cooling line. This water will be routed to a holding tank placed in the Absorber Service Building (LBNE 30).

#### **3.7.4.4 Absorber Temperature Monitoring**

Absorber-core blocks will be instrumented with at least eight thermocouples, distributed radially every 45° at a radius of approximately 400 mm. The output voltages from the thermocouples will be read out by five precision temperature loggers (for example, NI PXI-4351 modules), which can each be used to measure the temperatures from 16 thermocouples. The digitized signals will be analyzed by the data acquisition computer, which will provide a beam-permit signal if the temperature is within the specified limits.

This is important in the case of a missing or destroyed target, where the primary beam would directly hit the absorber, depositing maximum power and causing a fast temperature rise.

### **3.8 Target Hall Shielding (WBS 130.02.03.08)**

#### **3.8.1 Introduction**

Target Hall shielding (also called the target pile) is designed to (1) keep the accumulated radionuclide concentration levels in the surrounding soil below standard detectable limits; (2) keep prompt radiation levels low enough for electronics in the Target Hall to have adequate lifetimes; and (3) keep residual radiation rates on top of the shield pile low enough to allow personnel to access the top of the steel shielding pile for maintenance with beam off. It consists of two portions, the Target Hall Shield Pile and the Target Hall Air-Cooling Flows.

#### **3.8.2 Design Considerations**

Target pile size cannot be significantly modified or upgraded after completion. Therefore, this part of the neutrino beam has been designed for 2.3-MW beam-power operation, corresponding to the maximum anticipated power.

#### **3.8.3 Reference Design**

##### **3.8.3.1 Target Hall Shield Pile**

The Target Hall steel shield pile refers to the steel shielding surrounding the beamline components (baffle, target, Horn 1 and Horn 2) installed in the target chase. The chase runs the entire length of the steel shield pile, which extends from the primary-beam window down to the decay pipe. The chase is 54-in wide at the water-cooling panels in the region of the horns and 64-in wide elsewhere. Its height varies along the length of the shield pile; the chase

concrete floor has one vertical step. The beam center-line in the Target Hall region slopes downward at 101 mrad (5.79°) from upstream to downstream, as illustrated in Figure 3-44.

The chase acts as a collimator for pions from the target and horns that are not well-focused. This collimation reduces the beam power deposited in the decay pipe.

The shield will consist of two main layers. An inner, steel layer will absorb all of the stray particles from interactions of the primary beam, except neutrons below a few MeV energy. The outer layers are used to moderate and absorb most of the neutrons that escape from the steel layer. These outer layers consist of concrete blocks that are supplemented with borated polyethylene plates on top of the concrete.

The shielding is divided into two sections: (1) the bottom and side shielding which must appropriately shield the surrounding earth and ground water from tritium activation; and (2) the top shielding which must shield the upper Target Hall (see figure 3-45).

The LBNE steel, concrete, marble, and borated polyethylene shielding requirements are given in Tables 3-6 and 3-7. Additionally, there is a 120-in-thick concrete wall at the upstream end to separate the target pile and pre-target tunnel. For comparison, NuMI has 1 m of concrete and 52 in of steel shielding on the bottom and sides and 73-82 in of steel and 18 in of concrete on the top.

**Table 3-6:** Shielding requirements for the top of the target chase.

	Iron (in)	Marble+ Borated Poly (in)	Concrete (in)
Top of chase- All regions	18	0	0
Baffle	92	6	0
Horn 1	106	6	0
Between horns Sec. 1	116	6	0
Between horns Sec. 2	92	6	0
Horn 2	106	6	0
Downstream Horn 2	116	0	36

The open space between the steel shielding and the floor and walls of the Target Hall concrete pit form air cooling channels for the exterior surface of the steel pile. The channels are named “bottom” for the floor and “side” for the walls. The space between the top of the steel shielding pile and the poly layer is called the “top” channel. The poly layer is the cover over the Target Hall pit. The cooling airflow, discussed below, flows through these channels to enter the chase.

Shielding steel is stacked in a staggered and interlocking fashion so there are no line of-sight cracks through the steel shielding pile. Two methods are used to close the top of

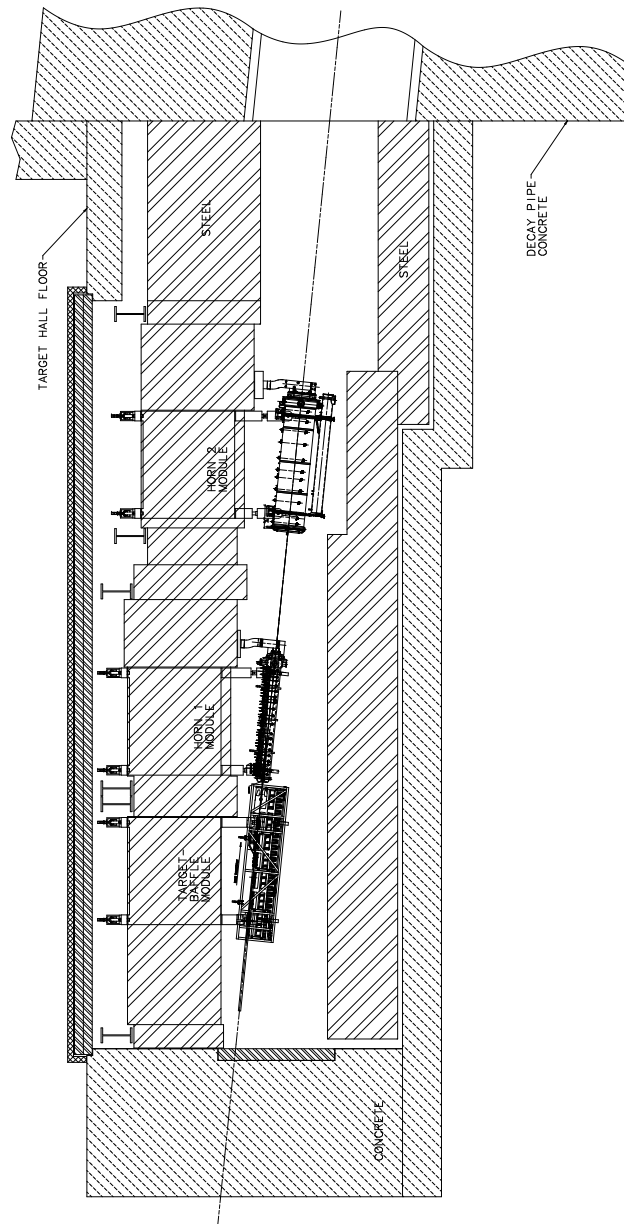
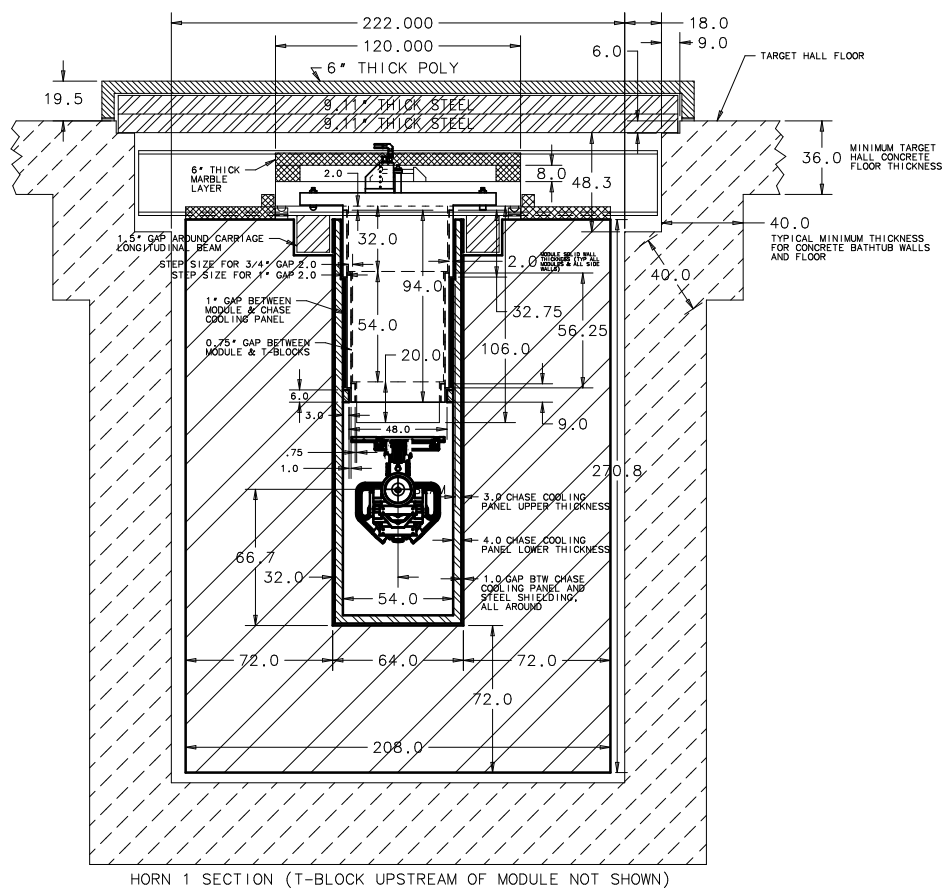


**Figure 3-44:** Beamline elevation view. The beam comes from left and the beginning of the decay pipe is at the right.



Created: 17:16:40 on 07-08-12 (D-M-Y) By: stefonik State: 1-INITIAL

**Figure 3-45:** Cross section of target chase steel shielding (cross-hatched areas). The secondary beam is confined to the rectangular opening in the center

**Table 3-7:** Shielding requirements for the walls and the floor of the target chase.

	Iron (in)	Concrete (in)
Upstream wall	12	140
Baffle floor	72	40
Baffle right wall	72	96
Baffle left wall	72	40
H1 floor	72	40
H1 right wall	72	85
H1 left wall	72	112
Btwn Horns floor Sec.1	72	40
Btwn Horns right wall Sec.1	52	112
Btwn Horns left wall Sec.1	52	112
Btwn Horns floor Sec. 2	72	40
Btwn Horns right wall Sec.2	52	112
Btwn Horns left wall Sec .2	52	112
H2 floor	52	40
H2 right wall	52	85
H2 left wall	52	40
DS of H2 floor	52	40
DS of H2 right wall	52	85
DS of H2 left wall	52	40

chase. Removable, specially made steel blocks called “T-blocks” are used where beamline components are installed. Steel blocks and slabs are used in the other areas.

### 3.8.3.2 Target Hall Air-Cooling Flows

Energy deposited by the 708-kW beam in the shielding pile and the beamline components is removed by an air-cooling system and cooling systems on the beamline components; water-cooled shielding is not required for 708-kW operation. Approximately 35,000 scfm cools the steel shielding at 708 kW. This airflow rate is obtained by scaling the 25,000 scfm airflow rate for the 46-in NuMI chase width to the 54-in LBNE chase width air using the cross sectional chase flow areas.

For the 2.3-MW beam, water-cooled shielding, i.e., carbon steel chase panels, T-blocks and module bottoms, intercept most of the beam energy leaving the chase. The air-cooling system and cooling systems on the beamline components remove the balance of the deposited beam energy. Water-cooled shielding will be installed for 708-kW operation but water cooling will be enabled only at 2.3 MW. Energy deposited by the 708-kW beam or the 2.3-MW beam in the decay pipe is removed by the air-cooling system, water cooling is not needed.

**Table 3-8:** Airflows in the target pile and the decay pipe.

	Flow (cfm)
Target pile chase supply duct	35,000
Top channel	20,000
Side channels (2)	5000 ea.
Bottom channel	5000
Chase return	35,000
Decay pipe side	50,000
Annular gap	50,000
4-m inner pipe	50,000
Combined return duct	85,000

The discussion below outlines the air-cooling system. The equipment needed for air cooling is provided by Conventional Facilities at the Near Site, and discussed in Volume 5 of this CDR.

A single air handler, located in the Air Handling Room, provides 85,000 scfm of dehumidified air to cool the shielding pile and the decay pipe. There are two supply ducts, one to the target pile and one to the decay pipe. Airflows to the shield pile and to the decay pipe are balanced with dampers in the air handler. The airflows mix after they traverse their cooling paths and return to the air handler in a single duct. The combined air return duct is connected to the upstream end of the 4-m-diameter decay pipe, just beyond the end of the steel shield pile. The supply and return ducts have labyrinths, i.e., multiple right angle turns, and steel shielding where the ducts enter or leave the shield pile or the decay pipe to attenuate radiation leakage out through the ducts.

The cooling airflow enters the target pile at the downstream end above the steel shielding and flows upstream in the top, bottom and side channels. All of the air exits the bottom and side channels at the upstream end of the pile, turns 180°, and enters the chase. All of the air flowing in the top channel flows vertically downward through clearances between the T-blocks and into the chase. The 35,000 scfm cooling airflow exits the chase at the downstream end, mixes with the cooling airflow from the decay pipe, and enters the air return duct. The flows are shown schematically in in Figure 3-46.

Approximately 50,000 scfm cools the decay pipe. The cooling airflow enters the annular gap of the concentric decay pipe at its upstream end and flows downstream. At the downstream end the air flows out of the annular gap into the 4-m-diameter decay pipe, turns 180°, and flows upstream. At the upstream end the 50,000 scfm mixes with the 35,000 scfm from the chase and enters the air return duct back to the air handler.

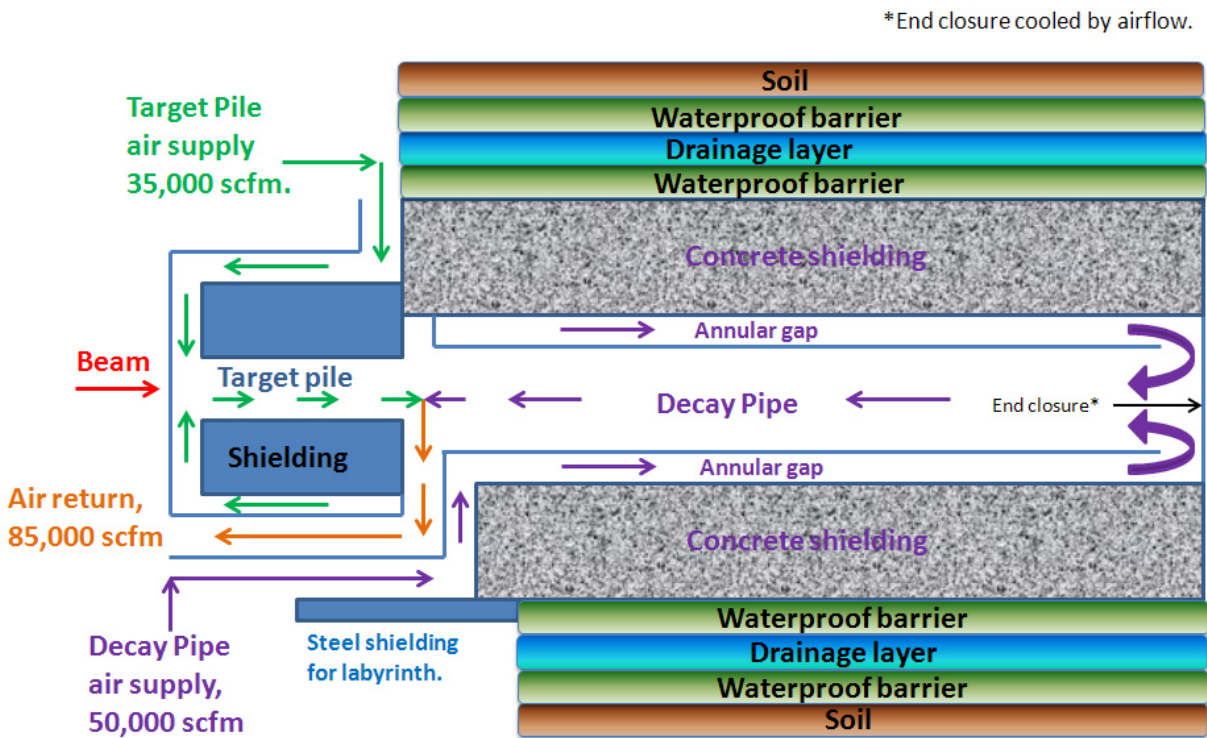


**Figure 3-46:** The flows for the Target pile and decay pipe air-cooling concept are shown schematically.

## 3.9 RAW Water Systems (WBS 130.02.03.09)

### 3.9.1 Introduction

Many components in Target Hall as well as the core of the absorber are water-cooled. Since these elements are operated in an environment with a high flux of energetic particles from the beam and target, the cooling water itself will be activated and cannot be allowed to mix with unactivated water. Therefore, these components are cooled using a closed-circuit water system; the heat being moved by conduction and convection to secondary water heat-exchanger/chiller system connected to the outside world. The closed-loop Radioactive Water Systems (RAW systems) are used extensively at Fermilab in removing heat from high-flux particle environments. They are generally of modular design with integral secondary containment systems, and easily transportable into their final location.

### 3.9.2 Design Considerations

All RAW equipment skids will have suitable containment for RAW leakage and tritium capture, and all should be designed with an intermediate loop between the RAW system and exposure to systems outside of the enclosures. All the RAW systems will require radiographic inspection of welds. Piping will be designed and installed in accordance with ASME B31.3 Code for Process Piping. Pressure vessels will be designed in accordance with ASME Boiler and Pressure Vessel Code Section VIII Division 1. Both will adhere to both FESHM [12] Chapter 5031 and the Fermilab Engineering Manual [13].

All RAW system volumes are expected to fall into the range of 100 to 200 gal each. RAW skids will have sufficient containment to capture these volumes. Also, Fermilab's guideline is to limit RAW activity to 670,000 pCi/ml [29]; LBNE will design the system to operate around an activity level of 500,000 pCi/ml. The activation limit is expected to be reached on a monthly basis for the horn systems and biannually or so for the remainder of the systems. Because of this, the addition of RAW capture and drainage systems are included. Their purpose is to help with the recapture of RAW waters from each of the skids in such a way as to limit manpower exposure and frequency of water change-out. Similarly, the Target Hall and Absorber Hall will have adequate space for the local storage of hot de-ionization (DI) bottles and components.

### 3.9.3 Reference Design

#### 3.9.3.1 Target Hall Systems

Located outside the Target Hall will be a RAW equipment room, which will hold the majority of the equipment for RAW skids, for cooling of the baffle, target, and horns 1 and 2.

The estimated overall heat load is around 100 kW. Due to the distance from the Central Utility Building (CUB), a local system will prove advantageous. Local chillers were selected for the reference design and the load is included in the CF Target Complex design of 1,200 tons.

The reference-design Target Hall RAW systems are as follows:

- Target and Baffle RAW skid
- Horn 1 RAW skid (supply at 16-18°C)
- Horn 2 RAW skid (supply at 16-18°C)
- RAW Exchange and Fill System
- Intermediate cooling system

Room must be provided for the addition of a Shielding RAW Cooling System for 2.3-MW operations.

#### 3.9.3.2 Absorber Hall Systems

Located outside the main Absorber Hall will be a RAW equipment room, which will hold the majority of the equipment for RAW skids, for cooling of the absorber.

The estimated total heat load for the Absorber Hall RAW systems is approximately 450 kW (at 708 kW beam power). The most likely source of outside cooling water would be for a chiller system at ground level and a recirculation and cooling system to supply the enclosure. While possible, a local pond water-cooling system would most likely prove too expensive for consideration.

The reference-design Absorber Hall RAW systems are as follows:

- Absorber RAW skid

- Intermediate cooling system
- RAW Exchange and Fill System

## 3.10 Radiological Considerations (WBS 130.02.03.10)

### 3.10.1 Overview

In this section, radiological issues for operation of the LBNE beam line with 2.3 MW beam power are considered, since retrofitting the LBNE facility for 2.3 MW after years of operation at 708 kW is very costly and not practical. The scope of these issues includes the primary transport line, target hall, decay pipe and the absorber hall. The analyses contained in this section are based on current requirements of the Fermilab Radiological Controls Manual, FRCM[29]. Other measurements and verification data available are also used where applicable. The posting and entry control requirements for access to areas outside of beam enclosures where prompt radiation exposure may exist for normal and accident conditions are given in the Fermilab Radiological Controls Manual. All results presented in the following subsections are based on the MARS modeling of the LBNE facility (See Section 3.12).

In NuMI (400kW), fractional beam losses are controlled to better than  $10^{-5}$ . Scaling to 2.3 MW this corresponds to controlling the losses at  $1.6 \times 10^{-6}$  for LBNE. Control of the LBNE beam average operational losses is assumed to be  $10^{-5}$  for shielding purposes, which gives a sensitivity/safety factor of more than 5. Larger, accidental beam losses are difficult to estimate from first principles. Again, the NuMI beam can be used as the analog to LBNE for this estimation. During the six years of NuMI primary beam operation, more than 50 million beam pulses have been transported to the NuMI target with a total of more than  $1.2 \times 10^{21}$  protons on target at 120 GeV. A total of 6 beam pulses have experienced primary beam loss at the 1% level, all due to Main Injector RF problems. Therefore, it is assumed that control of LBNE primary beam losses to less than 2 pulses/week is possible by using a control system similar to that developed for the NuMI beam.

The radiological requirements outlined in this section are applied to the designs of the technical systems and equipment for the Beamline discussed in this volume, as well as to the conventional facilities discussed in Volume 5 of this CDR.

## 3.10.2 Shielding

### 3.10.2.1 Primary Beamline

The Conceptual Design for the LBNE facility has been developed with external primary beam soil shielding of 23 feet (7.0 m). This provides an additional safety factor beyond the calculated LBNE required shielding for both the normal and accidental losses. The calculated soil shielding required for 2.3 MW beam, for unlimited occupancy classification, is 21 feet (6.4 m) for continuous fractional beam loss of  $10^{-5}$  level and 23 feet (7.0 m) for 2 localized full beam pulses lost per hour.

To reduce the accidental dose from muons at the site boundary to less than 1 mrem, 326 feet (99 m) of soil in the path of the muons is required. However, because of the offsite annual dose limit, the shielding for the longitudinal muons either must be increased to 400 feet (122 m) or beam control should limit full beam losses to less than one pulse per day.

### 3.10.2.2 Target Hall/Target Chase

The target hall shielding is designed to contain prompt radiation, residual radiation, activated air and accidental spills of radioactivated water, to reduce a thirty-year buildup of the radionuclides in the soil outside the shielding to below the standard detection levels. The goal of the design is to have an average dose rate of less than 100 mrem/hr in the target hall during the normal beam operations. A combination of steel, marble and borated polyethylene is used for shielding on top of the target chase. Because of the skyshine considerations, the walls and the ceiling of the target hall are required to be 5 feet (1.5 m) and 7 feet (2.1 m) of concrete, respectively. For the sides and the bottom of the target chase, combinations of steel and concrete shielding are used. Details of the target hall and the target chase shielding are given in Section 3.8.

### 3.10.2.3 Decay Pipe

Given the geology in the region near the Main Injector, if the Decay Pipe was constructed horizontally at the elevation of the Main Injector with enough shielding such that the production of radionuclides in the soil are below the *surface* water concentration levels, no additional mitigation would have been required. However, the Decay Pipe will be partly underground with the downstream end close to the aquifer. Under these conditions, it is prudent (ALARA) to reduce the concentrations by two orders of magnitude; e.g. tritium concentration to be 0.3 pCi/ml, which is below the standard level of detection. Based on the requirement set by the project[30], the decay pipe will use 18 feet (5.5 m) of concrete shielding. Additionally, to protect against tritium leaking out of the shielding and being released to the environment,

protective outer layers of water impermeable material and a water drainage layer are added to the decay pipe shield (see Section 3.6).

### 3.10.2.4 Absorber Hall Complex

The absorber (Section 3.7) and the Absorber Hall Complex shielding is based on the ground water management requirement[30] set by the project using the latest MARS model[31]. The shielding is designed to reduce a thirty-year buildup of the radionuclides in the soil outside the shielding to below the standard detection levels. The goal is to reduce the residual dose rates outside the absorber block to less than 100 mrem/hr and to preclude significant activation of the equipment in the absorber RAW room. During proton beam operations, the following areas will be designated as “limited occupancy” for the radiation worker: the service building, personnel elevator and stairway shaft, elevator lobbies at the three stops, the three sump pump rooms and the Instrumentation room . The rest of the complex is considered a high-radiation area and will not be accessible during beam-on periods.

## 3.10.3 Other Radiological Design Issues

### 3.10.3.1 Groundwater and Surface Water Protection

The production of potentially mobile isotopes such as tritium ( $^3\text{H}$ ) and sodium-22 ( $^{22}\text{Na}$ ) is an unavoidable consequence of high-energy particle collisions with nuclei. Since the primary transport line is located in the glacial till, with no direct connection to the aquifer, all radionuclides produced in the soil surrounding the enclosure will have to migrate down through the soil layers to reach the aquifer. These seepage velocities, for the layers in the glacial till, are very small and the concentrations of the radionuclides are reduced by 5 to 7 orders of magnitude.

The target hall and the target chase are also at grade level, located in the glacial till. The shielding of the target hall and the target chase is designed such that a 30-year accumulation of radionuclides in the soil immediately outside the shielding, assuming no dispersion, would result in maximum concentrations of 27% of the surface waters limits. Additionally, the target chase and the target hall will have a geomembrane barrier system, preventing water from coming in contact with the shielding.

For the rest of the beam line, from the decay pipe to the end of absorber hall, there will be sufficient shielding and water impermeable layers to render the concentration of the radionuclides of interest, accumulated in the soil over 30 years, to be less than the current standard detection limits [30]. The current accepted detection limits are 1 pCi/ml for tritium and 0.04 pCi/ml for sodium-22.

### 3.10.3.2 Tritium Mitigation

Tritiated water molecules (e.g. HTO) are highly mobile, especially in humid air, and can create significant concentrations in drain waters that are then collected in the pumping processes that keep the beam line areas dry. These basic processes, namely tritium production and migration, show that strategies to avoid unnecessary effluent will rely on isolating the materials in which the tritium is produced from water, and in the dehumidification of air in contact with these materials, together with subsequent collection and evaporation of the tritiated condensate. Additionally,

- There will be a geomembrane barrier system installed between the decay pipe concrete and the soil that is largely impervious to water. In this way the decay pipe concrete (in which tritium is created during operations) will be held at a low saturation. Numerical studies using the NuMI system indicate that if shielding concrete is unsaturated, the mobility of created tritium is low[32].
- The operational design of a sampling and monitoring program is straightforward, and allows for maintenance of the drainage system.

### 3.10.3.3 RAW Systems

The cooling water for the baffle, target, horns and the absorber will be highly activated after a short time of operation. The prompt dose rates from the RAW (RadioActive Water) skids belonging to these devices will be high and in addition to the short lived radionuclides, large concentrations of the tritium will build up in these systems. Shielding and cool-down times will be used to reduce the dose from these systems. Automated top off and top up with fresh water will be used to keep the tritium concentrations at manageable levels. Alarms and containment systems will be used to prevent spills and contamination of the soil and surface waters. Water from these systems will be disposed of as low level radioactive waste.

### 3.10.3.4 Activated Air

High levels of radioactive air will be produced in the target chase, decay pipe and absorber hall. The air to the chase and decay pipe is part of a closed, isolated loop. The two separate streams of air that feed the target chase and the decay pipe (Section 3.6) combine on return and then are routed to the air handling room. Additionally, the air from the absorber hall is sent to the air handling room, where it combines with the target chase and decay pipe air. In the air handling room, this air is chilled and dehumidified before returning to the decay pipe and the target chase. The air handling room structure and the doors are designed to be air-tight. A few percent of the target chase air leaks into the target hall, where it

is piped to the NuMI decay passageway and exhausted there. The transit time from the LBNE target hall to the NuMI exhaust is a sufficient to allow the airborne radionuclides to decay by several orders of magnitude. The current Fermilab radioactive air emissions permit allows the annual exposure of a member of public offsite to the radioactive air emissions, from all sources to be less than 0.1 mrem. It is the goal of the LBNE design is to have the air emissions contribute less than 30%-50% of this limit which allows for the emissions from other accelerators and beam lines at Fermilab.

### 3.10.3.5 Outside Prompt Dose

There are two ways where the prompt dose rates may reach outside the facility: (1) direct attenuated radiation outside the shielding and (2) skyshine, which is radiation, primarily neutrons, due to back scattering from air. FRCM Article 1104[29] describes the regulatory requirements/limits regarding the maximum annual allowable dose to the public. The LBNE primary beam transport line, target hall and the decay pipe and the absorber service building can contribute to outdoor doses. Based on the latest MARS calculations[33,34] both the annual direct and skyshine doses are calculated for both offsite and onsite locations. Direct accidental muon dose at the apex of the transport line is also included in the offsite dose.

### 3.10.3.6 Offsite Dose

To allow operations of other experiments, beam-lines and accelerators, the offsite goal for LBNE is set at  $1\pm 1$  mrem in a year, from all radiation sources generated by this beam-line. The total offsite dose, at the nearest site boundary, due to both direct and skyshine is estimated to be 1.32 mrem in a year.

### 3.10.3.7 Onsite Dose

Wilson Hall is the nearest publically occupied building to the LBNE beam line. Both the maximum direct and skyshine annual dose to the occupants of the Wilson Hall has been calculated. The total annual dose, at Wilson Hall, due to both direct and skyshine is estimated to be 0.06 mrem. Doses for other locations onsite, further away, will be less.

### 3.10.3.8 Residual Radiation

Based on the past experience and the difficulty of component replacement with the steep grades ( $\sim 10\%$ ) of the LBNE primary beam enclosures, the beam loss and beam control devices would be employed to keep the residual radiation inside the beam line to no more

than 50 mrem/hr on contact. This allows for repair or replacement of the beam line elements with little programmatic impact and keeping the dose to the workers ALARA.

There are other beam line devices, such as targets, horns, cooling panels or modules that are exposed to high levels of beam sprays and are expected to become highly radioactive. These devices may need to be repaired or replaced. The shielding of the work/repair cell used for these devices is designed such that for a 1000 R/hr object, the dose rate outside the cell is less than 1 mrem/hr. The shielding of the containers used for the over the road transport of such devices will be such that the dose rate outside the containers is less than 100 mrem/hr at one foot.

## **3.11 Remote Handling Equipment (WBS 130.02.03.11)**

### **3.11.1 Introduction**

Technical components installed in the Target Hall enclosure are subjected to intense radiation from the primary or secondary beam. The level of irradiation in some LBNE environments will reach levels that are unprecedented at Fermilab. These radiation levels will be too high for workers near such components. The failure of some of the technical components (such as target or horns) is likely over the lifetime of the LBNE experiment. Therefore remotely operated removal and handling systems are an integral part of the Target complex design. Because the remote handling systems are integrated into the infrastructure of the Target complex and cannot be upgraded after irradiating the Target complex areas, they must be designed to be sufficient for 2.3-MW beam power.

### **3.11.2 Design Considerations**

Components to be handled, serviced and/or stored range in size (from 0.20 m<sup>3</sup> to 26 m<sup>3</sup>), range in weight (from 10 kg to 30,000 kg) and range in estimated dose rate (from 5 R/hr to 8,000 R/hr on contact), as described in the Remote Handling Component Lists [35]. Shielding requirements for work cells and storage areas have been determined to be 3 ft of concrete or 11 in of steel to reduce dose rates to workers to below 5 mrem/hr at 1 ft. Storage and work cell areas must have redundant sump systems with emergency back-up power systems to mitigate contamination of in-flow water by radioactive particulate from serviced and/or stored components. Steel casks used to transport radioactive components will be sized to reduce dose rates to workers to below 5 mrem/hr at 1 ft where possible (limited by the crane capacity of 50 tons). Where not possible, it is expected that casks should be of sufficient thickness (4-in wall thickness) to allow brief hands-on access by radiation workers (300-500 mrem/hr at 1 ft maximum).

The design is based upon a conceptual design study performed by the Remote Systems Group at Oak Ridge National Laboratory. Since the study was performed, remote handling plans were revised significantly resulting in reduced scope and reduced cost. The final report of this study is available [36], and the applicable portions of that study are reflected in the following sections.

### 3.11.3 Reference Design

The LBNE remote-systems reference design includes equipment and systems in two functional locations. These are the surface Target complex (Target Hall enclosure and neighboring service areas) and the underground Absorber Hall. Along with shielded, remote-capable work areas, each of these three locations will have the variety of equipment, lifting fixtures and vision systems required to carry out needed operations.

#### 3.11.3.1 Target Complex Remote-Handling Facilities

The Target Hall enclosure contains the components for generating neutrinos and focusing them toward the near and far detectors. The beamline component arrangement is shown in Figure 3-47. The remote handling of components in the Target Hall enclosure chase will be accomplished with long-reach tools, a bridge crane and a shielded work cell. The high levels of radioactivity within the Target Hall while running beam restricts access to facility shut downs after a short cool-down period. The conceptual design closely resembles the layout for the NuMI Target Hall. Since this layout eliminates the possibility for personnel to access any portion of the Target Hall during facility operation, it will require a separate beam-on accessible service area for temporary storage of radioactive components and staging area for remote handling activities.

The main hallway for transport of equipment shielding, and components is located at the upstream portion of the Target Hall enclosure and connects to the Morgue/Maintenance areas (floors of both Target Hall and Morgue/Maintenance areas are at the same elevation). It is through this hallway that radioactive components must pass to get from the Target Hall to the maintenance and morgue (short-term storage) areas. Since most of the service areas are planned to be occupiable with beam on, a shield door must be provided to shield the service areas from the Target Hall. In addition, the air volume of the Target Hall enclosure and the air volume of the neighboring service areas must be separated to avoid radioactive-air contamination of the service areas. The shield door will incorporate an air seal to achieve this air-volume separation. This Target Hall shield door is included in the scope of the remote systems WBS. The layout of the Target Complex is shown in Figure 3-48 with an expanded view in Figure 3-49.

The Target Complex remote operations plan incorporates one hot storage rack in the Target

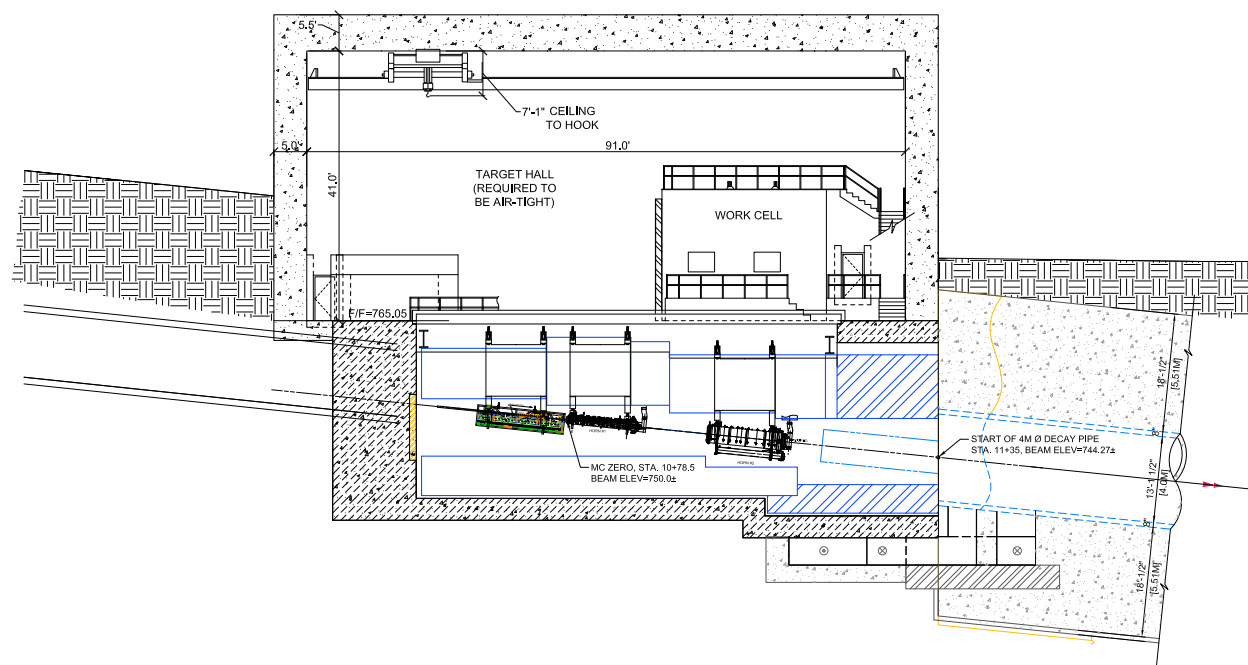


**Figure 3-47:** LBNE Target Hall enclosure beamline elevation section

Hall enclosure, designed to provide short- or long-term storage for Horn Module “T-blocks” during component replacement activities. The hot storage can also provide temporary storage of other components that the Morgue cannot accept at the time of removal from the chase. The T-block storage rack is configured as a pit with T-block mounts similar to the carriage mounts that exist in the chase. It is located in the Target Hall floor next to the chase with removable shielding covers.

The work cell and hot-storage rack are located at the downstream end of the Target Hall enclosure on the beam-left side of the chase. The work cell is primarily used to remotely remove a failed horn or target/baffle from an activated module and attach a new replacement component. Other remote handling activities such as emergency repairs will have to use the work cell in an ad-hoc way as current operations in NuMI target hall are conducted, or repair operations can use the remote handling facility at C-0 if over-road transport is available. See Figures 3-50 and 3-51.

The chase is covered with shielding composed of steel, marble and borated polyethylene. The borated polyethylene functions as a neutron shield. The marble functions as a residual radiation shield to help reduce the dose to workers during beam-off access. These chase shield covers shall be designed to be stackable such that, when accessing the target chase, the removed covers can be temporarily stored on an un-accessed section of the chase. The replacement of a horn or target is likely to require the greatest number of shield blocks to be removed. One should note that at this point in the conceptual design, Horn 1 with the module attached is the tallest item moved during operation. The shield blocks cannot be

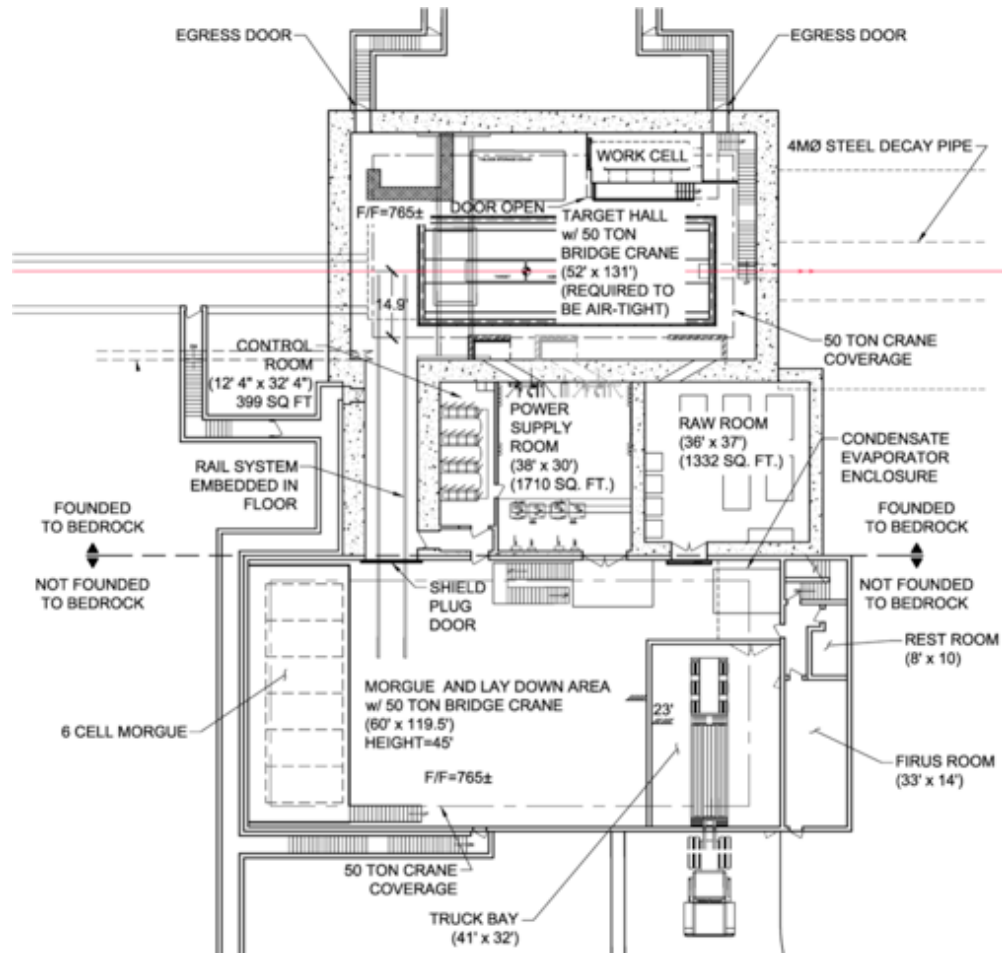
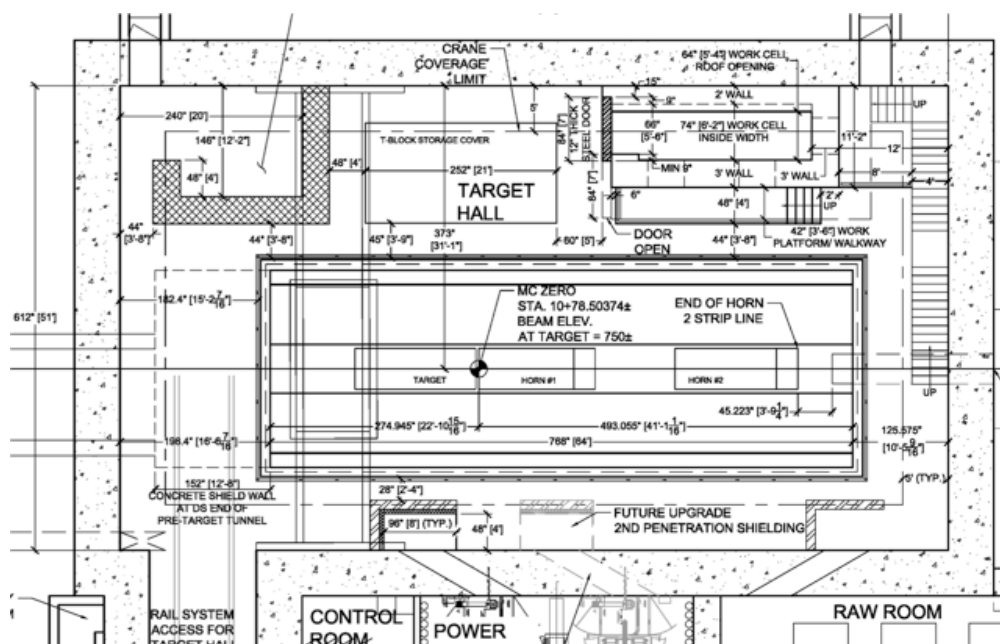


Figure 3-48: Target Complex Plan View



**Figure 3-49:** Target Complex Plan : expanded view of Figure 3-48

stacked so high as to block access of the horn to the work cell. It is not expected that shield blocks from the chase will be occupying the needed set-down space in front of the work cell, but if this situation arises, additional set-down space is available at the US end of the enclosure.

Similar to the NuMI work cell design, the Target Hall work cell conceptual design uses three shield walls fit together into a “U”-shape with a sliding shield door on the side facing the upstream end of the Target Hall. One of the side walls is incorporated into the Target Hall enclosure side wall to save on space and shielding. The door allows a horn module with horn attached to enter into the cell. The sliding shield door is fabricated from steel with a thickness of 12 in. The door translates using a v-groove track and multiple v-groove rollers along with an additional set of rollers at the top of the door to prevent door tipping. The shield door is moved by a power screw driven by an electric motor located outside the cell, which is similar to what has proven successful with NuMI. Proper controls must be added to allow the shield door to be remotely operated via the control area. The top of the work cell is covered with removable shield blocks that fit around the top of the module. The design of this cell minimizes construction cost while maintaining all required capability for completing a horn or target/baffle replacement operation. This cell is approximately 25-ft long, 12-ft wide and 19-ft tall (excluding the personnel safety railing). On the bottom of the cell is a lift table to accept failed components and mount replacement components to their mating modules. As in present NuMI operations, the activated modules must be replaced back into the chase in order to access the lift table area (to remove a failed component into a waiting cask).

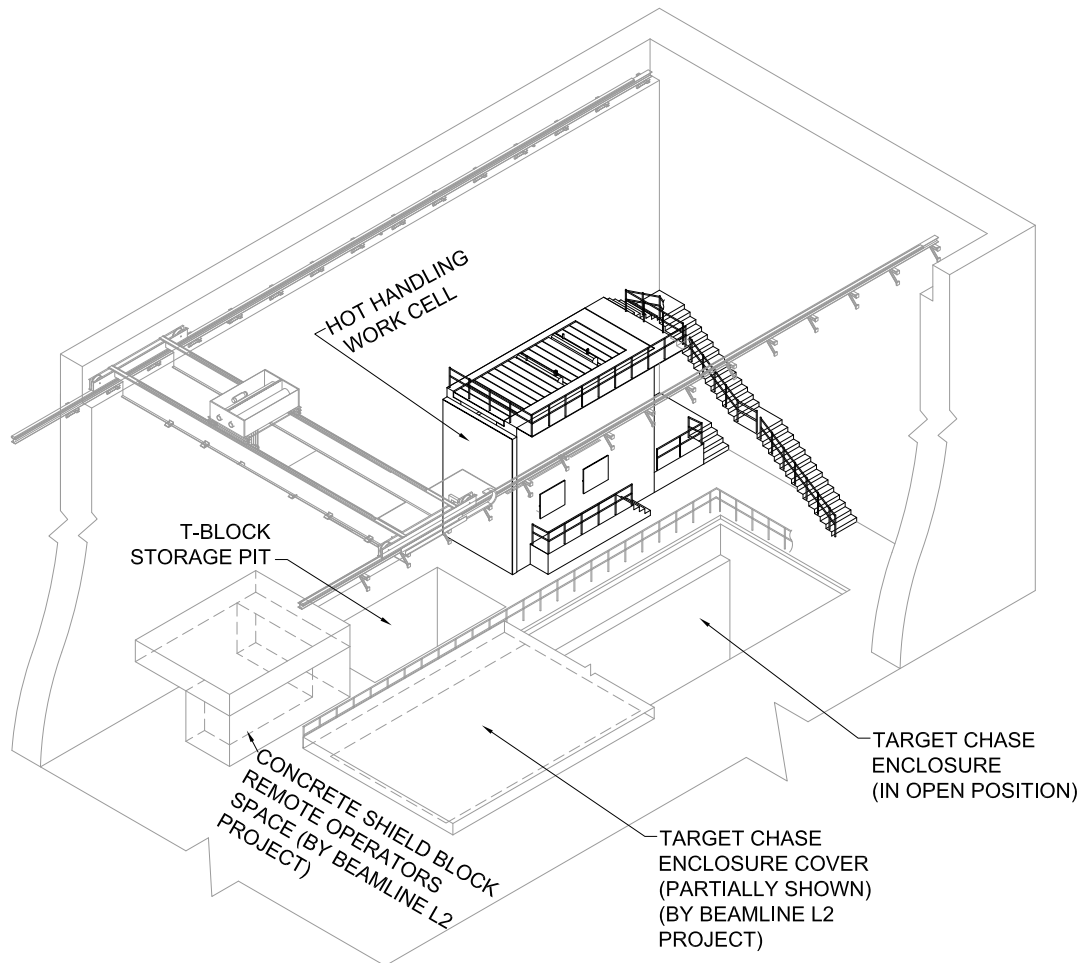


**Figure 3-50:** Target Hall work cell concept

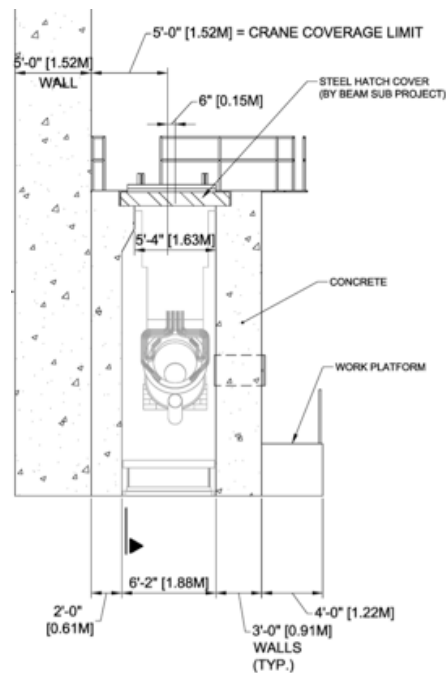


**Figure 3-51:** Target Hall work cell section, viewed from upstream

Lead glass block windows, similar to that in the NuMI work cell, will be utilized in the downstream and beam right walls to allow alignment activities (also similar to NuMI) as needed.

Before the horn/target replacement operation begins, the shield cask must be placed in the Target Hall, at the upstream end of the enclosure. The shield cask is designed to provide maximum shielding while maintaining a total loaded weight under 50 tons, the capacity of the service areas and Target Hall bridge cranes. The top loading shield cask comprises a shield container, a shield lid and an end load shield door (shutter type). The cask includes a drive system to push/pull a failed component into and out of the cask on a cart system. The top shield lid is removed and placed next to the shield container.

With the cell and cask prepared, the module with failed horn attached can be removed from the chase. The steel and borated polyethylene shielding about the failed horn is removed. The utilities connected to the failed horn are disconnected by hand or using long-reach tools. The marble and steel module shielding (T-blocks) are remotely removed from the module, placed in the T-block storage pit, and covered with the T-block storage pit shield covers. Multiple top shield blocks are removed from the cell using the bridge crane. Then the sliding shield door is remotely opened from the control room. The bridge crane remotely lifts the module and horn and transports them to the cell, placing the module on alignment feet located on corbels inside the cell. The work cell top shielding can be placed around the module, the shield door is closed and the shielding above the chase is returned.

After all the shielding is properly returned, personnel access to the Target Hall enclosure can be granted, and the failed component can be removed from the module. This is accomplished by locating the lifting table under the failed horn in the cell and then elevating the platform until the horn's weight is fully supported. Using a long-reach tool through openings in the shielding, the connections between the failed horn and module are released, similar to what has proven successful with NuMI. With the component disconnected from the module, the elevating platform is lowered. With personnel out of the Target Hall enclosure, the shielding over the chase is again removed, the sliding shield door is remotely opened and the activated module is placed back into the chase. Chase shielding panels are re-installed, the work cell door is closed, and work cell cover shielding is replaced. Now, the area can be prepared for the transport of the failed component to the cask. When all is ready, the work cell top shielding is removed, the door is remotely opened and the bridge crane is used to pick up the failed device and place it into the shield cask, and the shield cask is capped with the shield lid. The cask is moved into the Morgue area utilizing a motorized cart on rails (similar to the NuMI system). There, the Morgue crane is used to move the cask into position next to a Morgue cell. Then the end load door system is used (similar to the C-0 Remote Handling Facility) to push the component into the Morgue cell while shielded.

The replacement horn is transported onto the lift table in the work cell. Once again using the same procedure, the activated module must be transported back into the work cell positioned above the new component and all shielding put in place. Now, personnel can safely access the work cell and use long-reach tools to connect the replacement component to the module. The module and replacement component are now ready to be returned to the chase and personnel must leave the Target Hall enclosure. The shielding above the chase and work cell are removed along with the marble and steel (T-block) shielding in the module. Then the sliding shield door is opened. The bridge crane transports the module with replacement horn to the chase, and the marble and steel shielding can be returned.

The cell's removable shield blocks are then returned, and the shield door is shut. With all the shielding in place, personnel access is allowed. The technicians can enter the Target Hall enclosure and connect the component utilities by hand or using a long-reach tool. Once the utilities are connected, the component's alignment can be checked and adjusted if needed. Then the steel and borated polyethylene shielding above the chase can be returned and air seal established. With all the shielding in place and the component functioning properly, the facility can return to operation.

The work cell conceptual design provides a basic method for horn replacement while also providing a work area for ad-hoc repairs. This concept is not capable of quickly replacing the horn or target if the situation arises. However, this concept's minimal size and limited use of expensive equipment results in a very cost-effective solution.

The specifications for a remotely operated crane can be driven by either regulatory requirements or operational or mission requirements. Facility safety assessments will determine issues such as whether airborne contaminants are a concern if a crane failure were to occur,

or whether significant radiation exposures to personnel or the public could result. These types of situations might cause the crane to be considered to be a Credited Engineered Control, which would impose higher design and operational standards. If that type of environment or risk is not applicable, then operational or mission requirements could also impose these higher crane standards. This would be the case if the risk to the Project were such that if a load was dropped or a crane failure occurred with a suspended radioactive load, then the consequences would be extremely severe in terms of personnel safety or recovery time and expense.

In general, cranes used in radiation environments have features that are driven by requirements in one or more of these areas:

1. Being able to support and hold a load during and after a defined seismic event
2. Having dual load paths and redundant mechanisms to ensure loads cannot fall
3. Having features that allow recovery from a crane failure by being able to manually lower a load and move the crane to a safe area for repair

For LBNE, the use of the crane to lift a radioactive load will occur only after facility start-up has begun. After that point, crane usage will be intermittent, with potentially weeks or months between uses. With that type of usage, the probability of a seismic event occurring while holding a load becomes extremely small, so from this standpoint a fail-proof (ASME NOG-1) crane is not considered necessary. However, when dealing with unshielded radioactive loads, the incorporation of redundant emergency drive systems is desired to enable putting unshielded radioactive loads in a safe condition in the case of a crane drive failure. In addition, some custom provisions to prevent “two-blocking” and removing the crane electronics from the Target Hall enclosure (to avoid exposure to beam-on conditions) are recommended. These features and other crane specifications are listed in Table 3-9.

Control of the crane and work cell door must take place in a shielded environment. This environment is envisioned to be a “control cave” built of concrete shielding blocks in the upstream, beam-left corner of the Target Hall enclosure. The control cave shall have a roof and labyrinth to allow operators to work in a low dose area during unshielded lifts in the enclosure. An emergency egress door assures that operators can exit the enclosure in case of emergency.

With no personnel allowed in the Target Hall enclosure during most of the maintenance operations, a remote viewing system is essential. Similar to current NuMI operations, the Target Hall viewing system will consist of several cameras on PZT mounts that can be placed in multiple locations (including on the crane bridge). The system includes transceivers for signal and control communications and a portable control station consisting of video monitors and camera controls. The portability of this system means that only one system needs to be

**Table 3–9:** Target Hall crane characteristics.

Feature	Value or Description
Capacity	50 tons in a true vertical lift configuration
Lift	50 ft
Speed	Creep modes for all axes of travel
Reeving	Double reeved, single-failure-proof with provisions to prevent "two-blocking"
Radiation Environment	Total Absorbed Dose: $10^4$ rads - Maximum Dose Rate: $10^2$ rads/hr
Hook Rotate Capability	Continuous
Hook	Supported by two independent drive systems
Auxiliary Hoist	5T capacity, 50ft lift, no powered hook rotate
Brakes	Shall restrain all loads without slip or overtravel
Electronics	All electronics, including axis drive amplifiers, control circuits, and memory devices shall be located outside the Target Hall
Load Sensing with Overload Alarm/Interlock	Capability required
Cable Slack Detector	Capability required
Video Cameras (by Others)	Mounts and cable accommodation required
Lights (by Crane Vendor)	Mounted on bridges
Variable-speed Control	Local pendant and wired remote from control room
Recoverability Features	Custom redundant drives and/or manual winch for bridge recovery

purchased for the project and can be used in the Target Hall, the Morgue and the Absorber Hall as needed.

CCD cameras have a limited radiation tolerance, approximately  $10^3$  rads total integrated energy, and if it weren't for the neutron radiation could potentially be left in the Target Hall during beam-on. However, the neutron exposure would render the cameras inoperable, so during remote operation, the cameras will be removed from the Target Hall and placed in a protected area. Given the relatively low background radiation levels expected in the Target Hall during maintenance operations, the high cost ( $> \$60,000$  each) of radiation hardened tube cameras is not justified, so the CCD cameras will be considered disposable.

The Morgue and Maintenance area of the Target Complex is an area for short-term storage of spent components. In addition, it will serve as a maintenance area for in-beam components. These facilities are described in this section from the perspective of remote handling activities and equipment that will occupy this area. The building, including the cast-in-place concrete shielding for the morgue, will be provided by Conventional Facilities (see Volume 5 of this CDR for construction details).

The services areas of the Target Complex will be constructed with thick concrete walls sized to reduce the dose rate external to the building (i.e., the residual dose rate from radioactive components being serviced/stored inside) to acceptable limits. Some pertinent characteristics of this facility include:

- Integrated truck bay for surface-level loading/unloading
- Overhead bridge crane accessing both a truck bay and Morgue/Maintenance areas
- Shielded storage and repair areas for activated components, referred to as the morgue

Figure 3-48 provides a plan view of the services areas of the Target Complex. It is a dual-level facility with a ground-level truck bay of approximately 1,200 ft<sup>2</sup> and an elevated morgue maintenance level of approximately 7,200 ft<sup>2</sup>. From a radiation protection perspective, the truck bay is expected to be open access for personnel, while the morgue will be limited access. Each level is covered with the same 50-ton overhead bridge crane. The Target Hall enclosure is connected through a large hallway at the upstream end. As the Target Hall enclosure ventilation system must be separated from the neighboring service areas, a sealed shield door in this connection hallway is required during beam-on operations.

It is assumed that the Morgue will be a radiation buffer area, which requires that radiation levels in personnel-accessible areas are less than 5 mR/hr. A calculation was made to determine the thickness required to reduce the radiation from an assumed unshielded dose rate of 1,100 R/hr to a shielded rate of 5 mR/hr. The result showed that 3 ft of concrete or 11 in of steel is needed between the component and personnel in the facility or to the exterior of

**Table 3-10:** Morgue storage requirements.

Component	Replacement Frequency at 708 kW, #/yr	Storage Quantity at 708 kW, 2 yrs	Replacement Frequency at 2.3 MW, #/yr	Storage Quantity at 2.3 MW, 2 yrs
Target/Baffle carrier	2	4	5	10
Horn 1	0.5	1	0.5	1
Horn 2	0.5	1	0.5	1

the building. All transport activities of radioactive components in the Morgue area will be shielded to the extent possible with the crane capacity of 50 tons

Groundwater activation is not a concern for components being handled at the Morgue because they will not have enough energy to activate the water. However, surface water contamination due to collection of activated dust and loose particles in a flood scenario will be a concern, and the morgue level will require a redundant sump system and back-up power generator.

The LBNE Target Hall Complex is configured to provide short-term storage space of spent components in a 6-cell morgue for two years of 708 kW operation, with the expectation that, after two years of decay time, radioactive components could be moved to a long-term storage location. If the morgue storage requirements increase (due to shorter than assumed component lifetimes and/or higher beam power operations), the building could be expanded by Fermilab to allow for more storage capacity in the future. The expected storage requirements for the morgue are shown in Table 3-10. for both the 708 kW and 2.3 MW cases. Because the horns are the largest components (with Horn 2 being somewhat larger than Horn 1), storage cells are designed to accommodate one Horn 2. For the 708 kW two-year storage space requirement, a total of six cells are allocated to the facility concept.

The longer-term storage location is assumed by LBNE to be provided by Fermilab. This facility is required to be available to accept LBNE components after the LBNE Beamline has been running for 2 years, presently scheduled to be ~2024. At the present time, the Associate Lab Director for Accelerators is assessing long-term radioactive storage needs at Fermilab which is expected to result in a plan for a long-term storage facility.

Spent components would be transported from the Target Hall enclosure to the Morgue/Maintenance area of the Target Complex in a shielded steel transport cask. The cask thickness would be determined by crane capacity in the Target Complex (50 ton) rather than the thickness required to reduce dose rates to a level that allows long-term direct human contact with the container. For horns, an estimated cask thickness is 4 in. Because hands-on contact may be limited, the casks must be able to be remotely loaded and unloaded. The casks and morgue cells will be side loaded, enabling the radioactive component to be transferred from one to the other largely under shielding. For NuMI and NOvA components, a system that

achieves this has been already designed and used in operation.

Figure 3-52 shows a picture of the morgue/cask transfer system in place at C-0 Remote Handling Facility. The component in the cask is supported by a rolling cart and pushed/pulled by a serapid chain mechanism mounted to the back of the cask. Temporary shielding is set around the gap between the cask and the morgue when the morgue and cask doors are removed.



**Figure 3-52:** Photo of cask-to-morgue cell transfer system used at C-0 Remote Handling Facility

The cask and morgue doors are designed to be remotely operated using the building crane, as is the temporary shielding. The area above the morgue cells may be used for storage or for storage cell upgrade (to provide an additional 6 cells in a second layer). The above floor design reduces the possibility of water contamination issues due to flooding.

To separate the air volumes of the Target Hall enclosure and the service areas of the Target Complex, a Target Hall-connecting hallway shield door and air seal must be constructed. The

door is expected to consist of 6 inches of steel and 1 inch of borated polyethylene mounted on rails to allow motorized movement. The exterior side of the door will be lined with galvanized steel sheet to form the air barrier. The air seal at the edges of this barrier is conceived to be either double O-rings with toggle clamps or a double inflatable air diaphragm with passive clamps. An air monitoring station, located in the Power Supply Room, to monitor the air activation on the Target Hall side of the door will provide information needed prior to granting removal of the cover.

### 3.11.3.2 Absorber Hall Remote Handling Facilities

The Absorber Hall remote handling facilities are similar in concept to those for the Target Hall in that they will include a bridge crane, cask system and long-reach tools to enable the replacement of the hadron monitor upstream of the hadron absorber. However, unlike in the Target Hall, replacement of components will not require a work cell and all hadron monitor replacement crane operations are planned to incorporate shielding that allows for some minimal hands-on access. In addition to hadron monitors, water-cooled absorber modules and steel shielding may fail, and some provisions must be made to allow replacement. Although the absorber components are designed to last the lifetime of the facility and will include redundant water-cooling lines, the consequences of complete failure are significant. Therefore, provisions will be made in the design of the Absorber Hall components and shielding to allow future replacement. However, because of the low probability of complete failure, design and construction of remote handling equipment for absorber modules and water-cooled shielding will not be included in the LBNE project. If complete failure occurs during operation, a long downtime (6 months to 1 year) would then be required to design, build, develop procedures and safely replace the failed component(s).

The conceptual design of the Absorber Hall is shown in Figures 3-53 and 3-54. The hadron monitor and the absorber modules are located under steel and concrete shielding blocks. The hadron monitor is the furthest upstream component in the absorber assembly. Directly to the beam-right of the absorber assembly is an empty, shielded pit volume called the morgue. This morgue has been designed to accept three hadron monitors or absorber modules. In order to replace a hadron monitor, first, with shielding in place, utilities to the component must be disconnected by hand at the top of the absorber pile. After disconnecting utilities, using the crane and appropriate lifting fixtures, the top layer of shielding blocks are removed as necessary to uncover the hadron monitor shielding module. Although this step can be done remotely, it is expected that dose rates will be low enough ( $<300$  mrem/hr) to allow limited hands-on access, if necessary. Next, a special open-top cask (called a “castle”) is placed over the hadron monitor module. On the side of the castle, a special cask and monitor exchange system will be installed and readied for removing the spent hadron monitor (see Figure 3-55). The hadron monitor module is then drawn upward into the castle using the crane (during this step the monitor gas and signal lines are wound into a spool located within the cask). Once the hadron monitor is level with the side cask, the monitor is pulled from the castle

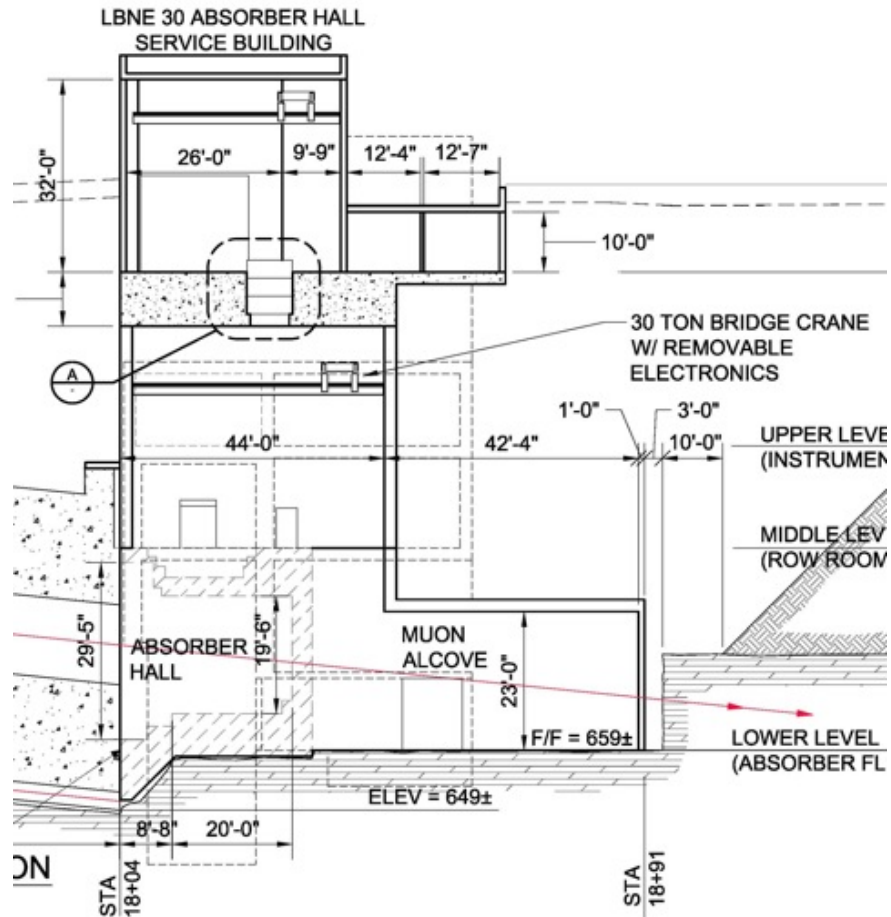


**Figure 3-53:** Absorber Hall section. The beam comes from the left. The downstream end of the decay pipe is bottom left.

into the side cask using a mechanism very similar to the one currently used for the NuMI hadron monitor exchange. Then the shutter doors on the side cask and castle can be closed and the cask containing the spent hadron monitor can be moved to a storage location (the side morgue) or out of the Absorber Hall as appropriate. The new monitor is installed in the reverse order and the top layer of shielding blocks is replaced. Finally, after a system check-out procedure, utilities can be re-connected and operation can be resumed.

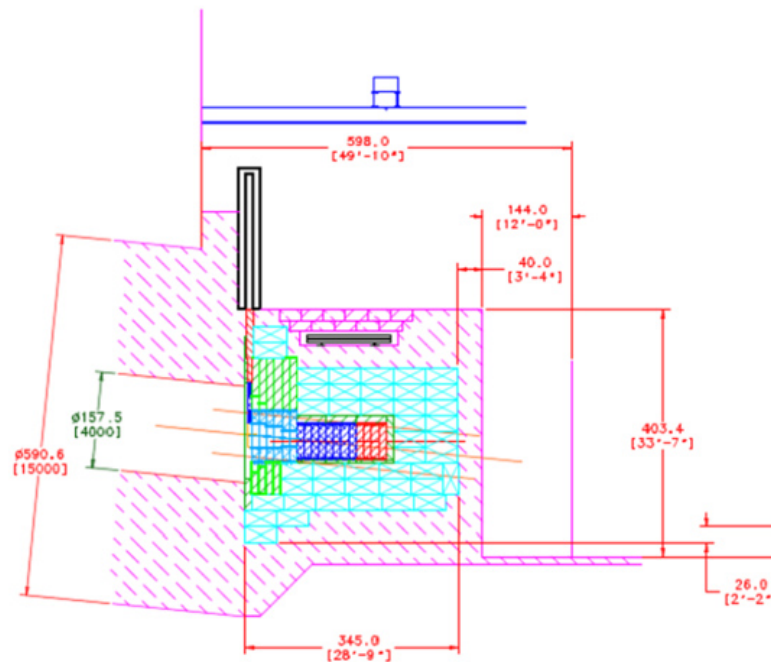


**Figure 3-54:** Absorber Hall section showing details of the absorber core and shielding arrangement. The aluminum core is colored dark blue. The shielding is shown in cyan and magenta. The beam comes from the left.

There are no plans within the Project to provide support for removal of radioactive items from the Absorber Hall morgue to the surface. However, nothing in the Project plan precludes doing so in the future should it be necessary. Shielded casks could be built to shield radioactive components during transport, and the Absorber Hall bridge crane could be used to load and unload those casks.

The Absorber Hall bridge crane has a very similar function as the Target Hall bridge crane. This crane is actually located in the near-surface building (LBNE-30) above the Absorber Hall itself. The use of the crane to lift a radioactive load will occur only after facility start-up has begun. After that point, crane usage will be intermittent, with potentially weeks or months between uses. With that type of usage, the probability of a seismic event occurring while holding a load becomes extremely small, so from this standpoint a NOG-1 crane is not considered necessary. In addition, because the hadron monitor exchange system incorporates shielding casks (castle) at every step, recovery systems in case of crane failure are not neces-

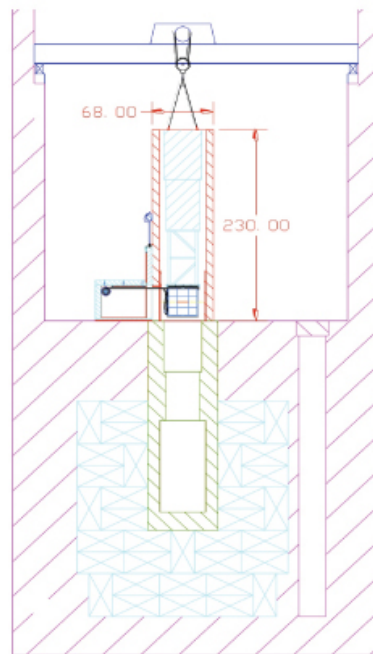


**Figure 3–55:** Cross section of Absorber Hall beam view showing hadron-monitor replacement concept

sary. A standard, industrial 30 ton bridge crane (with provisions to remove electronics from the Absorber Hall during beam operation, if deemed necessary) is sufficient. In addition, since true remote operations using the crane are not planned for hadron monitor exchange, a control room for the Absorber Hall is not required.

## 3.12 Modeling (WBS 130.02.03.12)

### 3.12.1 Introduction

This section describes the simulation of the neutrino beam and its effects on nearby materials using software models. The simulations use the MARS package, which is well documented and benchmarked [15] [37]. The MARS model of the reference design will describe the target, horns, decay pipe and absorber, as well as all of the shielding. In particular, MARS will be used for estimating:

- Beam-energy deposition in components, required for engineering considerations and estimating cooling capacities
- Prompt (beam-on) dose rates within halls outside of shields
- Residual dose rates from components within or outside shielding
- Radionuclide production in components, shielding and rock

### 3.12.2 Design Considerations

The level of detail in the model will follow the reference design as it evolves. The model already provides a basis for estimating the total thickness of shielding needed. Later, for example, as the block size and stacking pattern become set in the design, these details will be incorporated into the model. Thus, the effect of voids or cracks, which are small in a good design, will be studied at a later time. An estimate for the locations of excavated rock boundaries is needed for estimating tritium production and groundwater concentrations.

The composition of materials used in the MARS model needs to match that of the design materials to the known accuracy. The atomic mass fractions are usually sufficient for the simulations. Items to be modeled include rock, shielding materials and the materials incorporated into technical components. Components present in an engineering design or plan whose effect is negligible, e.g., bolts, will not be included.

### 3.12.3 Reference Design

A realistic MARS model has been built for the LBNE target, horns, target station and its shielding, decay pipe and tunnel shielding, and the hadron-absorber system. In the model as in the conceptual design, the proton beam is tilted down by 101 mrad, and the 25-m target station and decay channel follow this tilt while the hadron-absorber system is arranged horizontally. The hadron-absorber system includes an aluminum mask that protects the water cooling pipes, a 2.4-m long aluminum core followed by a 2.7-m long iron core surrounded by massive iron shielding in a concrete shell, all in an 18-m long service building. Horn magnetic fields and all details of geometry and materials distributions are included in the model.

In the reference model, a 120-GeV proton beam hits a 0.96-m long cylindrical graphite target at an intensity of  $1.6 \times 10^{14}$  protons per pulse. A 60-GeV case is also being considered. We model in great detail both 708-kW and 2.3-MW normal operation (1.33-s repetition rate,  $4.9 \times 10^{13}$  and  $1.6 \times 10^{14}$  sec<sup>-1</sup>, respectively) as well as an accident scenario. The latter is a 3.07-MJ beam accident (“target destroyed”), in which a proton beam interacts with 1-atm air (or helium) in the decay pipe and hits the absorber. Substantial modeling efforts are being conducted in the primary-beamline and baffle areas.

MARS is used to calculate energy deposition (peak values and total dynamic heat loads), integrated absorbed dose and residual activation in all the system components (target, horns, decay pipe, shielding, all the components of the hadron absorber, etc.), prompt-dose-equivalent distributions in and out of the service buildings, and radiation load on groundwater and air outside the shielding. These calculations will help in the design of optimal subsystems (target station, decay channel and hadron absorber) and will aid in the evaluation and minimization wherever possible of residual dose levels. They will also help optimize hands-on maintenance conditions, keep impact on the environment below the regulatory limits, and estimate and maximize wherever possible the component lifetime.

## 3.13 R&D Program

This section summarizes the R&D work on the components of the Neutrino Beam. There are detailed plans for ongoing and projected activities for high-power target systems.

As discussed in Section 3.3, at this time contract work has been funded to Rutherford Appleton Labs (UK) for target and window designs suitable for both 708 kW and 2.3 MW operation [19], to IHEP for design work on an alternative target design described in the document [38], and to Brookhaven for target-material irradiation studies. This work is expected to continue after CD-1.

## 4 System Integration (WBS 130.02.04)

### 4.1 Introduction

This chapter covers the System Integration activity of the LBNE Beamline L2 Project. The System Integration team's responsibilities can be broken into two major areas: first, the oversight of systems for Controls, Alignment and Interlocks, and second, coordination of interfaces and installation between each of the systems of the Beamline L2 Project. The Controls, Alignment and Interlocks must function across the entire L2 project and must therefore be properly supported by all the interfaces in addition to the relevant components. Interface coordination involves both achieving consensus as to the location and nature of each interface and the party responsible for it. The coordination activity must also ensure proper distribution of requirements and specifications so that all the needed components are accounted for, and that they will be constructed such that they will fit together properly during installation and operate successfully.

System Integration thus has the primary responsibility of facilitating good communication throughout the L2 project in order to prevent deficiencies and scope-related problems, and for any that are introduced, to spot them early on and make sure they get corrected.

### 4.2 Controls (WBS 130.02.04.02)

#### 4.2.1 Introduction

Any high-energy external beamline requires a robust control system to ensure proper operation. The control issues for a beamline like LBNE's are well understood. The control system must be able to

- reliably log data for every beam pulse (this implies a digitization with appropriate throughput)

- plot both real-time and logged data in strip-chart form and capture all operational information for the beamline devices in a database
- issue alarms for off-nominal conditions and provide power-supply controllers with ramping capability
- handle the so-called slow-control subsystems: water, vacuum and temperature
- provide environmental monitoring
- display information from the position and loss monitors along the beamline and provide an auto-tuning facility to keep the beam centered over its length without significant human intervention

The LBNE beamline consists of a large number of components, and the control system must have sufficient bandwidth to collect the necessary information from each component for each beam pulse.

The Accelerator Controls Network (ACNET) provides services for process control, monitoring, timing, save-and-restore and data logging for the Fermilab accelerator complex. Since the LBNE beamline is an extension of the accelerator complex, its control requirements will be supported via ACNET.

Given LBNE's very high beam power, 700 kW with a possible upgrade to 2.3 MW, the beam energy delivered per pulse, if misdirected, is sufficient to damage beamline components. This necessitates the use of a beam-permit system to verify a host of parameters about each beam pulse before it's extracted and to issue a "permit" if everything is in order. The beam-permit system must also be able to determine when a single bad pulse has been extracted and ensure that no further pulses are extracted until the problem is resolved. LBNE will use a system developed for NuMI that has also been used for several other Fermilab beamlines.

## 4.2.2 Reference Design

### 4.2.2.1 ACNET Controls

Controls for LBNE will be made up of standard Fermilab accelerator-control system interface and networking components. These include VME, HRM and PLC hardware with appropriate modules to provide control and monitoring of technical equipment along with commercial Ethernet switches and hubs for the networks. It should be noted that there are no plans to support the older CAMAC systems in the new LBNE areas. However, since it is unlikely that CAMAC will have been fully replaced in the MI by then, any LBNE equipment that might be installed in the MI-10/14 service buildings may be connected to ACNET via CAMAC.

ACNET services for LBNE will include connections to existing accelerator-timing systems (TCLK and MIBS from MI-8) and to the LBNE Beam-Permit System via fiber cables.

ACNET consoles provide the ability to monitor and control accelerator operations throughout the complex. This will include the LBNE beamline and technical components. While operations are typically directed via consoles in the Main Control Room remote consoles are available at a number of locations around the complex.

New controls for LBNE will be installed in five locations (Primary Beam Service Building (LBNE 5) Controls Room, Target Hall (LBNE 20) Controls Room, Target Hall Power Supply Room, Absorber Service Building (LBNE 30) Controls Room and Absorber Hall Instrumentation Room). LBNE user-interface displays will be configured to show the LBNE beamline as a single entity from the extraction kicker (described in Section 2.6.3.6) to LBNE target (described in Section 3.3).

#### 4.2.2.2 Beam-Permit System

The LBNE Beam-Permit System works in two modes to prevent extraction of errant pulses that could cause damage: *current-pulse mode* to inhibit a faulty pulse from being extracted and *next-pulse mode* to prevent extraction of subsequent pulses in case of a problem.

In current-pulse mode, the beam permit system examines a few hundred parameters in the last few milliseconds before beam delivery to ensure everything is ready for the beam. All magnet power supplies are examined, and ramping to the flat-top level is checked. Beam positions of the circulating MI beam near the LBNE kicker will be examined to test the real-time orbit in the accelerator. Kicker charge level will also be checked to ensure that the desired extraction angle will be achieved. In addition, the beam-permit system will examine parameters of the MI radio frequency (RF) system to assure that the accelerating voltage is correct for nominal extraction. If anything wrong is sensed in any of the data, the kicker will be inhibited and the beam will be sent to the MI Beam Abort.

In next-pulse mode, the beam-permit system takes many measurements after a pulse has been delivered to ensure that it was delivered properly. Chief among these are measurements from the total and local loss monitors distributed along the beamline. These monitors are sensitive to losses on the order of one part in  $10^4$  and can sense an errant beam pulse immediately after its delivery. Other measurements are taken from the beam-position monitors near the target, which indicate the proper delivery of beam, and from an array of sensors reading out target data. In the case of an errant beam pulse, subsequent pulses are inhibited.

When the system is tripped in either mode, further delivery of the beam is inhibited until a control-room operator provides a manual reset. Repeated permit-system trips caused by beam losses escalate the authority level required to restart the beam; authority moves to

beamline experts or safety personnel, depending on the circumstances.

The permit system has proven to be an excellent diagnostic for beamline and MI operations. If trips are kept at a low value, on the order of 5 to 10 per day, one can be reasonably sure that the beamline integrity is intact. After a down period, the permit system is used to check that the beamline is ready for re-establishment, and a single pulse is generally all that is required for start-up.

## 4.3 Radiation-Safety Interlock Systems (WBS 130.02.04.03)

### 4.3.1 Introduction

This section describes the philosophy, policies, procedures, design, fabrication, installation, checkout and commissioning for the Radiation Safety Interlock Systems (RSS), Radiation Monitors, Radiation Air Monitors, and Radiation Frisker Stations. Underlying all safety-system designs is a commitment to providing the necessary hardware, procedures, and knowledge to personnel to ensure their well-being. Inherent in each of these systems is the concept of redundancy.

The RSS systems are designed to protect personnel from exposure to particle beams. They are intended to prevent injury, serious overexposure or death from beam-on radiation, X-Rays or high-voltage/high-current power supplies. This includes the enclosure access-control interlocks, exclusion-area boundary gates, access keys and cores, emergency stop system, audio warning system, electrical-safety system, electrical-safety system interface units, the beamline critical-device-control contactors, critical-device controllers and associated interconnect cabling.

The Radiation Monitors are used to detect stray radiation during beamline operations. This includes Fermilab's "Chipmunk" radiation monitors (so-called because they emit an audible "chip" sound), multiplexing (mux) monitoring network, safety-system radiation-monitor interlock components and electronic berm components.

The Airborne Radiation Monitors are used to monitor the amount of radionuclides that are released to the environment during beam operations. This system includes the airborne-radiation monitors and the associated enclosure to house the components.

The Radiation Frisker Stations are used to survey personnel and materials being removed from the beamline, Target Hall and absorber enclosures. These include the portable and wall-mounted laboratory frisker and "wallflower" detectors and installation at the enclosure entry points.

### 4.3.2 Methods

The principal method employed by the interlock systems is to establish and maintain exclusion areas surrounding active accelerator areas, maintaining sufficient distance between beamline operating components and the closest point of approach. When potential exists for personnel to be within the defined exclusion area, the Radiation Safety Interlock System disables all operations that may create hazardous conditions.

Electrical-safety systems, a subset of the Radiation Safety Interlock System, have been developed to provide protection from high voltage, high current, and x-ray producing devices.

Another method is redundancy. All hardware is designed such that no single failure will result in the loss of protection. To accomplish this, two separate circuits are used to detect a given condition. For example, two separate switches monitor each door to detect its status. Each of these switches in turn is connected to a separate control circuit. Thus if one switch were to fail, the other would still operate, providing the necessary protection. An extension of the redundancy concept is used in the control of radiation-safety-system critical devices, i.e., one that prevents beam from entering an area. Two critical devices will be controlled by a single radiation-safety system.

Another key principle used in designing all safety systems, is the idea of “fail-safe” circuits. All circuits are designed in such a way that if a circuit fails, the failure would initiate a system shutdown, resulting in a safe condition. For example, if the cable that controls a device were cut, the device could not be enabled. In this way personnel are still safe. Since not all component failures can be detected by the interlock systems, functional testing in accordance with the Fermilab Radiological Control Manual (FRCM) [29] needs to be performed at periodic intervals and test results documented to ensure reliable operations.

“Search and secure,” a walkthrough of an area in a predefined sequence by at least two qualified persons to ensure that the area is unoccupied, is perhaps the most important method to ensure radiation and electrical safety. This is required each time before beam or power supplies are enabled. The search sequence will be programmed into a Programmable Logic Controller (PLC) for the LBNE Radiation and Electrical-Safety systems. The order in which the interlocks are reset will be designed so as to ensure that no personnel are missed by the search team.

Once an area has been searched and secured, status displays on the outside of each access door and each section gate indicate to individuals that the area is interlocked and that access is forbidden to unauthorized personnel. Immediately before beam is brought into an area or power supplies are enabled, a prerecorded message consisting of a siren and verbal announcement will be played to allow personnel, which in the unlikely event of being missed on a search, have time to safely exit the area. Audio warning speakers will be located at approximately 125-foot increments. All doors to an area are locked and the keys to open

these doors are interlocked and guarded in the Main Control Room. Distribution of these keys is not taken lightly. Only authorized personnel are allowed access. The type of access determines the authorization level required for the individual.

### 4.3.3 Reference Design

The Radiation Safety Interlock Systems (RSS) for LBNE extends throughout the underground enclosures with the exception of the following areas, which are to remain accessible during LBNE beamline operations.

- LBNE Target Hall Power Supply and Utility Rooms, Controls Room, Morgue service area and truck bay
- LBNE Absorber Hall access shaft
- LBNE Below-Ground Absorber Hall elevator landing area
- LBNE Absorber Sump and Pump Room and Instrumentation Room

Areas of exclusion during LBNE beam operations are divided into three separate areas. The primary beam enclosure is interlocked to the Booster RSS (not under LBNE control). The remaining exclusion areas, the Target Hall and absorber are interlocked to the LBNE RSS. The primary beam enclosure and Target Hall are contiguous with the decay-pipe region separating the Target Hall and absorber.

The LBNE RSS must be cleared for beam to be transmitted down the beamline. The state of the RSS is also an input to the LBNE Beam-Permit System. While not integral to the LBNE RSS, radiation “stack” monitors sample and record levels of activated air from the Pre-Target, Target Hall and absorber areas.

#### 4.3.3.1 Critical-Device Controller

In support of LBNE operations, two critical devices will be utilized and controlled by the LBNE Critical Device Controller (CDC). This controller will be permitted when it is safe to extract MI beam into the LBNE beamline. The controller will be connected to the power supplies feeding two separate bend magnet strings, both of which are required for beam to be transported to the LBNE beamline. Should the controller detect a failure of either power supply not turning off, the controller will send a failure mode signal to the Booster RSS disabling any further beam to the MI.

### 4.3.3.2 Exclusion Areas

A new extraction pipe will be installed inside the MI enclosure connecting to the primary beam enclosure. The upstream section of the LBNE beamline, the beamline service building access point, LBNE 5, and the enclosure down to the upstream end of the Target Hall will be interlocked to the Booster CDC.

The Target Hall Complex will be interlocked as a separate enclosure allowing for work in the Target Hall while the upstream LBNE enclosure is interlocked in support of MI area operations.

The LBNE absorber is accessible from the LBNE 30 Service Building through the access shaft. The absorber will be interlocked as a separate enclosure.

It is expected that no more than two personnel will be required to satisfactorily search and secure areas in the domain of the LBNE RSS.

### 4.3.3.3 Electrical-Safety System

Electrical hazards from exposed conductors and connections will inevitably exist in the LBNE beamline from the point of extraction to the magnetic focusing horns. These hazards are typically associated with the beamline magnetic elements, introduced in Section 2.2, such as the extraction kickers, the Lambertsons, the dipole and quadrupole magnets and the focusing horns. The Electrical Safety System (ESS) extensions of the MI and LBNE RSS provide permitting inputs to associated power supplies in order to partially mitigate the hazard of exposed and otherwise unguarded conductors. The ESS connections will be available at the MI-10, LBNE 5 and Target Hall areas. Trim and correction-element conductors and connections are guarded and connection of their associated power supplies to an ESS is not necessary.

Accommodating access into the MI and LBNE is further provided by connection of selected supplies to the pulsed power feeder 96/97. This feeder is de-energized during MI access.

### 4.3.3.4 Radiation-Loss Monitoring

Fermilab has several radiation-monitoring devices available to detect beam losses. Although the radiation-shielding assessment has not been completed, some areas of concern have been identified. Given the shape of the beamline, one area is just downstream of the apex of the embankment. Excessive beam losses in this region could potentially lead to muons directed off-site. One of the radiation-monitoring devices, called a “Scarecrow,” will be placed here. If

excessive beam losses are detected, the system will trip the LBNE Critical Device Controller (CDC) preventing further beam transport.

Non-interlocked Chipmunk monitors will be placed at various locations around the Target Hall and absorber areas to monitor for excessive radiation rates. Fermilab's MUX monitoring network will be extended into the LBNE area for recording of both interlocked and non-interlocked radiation-monitoring instruments.

#### **4.3.3.5 Airborne-Radioactivity Monitors**

Airborne Radiation Monitors are used to monitor the amount of radionuclides released to the environment during beam operations. Airborne activation results primarily from the direct interaction of primary and secondary particles with the air (or other gaseous medium). Dust, from natural erosion, wear or work on radioactive accelerator components is a secondary source, as is the emission of gaseous radioactivity from "hot" liquids in the radiation environment produced by the accelerator. Since the vast majority of the radioactive atoms produced are short-lived, delayed ventilation, with a delay time of one hour from production to exhaust, is used to reduce the radioactivity by roughly one order of magnitude at the air exhaust stack. Activation from the downstream LBNE primary beam, the Target Hall and the absorber areas will be monitored.

#### **4.3.3.6 Enclosure Radiation Monitors**

Radiation frisker stations are used to survey personnel and materials being removed from the primary beam, Target Hall and absorber enclosures. Fermilab has a standardized pair of instruments for frisking and determining a material's radioactive class. The laboratory standard frisker and wallflower detectors will be installed at each enclosure entry point. Emergency-exit locations will not be outfitted with frisker stations.

## **4.4 Alignment (WBS 130.02.04.04)**

### **4.4.1 Overview**

This section summarizes the concepts, methodology, implementation and commissioning of the geodetic surveying (global positioning) efforts for determining the absolute positions of the LBNE beamline components at Fermilab and the location for the Far Detector at SURF. This information is critical to achieving proper aim of the neutrino beam. From this

**Table 4-1:** Alignment tolerance requirements ( $1-\sigma$ )

Beam position at target	$\pm 0.45$ mm
Target position - each end	$\pm 0.5$ mm
Horn 1 position - each end	$\pm 0.5$ mm
Horn 2 position - each end	$\pm 0.5$ mm
Decay pipe position	$\pm 20$ mm
Downstream Hadron monitor	$\pm 25$ mm
Muon monitors	$\pm 25$ mm
Far Detectors	$\pm 21$ m

information, the beam orientation parameters are computed, as well as the alignment of the LBNE beamline.

#### 4.4.2 Design Considerations

Clearly, directing the neutrino beam to intersect the Far Detector located 1,300 km distant from the source, is of paramount importance. Physics requirements will drive the absolute and relative alignment tolerances.

The divergence (spatial spread orthogonal to the line of travel) of the neutrino beam at this distance is on the order of kilometers. The spectrum of neutrino energies varies with their offset from the beam's center line, higher-energy neutrinos are closer to the center, lower-energy ones are farther out. Based on NuMI's requirement for the energy spread, LBNE will require that the combined effect of all alignment errors must cause less than 2% change in any 1-GeV energy interval in predicting the Far Detector energy spectrum.

To accomplish this, and prorate from NuMI to SURF, the neutrino-beam center must be within  $\pm 133$  m from its ideal position at the far detector, corresponding to an angular error of  $\pm 10^{-4}$  radians. Achieving this tolerance requires precise knowledge of the geometry of the neutrino beam. Table 4-1 lists alignment tolerance requirements for the low-energy beam for NuMI, which will also be established for LBNE, with the exception of the Far Detector which was prorated to SURF. A Monte Carlo (PBEAM\_WMC) was used to calculate the effect of misalignments of each beamline element for the determination of the Far Detector spectrum (without oscillations) from the NuMI's measured near-detector spectrum.

The requirement on the relative alignments of the beamline components and the target-station components (target and horns) is that they be within  $\pm 0.35$  mm (requirement based on NuMI). To accomplish this, high-accuracy local geodetic and underground networks will be established to support the installation and alignment of the primary-beam components, neutrino-beam devices and the near detector.

### 4.4.3 Reference Design

#### 4.4.3.1 Geodetic Determination of the Global Positions

The computation of the geometric parameters of the beam trajectory, expressed in terms of the azimuth and the slope of the vector joining the two sites, requires precise knowledge of the absolute positions of the two ends of the vector, at the near and far sites.

The geodetic orientation parameters of the beam, based on the absolute and relative positions of the target at Fermilab and the far detector at SURF, will be determined with GPS to a high level of accuracy in conjunction with the national Continuously Observed Reference Station (CORS) network. All other geodetic aspects related to the project, i.e. local geoid modeling, deflection from the vertical, differential tidal variations, plate tectonics, point velocities and precise azimuth determination, will be resolved and confirmed for quality assurance.

The development in the past decade of the CORS System led us to conclude that direct GPS observations of long baselines between monuments located at Fermilab and the SURF site, combined with CORS data, would provide the most precise and reliable results. Connections derived from two or more CORS stations will ensure unprecedented positional integrity without the expense of sending additional receivers and personnel into the field.

As a result of the ongoing collaboration, a Cooperative Agreement with the National Geodetic Survey (NGS) will be established for determining the coordinates of several points belonging to the Fermilab and SURF networks in conjunction with the CORS system. In addition to the data analyzed at Fermilab, NGS will compute an independent solution and provide geodetic coordinates for the two sites using the adjacent CORS network.

The GPS observation campaign will follow the NGS specifications. Except for station occupation time, the specifications are similar to the High Accuracy Reference Network procedures regarding equipment setup, GPS-receiver controls, weather-data collection, and documentation. During three days of observations and using four dual-frequency receivers, three sessions of 9-10 hours of data at each site will be collected, staggering the observation start times in order to observe the complete satellite constellation orbital period of 12 hours.

The network for determining accurately the coordinates for the Fermilab-SURF baseline is formed by four CORS stations and the two primary LBNE monuments: 66589 at Fermilab, the closest to the designed LBNE Target Hall, and a new monument near SURF's Yates access shaft, for which the most GPS observation data will be collected. From the CORS stations adjacent to the main Fermilab-SURF baseline four were selected, two on each side of the vector in a balanced manner. Figure 4-1 shows a map of the Midwest CORS stations with the proposed network superimposed.

The vector solutions for the network will be processed by combining the GPS data collected

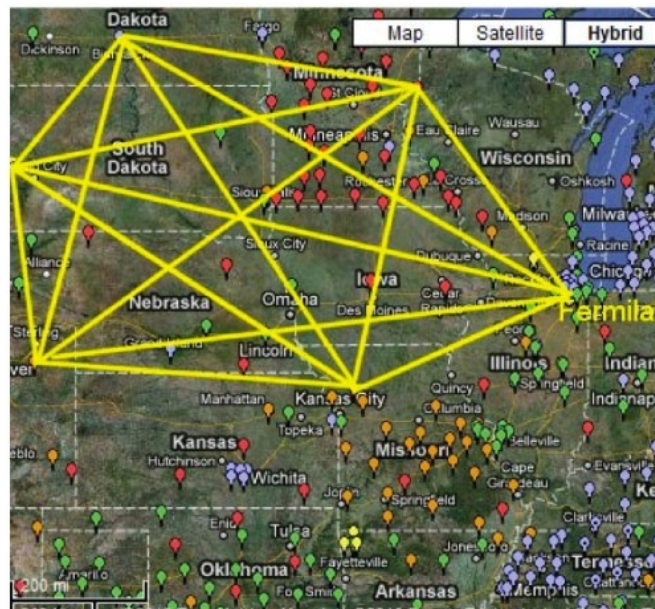


**Figure 4-1:** GPS network tying Fermilab and SURF to the CORS system

by Fermilab with the data collected by the CORS stations that are made available for retrieval via the Internet. To improve the accuracy of the baseline GPS-vector computations, the satellites' precise orbits, made available by NGS, will be used. Observed meteorological data will also be used for modeling the tropospheric effect on the GPS signal propagation.

A minimal-constraint, least-squares adjustment consisting of 72 observations (24 vectors) will be performed. Simulations and past experience from NuMI show the standard deviations of the adjusted coordinates to be in the millimeters range in all three coordinates (longitude/latitude 1–3 mm, ellipsoid height 7–10 mm) at 95% confidence level. As a measure of internal consistency, the *rms* of the residuals of the adjustment were 2 mm in both latitude and longitude and 6 mm in height as shown in Figure 4-2 *a* and *b*.

The high quality of this network will be further confirmed by computing standard deviations for the spatial distances and height differences for all adjusted vectors using variance-covariance propagation. Past experience from NuMI shows that standard deviations for the spatial distances are less than 5 mm (this includes lines across the network). The height differences have standard deviations of 10–15 mm.

Past experience from NuMI shows that a comparison between the two sets of results, computed independently by Fermilab and NGS, indicated differences on the mm level for the longitude and latitude and amounting up to 10 mm in height. These differences can be explained by the fact that the computations were performed independently in two reference frames: (International Terrestrial Reference Frame (ITRF96) and North American Datum (NAD 83) and that temporal tidal variations were not accounted for in the computations.

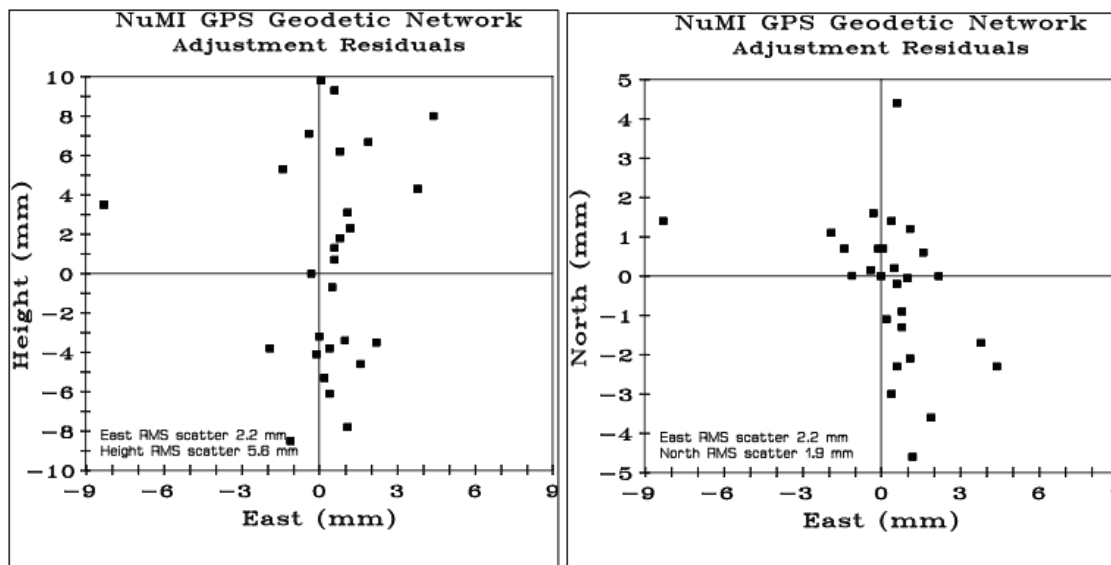


**Figure 4-2:** Residuals in latitude/longitude and residuals in height.

The NAD 83 reference frame is defined such that the North American tectonic plate does not move as a whole relative to it. On the other hand, relative to the ITRF, even points located on the rigid part of the North American tectonic plate move continuously at rates ranging from 9 to 21 mm/year in the United States.

#### 4.4.3.2 Primary Surface Geodetic Network at Fermilab

The geodetic reference for supporting the construction and positioning of the LBNE project is derived from a high-accuracy local surface network. The existing Fermilab/MI master control network, which has a relative positional accuracy better than 2 mm, includes the monuments surveyed during the CORS tie campaign, and will be supplemented with six geodetic monuments, providing densification around the access points. Figure 4-3 shows a simplified version of the network geometry.

The LBNE absolute-positioning-tolerance requirements call for extensive combined GPS, terrestrial and astronomic surveys. The computations will be performed in the NAD 83 system, which uses the Geodetic Reference System (GRS 80), which consists of a global reference ellipsoid. Simulations and past experience from NuMI show that minimal-constraint least-squares adjustment consisting of more than 410 observations will yield absolute error ellipses in the mm range at the 95% confidence level.

Precise astronomical azimuth determinations will be performed on two MI geodetic monuments surveyed during the CORS campaign. Those monuments, with wide visibility over the LBNE upstream area covering the entire beamline, will be used extensively during the

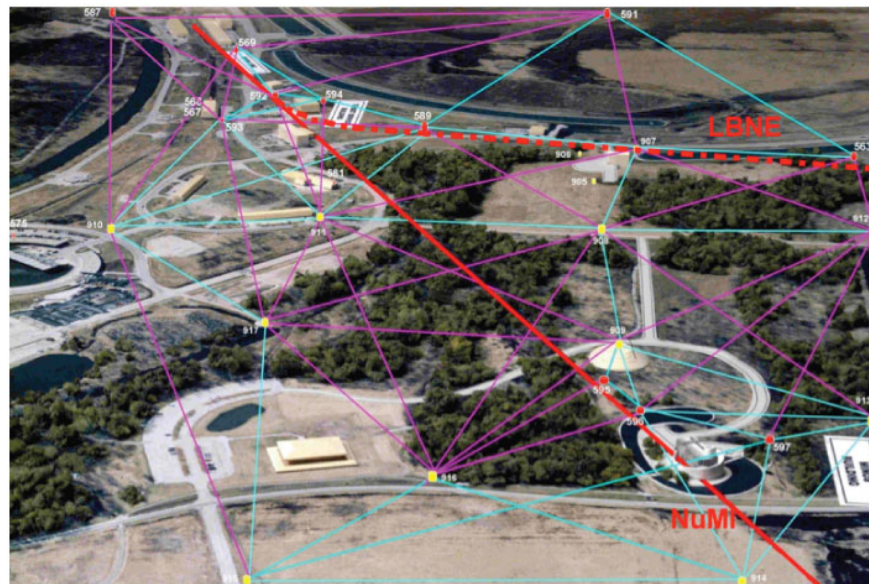


**Figure 4-3:** Fermilab LBNE surface geodetic network.

project as reference for transferring absolute coordinates from the surface into the underground tunnels and halls. They will also serve as a calibration baseline for the surveying tool, a DMT-brand Gyromat 2000 precision gyroscope. Based on experience from NuMI, the standard deviation of the azimuth over three nights of observations was 0.66 arc seconds (0.003 mrad).

The vertical alignment of the beamline components along the vector joining the two sites relies on leveling measurements, which use as a reference surface the geoid, defined as the equipotential surface of the Earth's gravity field at mean sea level. The general shape of the geoid over a large area, in other words, is determined by gravitational parameters.

The non-homogeneity of the earth and the surrounding Fermilab topography may not change dramatically enough to raise major concerns for distortions of the gravity equipotential surfaces. However, for the purpose of aiming the neutrino beam correctly, it is important to consider local variations in the gravity field in order to precisely determine the gravity vector at the origin. This information also allows precise determination of the magnitude of corrections that will compensate for deflections from the vertical.

Since the LBNE beamline originates from the MI, the study of the local geoid model covering the Fermilab area developed in the mid-1990s was used to help determine the exact spatial geometric relationship between the Tevatron and the new MI. With both high-precision GPS and geodetic leveling measurements available for a rather large number of monuments covering the site, the geoid height at those points was calculated differentiating between GPS ellipsoidal height and the orthometric height from geodetic leveling. The local geoid model then used a best-fitting surface employing a second-order polynomial and a spline function

to interpolate heights at other points where surveying data was not available. The results show that the accuracy for computing relative geoid heights and the two components of the deflection of the vertical were in the range of  $\pm 3$  mm and respectively  $\pm 0.1$ -  $0.2$  arc seconds with respect to the local origin.

The local geoid model was compared with the Geoid93 model provided by the National Geodetic Survey (NGS). Based on over 1.8 million terrestrial and ship gravity values, the model uses a Fast Fourier Transform (FFT) method to compute the detailed geoid structure which, combined with an underlying OSU91A geopotential model, produces a geoid height grid with a  $3' \times 3'$  spacing in latitude and longitude referred to as the Geodetic Reference System 1980 (GRS 80) normal ellipsoid. The values for the intermediary points are then interpolated by using locally a biquadratic fit function. NGS estimates that the comparison of the Geoid93 model with combined GPS and levelling yields roughly a 10-cm accuracy (one sigma) over length scales of 100 km. Better accuracy is expected over shorter lengths.

The comparison between the two models shows differences up to 5 mm, consistent with the expected values. Furthermore, this is also an indication that there are no local gravity anomalies (local variations in the gravity field) not modeled by the national model for this area, at least at this level of sensitivity. The LBNE beamline falls in the 1.5-mm range of those differences, well within the estimated accuracy for the local or the national geoid models. The national geoid model was considered sufficient to cover the tolerance requirements for the project. As a result, the Geoid93 and Deflec93 provided by NGS were used in the LBNE geodetic computations.

#### 4.4.3.3 High-Accuracy Sub-Surface Control Network

The final primary-beam trajectory is of crucial importance to LBNE. To minimize the relative errors between the beamline components, target and horn alignment and to provide dynamic monitoring of their relative positions, a high-accuracy control network with strict tolerances will be implemented. Relative component positions established to  $\pm 0.35$  mm ( $1\sigma$ ) are expected throughout the extraction enclosure, transfer tunnels and Target Hall. The residuals from the NuMI Target Hall to the MINOS Near Detector, as shown in Figure 4-4, provide an example of the degree of coordinate uncertainty in a measured system like LBNE.

Network simulations of different models have led to an optimized design of the number (six) and locations of vertical sight risers. This is sufficient to provide azimuthal constraints and to control the scale of the network.

The configuration of the control network is limited by the geometry of the tunnels and halls. Studies and past experience with NuMI have led to a configuration based on chains of polygons. In order to improve the isotropy of the network and compensate for the weaknesses caused by the poor ratio between the sides of polygons, additional measurements spanning

adjacent polygons are added.

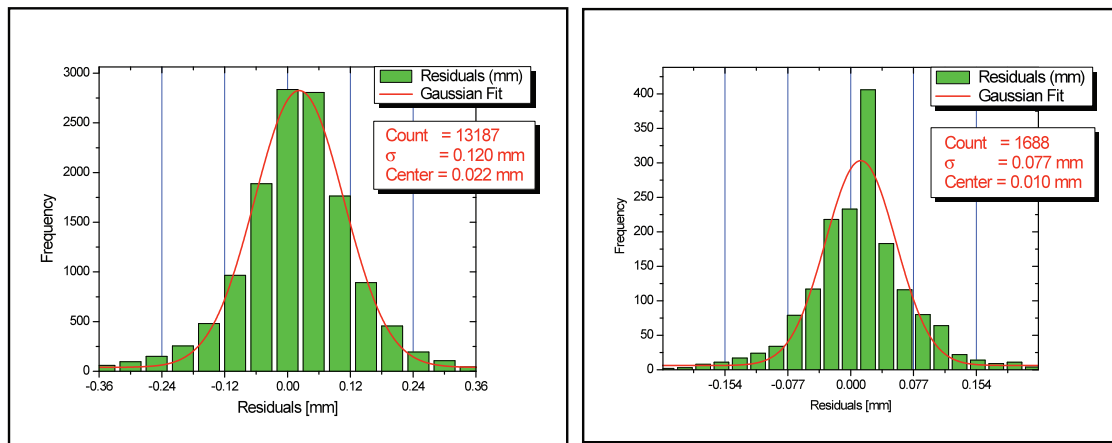


**Figure 4-4:** Distribution observation residuals for the Target and Near Detector Halls in MINOS

## 4.5 Installation Coordination (WBS 130.02.04.05)

This activity provides the management oversight of the day-to-day activities taking place in the installation areas and the framework for sequencing and scheduling the installation tasks. Therefore its role is primarily the *coordination* of installation activities and will be led by an Installation Coordinator. The responsibility for the design, fabrication and installation of each element of the Beamline L2 Project resides in its appropriate subsystem.

Installation coordination will be managed similarly to NuMI installation. Each area (e.g., Target Area, absorber and so on) will have a Floor Manager whose job it is to oversee the overall installation activity taking place in the area and to supervise the daily activities of task managers who are leading the work crews in each area. Floor Managers will report directly to the Installation Coordinator.

During installation, a regular end-of-week installation meeting will be held with the Installation Coordinator and Deputy, the Floor Managers from all areas, and the ES&H Manager to review the progress of the week and discuss issues that have arisen.

In an additional weekly meeting, the Floor Managers will meet with the L3 and L4 managers to review progress, relate information from the previous installation meeting and discuss the tasks being considered for the upcoming time periods. This discussion will include lab and project management and ES&H representatives. It is expected that as issues arise which impact cost and schedule, they will be discussed if not resolved.

Daily “toolbox” meetings for everyone working in the areas will be held to outline the activities of the day and discuss any specific issues or concerns.



## References

- [1] Particle Physics Project Prioritization Panel, “US Particle Physics: Scientific Opportunities; A Strategic Plan for the Next Ten Years,” 2008. [http://science.energy.gov/~media/hep/pdf/files/pdfs/p5\\_report\\_06022008.pdf](http://science.energy.gov/~media/hep/pdf/files/pdfs/p5_report_06022008.pdf).
- [2] T. Akiri *et al.*, “The 2010 Interim Report of the Long Baseline Neutrino Experiment Collaboration Physics Working Groups.” arXiv:1110.6249.
- [3] LBNE Project Office, “LBNE Project Management Plan,” tech. rep., FNAL, 2011. LBNE Doc 2453.
- [4] “Draft MOU between LBNE and the Fermilab Directorate,” 2012. <http://lbne2-docdb.fnal.gov:8080/cgi-bin/ShowDocument?docid=6319>.
- [5] “Alternatives Analysis.” LBNE Project Management Team - LBNE Doc 4382, 2012.
- [6] V. Papadimitriou, “Decision on the depth and extraction point of the LBNE Neutrino Beamline,” tech. rep., FNAL, 2011. LBNE:DocDB-5122.
- [7] I. Kourbanis, “MI Beam Power for Different Energies,” tech. rep., 2010. LBNE Doc 3716 <http://beamdocs.fnal.gov/AD-public/DocDB/ShowDocument?docid=3716>.
- [8] “Accelerator Performance Charts.” <http://www-bd.fnal.gov/pplot/>.
- [9] “Methodical Accelerator Design (MAD).” CERN - Accelerator Beam Physics Group <http://mad.home.cern.ch/mad/>.
- [10] D.Harding. Magnet Test Facility measurement database private communication (Fermilab AD) .
- [11] V. Bocean (Fermilab PPD/Alignment) private communication.
- [12] Fermilab, “Fermilab ES&H Manual .” <http://esh.fnal.gov/xms/FESHM>.
- [13] “Fermilab Engineering Manual, v07/10,” tech. rep., 2010. [http://www.fnal.gov/directorate/documents/FNAL\\_Engineering\\_Manual.pdf](http://www.fnal.gov/directorate/documents/FNAL_Engineering_Manual.pdf).

- [14] I.Baishev, A.Drozhdin, N.Mokhov, and X.Yang, “STRUCT Program User’s Reference Manual,” 1994. SSC Doc: SSCL-MAN-0034 <http://www-ap.fnal.gov/users/drozhdin/>.
- [15] N. Mokhov and S. Striganov, “MARS15 Overview, Hadronic Shower Simulation Workshop AIP Proceedings 896,” tech. rep., 2007. Fermilab-Conf-07-008-AD.
- [16] “NuMI Technical Design Handbook, Sec. 4.4,” tech. rep., 2003. [http://www-numi.fnal.gov/numwork/tdh/tdh\\_index.html](http://www-numi.fnal.gov/numwork/tdh/tdh_index.html).
- [17] V.Zarucheisky *et al.*, “NOvA Target Hall Baffle Specification,” 2010.
- [18] M.Martens, J.Hylen, and K.Anderson, “Target and Horn Configuration for the NOvA Experiment,” tech. rep., 2009. [http://www.fnal.gov/directorate/documents/FNAL\\_Engineering\\_Manual.pdf](http://www.fnal.gov/directorate/documents/FNAL_Engineering_Manual.pdf).
- [19] C.Densham *et al.*, “Conceptual Design Study of the LBNE Target and Beam Window,” tech. rep., 2010. LBNE Doc 2400.
- [20] N.Simos *et al.*, “Long Baseline Neutrino Experiment (LBNE) Target Material Radiation Damage from Energetic Protons of the Brookhaven Linear Isotope Production (BLIP) Facility,” tech. rep., 2012. LBNE Doc 5724.
- [21] B.Lundberg, “Specifications for Beam Simulations,” tech. rep., 2009. LBNE Doc 2161.
- [22] “NuMI Technical Design Handbook, Sec. 4.2.4,” tech. rep., 2003.
- [23] N.Mokhov, “The Mars Code System User’s Guide,” tech. rep., 2009. Fermilab-FN-628.
- [24] “Beamline Requirements Documentation,” tech. rep. LBNE Doc 4335 <http://lbne2-docdb.fnal.gov:8080/cgi-bin/ShowDocument?docid=4335>.
- [25] N.Mokhov *et al.*, “LBNE Target Station, Decay Volume and Hadron Absorber: Radiation and Thermal Analysis Modeling,” tech. rep., 2011. LBNE Doc 2241.
- [26] “National instruments.” <http://www.ni.com/>.
- [27] “ANSYS Engineering Simulation.” <http://www.ansys.com>.
- [28] E.Rivera, “NuMI Hadron Absorber Finite Element Analysis for NOvA Beam Energy’,” tech. rep., 2010.
- [29] “Fermilab Radiological Control Manual, and references therein,” tech. rep. /url-<http://esh.fnal.gov/xms/FRCM>.
- [30] D. Reitzner and K. Vaziri, “LBNE Groundwater Shielding Requirements for Shallow and Deep Beam,” tech. rep., Fermilab. LBNE Doc 4052 <http://lbne2-docdb.fnal.gov:8080/0040/004052/004/ShieldingRequirementsGroundwater5.docx>.

- [31] N. Mokhov, “LBNE Absorber MARS Studies.” LBNE Doc 2205 [http://lbne2-docdb.fnal.gov:8080/0022/002205/001/LBNE\\_ABS\\_norm\\_mokhov\\_031610.pdf](http://lbne2-docdb.fnal.gov:8080/0022/002205/001/LBNE_ABS_norm_mokhov_031610.pdf).
- [32] “LBL Consultant Report on NuMI Tritium in Beampipe Shielding,” tech. rep. LBNE Doc 2533.
- [33] N. Mokhov, “Target Chase MARS Calculations.” LBNE Doc 3216 <http://lbne2-docdb.fnal.gov:8080/0032/003216/001/LBNE-doc-3216-mokhov-120810.pdf>.
- [34] D. Reitzner, “LBNE Dose at Site Boundary.” LBNE Doc 4128 [http://lbne2-docdb.fnal.gov:8080/0041/004128/002/skyshine\\_on\\_axis\\_MI10\\_revisited.pptx](http://lbne2-docdb.fnal.gov:8080/0041/004128/002/skyshine_on_axis_MI10_revisited.pptx).
- [35] P. Hurrh, “LBNE Remote Handling Component List and Shielding Calculations,” 2012.
- [36] V.Graves, A.Carroll, and T.Burgess, “Conceptual Design of the Remote Handling Facilities for the Long-Baseline Neutrino Experiment,” tech. rep., 2010. ORNL/TM-2010/125, LBNE DocDB 2483.
- [37] N. Mokhov, “Recent MARS15 Developments,” tech. rep., 2010. Fermilab-Conf-10-518-APC.
- [38] V.Garkusha *et al.*, “700 kW target design study - IHEP 2009 Accord report,” tech. rep., 2010. LBNE Doc 2423.